Cinnamic acid terminated dendrimers Synthesis, characterization, biological evaluation and NMR metabolomics analysis

DOCTORAL THESIS

Ana Cristina Dias Oliva
DOCTORATE IN CHEMISTRY

ORIENTATION
João Manuel Cunha Rodrigues

COORIENTATION
Helena Maria Pires Gaspar Tomás

Cinnamic acid terminated dendrimers – Synthesis, characterization, biological evaluation and NMR metabolomics analysis

A thesis presented to the University of Madeira to obtain the Doctoral degree in Chemistry

Ana Cristina Dias Olival

Under the supervision of:
Doctor (Ph.D.) João Manuel Cunha Rodrigues
Doctor (Ph.D.) Helena Maria Pires Gaspar Tomás

Faculdade de Ciências Exactas e da Engenharia
Centro de Química da Madeira
Funchal, Portugal

August 2022

The work presented in this dissertation was performed in the Centro de Química da Madeira (CQM) at the Molecular Materials Research Group (MMRG), University of Madeira, under the scope of the PD-F FCT Ph.D. Programmes (Doctoral Program in Nuclear Magnetic Resonance Applied to Chemistry, Materials and Biosciences (PTNMR Ph.D.), supported by ARDITI - Agência Regional para o Desenvolvimento da Investigação, Tecnologia e Inovação through the Ph.D. grant REF: M1420-09-5369-FSE-BD-CQM. The support of PROEQUIPRAM - Reforço do Investimento em Equipamentos e Infraestruturas Científicas na RAM (M1420-01-0145-FEDER-000008), project M1420-01-0145-FEDER-000005-CQM^{+} (Madeira 14-20 Program), and FCT-Fundação para a Ciência e a Tecnologia through the CQM Projects: UID/QUI/00674/2015, Pest-OE/QUI/UI0674/2019. Base Fund UIDB/00674/2020 and Programmatic Fund UIDP/00674/2020 were also acknowledged.

Acknowledgments

The preparation of this dissertation would not have been possible without the support and guidance of several persons and entities involved in my academic life.

First, I would like to thank Professor João Rodrigues and Professor Helena Tomás for the opportunity they gave me to carry out the dissertation project under their guidance, for all the support, encouragement, interest, enthusiasm, and concern shown throughout these years and during my study and training.

The University of Madeira and especially the CQM- Centro de Química da Madeira (Madeira Chemistry Research Centre) for welcoming me, making available the infrastructure, and providing the necessary conditions to carry out my research.

This project would not be possible without the support of ARDITI (Regional Agency for the Development of Research, Technology, and Innovation) through the Ph. D. grant M1420-09-5369-FSE-BD-CQM.

The Hospital Nélio Mendonça, especially to the haematology service for providing the blood used for the haematotoxicity tests.

To the non-teaching staff of the chemistry department, Paula Andrade, Paula Vieira, and of CQM, Teresa Abreu, and Yessika Oliveira, for the continuous support whenever I needed it.

To the laboratory colleagues, especially to Rita Castro, Mara Gonçalves, Cláudia Camacho, Dina Maciel, Nilsa Oliveira, Carla Alves, Filipe Olim, Duarte Fernandes, Lydia dos Orfãos, Carla Miguel for sharing knowledge, and for the good working environment that I felt in the laboratory.

To Doctor João Figueira (Umeå University) and Engineer Phil Stone (from Dias de Sousa S. A.), for answering my technical doubts and existences central to my work's development.

Professor José Camara, Professor Paula Castilho, and Professor Pedro Pires gave accurate comments that helped me organize and forward ideas.

Many thanks to Catarina Silva. Without her, I wouldn't have developed the idea for this project, which gave me so much satisfaction.

To the colleagues that along the years have become friends, Joselin Aguiar, João Gonçalves, Mariangie Castillo, Vera Alves, João Serina, Gonçalo Martins, Vítor Spínola, Fátima Mendes and Rosa Perestrelo for the conviviality, atmosphere of mutual help during these last years.

To my family, my source of inspiration. Without them, I would not have got here.

A special thanks to my parents, Maria da Conceição and Manuel Andrade, and my brothers, Luis Miguel, Manuel Adrian, and Jesus Alberto, for supporting me all the time.

To Henrique Sousa, for listening, for always giving the right opinions, and for the unconditional support and joys he gives me in my life.

Abstract

Given the widespread use and enormous therapeutic potential of nanoparticles, the study of their biological effects is a relevant and current issue.

In this project, were synthesized new cinnamic acid-terminated PAMAM G4NH2 dendrimers (CATDEN) to target the monocarboxylate transporter (MCTs) overexpressed in cancer cells. The cinnamic acid chosen was alpha-cyano-4-hydroxycinnamic acid, given its effectiveness *in vitro* and *in vivo* in inhibiting MCTS. The metabolic profile of cell extracts and cell culture supernatants were studied by NMR metabolomics methods to evaluate the dendrimer's mechanism of action.

After statistical analysis, the results showed that all cell lines were affected by the treatment with the PAMAM G4NH_2, with the assays in human osteosarcoma cells (CAL-72) showing higher discrimination between treated and non-treated cells.

The results suggested that native dendrimer and CATDEN influence metabolic alterations in energy production (glucose metabolism) and protein synthesis (amino acid catabolism). This finding indicates that the cytotoxicity associated with PAMAM may result from the depletion of the components of the medium.

Furthermore, CATDEN dendrimers were also used to encapsulate the anticancer drug DOX. Our results indicated that in CATDEN, even with a lower encapsulation capacity (probably due to steric hindrance), the release of DOX is similar to that of the commercial dendrimer not functionalized with cinnamic acid. The cytotoxicity of both dendrimer/DOX complexes is shown to be superior when compared to free DOX.

Key Words: NMR, cinnamic-acid, metabolomics, dendrimers, PAMAM, doxorubicin

Resumo

Dada a utilização generalizada e o enorme potencial terapêutico das nanopartículas, o estudo dos seus efeitos biológicos é uma questão relevante e atual.

Neste projeto, novos dendrímeros funcionalizados com ácido cinâmico (CATDEN), tendo por base os dendrímeros PAMAM, foram sintetizados com o intuito de serem direcionados ao transportador de monocarboxilato (MCTs) sobreexpresso em células cancerosas. O ácido cinâmico escolhido foi o ácido alfa-ciano-4-hidroxicinâmico, já que que apresenta eficácia *in vitro* e *in vivo* na inibição dos MCTS. O perfil metabólico dos extratos celulares e sobrenadantes de cultura celular foram estudados usando métodos de metabolómica aplicados à técnica de RMN para avaliar o mecanismo de ação do dendrímero.

Após análise estatística, os resultados mostraram que todas as linhas celulares foram afetadas pelo tratamento com o PAMAM G4NH_2, sendo que os ensaios com células de osteossarcoma humano (CAL-72) mostraram uma maior discriminação entre células tratadas e não tratadas.

Os resultados sugerem que tanto o dendrímero nativo (PAMAM G4NH_2) como o dendrímero CATDEN afetam os processos metabólicos de produção de energia (metabolismo da glucose) e síntese de proteínas (catabolismo de aminoácidos). Esta constatação parece indicar que a citotoxicidade associada aos dendrímeros pode ser resultado da depleção dos componentes do meio.

Além disso, os dendrímeros CATDEN também foram utilizados para o encapsulamento do fármaco anticancerígeno, DOX. Os nossos resultados indicaram que os dendrímeros CATDEN, mesmo com uma capacidade de encapsulação inferior (provavelmente devido ao impedimento estérico), a libertação da DOX é similar à do dendrímero comercial não funcionalizado com o àcido cinâmico. A citotoxicidade de ambos os complexos, dendrímero/DOX mostra ser superior quando comparada com a DOX livre.

Palavras-chave: NMR, acido-cinâmico, Metabolómica, Dendrimeros, PAMAM, doxorubicina

Preamble

The present work was developed at the Madeira Chemistry Centre (CQM), University of Madeira (Portugal), specifically in the Molecular Materials and Coordination Chemistry Lab, the Biochemistry and Cell Culture lab, and the Nuclear Magnetic Resonance (NMR) Lab.

The general objective of this Ph.D. project was to synthesize and characterise a new family of cinnamic acid ¬terminated dendrimers and study their influence on cancer by NMR metabolomics. Given the potential application of these molecules as cancer therapy and/or diagnostic agents, their use as vehicles for the transport of drugs will be simultaneously investigated.

The thesis is subdivided into 5 chapters: Chapter 1 presents an overview of state of the art in the field of metabolomics, focusing mainly on the application of NMR-based metabolomics in mammalian cell lines and the toxicology evaluation of nanomaterials like dendrimers. Chapter 2 describes the experimental methods used throughout this work, including the synthetic procedure and chemical characterization for the cinnamic acid, terminated dendrimers, the procedures used in cell culture and biological assays, sample collection and preparation, NMR analysis, and statistical treatment of the data. Chapter 3 presents the metabolomics analysis of different cell lines exposed to native PAMAM dendrimer generation four, based on NMR analysis of culture media supernatants (exometabolome) and polar cell extracts (endometabolome), showing the wide range of applications that NMR and chemometrics allow to explore. Chapter 4 details the preparation and characterization of novel cinnamic acid terminated dendrimers used as scaffolds to encapsulate anticancer drugs doxorubicin. Chapter 5 shows the results of the metabolic profile of an osteosarcoma cell line after the treatment with one of the novel cinnamic acid-terminated dendrimers. Finally, based on the integration of the results presented throughout the previous chapters, the main conclusions of this work are presented and discussed in Chapter 6.

List of communications

Oral communications

Internationals

Olival, A.; Tomas, H; and Rodrigues J. Study of the in vitro cellular effects of PAMAM dendrimers using ^{1}H NMR. MAD-Nano18, Madeira International Conference on Emerging Trends and Future of Nanomaterials for Human Health, 30th November to 2nd December 2018, Funchal, Portugal.

Olival, A.; Tomas, H; and Rodrigues J. Cinnamic acid functionalized PAMAM dendrimer generation 4: drug delivery and cytotoxicity. IDS11 - 11th International Dendrimers Symposium, 14th to 18th December 2019, Funchal, Portugal.

Nationals

Olival, A.; Tomas, H; and Rodrigues J. Study of the in vitro cellular effects of PAMAM dendrimers using ^{1}H NMR. 4th CQM Annual Meeting, 3rd to 4th February 2017, Funchal, Portugal.

Olival, A.; Tomas, H; and Rodrigues J. PAMAM Dendrimer Effects on the Metabolic Profile of Different Cell Lines by ^{1}H NMR Analysis. 5th CQM Annual Meeting, 1st to 2nd February 2018, Funchal, Portugal.

Olival, A.; Tomas, H; and Rodrigues J. Effect of Functionalization of PAMAM Dendrimers with Cinnamic Acid in Drug Encapsulation. 6th CQM Annual Meeting, 26th to 27th Abril 2019, Funchal, Portugal.

Poster communications

Olival, A.; Tomas, H; and Rodrigues J. Evaluation of the nanotoxicity of PAMAM dendrimers by ^{1}H NMR Metabolomics in different cell lines. MAD-Nano18, VIII Ibero-American NMR Meeting – VIII Iberic-American Meeting of RMN, 26th to 29th December 2018, Lisboa, Portugal.

Olival, A.; Tomas, H; and Rodrigues J. ^{1}H NMR analysis of the metabolic profile of different cell lines. Ciência 2018 - Encontro com a Ciência e Tecnologia em Portugal, 2nd to 4th December 2018, Lisboa, Portugal.

Index

Index of Figures

Index of Tables

Abbreviations

δ	Chemical shift (expressed in ppm)
A2780	Human ovarian carcinoma cell line
ACCA	Alpha Cyano 4-hydroxycinnamic Acid
ANOVA	Analysis of Variance
CACO	Human colorectal adenocarcinoma cell line
CAL-72	Human bone cancer cell line
^{13}C NMR	Carbon Nuclear Magnetic Resonance
DMEM	Dulbecco's Modified Eagle Medium
DNA	Deoxyribonucleic acid
FBS	Fetal Bovine Serum
FTIR	Fourier Transform Infrared Spectroscopy
^{1}H NMR	Proton Nuclear Magnetic Resonance
HMDB	Human Metabolome Data Base
HSQC	Heteronuclear Single Quantum Coherence Spectroscopy
NIH 3T3	Mouse embryonic fibroblast cell line
NMR	Nuclear Magnetic Resonance
MALDI	Matrix-assisted Laser Desorption/ionization
MCT	Monocarboxylate Transport
ppm	Parts per million
PBS	Phosphate-Buffered Saline
PCA	Principal Component Analysis
PLS-DA	Partial Least Squares regression
RPMI	Roswell Park Memorial Institute
RT	Room Temperature
VIP	Variable importance in a projection
UV-Vis	Ultraviolet-Visible spectroscopy
TSP	3-(Trimethylsilyl)propionic-2,2,3,3-d_4 acid sodium salt

Chapter 1 - State of the art

1. Metabolomics

The Human Genome Project[1] has motivated the scientific community to pursue an understanding of the cellular functioning of organisms and their biological changes. This led to the emergence of the omics sciences that took a holistic view of the molecules contained in cells, tissues, or organisms. The suffix "-omic" came from the Greek suffix "ome", which can be understood as "set of a substance" and has been added to denote studies performed on a very largescale data analysis (Figure 1). They are genomics (the study of changes in genes), transcriptomics (the study of changes in transcripts), proteomics (the study of changes in proteins), and metabolomics (the study of changes in metabolites).[2]

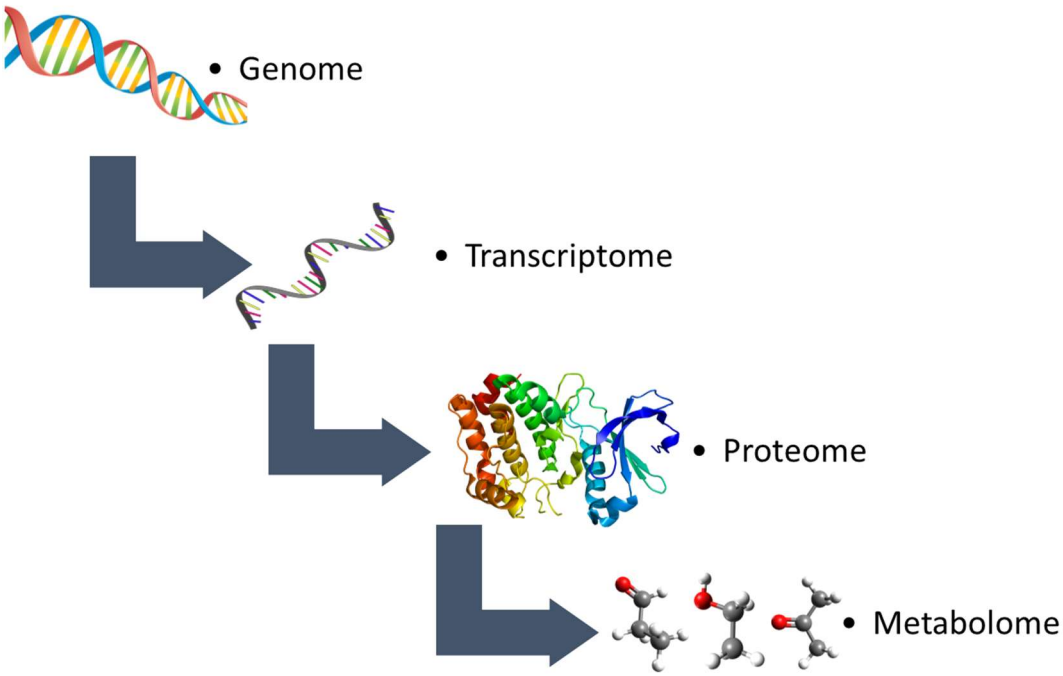

Figure 1. Omics science.

The first to use the term metabolomics was Oliver Fiehn in 1998[3]. He later defined it in 2002[4] as "the complete set of low-molecular-weight metabolites/intermediates that are context-dependent, varying according to the physiology, developmental or pathological state of the cell, tissue, organ or organism." However, the first to define it was Jeremy Nicholson in 1999[5] as "the quantitative measurement of the dynamic multiparametric

metabolic response of living systems to pathophysiological stimuli or genetic modification".

Since then, the term has come to designate a global and interactive approach to the analysis of highly complex and interconnected reactions, whereby even small changes, such as a decrease in concentration or activity of an enzyme, can cause simultaneous modifications in the concentration of hundreds of metabolites.

Metabolites are intermediate or final products of metabolism in a biological sample[6], and the set of all low molecular mass metabolites (up to 1500 Da) present or altered in a biological system is called the metabolome.[3] In this way, the metabolome provides a direct link between the genome, the transcriptome, and the proteome. It can reveal which factors directly influence a given biological function.[7] Indeed, the metabolome is the closest one to the physiological state of an organism because it is the ultimate response to disease or environmental influences.

Metabolomics has been applied in different areas of knowledge, such as clinical analysis, disease, diagnosis, food (detection of adulteration of food), nutrition (diet), sports, environmental, forensic toxicology (monitoring the effects of drugs), or analysis of pathological organisms (parasites, bacteria, fungi), among others.[8]

Most of the human genome, transcriptome, and proteome are now known, and the data are available. Unfortunately, the same cannot be said of the human metabolome. In 2004, the Human Metabolome Project (HMP) was created by Wishart Research Group[9,10] (University of Alberta, Canada). This project was launched as part of an effort to identify and quantify all detectable metabolites (>1 μM) in the human body.[11] The project's main purpose is not only to identify and quantify but also to catalog and store all metabolites that can potentially be found in human tissues and biofluids to make the information available for all researchers through the Human Metabolome Database (www.hmdb.ca).

1.1.Metabolomics workflow

Metabolomics mainly aims to discover a set of metabolites that differentiate samples from two or more different groups. To develop metabolomic studies, the Metabolomics Society

(http://metabolomicssociety.org/) in 2005 recommended the following a specific workflow to achieve appropriate and reliable results (Figure 2).

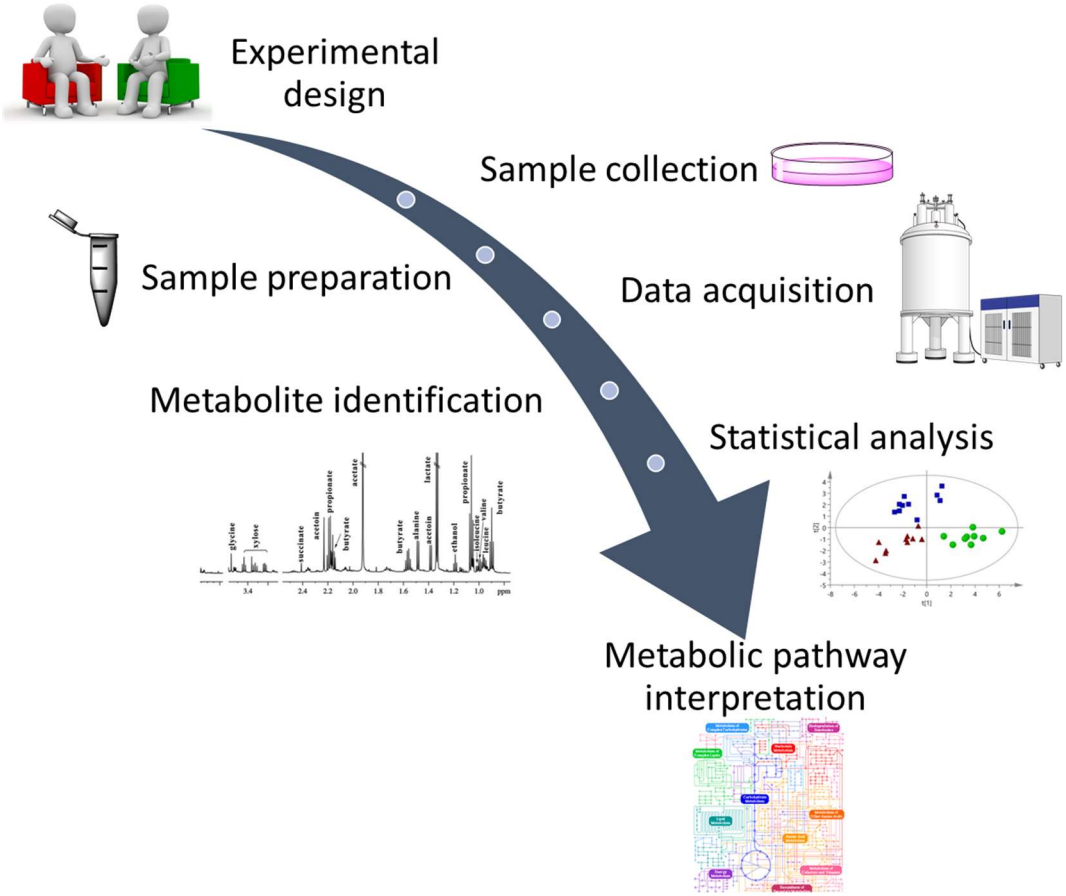

Figure 2. Workflow of a metabolomic study.

Metabolomics Standards Initiative (MSI) (http://www.metabolomics-msi.org/) defined a standardization in the procedure adopted in studies and publications of papers in metabolomics, intending to provide a clear description of the biological system studied and all the components of the study, as well as allowing the data to be effectively applied, shared and reused.

In the first step, a biological problem to be studied should be previously defined to choose the type of metabolomics approach that will be employed. Because it is from this choice that the steps of the experimental planning and analysis are defined since these decisions are interrelated, and the conduction of the whole metabolomics experiment will directly affect the final result.[12,13]

Two different approaches can be used in metabolomics. The most suitable one for the study's purpose depends on the information obtained from the metabolomic analysis.

Targeted metabolomics is the quantitative analysis of one or more pre-selected metabolites of a particular chemical class or associated with specific metabolic pathways. In contrast, untargeted metabolomics is based on the qualitative analysis of the most significant possible number of metabolites belonging to several chemical classes contained in the biological system under study. An untargeted approach represents an unbiased tool to investigate the relationship between interconnected metabolites from multiple pathways that provides an impartial overview of the metabolome.[14]
The following steps are the experimental planning and the sample preparation. The experimental planning involves choosing the type of sample (type of biological fluid, cells, tissue, etc.), the definition of the number of samples that will be evaluated in each group studied, and how these samples will be collected and stored before further manipulation. The sample collection is one of the most important and time-consuming steps due to the biological samples' complexity, heterogeneity, and wide concentration range of the metabolites present.[15]

Covering the entire metabolome of a biological organism is not an easy task since there is a large chemical diversity of metabolites with varying concentrations. Therefore, it is not possible to find a single analytical technique capable of doing so.[16,17]

Metabolomics has developed alongside pioneering analytical instrumentation. The acquisition of metabolic data is performed using powerful analytical tools, such as nuclear magnetic resonance (NMR)[18,19] and mass spectrometry (MS)[20], which provide structural information on various chemical classes, and are the most widely used analytical techniques in metabolomics studies.[21]

Mass spectrometry provides rapid determination and quantification with high sensitivity and selectivity of known and unknown molecules.[14] This information is obtained by measuring the mass-to-charge ratio (m/z). It can be used through direct infusion mass spectrometry (DIMS), which often makes the analysis difficult due to ionisation suppression problems, or it can also be used through matrix-assisted laser ionisation and desorption ionization mass spectrometry (MALDI-MS). The latter is widely applied mainly in the analysis of cellular compartments.[22,23] The constant problems of ionization suppression of the signals obtained in the analysis by DIMS due to complex matrices are circumvented by coupling it to separation analytical techniques such as gas chromatography (GC), high-performance liquid chromatography (HPLC), and capillary

electrophoresis (CE).[16] In addition, the retention time information, or migration of the previously separated metabolite, helps to confirm the identification of the metabolite using authentic analytical standards.

Nuclear magnetic resonance spectroscopy presents many advantages over MS.[24,25] It is more reproducible and does not destroy the sample after analysis, despite contaminating it with deuterated solvents, allowing the re-use of the same sample for consequent analysis. On the other hand, it has low sensitivity and selectivity, presenting spectral regions with overlapping signals, compromising the interpretation of results; furthermore, high-resolution equipment is required.[21,26,27] The most important nuclei in biomolecular NMR studies are ^{1}H, ^{13}C, ^{15}N, and ^{31}P. Among these nuclei, the proton is the most used nucleus in this field because the natural abundance is near 100%. NMR is a simple, robust, and comprehensive technique that requires little or no sample manipulation, and intact biological samples (solids and semi-solids) can be analysed[28,29] using high-resolution magic-angle-spinning NMR spectroscopy.[30]

The metabolomic process involves the simultaneous use of analytical chemistry techniques to generate metabolite profiles and data mining techniques to retrieve metabolically relevant information.[31]

The data generated by metabolomic analyses are abundant and complex; therefore, appropriate data handling tools should be employed in their processing to avoid errors and maintain the integrity of the biological variations inspected.[32] The metabolomics researchers employ chemometrics to extract the most relevant information from the data set using mathematical and statistical models through multivariate and univariate analysis methods.[33] In multivariate analyses, the classification and discrimination of entities or metabolites responsible for differentiating the groups of samples are performed by evaluating the set of the data matrix extracted in the previous work step. Unsupervised methods are applied, such as principal component analysis (PCA), and supervised methods like partial least squares discriminant analysis (PLS-DA). In univariate analyses, the study variables (entities or metabolites) are assessed separately and, unlike multivariate methods, the relationships between them are disregarded. Statistical tests such as ANOVA, Student's t-test, or Mann-Whitney U test are often used.[32]

The overall preferred software platform for metabolomics data analysis is MetaboAnalyst 5.0, which handles most of the common metabolomic data types from the commonly used metabolomics platforms (MS and NMR) for most metabolomics experiments (targeted, untargeted, quantitative). These include data processing, data normalization, statistical analysis, and high-level functional interpretation.[34]

The biological interpretation aims to find the answers to the questions raised at the beginning of the working flowchart or makes it possible to generate a new hypothesis. This interpretation is performed by correlating the altered metabolites with metabolic pathways, using libraries such as KEGG[35,] MetaboLights,[36] among others.

2. NMR metabolomics

NMR has played a considerable role in the development of the metabolomics of biology systems due not only to the advantages mentioned above but also because it allows the analysis of complex mixtures with the capacity to accurately quantify small endogenous metabolites produced by or used by the cells or tissues in culture.[37] It is a frequently used strategy to elucidate unknown compounds and metabolic changes in biological samples.

2.1. Principles of nuclear magnetic resonance spectroscopy

Nuclear magnetic resonance spectroscopy is one of the main tools used to characterise organic molecules and study inorganic and organometallic compounds. NMR is a spectroscopic technique since it uses electromagnetic radiation, in this case, radiofrequency, and is based on the behaviour of atomic nuclei under the effect of a magnetic field. It is an essential technique for research at the molecular level, allowing the obtention of structural and dynamic information for any state of matter.

The NMR spectroscopy technique can be used for research and development and also as a routine technique for qualitative (identification of unknown compounds or mixtures) and quantitative analysis (determining the purity of the sample or mixtures), such as food products and biological fluids, in a non-invasive and non-destructive way.

The usual NMR spectra are graphs of the probability of energy absorption or emission as a function of frequency (ν), where the position, intensity, and shape of the peaks matter.[38]

Nuclear magnetic resonance spectroscopy has grown rapidly due to continuous technological advances and the usefulness of this method in chemistry.

2.1.1. Magnetic properties of the nuclei

The nuclear magnetic resonance technique is based on the selective absorption of radio waves by samples placed in a magnetic field.

NMR spectroscopy, as a form of spectroscopy, is an example of the interaction of matter with electromagnetic radiation, but differently from other spectroscopic techniques, it requires a strong static magnetic field, in which energy is absorbed or emitted according to the Bohr frequency condition $\Delta E = h\nu$

As it is of common knowledge, the atom is formed by protons (positively charged), electrons (negatively charged), and neutrons (neutral particles). The rotation of the charged particles - charge rotation - generates a magnetic movement oriented along the spin axis, which means that these nuclei act as tiny magnetic bars. This is a property of the nucleus of an atom, which consists of what is known as *nuclear spin* (*I*).

In the absence of an external field, the orientation of the spins is random, with zero magnetization. In the presence of a magnetic field, the magnetic nuclei adopt one of the permitted orientations of different energy (Figure 3). When it presents a spin I "≠" 0, the nucleus can be considered with charged particles that revolve around its axis, rotating a nuclear magnetic. Nuclei ^{1}H, ^{13}C, ^{19}F, and ^{31}P have I=½, which allows being analysed using NMR. The most important nuclei for biomolecules have I = ½.

The signal from NMR spectroscopy thus results from the difference between the energy absorbed by the spins making a transition from the lower energy state to the higher energy state and the energy emitted by them simultaneously making a transition from the higher energy level to the lower energy level.[39] Since the ability to detect these small population differences is pronounced, NMR spectroscopy becomes a sensitive method, though not as sensitive as desired.

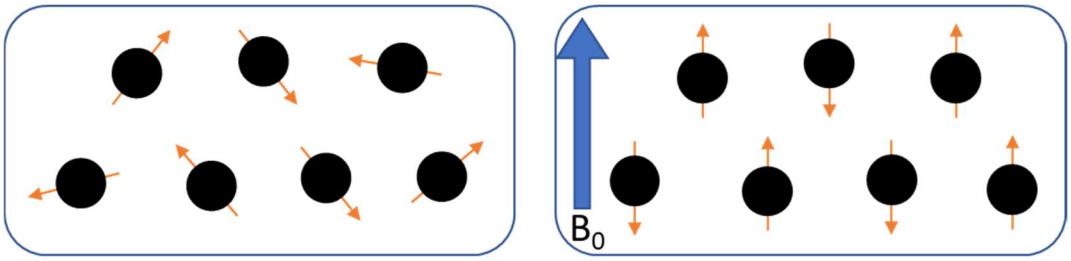

Figure 3. Left - Randomly oriented spins in the absence of a magnetic field. Right - Aligned spins in the presence of an applied magnetic field (B_0).

2.1.2. Chemical shift

The chemical shift is the relative difference in the resonance frequency of the core and the reference substance. The intensity of the magnetic field in which the absorption of radiation occurs depends on each proton's magnetic neighborhood. Chemical shifts (δ) are measured on a Hertz (Hz) scale but expressed in part per million (ppm) since they are very small concerning the intensity of the magnetic field.

The different species of protons have different electronic environments, thus determining the exact location of the spectrum in which the proton absorbs. The absorption of energy from protons in magnetic fields of different intensities or different frequencies of electromagnetic radiation causes them to appear at different positions in the NMR spectrum, this is because some nuclei are located in regions of a different density than others in the same molecule.[39]

2.1.3. Shielding effects

The shielding effect produces variations in the positions of the absorption signals in the NMR spectrum. This variation results in a change in the chemical shift of the protons. This parameter is used to determine the density and distribution of the electronic cloud in the surroundings of the nucleus, making possible the deduction of the structural characteristics of the molecule in the region of each of the protons. This information from an NMR spectrum is particularly relevant for determining the carbon backbone of a molecule.

The presence of functional groups in the neighbourhood nucleus area gives the changes in the shielding effect. For example, the presence of an electronegative atom removes

electrons from the observed nucleus, causing a deshielding effect by reducing the density of the electronic cloud (Figure 4).

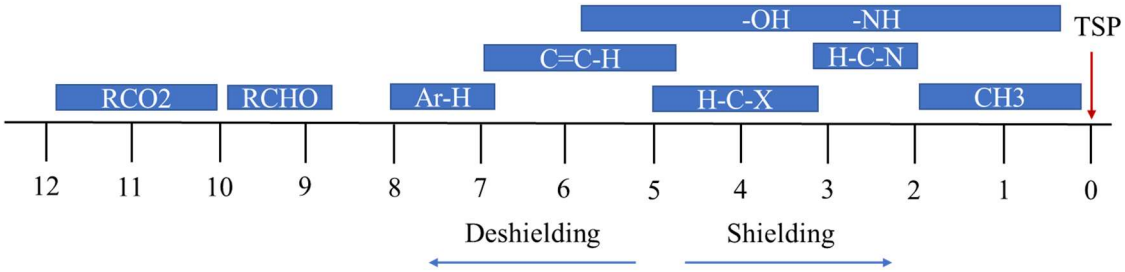

Figure 4. Shielding and deshielding effect for various functional groups in the proton chemical shift. Resonance at 0 ppm is the reference signal from TSP.

References compounds are used to look at the frequencies of the different nuclei of a sample independently from the magnetic field employed. Two of the compounds with maximum shielding are tetramethylsilane (TMS) for organic solvents and sodium salt of trimethylsilyl propionic acid (TSP) for aqueous solutions (Figure 5). The position of TMS and TSP in an NMR spectrum is always assigned a value of zero.

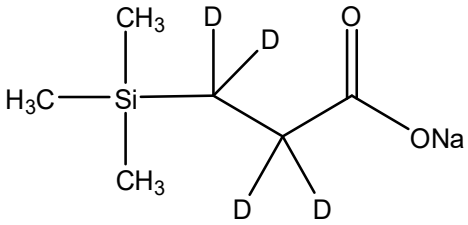

Figure 5. TSP structure.

2.1.4. Quantification

The magnitude or intensity of a signal is given by a vertical axis in the spectrum and is proportional to the molar concentration of the sample. Consequently, a small or diluted sample gives a weak signal, but higher concentrations double or triple that signal.

However, what is important in analysing a signal in the spectrum is not its height but the area implied by the signal. These areas, when accurately measured, are directly proportional to the number of each nucleus (^{1}H, ^{13}C, ^{15}N, etc.) present in a sample.[40]

Hence, from the areas of the two signals A_{sample} (A_s) and $A_{Standard}$(A_{std}), and the weight of the internal standard taken, the amount of the sample component present is calculated according to the expression:[41,42]

$$m_x = m_{std} \frac{MW_s}{MW_{std}} \frac{n_{std}}{n_s} \frac{A_s}{A_{std}}$$

Where:

m_x = mass of the sample

m_{std} = mass of the standard

N_{std} = the number of protons in the groups of the standard

N_s = the number of protons in the groups of the sample

MW_{std} = the molecular weights of the standard

MW_s = the molecular weights of the sample

The success of untargeted metabolomics depends on the relative quantification of the metabolites. The most used nucleus in metabolomics is ^{1}H because it is inherently quantitative. However, internal standards with known concentrations are typically employed to quantify the metabolites.[27] Particular attention must be paid to selecting the internal standard(s) utilized for a sample type or specific analysis.

3. NMR metabolomics in mammalian cells

NMR spectroscopy is a common technique in metabolic studies because it helps to identify and quantify most of the metabolites present in biofluids, cell extracts, and tissues without prior knowledge of the samples.

Metabolomics studies in mammalian cell cultures have many advantages over the techniques used to test *in vitro*, such as a high control over experimental variables, lower biological variability, less rigorous ethical issues, and lower costs. The concentrations of metabolites represent sensitive markers of both genetic and phenotypic changes.[43] Chemical shifts can provide crucial evidence for the identification of specific metabolites.[44]

To increase the statistical accuracy of the results, it is essential to include replicates in the experimental design. Biological replicates are cultures grown independently, and technical replicates can be different aliquots of cells from the same culture or multiple

measurements of the same extracts. The study should include all the steps applied to independent cell line cultures and at least three technical replicates[43]. However, growing sufficient cell numbers can be demanding in a study involving several experimental conditions and replicates of each condition. For instance, the number of cells needed for a common NMR acquisition is 3~5 million per sample.[45]

Quenching is the process of stopping cell metabolism, and it is a crucial step in metabolomics studies because the rapid turnover of many metabolites makes the sample no longer representative of the culture from was drawn. In standard cell culture, the traditional first method used is trypsin to detach cells from their growth surface, but the detachment of cells from the extracellular matrix alters their physiology, thus making it a method not ideal for metabolomic application.[46] There are several ways to stop enzymatic activity: cold methanol[46], cold isotonic saline solution[47], or liquid nitrogen. The latest is the one that shows the highest reproducibility and stability.[48]

The adequate quantification of the metabolites is influenced by the signals being well separated from the interfering signals, which allows a good integration. However, it is commonly challenging to quantify metabolites due to the presence of proteins in mammalian cells. These proteins produce a broad signal in the NMR spectrum, making an accurate quantitation challenging in such circumstances. To overcome this issue, a metabolite extraction must be performed to obtain more information from the sample. However, no universal method can extract the entire cellular content. The intracellular metabolites are extracted using a solvent system with variations in polarity, for example, perchloric acid, acetonitrile/water, methanol, and methanol/water.[47] In the NMR-based analysis of mammalian cells, a higher portion of intracellular metabolites are extracted using methanol/chloroform/water.[49,50] This dual-phase extraction mixture allows the characterization of polar and lipophilic compounds separately. However and despite the reported limitations, the application of metabolomics in mammalian cell culture has shown its value in numerous areas such as: cell culture monitoring[51,52], toxicology[53,54], and drug testing[55].

NMR metabolomics has already been achieved in different mammalian cells cultures: HepG2 (human liver carcinoma cells)[56], MDA-MB-231 (human breast adenocarcinoma)[57], MCF7 (human breast adenocarcinoma)[58], NIH 3T3 (mouse embryonic fibroblast cells)[59,60], L02 (human fetal hepatocyte line)[61], CHO (Chinese

hamster ovary)[52,62,63], RPE (human retinal pigmented epithelium)[64], amount others. However, to accomplish the metabolomic analysis in cell cultures, some considerations, such as the number of cells, detachment procedure, quenching, and metabolite extraction methods, need to be taken.

NMR has been used to study aspects of the cancer metabolome due to the capacity to understand the characteristic patterns of metabolites seen in tumours and how those patterns can be disturbed in experiments or during anticancer therapy. Understanding cancer metabolism involves applying analytical methods to evaluate metabolite levels in biological samples from healthy and diseased tissues.

3.1.Introduction to cancer

Cancer is a complex disease that involves numerous changes in the cell's physiology. Cancer cells grow and divide unregulated, forming malignant tumours.[65]

Hanahan and Weinberg[65,66] suggested ten essential changes in cell physiology (Figure 6) that may be underlying the growth of malignant cells. The following ten changes have been described as common to almost all cancers:

Self-sufficiency in signs of growth: Normal tissues carefully control the production and release of signals to promote cell growth and division. When these signals are absent, cell proliferation is stopped. However, cancer cells can sustain chronic proliferation without signs of external growth. Alternatively, cancer cells can send signals to stimulate normal stromal cells (organ support tissue) associated with the tumour, which provides cancer cells with various growth factors.

Insensitivity to growth suppressors: In addition to the ability to positively induce and sustain growth signals, cancer cells can bypass processes that negatively regulate cell proliferation. Many of these processes depend on the actions of tumour suppressor genes. Two very important tumour suppressors are RB (retinoblastoma-associated) and TP53 (tumour protein 53). The cancer cells select these tumour suppressors because they control important resources for cell proliferation, senescence, and apoptosis.

Apoptosis - Evasion of programmed cell death: Apoptosis is a coordinated process that initiates cell death following various cell injuries. Avoidance of apoptosis is a predictable

physiological response in tumour cells. In contrast to normal cells, acquired resistance to apoptosis is a characteristic of most types of cancer cells.

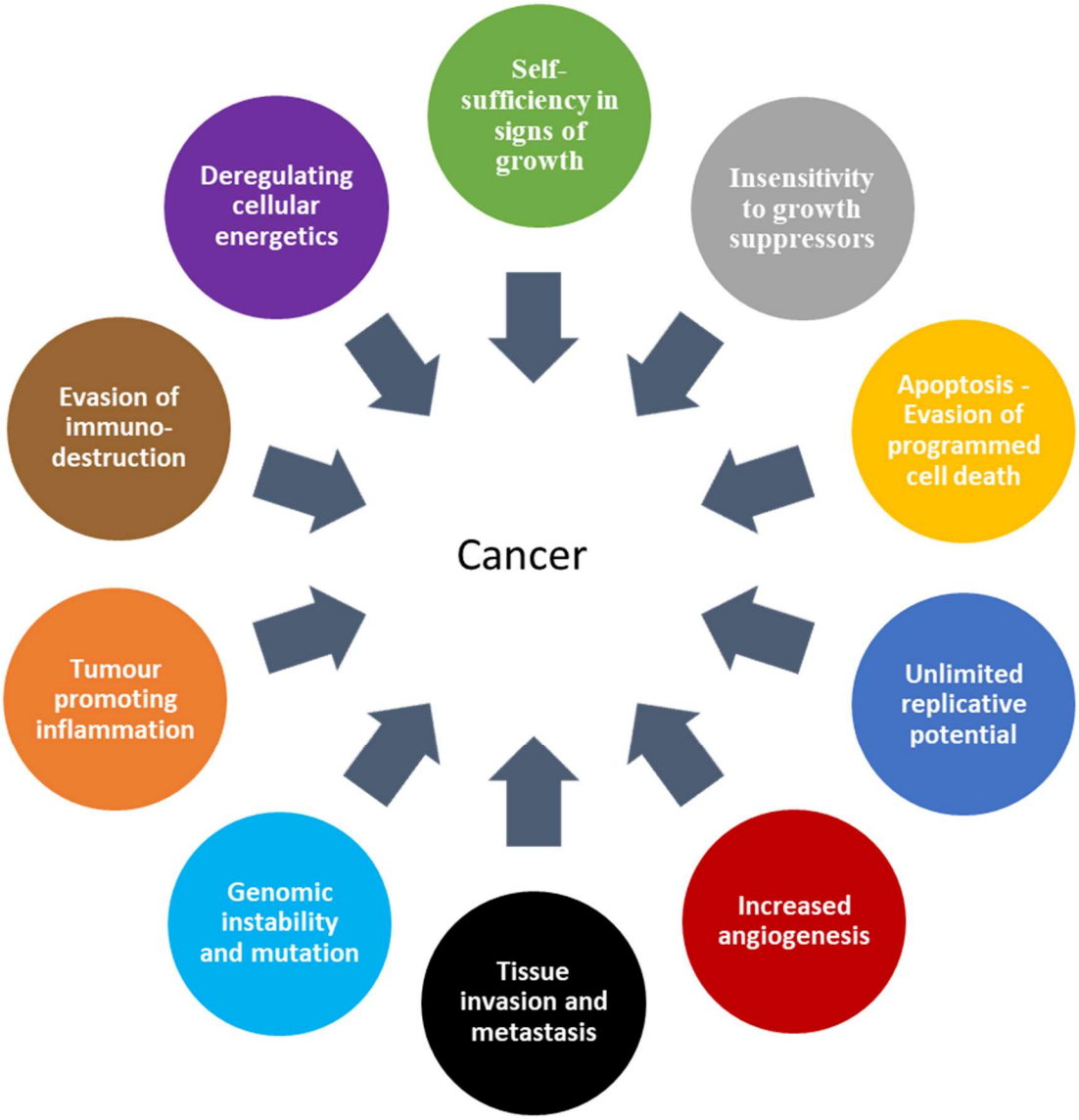

Figure 6. Hallmarks of cancer.

Unlimited replicative potential: Non-cancer cells, after a limited number of divisions, become senescent, while cancer cells have unlimited replicative potential that allows them to grow and divide indefinitely. This proliferation limit can be exceeded by inactivating the tumour suppressor genes previously described and has been associated with two distinct barriers: senescence, which is the gateway into a typically irreversible viable non-proliferative state, and apoptosis, which is the induction of cell death.

Increased angiogenesis (neovascularization): Angiogenesis involves neovascularization or the formation of new capillary vessels from existing blood vessels,

and it is related to the processes of tissue inflammation, wound healing, and tumorigenesis. Angiogenesis is necessary for most tumours to grow since it provides them with essential nutrients for energy and removes toxic waste products such as lactic acid and ammonia.

Tissue invasion and metastasis: During the growth of most types of cancer, cancer cells separate from the primary tumour, enter the bloodstream and the lymphatic system, evade the attack of the immune system, invading adjacent tissues by penetration of tumour cells into neighbouring tissues. This sequence of steps is called metastasis. Metastasis is the general term used to describe the spread of cancer cells from the primary tumour to surrounding tissues and even distant organs, being one of the primary causes of cancer mortality. Both processes are closely allied on a mechanistic level because they use similar operational strategies.

Genomic instability and mutation: The development of genomic instability in cancer cells generates random mutations and consequently allows the manifestation of the physiological changes that lead to cancer.

Tumour promoting inflammation: The inflammatory state of cancer cells is stimulated by the immune system cells, which promotes tumour progression by blocking apoptosis and exaggerating the production of inflammatory substances such as cytokines and prostaglandins.

Evasion of immunodestruction: The immune system plays an essential role in identifying, resisting, and eliminating neoplasms. Cells and tissues are constantly monitored by an immune system that is always on alert. This immune surveillance recognizes the antigens produced by cancer cells and destroys abnormal cells using T cells. This sequence of processes constitutes an effective barrier to tumorigenesis and tumour progression. Solid tumours appear to have eluded the immune system by developing immune tolerance against tumour antigens. With this developed capacity, cancer cells evade their detection and eradication by the immune system.

Deregulating cellular energetics: The essence of neoplasm is represented by the chronic and often uncontrolled proliferation of cells and the corresponding adjustments of energy metabolism to boost growth and cell division. Energy metabolism consists of a set of

biochemical transformations that take place in the cell to obtain energy. One of the ways to obtain energy is glycolysis.

In normal cells, glycolysis is a sequence of enzymatic reactions that occur in the cytoplasm, through which the glucose molecule, with six carbon atoms, is transformed and cleaved, giving rise to two pyruvate molecules, with three carbons and a reduced amount of ATP. The pyruvate produced can be catabolized aerobically by pyruvate dehydrogenase and enter the citric acid cycle generating electron-carrying molecules, such as nicotinamide and reduced adenine (NADH) dinucleotide. These molecules allow the production of large amounts of ATP at the level of the electron's transport chain and oxidative phosphorylation. Thus, glucose is completely oxidized to produce CO_2 and H_2O (Figure 7).

However, glycolysis can also be performed anaerobically (without oxygen). In these cases, the final product of glycolysis is no longer pyruvate and becomes a smaller molecule, lactate. Anaerobic glycolysis produces two molecules of lactic acid for each molecule of glucose. The lactic acid produced is transported out of the cell by monocarboxylate transporters (MCTs). These transporters are crucial for intracellular pH regulation since they keep the efflux of lactic acid from the cells produced, avoiding the decrease of the pH of cytosol, which can lead to cell apoptosis.[67] This high level of lactate production is a phenomenon generally observed in solid tumour cells under hypoxia conditions.[68]

Unlike normal cells, which produce ATP through oxidative phosphorylation, tumour cells show a metabolic shift, the so-called "Warburg effect", which produces energy through aerobic glycolysis.[69] This effect was proposed by Otto Warburg after observing that most tumour cells produce ATP by converting an excessive amount of glucose into lactate, even in the presence of oxygen.[70]

The reprogramming of the energy metabolism of tumour cells is contradictory because when opting for anaerobic glycolysis, the cells choose a less efficient way of producing ATP molecules. But despite being less advantageous in terms of energy, the increase in lactate production leads to a decrease in the pH of the extracellular medium, which is thought to confer proliferative advantages to the tumour.[71]

The increase in glycolysis in cancer cells facilitates those glycolytic intermediates that are used to feed cellular biosynthetic pathways, including those that generate macromolecules, such as nucleosides and proteins, necessary for the constitution of new cells. Some tumours have two subpopulations of cancer cells that differ in their energy generation pathways. One subpopulation is dependent on glucose consumption, and the produced lactate is used for export, while the cells of the second subpopulation import the lactate produced by neighbouring cells, which is used as an energy source.[66]

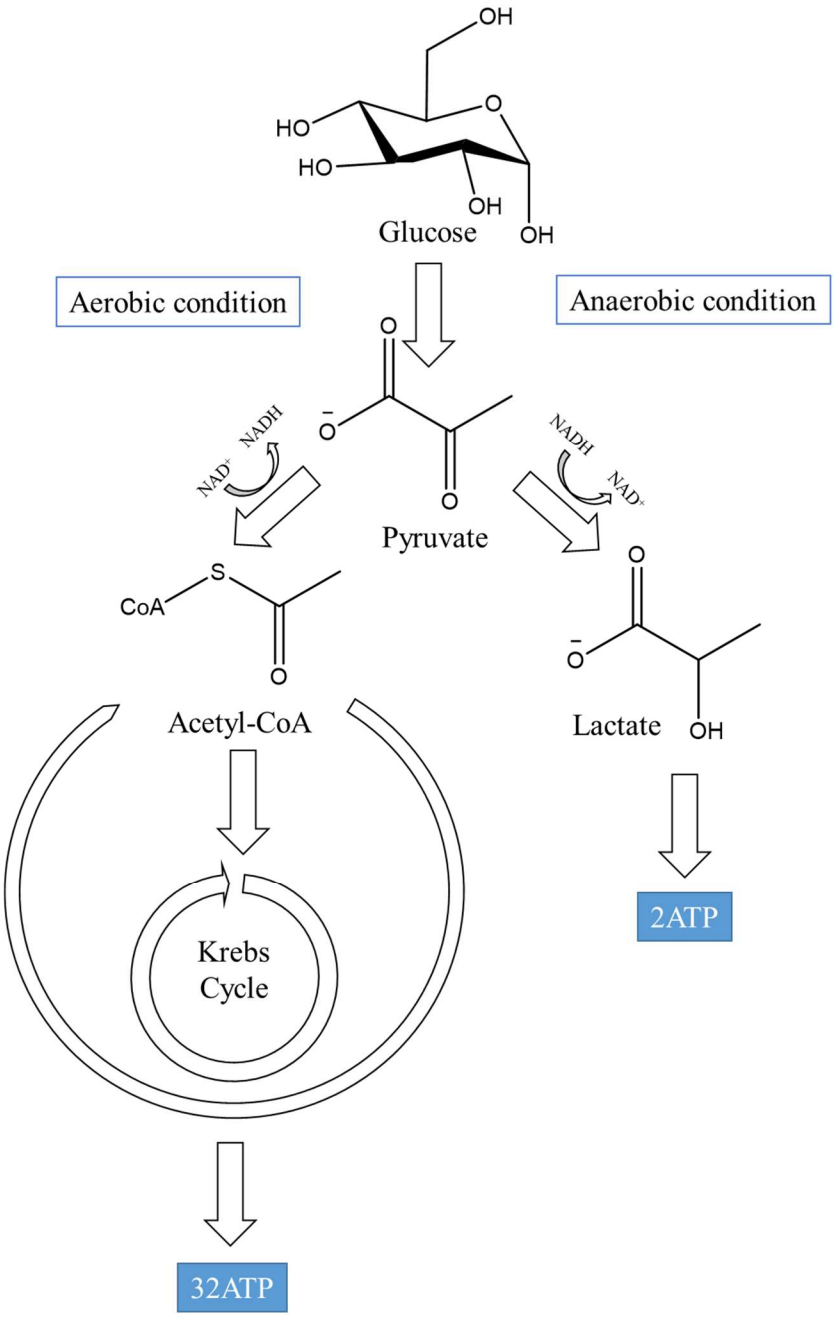

Figure 7. Glycolysis aerobic vs. anaerobic glycolysis (adapted[72]).

3.1.1. *Monocarboxylate transporters*

Monocarboxylate transporters (MCTs) are molecules belonging to the SLC16 gene family, currently composed of 14 members. MCT1, MCT2, MCT3, and MCT4 isoforms are proton symporters, which mediate the transport of molecules with a carboxylic group, such as pyruvate, lactate, and ketone bodies, through membranes with proton co-transport.[67,73]

MCTs are proton-linked plasma membrane reversible symporters[67] that consist of 12 transmembrane domains (TMDs) with a large loop between domains 6 and 7, with their N and C terminals inside the cell, with most of the regions belonging to the conserved TMDs, with the most variable regions corresponding loop and terminal C (Figure 8).[74]

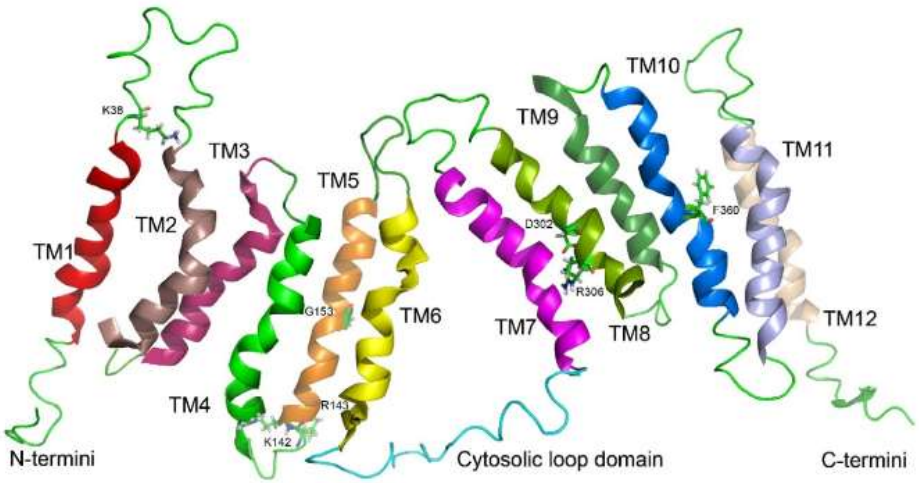

Figure 8. Proposed structure of MTC's.[75]

MCTs have the function of transporting lactic acid both to the extracellular medium and mainly to the cytosol, where lactic acid is necessary for gluconeogenesis. All cells export lactic acid under hypoxic conditions and use any expressed MCT isoform. In most tissues that depend on aerobic glycolysis for their energy metabolism, under normoxic conditions, the efflux of lactic acid is carried out by MCT4.[76]

In general, MCTs contribute to the maintenance of the cytosol pH and have been proven to be involved in cancer, facilitating the survival of glycolytic tumours.[77] MCT1 and MCT4 are highly associated with an increase in tumour aggressiveness.[78] MCT1 can be found in all tissues but sometimes only in certain tissue sites.[67] MCT4, although present in most tissues, is strongly associated with tissues with a high rate of glycolysis, such as

skeletal muscle and tumour tissues, where it is involved in the removal of lactic acid produced from glycolysis.[79]

The inhibition of MCTs by small-molecule inhibitors leads to lactate influx/efflux impairment. Both impairments can further induce apoptosis by acidification or inducing glucose deprivation of the cytosol in cancer cells, respectively[80,81]. Thus, the inhibition of MCTs, especially MCT1–4, could be a powerful approach to killing or greatly reducing cancer cells' growth (Figure 9).

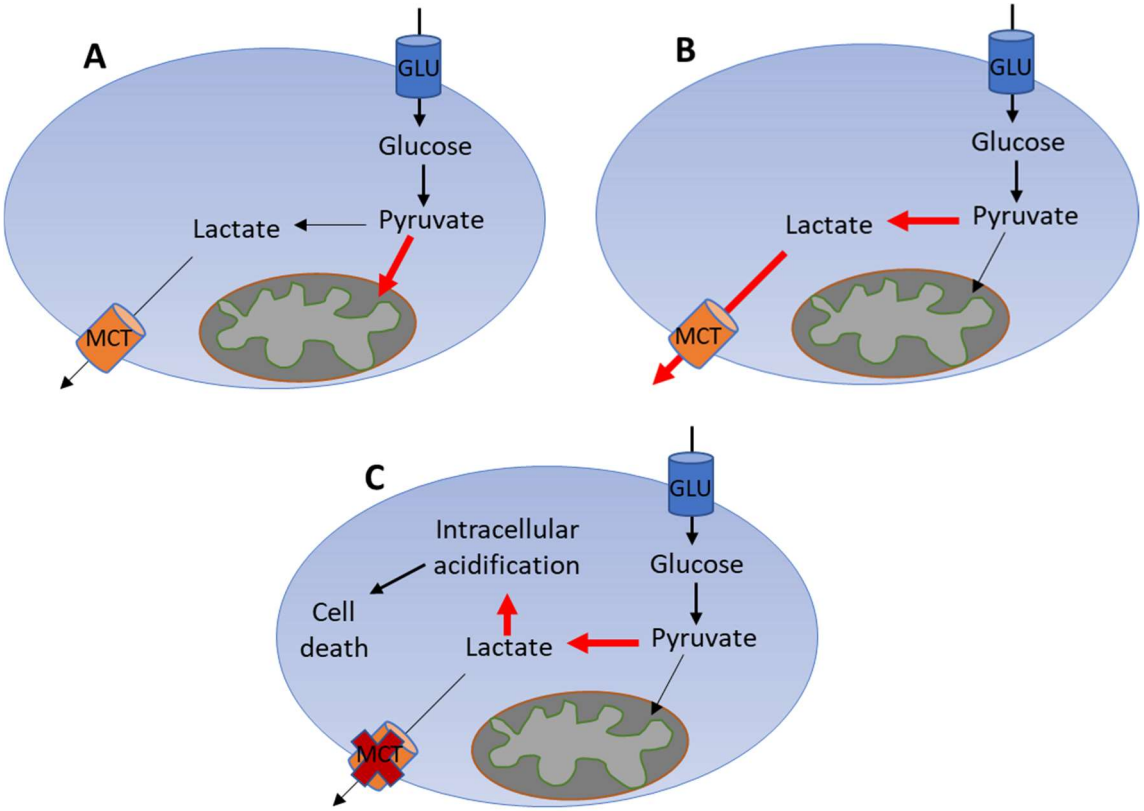

*Figure 9. **A**) role of MTC´s in metabolism in normal cells. **B**) in cancer cells. **C**) cancer cells after blocking the MCT.*

MCT´s can represent an attractive target for cancer therapy because they would induce apoptosis due to cellular acidosis and reduce tumour angiogenesis, invasion, and metastasis.

To date, some inhibitors of MCT have been reported with promising activity in experimental cancer models, including AZD3965 for MCT1 (clinical phase I) and AZD0095 for MCT4.[75] Blockade of MCT1 has profound effects on human cancer cell metabolism that extend beyond intracellular lactate accumulation, effects were observed

on mitochondrial activity by increased oxidative metabolism, improved bioenergetics, and decreased phosphocholine levels.[82]

One of the important discoveries in the MCTs field was the α-cyano-4-hydroxycinnamate acid (ACCA) inhibitor. The ACCA is a non-selective inhibitor of several MCT with a K_i (inhibitor constant: the concentration required to produce half-maximum inhibition) against MCT1 of 166mM, MCT2 of 24mM, and MCT4 of 994mM (Figure 10).[83]

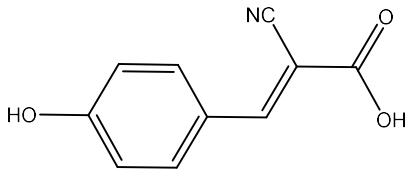

Figure 10. Molecular structure of α-cyano-4-hydroxycinnamic acid.

ACCA slowed down tumour growth and potentiated radiotherapy's effects on tumors expressing MCT1 in mice by reflecting an acutely improved tumour oxygenation, where hypoxic tumour cells will die of "starvation" due to increased glycolysis in well-oxygenated cells.[80]

In the work of Calori et al.[84] ACCA was used as a vector of liposomes for targeting cancer cells that overexpress MCT-1. They also demonstrate that ACCA decreases oxidative stress induced by reactive oxygen species generated *in situ* in a clinical modality known as Photodynamic Therapy. Sattler et al.[85] developed a fluorinated analog of ACCA as a radiolabelled MCT1/4 inhibitor to be used for imaging cancer metabolism with PET. Jonnalagadda et al.[86] developed potential anticancer agents based on the α-cyanocinnamic acid structural template, and the *in vitro* results confirm that the compounds disrupt glycolysis and oxidative phosphorylation (OxPhos) efficiently in MCT1 and MCT4.

4. Metabolomics for nanoparticles

Nanotechnology has many crucial advances in developing biomedical applications like targeted drug and gene delivery, imaging, biological sensors, and especially cancer treatment, where it provides greater therapeutic efficiency than isolated drugs.[87]

This rapid increase in manufacturing and use has raised questions about the novel physicochemical properties of nanomaterials and their potential toxicity.[88]

In 2010, Oberdörster[89] defined nanotoxicology as "*the study of the adverse effects of engineered nanomaterials on living organisms and the ecosystems, including the prevention and amelioration of such adverse effects*."

Evidence indicates that nanomaterials generate reactive oxygen species (ROS), resulting in inflammation, apoptosis, necrosis, fibrosis, hypertrophy, metaplasia, and carcinogenesis. This oxidative stress is generally difficult to measure by conventional methods.[88]

Several methods are accessible for nanoparticle toxicity assessment in biofluids, cells, tissues, and organisms. They can be categorized as *in vitro* (proliferation assays, apoptosis assay, necrosis assay, oxidative stress assay, endotoxin assay, inflammation assay) and *in vivo* (effects on organ systems, mechanistic studies, and LD_{50}) assays.[90,91]

These traditional approaches to evaluate toxicity have some weaknesses, for example, whether studying nanoparticles, for example, external factors (media pH, additives to the cell culture) and limited ability to detect minuscule variations within a cell can result in unreliable results.

Omics technologies have been used in nanotoxicity investigations using high-throughput screening information instead of focusing on a single molecule. Since there are limitations to traditional toxicological methods, omics approaches provide a more comprehensive understanding of the biological events triggered by NPs on cellular models.[92] Evaluation of metabolic changes induced by nanomaterials on cellular models through NMR or MS-based metabolomics is increasing due to its usefulness for revealing unexpected biological effects and assisting the understanding of the mechanisms of nanomaterials toxicity.[93]

The enhanced sensitivity of metabolomics methods over conventional histopathology and serum chemistry analysis was demonstrated by Lu et al.,[94,95] that noted changes in metabolites involved in energy, amino acid, lipid, and nucleotide metabolism. The significantly altered metabolites suggested impairment of the Krebs cycle and were also consistent with the manifestation of oxidative stress.

Metabolic profiling requires exploring alterations in the concentrations of endogenous metabolites within biofluids or tissues after a perturbation. These changes can be

measured regarding the perturbed molecular pathways and clarify the mechanism following exposure to nanomaterials.

The study of metabolic responses of cultured mammalian cells to nanomaterials has only a decade, but the number of scientific papers reporting metabolomics applications in nanotoxicology has continuously grown over the last years. The nanoparticles investigated through metabolomics included Ag[56], Au[96,97], Cu[98], ZnO[99,100], and graphene[101], among others.

One of the nanomaterials most used for biomedical applications are dendrimers. Nevertheless, to the best of our knowledge, dendrimers have been scarcely studied in terms of their metabolomic profile. Only very recently, some authors, such as Lykogianni et al.[102] and Elmi et al.[103], started to use the metabolomic approach to study the metabolic profile of the native dendrimer before their applications.

4.1.Dendrimers

Dendrimers, also called in the early days 'cascade molecules', are polymeric macromolecules with a tree-like structure, displaying a highly branched, well-defined arrangement that assumes a nanoscale size.[104–106]

In 1978, Vögtle[107] and his collaborators published an innovative "cascade" methodology that allowed the synthesis of dendritic architecture, and from that moment on, it was possible to synthesise these molecules more efficiently and study them for future applications.

The term dendrimer has Greek origins from the word "*dendron*", meaning "tree/ramification" due to its resemblance to a tree, and the word "*meros*", meaning "part".

The general structure of the dendrimer has three fundamental components (Figure 11):[104]

a) Central core with two or more identical reactive groups
b) Branches that are composed of repeating units (generations), which diverge radially from the central core
c) Terminal functional groups located at the surfaces influence the properties of dendrimers.[108] These groups may have a negative, positive or neutral charge.

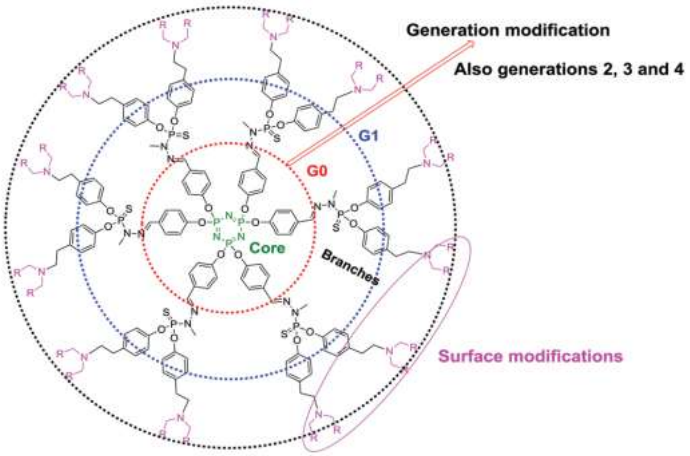

Figure 11. 2D chemical structure of a dendrimer of generation 1 as a representative example of a phosphorus dendrimer skeleton.[109]

Both the number of generations of the dendrimer and the chemical composition of its structural components are factors that will influence its size, shape, and reactivity. Since it is possible to control these same factors during the synthesis of dendrimers, they are considered one of the most versatile and customizable nanoparticulate forms.[110]

The dendrimer size is relevant in the three-dimensional form, with low generation dendrimers generally presenting a more open structure, while those with a high generation become denser and have a more globular structure.[111] As the size of the dendrimer increases one generation, its molecular weight doubles in size.[112] Furthermore, the size of dendrimers is very similar to that of biological structures existing in humans, thus allowing for a unique interaction with biological systems at a molecular level.[113]

Regarding their properties, dendrimers present a three-dimensional architecture that makes them convenient for the release of drugs at a specific target site due to their unique characteristics, such as their high functionalisation capacity and low polydispersity. The fact that they have an easily modifiable surface is also a relevant property of these, making them polyvalent and thus allowing the conjugation of the dendrimer with both ligands and drugs.[111]

Dendrimers increase the solubility and bioavailability of drugs that are not very water-soluble due to the capacity to possess a hydrophobic central nucleus and a hydrophilic surface. The solubility conferred by the dendrimer is affected by several factors, such as the number of generations, pH, core, temperature, polymer architecture, and functional

groups. The drugs can remain in the empty intramolecular cavity or be conjugated to the surface groups of the dendrimer for subsequent controlled release.[104,106]

Several classes of dendrimers have been synthesized, with significant changes among them regarding the elements that integrate the core, the branching units, and the surface groups.[114] Generally, the synthesis of dendrimers involves repeating a sequence of reactions composed of two steps, which correspond to the generation growth and activation steps. To obtain dendrimers without structural defects and high yields, these reactions must be complete. These molecules can be synthesised using mainly two distinct strategies: divergent synthesis, developed by Tomalia et al. and Newkome et al., or convergent synthesis, developed by Hawker and Fréchet.[115] The main differences between both strategies are restricted to the direction of the synthesis process and generation limits.

Divergent synthesis: The divergent synthesis is based on the successive addition of repeated monomers that proceed radially outwards, starting from the central core. This determines the number of branching points.[116] Using amine core with methyl acrylate, the synthesis is initiated by adding three arms using the Michael addition reaction; in a second step, an ethylenediamine molecule is reacted on these formed three arms through an amidation reaction (Figure 12).[117] As more monomers are added, an increase in the molecular weight and number of groups present on the dendrimer surface is observed.[105] The purity is compromised for getting a higher yield. Lesser purity in the divergent synthesis of dendrimers is basically due to missing repeat units, intramolecular and intermolecular cyclization, ester hydrolysis, and retro Michael reaction.[117]

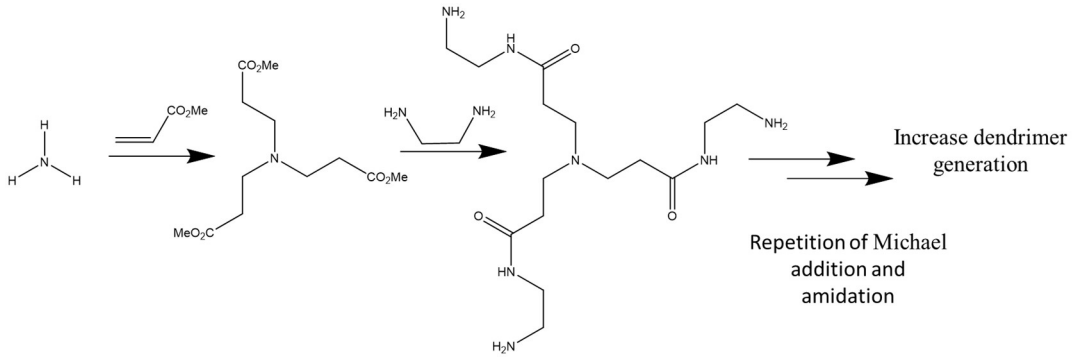

Figure 12. Divergent approach for synthesising dendrimers (adapted [116]).

Convergent synthesis: In contrast to divergent synthesis, dendrimers can also be synthesized starting from the surface according to a convergent approach. In this case,

the growth of the molecule starts from the ends of the chain, synthesizing first the various branching points that will constitute the dendrimers, and, finally, these branching points are joined to a central core (Figure 13).[105,116] Convergent approach overcomes the purity and structural defect issues of divergent synthesis, but the yield is sacrificed.[117]

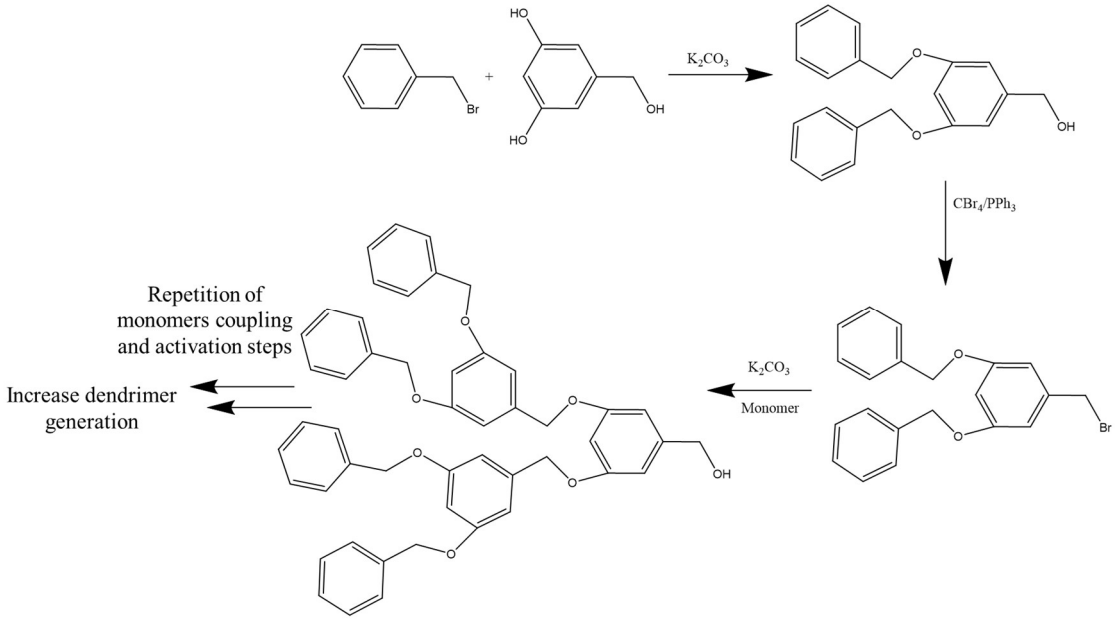

Figure 13. Convergent approach for synthesizing dendrimers(adapted [116]).

Comparing both methods, it is verified that the convergent approach allows greater control of the final dendritic architecture.[118] Both synthesis approaches involve stepwise processes that are tedious and time-consuming. In addition to the time-consuming production, these synthesis models are costly. However, the added value conferred by dendrimers' structural features and properties justifies the high cost of their production.[116]

Many types of dendrimers have been synthesised in the last decades: polypropylene imine[119], glycodendrimers[120], metallodendrimers[121,122], triazine based[123], phosphorous dendrimers[124,125], poly(alkylideneamine)[126] and PAMAM (Polyamidoamine).[127]

The dendrimers most described in the literature are the PAMAM because they were the first to be synthesised, characterised, and marketed.[111] PAMAM dendrimers are branched macromolecules that grow, in this case, from a central molecule (divergent synthesis), ethylenediamine (EDA), a diamine. This dendrimer has tertiary amines in the branches and primary amines in the periphery. The increase of one dendrimer generation leads to an exponential increase in primary amines and about 10Å in diameter (Figure 14).

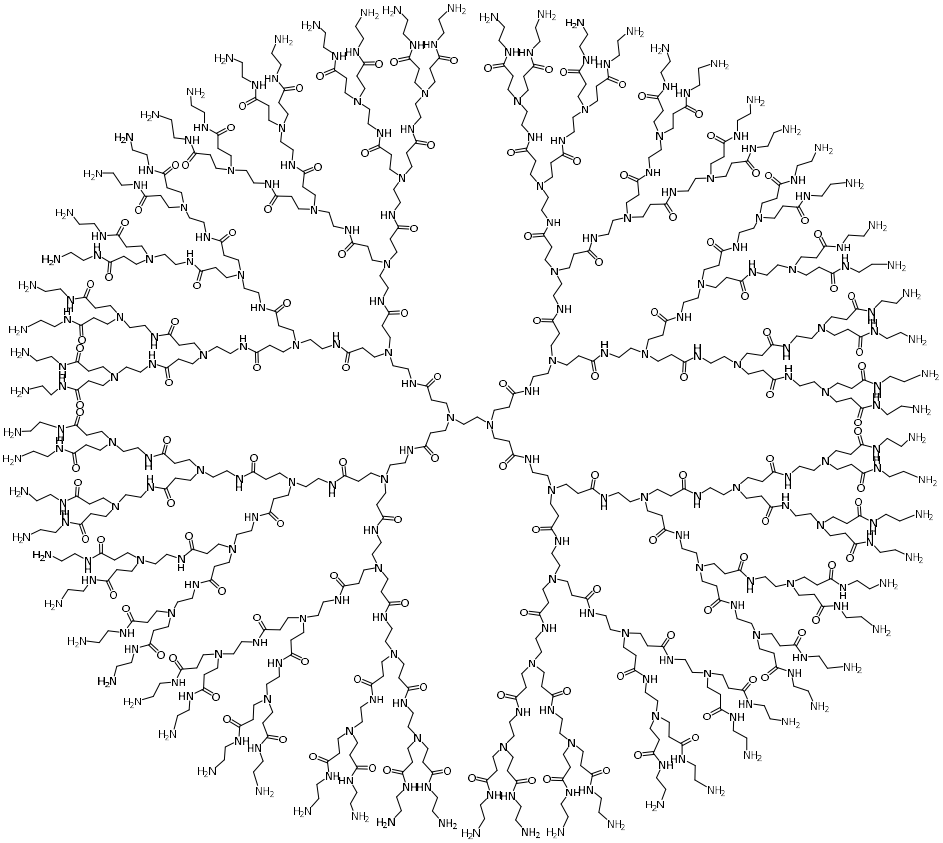

Figure 14. PAMAM (NH_2) generation four (G4) (adapted[128]).

The stability of PAMAM dendrimers is affected by pH since it influences protonation and, consequently, its solubility[129]. PAMAM dendrimers are biocompatible, although they may present some cytotoxicity,[104,130–133] which depends on the number of generations, concentration, time of exposure to cells, and largely due to the presence of positive charges on the surface conferred by the primary amines protonated at physiological pH. This positive charge leads to an interaction between dendrimer and the negatively charged cell membranes and consequently to the formation of nanopores in the cell membrane, its damage, subsequent leakage of cellular content, and eventually cell death.[133]

Mukherjee et al.[130] suggest that the toxic pathway of the cationic PAMAM dendrimers comes from the localization in the mitochondria leading to ROS production and resulting in oxidative stress, apoptosis, and DNA damage.

One strategy to decrease the toxicity of dendrimers is based on the alteration of the surface groups to protect cationic groups, such as amine groups, with neutral or anionic units,

thus decreasing the cytotoxicity inherent to them by preventing electrostatic interactions between the dendrimers and the cell membrane.

Dendrimer functionalization is the process of integrating multiple active sites in dendrimers to build macromolecules with multifunctional architecture.[115] They have been subject to modifications with amino acids[134], hydrophobic chains[135], cholesterol[136], PEG[137,138], cyclodextrins[139], antibodies[140], sugars[141,142], lipids[143], among others.

Dendrimers have been conjugated to molecules that improve their cytotoxicity and other properties such as transfection efficiency, internalization, targeting the molecules to the target cells, etc., whatever conditions, *in vitro* or *in vivo.*[144]

This functionalization makes dendrimers one of the best candidates for targeted drug delivery. The positive charge of cationic dendrimers facilitates the interaction with cell membranes, and the targeted moieties can be used to deliver the drug to the desired location. Dendrimers can also control drug delivery systems, ensuring the release of the drug for a prolonged time.[145] This application leads to better efficiency of the drugs with a narrow therapeutic index, as is the case with doxorubicin, which is often delivered in suboptimal dosages to avoid side effects in the patient.[146]

The dendrimer's core, interior, and surface may be manipulated to produce a large range of new emerging properties that suit various applications (Figure 15), like environment[147], sensors[148], catalyst[149], biomedical[111,127,150–152], nanotechnology[153,154] and industrial processes[155,156]. Currently,there are at least 26 dendrimers in clinical trials[157]. One good example is a dendrimer based on poly-L-Lysine used against sexually transmitted diseases developed by Starpharma company called VivaGel®[158].

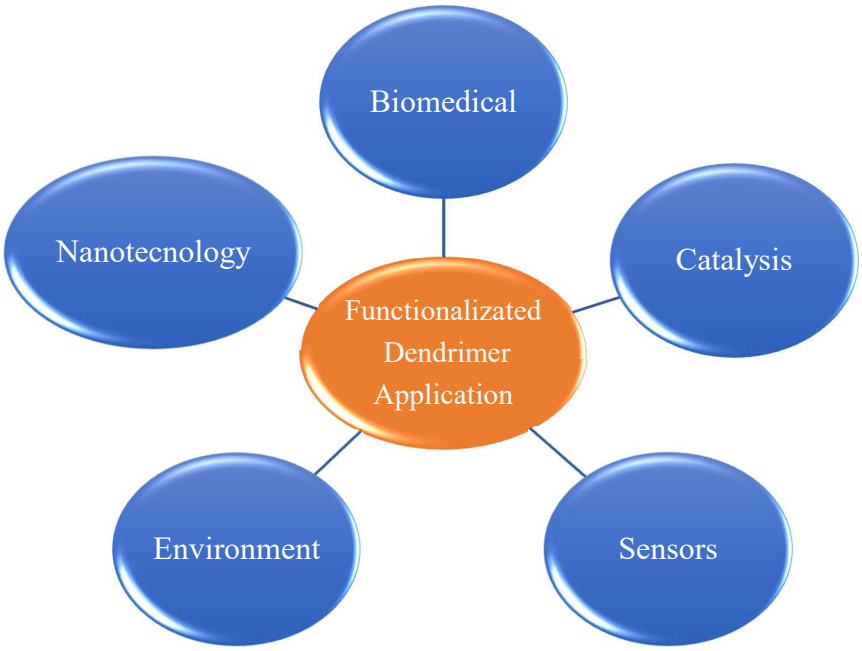

Figure 15. Applications of functionalized dendrimers.

Chapter 2- Materials and methods

1. Reagents and equipment

Ethylenediamine core amine-terminated G4 PAMAM dendrimers ($G4NH_2$) in methanol were purchased from Dendritech (Midland, MI, USA), and before use, they were purified using a dialysis membrane with a molecular cut-off of 10000 Daltons against distilled water. α-Cyano-4-hydroxycinnamic acid ≥98% (ACCA) and N-hydroxysuccinimide ≥98% (NHS) were obtained from Sigma-Aldrich. 1-(3-dimethylaminopropyl)-3-ethylcarbodiimide hydrochloride >98% (EDC-HCl) was bought from TCI Chemicals. Doxorubicin hydrochloride analytical grade (DOX) was purchased from Ourchem (Sinopharm Chemical Reagent Co., Ltd, Shanghai, China). Methanol 99,99% and chloroform 99,98% were bought from Fisher Chemical. Dialysis membranes were purchased from SpectrumLabs. 3-(Trimethylsilyl)propionic-2,2,3,3-d_4 acid sodium salt (TSP) and deuterium oxide (D_2O) were supplied by Acros Organics (Geel, Belgium), and dimethylsulfoxide-d_6 99,80% by VWR (Pennsylvania, USA). Potassium dihydrogen phosphate (KH_2PO_4), sodium azide, and potassium deuteroxide solution (KOD) were purchased from Panreac (Barcelona, Spain) and Sigma Aldrich (St. Louis, Missouri,, USA). All reagents were used as received unless otherwise reported.

NMR spectral acquisition was performed using a Bruker Advance II Plus NMR spectrometer equipped with a 400 MHz magnet UltraShield™ 400 Plus at 25 ºC. Attenuated total reflection Fourier Transform Infrared (ATR-FTIR) spectroscopy was carried out with a Perkin Elmer Spectrum Two™ spectrometer (Perkin Elmer, Waltham, MA, USA). Zeta potential was measured by Zetasizer Nano ZS (Malvern Instruments, UK) at 25 ºC with disposable folded capillary cells (DTS1060C, Malvern). Matrix-assisted laser desorption/ionization time-of-flight mass spectrometry (MALDI-TOF MS) was done at an Autoflex maX device (Bruker Daltonics, Bremen, Germany) equipped with the Smartbeam-II™ laser emitting at 355 nm using as a matrix 2,5-dihydroxybenzoic acid (DHB). (100 mg/mL, can:0.1% TFA, 2:1). Ultraviolet-Visible spectroscopy was obtained using a quartz cuvette, and the absorbance was measured using a Perkin Elmer Lambda 25 spectrophotometer. The acquisitions were made with the Perkin Elmer UV WinLab Software (version 5.2.0.0646). Photoluminescence Spectroscopy was obtained using a quartz cuvette placed into a Perkin Elmer LS 55 Fluorescence Spectrometer (Perkin Elmer FL WinLab Software, version 4.00.03). Elemental Analysis was performed at the Laboratorio de Análisis Químico Elemental, Servicio Interdepartamental de

Investigación (SIdI), Madrid University, Madrid (Spain) using an Elementary Chemical Analyzer LECO CHNS-932.

Cell viability, *in vitro* release of DOX, hemolytic toxicity, and quantification of glucose and lactate were measured by a Perkin Elmer Victor 3 Multilabel Reader (Perkin Elmer, Waltham, Massachusetts, USA). The acquisitions were made with the Wallac 1420 Workstation Software (version 3.00.0.53)

2. Cell culture grown

NIH 3T3 cells (mouse embryonic fibroblast) and CAL-72 cells (human bone cancer cell line) were cultured in DMEM (Dulbecco's modified Eagle's medium), CACO-2 (human colorectal adenocarcinoma) in MEM (Minimum Essential Media) supplemented with 1% NEEA and A2780 cells (human ovarian carcinoma) in RPMI (Roswell Park Memorial Institute-1640) supplemented with 2mM glutamine. Culture mediums were purchased by Life Technologies (Thermo Fisher Scientific, Califórnia, EUA) and supplemented with 10% heat-inactivated fetal bovine serum (Gibco^{TM} Life Technologies, Thermo Fisher Scientific, Califórnia, EUA) and 1% antibiotic–antimycotic 100X solution (containing penicillin, streptomycin and amphotericin B (Gibco^{TM} Thermo Fisher Scientific, Califórnia, EUA). Cells were grown in a humidified incubator (Nuaire NU-5500E DH Air Jacketed Co2 Incubator, Plymouth, Minnesota, USA) at 37ºC and 5% CO_2. The subconfluent cells were harvested using a trypsin–ethylenediaminetetraacetic acid solution (Sigma-Aldrich).

2.1. Cellular viability

The antiproliferative activity was determined by placing the cancer cell lines on 96-well plates at a different density for each cell line: 5000 cells (NIH 3T3 and CAL-72) per well and 10000 cells (A2780, CACO-2).

Cells were seeded in 100µL of culture medium and were allowed to adhere overnight. Then, after media removal, they were treated with the compounds under evaluation at different concentrations. For this, a stock solution of each compound was prepared in distilled water/DMSO, and serial dilutions with distilled water/DMSO were made to attain the desired concentrations. In the end, 10µL of the different solutions were added

to each well together with 990µL of cell culture medium. The respective controls were performed with an adequate 1% (v/v) of distilled water/DMSO. The effect of the compounds was assessed indirectly by resazurin reduction assay. After cell incubation with compounds for 24 h, the culture medium was removed and replaced with a fresh medium containing resazurin at a concentration of 0.1mg/mL (Sigma-Aldrich) for 4 h. Afterwards, aliquots of the cell supernatant were transferred to 96-well opaque plates, and the resorufin fluorescence (λ_{ex} = 530 nm, λ_{em} 626 = 590 nm) was measured using a microplate reader.

The percentage (%) of cell viability was determined considering the value obtained by the negative control as 100%. Cytotoxicity was expressed as the IC_{50} value (the value that inhibits cell growth at 50%), and the IC_{25} was calculated from at least 3 independent experiments (n = 3) by nonlinear regression.

3. Metabolomics experiments

3.1. Extraction of metabolites

The methodology used for the global assessment of the cells metabolome was based on the metabolomics workflow recommended by the Metabolomics Standards Initiative and several published protocols .[52,159]

Four replicates of the dendrimer-treated and control group were prepared for the metabolomic study. Cells were seeded in a Petri dish at a density of $5x10^6$ cells/dish for NIH 3T3, A2780, and CACO-2 and $3x10^6$ cells/dish CAL-72.

Cells were exposed to the compounds with the $IC_{25,}$ and IC_{50} values were established according to the viability results. After 24h of treatment, the culture medium was collected and then centrifuged in a benchtop centrifuge to remove cells and cell debris from the media. The media was freeze-dried and stored at -80ºC.

The cells were washed 3 times with phosphate-buffered saline (PBS 1X) to remove any remnants of the culture medium. Then they were scraped from the plate with a rubber scraper. The detached cells were quenched by immersion in liquid and sonicated to release the intracellular metabolites.

Endometabolites were extracted using methanol: chloroform extraction procedure introduced by Bligh and Dyer in 1959[160] with slight modifications introduced by Lauri at

al[161] (Figure 16). Methanol and chloroform were added to the solution containing the cells to obtain a volume ratio of 1:1:1. Cells were incubated for 20 min on ice and vortexed frequently. The cell extracts were centrifuged at 4000 x g at 4ºC for 20 min. The aqueous phase was collected and dried using a rotavapor to remove methanol and freeze-dry to remove water. The dried aqueous extracts with metabolites of interest were stored at -80°C.

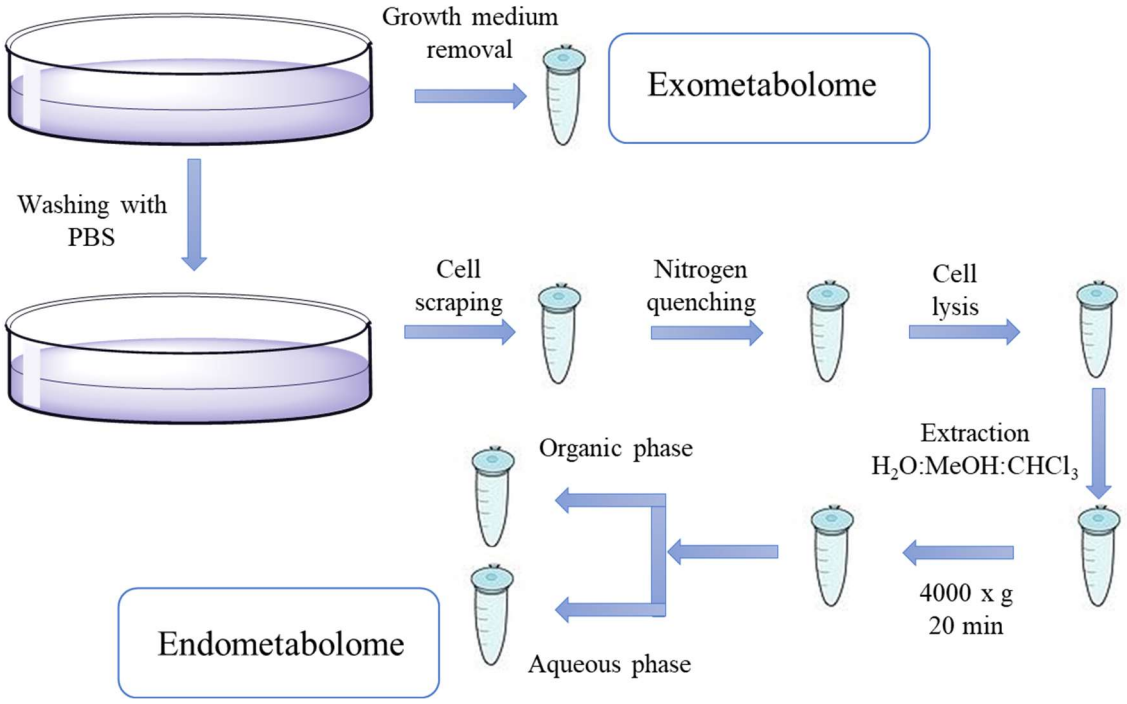

Figure 16. Schematic representation of metabolites extraction for metabolomics experiments.

3.2. NMR measurements

All dried extracts were dissolved in 540 µL D_2O and then mixed with 60 µL of a buffer solution (KH_2PO_4, 1.5 M in D_2O) containing 0.1% of TSP-d_4 (used as chemical shift reference) and sodium azide (NaN_3, 2 mM). The pH was adjusted to 7 using KOD. Samples were transferred into 5-mm NMR tubes. Representative samples of control cell extracts were examined by two-dimensional spectroscopy (HSQC) to assist in signal assignment and metabolite identification. All NMR spectra acquisition and pre-processing were performed under the control of a workstation with TopSpin 3.6.1 (Bruker BioSpin). ^1H NMR spectra were acquired using a 1D nuclear Overhauser enhancement spectroscopy (NOESY) pulse sequence (noesypr1d) to suppress water using the following parameters: SW 4807.692 Hz, TD 64 K data points, relaxation delay 5 s, 128 scans. All

samples were automatically tuned, matched, and shimmed. Each free induction decay (FID) was zero-filled to 128 K points, applied a Fourier transformation, processed using a line broadening (1.0 Hz), and automatically corrected the baseline and phase. The ppm scale was referenced according to the TSP signal at 0.00 ppm.

3.3. Metabolite identification and quantification

The metabolite identification was achieved by peak fitting routing within the 400MHz library spectra database from Chenomx NMR Suite 3.6.1 (Chenomx Inc., Alberta, Canada), the analysis and comparison with HMDB: Human Metabolome Database (http://www.hmdb.ca) chemical shifts databases, cross-checked with the literature[58,61,161–163], and by analysis of 2D NMR experiments.

The relative concentrations of metabolites were determined using Chenomx NMR Suite 8.5.1, which compares the integral of a known reference signal (TSP) with signals derived from a library of compounds containing chemical shifts and signal multiplicities. The metabolites not available in the library were identified by running a standard solution, and the relative concentration was calculated manually.

3.4. Statistical analysis

Statistical analysis was performed using a comprehensive Web application for metabolomic data analysis and interpretation, MetaboAnalyst software version 5.0.[164]

First, a normalization step was carried out to correct variations in the overall concentrations of the samples. Each spectrum was normalized to the unit area, obtained by dividing every variable by the sum of the absolute value of all its variables to avoid the contribution of sample dilution. To make features more comparable, raw data were Pareto-scaled.[165] Each compound concentration was normalized by dividing the measured concentration into the total concentration of all metabolites in that sample.[166]

Then, an unsupervised multivariate statistical method of principal component analysis (PCA) was firstly used to detect the inherent clustering and obvious outliers between the different groups. Subsequently, a supervised multivariate statistical method PLS-DA was applied to sharpen the separation between better groups and demonstrated that the samples tended to be grouped according to the treatment condition. Metabolites contributing to the groups' separation would be considered potential biomarkers.

A univariate statistical ANOVA was then carried out to screen out some low-abundant important metabolites that might be obscured in multivariate analysis. Metabolites with significant differences ($p < 0.05$) were considered as potential biomarkers. The Pearson's correlation was used to generate a heat map to identify clustering patterns between the metabolites.

3.5. Metabolic pathways analysis

The metabolic profile alterations were evaluated by the pathway analysis module available in the MetaboAnalyst. Two pathways' libraries were analysed: KEGG[35] and SMPDB[167]. The algorithm for pathway enrichment analysis was Globaltest[168], designed to estimate the association between concentration profiles of a matched metabolite set and the class label. The betweenness centrality algorithm was used for topological analysis to estimate the impact of the changed metabolites within a given metabolic network.

4. Synthesis of cinnamic acid terminated dendrimers

Cinnamic acid was conjugated to the PAMAM G4NH_2 dendrimer using EDC as a coupling agent and NHS as a stabilizer. For the -COOH activation, the ACCA was placed into a flask and the EDC.HCl was added drop-by-drop followed by the addition of NHS and allowed to react for 1h, RT, at 1250rpm. When the activation ended, PAMAM G4NH_2 in water was added, drop-by-drop to the solution under stirring. ^{1}H NMR was used to follow the reaction. After 1h, dialysis was performed against distilled water for 4h using a 15000Da MWCO, and the content of each membrane was transferred into a falcon tube, frozen, and lyophilized for 3 days. The final compounds were obtained as a oil and preserved in the fridge at 5ºC. All dendrimers were characterised by NMR, FTIR, UV-Vis spectroscopies, mass spectrometry (MALDI-TOF), elemental analysis, and zeta potential.

G4NH_2-25ACCA: G4NH_2 dendrimer (245.27mg, 0.017mmol), ACCA (104.44mg, 0.55mmol), EDC.HCl (105.84mg, 0.55mmol), NHS (119.88mg, 0.555mmol), yield: 100% (370mg, 0.017mmol). Characterisation: ^{1}H NMR (400 MHz, D_2O) δ 2.446 (m, 233H), 2.652 (m, 110H), 2.727 (s, 31H), 2.813 (m, 214H), 3.174 (t, 100H), 3.299 (m, 182H), 3.517 (m, 98H), 6.911 (d, 52H), 7.830 (d, 51H) and 7.968 (s, 25H) ppm. ^{13}C NMR (101 MHz, D_2O) δ 24.78, 32.03, 36.77, 38.77, 48.60, 50.97, 116.51, 132.78, 151.97, 158.44, 168.70 and 175.01 ppm. ^{15}N NMR (40 MHz, D_2O) δ 28.98,

116.67 ppm. FTIR-ATR: 3263 cm^{-1} (primary amino groups), 2209 cm^{-1} (cyano group), 1633 $cm^{-1,}$ and 1539 cm^{-1} (carboxylic acid and amide groups). Elemental Analysis (T/C)%: C(56.63/49.64), H(7.48/7.27), N(20.83/17.44); Hygroscopic. MALDI TOF: m/z = 17770 g/mol [M – $C_{187}H_{131}N_{25}O_{25}$].

G4NH$_2$-32ACCA: G4NH$_2$ dendrimer (223.272mg, 0.016mmol), ACCA (142.62mg, 0.753mmol), EDC.HCl (144.52mg, 0.753mmol), NHS (163.69mg, 0.753mmol), yield: 100% (332mg, 0.015mmol). Characterisation: ^{1}H NMR (400 MHz, D_2O) δ 2.428 (m, 236H), 2.659 (m, 136H), 7.722 (s, 24H), 2.826 (m, 226H), 3.182 (t, 93H), 3.287 (m, 192H), 3.520 (m, 89H), 6.898 (d, 63H), 7.778 (d, 63H) and 7.924 (s, 31H) ppm. ^{13}C NMR (101 MHz, D_2O) δ 24.58, 31.69, 35.36, 36.52, 38.76, 48.43, 50.86, 103.61, 116.10, 119.06, 123.14, 132.64, 151.65, 161.02, 168.43 and 174.76 ppm. ^{15}N NMR (40 MHz, D_2O) δ 28.56, 116.08, 231,35 ppm. FTIR-ATR: 3262 cm^{-1} (primary amino groups), 2211 cm^{-1}(cyano group), 1622 cm^{-1} and 1549 cm^{-1} (carboxylic acid and amide groups). Elemental Analysis (T/C)%: C(57.46/49.60), H(7.21/7.15), N(20.06/16.88); Hygroscopic. MALDI TOF: m/z = 18974 g/mol [M – $C_{258}H_{177}N_{32}O_{32}$].

G4NH$_2$-48ACCA: G4NH$_2$ dendrimer (229.46mg, 0.016mmol), ACCA (294.14mg, 1.55mmol), EDC.HCl (297.06mg, 1.55mmol), NHS (336.47mg, 1.55mmol), yield: 96% (351.91mg, 0.015mmol). Characterisation: ^{1}H NMR (400 MHz, D_2O) δ 2.563 (m, 277H), 2.916 (m, 100H), 3.091 (m, 192H), 3.193 (t, 72H), 3.278 (m, 161H), 3.392 (m, 128H), 3.526 (m, 60H), 6.857 (d, 98H), 7.687 (d, 98H) and 7.80 (s, 48H) ppm. ^{13}C NMR (101 MHz, D_2O) δ 30.38, 30.67, 31,57, 35.34, 36.45, 48.83, 51.16, 104.13, 115.66, 118.89, 123.64, 132.47, 151.45, 159.68, 168.22, 171.83, 172.76, 173.03 and 173.57 ppm. ^{15}N NMR (40 MHz, D_2O) δ 28.98, 30.73, 115.50, 119.59 ppm. FTIR-ATR: 3261 cm^{-1} (primary amino groups), 2211cm^{-1} (cyano group), 1623cm^{-1}, and 1556cm^{-1} (carboxylic acid and amide groups). Elemental Analysis (T/C)%: C(59.01/51.65), H(6.69/6.73), N(18.61/15.15); Hygroscopic. MALDI TOF: m/z = 21726 g/mol [M – $C_{290}H_{240}N_{48}O_2$].

G4NH$_2$-64ACCA: G4NH$_2$ dendrimer (216.94mg, 0.015mmol), ACCA (277.15mg, 1,47mmol), EDC.HCl (280.85mg, 1,47mmol), NHS (31.11mg, 1.47mmol), yield: 100% (399.44mg, 0.015mmol). Characterisation: ^{1}H NMR (400 MHz, D_2O) δ 2.562 (m, 278H), 2.830 (s, 13H), 2.932 (m, 75H), 3.113 (m, 196H), 3.193 (t, 93H), 3.274 (m, 136H), 3.392 (m, 128H), 3.523 (m, 77H), 6.767 (d, 129H), 7.686 (d, 129H) and 7.849 (s, 64H) ppm. ^{13}C NMR (101 MHz, D_2O) δ 29.63, 31.58, 34.69, 35.36, 36.36, 38.08,

38.58, 48.75, 51.03, 103.85, 115.49, 118.78, 123.54, 132.40, 151.52, 159.50, 168.20 ppm. ^{15}N NMR (40 MHz, D_2O) δ 30.68, 115.80 ppm. FTIR-ATR: 3252 cm^{-1} (primary amino groups), 2211 cm^{-1} (cyano group), 1621 cm^{-1} and 1560 cm^{-1} (carboxylic acid and amide groups). Elemental Analysis (T/C)%: C(60.23/53.06), H(6.28/6.31), N(17.48/14.81); Hygroscopic. MALDI TOF: m/z = 24478 g/mol [M – $C_{543}H_{373}N_{53}O_{64}$].

5. Preparation of doxorubicin-encapsulated dendrimers

The prepared dendrimers were dissolved in 5ml of water, and doxorubicin hydrochloride was dissolved in 1ml of methanol and neutralized with 20 µl of triethylamine. The DOX solution was dropped into the dendrimer solution and maintained under stirring overnight to allow the evaporation of methanol at room temperature. The dendrimer/DOX mixture solution was centrifuged (20627 x g for 5 min) to precipitate the non-complexed free DOX. The precipitate was then washed with water, centrifuged 3 more times, and dissolved in methanol to determine the DOX encapsulation efficiency by UV-Vis. All the supernatants were lyophilized to obtain the complex dendrimer/DOX.

G4NH$_2$/DOX: G4NH$_2$ dendrimer (23.58mg, 0.0017mmol), DOX (4.81g, 0.0083mmol).

G4NH$_2$-48ACCA/DOX: G4NH$_2$-48ACCA dendrimer (30mg, 0.0014mmol), DOX (4g, 0.0067mmol).

The encapsulation efficiency (*EE* (%)) and loading capacity (*LC* (*wt*%)) were calculated according to the following equations:

$$EE\ (\%) = \frac{DOX\ added - free\ Dox}{DOX\ added} \times 100$$

$$LC\ (wt\%) = \frac{Weight\ of\ loaded\ DOX}{Weight\ of\ DOX - encapsulated\ dendrimer} \times 100$$

5.1. *In vitro* release

DOX-encapsulated dendrimers were weighed according to the amount of doxorubicin inside the dendrimer. The amount of DOX was established in 2.5µM, which was dissolved in 300 µL PBS pH 7. The solution was placed in a mini dialysis device of 2k MWCO and then placed in a glass bottle with 5ml of PBS pH 7. At different time intervals, 100 µL of PBS were removed and transferred to a 96-wells opaque plate, and the DOX release was measured. The volume removed from the dialysis device's glass

bottle was replaced with 100 µl of fresh PBS pH 7 to the glass bottle. The DOX released into the supernatants was determined by UV-Vis spectroscopy.

The cumulative release (C_r) of doxorubicin against time was calculated with the following equation:

$$C_r\ (\%) = \frac{V_0 C_n + V_t \times \sum_1^{n-1} C_i}{m_{DOX}} \times 100$$

Where:

V_0 is the volume of release media,

C_n is the measured concentration of DOX in a certain time point,

M_{DOX} is the initial mass of DOX

V_t is the volume of the aliquots previously removed

C_i is the correspondent DOX concentrations in those aliquots

5.2. Size and zeta potential

All dendrimers were dispersed in water, PBS, DMEM, or RPMI at a 0.1mg/mL final concentration. The measurements were done for three independent experiments, corresponding to 11 runs for size and 35 runs for zeta measures. Disposable folded capillary cells were used for the zeta potential analysis. The other equipment parameters were default values.

5.3. Uptake study

For the cell uptake study, CAL-72 cells were plated for 24 h before the incubation with freshly prepared DOX or DOX-encapsulated dendrimer solutions at the same DOX concentration (the final concentrations in the wells were 1 µM) at 37 °C for 48 h and 24h.

Subsequently, the cells were washed with sterilized PBS buffer, fixed with 3.7% formaldehyde for 10mim, permeabilized with Triton-x 0,1% for 10 min, and stained with 40,6-diamidino-2- phenylindole (DAPI; Sigma) for 10 min. The cells were washed with PBS solution for analysis by optical fluorescence microscopy (Nikon Eclipse TE 2000E inverted microscope).

5.4. Hemolytic toxicity

The hemolytic toxicity was carried out using fresh and healthy human blood supplied by Hospital Nélio Mendonça (Funchal, Madeira) following the

cyanmethemoglobin method adapted from CLSI (The Clinical & Laboratory Standards Institute), ASTM (American Society for Testing and Materials), and ICSH (International Council for Standardization in Heamotology).[169–171]

The cyanmethemoglobin reagent was prepared by dissolving 50 mg potassium ferricyanide, 12.5 mg potassium cyanide, and 35 mg potassium dihydrogen phosphate in 250 ml of distilled water with 250 µl Triton-X, and its pH was adjusted to 7.4.

The standard curve for hemoglobin was plotted using hemoglobin from bovine blood and applied to determine the hemoglobin concentrations in the samples.

To quantify the total hemoglobin concentration in the original blood, a 250-fold dilution of blood was prepared in cyanmethemoglobin reagent (20 µl of blood in 5 ml of reagent), and the absorbance was measured at 550 nm. The concentration of hemoglobin was calculated with the following equation:

$$[Hg] = \frac{A_{550} \times D_f}{F}$$

Where:

A_{550} is the absorbance at 550nm,

D_f is the dilution factor (1:250),

F is the slope of the equation of the standard hemoglobin curve

The total concentration of hemoglobin in test tubes was calculated with the following equation:

$$T\ (g/L) = \frac{[Hg]}{D_f}$$

Where:

$[Hg]$ is the hemoglobin concentration in the original blood,

D_f is the dilution factor (1:80).

For hemotoxocity evaluation, all dendrimers as well free-DOX were diluted to a final concentration of 5 µM, 10 µM, 25 µM, and 50 µM in PBS. A 10% (v/v) blood solution was also prepared in PBS and added to each compound solution, including a positive (distilled water) and negative control (PBS) in a 1:8 ratio. Following the incubation for 3h at 37 °C, the mixture was centrifuged at 1598 x g for 15 min, the

supernatant was transferred to 96 well cell culture plates, and added cyanmethemoglobin reagent in a 1:5 proportion. The absorbance of the supernatants was measured at 550 nm

$$S = \frac{A_{550} \times D_f}{F}$$

A_{550} is the absorbance at 550nm of the supernatants,
D_f is the dilution factor (1:5),
F is the slope of the equation of the standard hemoglobin curve

Finally, the percentage of hemolysis was then calculated for each situation from the ratio between the hemoglobin concentration in the sample's supernatant and the total value that was initially present, with the following equation:

$$Hemolysis\ (\%) = (S \times T) \times 100$$

6. Lactate and glucose quantification

CAL-72 cells were plated in Petri dishes with a density of $3x10^6$cells/dish, allowed to adhere overnight, and subsequently incubated with the amount relative to the IC_{50} values of the $G4NH_2$, ACCA, and $G4NH_2$-48ACCA, previously calculated. Control assays were added with 1% DMSO. After 24h, the medium was collected, centrifuged, and kept to analyse the exometabolome. The cells were washed with PBS, scraped, transferred to a tube, submerged into liquid nitrogen, and sonicated. Before the extraction of the metabolites, samples of the lysed cells were taken to quantify the protein by BCA quantification. The metabolites were extracted using the same procedure used for metabolomics. The medium and aqueous extracts were freeze-dried.

Enzymatic colorimetric kits were used for lactate (Lactate, LO-POD, Enzymatic colorimetric, Spinreact, S.A.U., St. Esteve de Bas, Spain) and glucose (Glucose, HK, Enzymatic colorimetric, Spinreact, S.A.U., St. Esteve de Bas, Spain).
The assays were carried out in a 96-well plate, where 2 µl of supernatant from each assay and 200 µl of the previously prepared working solution were added. A blank was also prepared, containing 200 µl of the working solution and 2 µl of PBS. They were incubated for 5 min, the absorbance was read, and the amount of lactate and glucose (mg) was calculated using the formulas:

$$[Lactate] = \frac{abs\ sample}{abs\ standard} \times 10\ (Concentration\ of\ standard\ solution)$$

$$[Glucose] = \frac{abs\ sample}{abs\ standard} \times 100\ (Concentration\ of\ standard\ solution)$$

Total protein was assessed using the BCA (Pierce™ BCA Protein Assay Kit, ThermoFisher Scientific, Waltham, Massachusetts, USA) assay for the aforementioned time points. Data were collected from two independent experiments, each in triplicate. Results are expressed as total μg/total biomass.

Chapter 3. ^{1}H NMR metabolomics of PAMAM G4NH$_2$

Nanotechnology offers a wealth of tools that provide cancer researchers with new and innovative ways to diagnose and treat diseases. By using nanotechnology in drug design and delivery, researchers are trying to push nanomedicine to be able to deliver the drug to the targeted tissue, release the drug at a controlled rate, develop a biodegradable drug delivery system, and be able to escape from degradation processes of the body.

In this context, dendrimers are being studied as drug/gene delivery vehicles and carriers for molecules/chemical groups and/or inorganic particles used as contrast agents in medical imaging.[172]

Current problems for nanomedicine involve understanding the issues related to toxicity and the environmental impact of nanoscale materials. Because of quantum size effects and large surface area to volume ratio, nanomaterials have unique properties that affect their toxicity compared to their larger counterparts.

Metabolomic technologies can provide high-throughput screening information for oxidative stress biomarkers following nanomaterials' introduction into biological systems.[88]

This work aims to use nanotechnology as a platform to study the biochemical disorders induced by dendrimers in cell culture using NMR metabolomics. These two fields will be complementarily used to identify metabolic targets and understand the cytotoxicity mechanism and changes in the metabolic profile of cells treated with dendrimers.

The main objective of this chapter was to study the *in vitro* metabolic cellular effects of generation 4 polyamidoamine (PAMAM) dendrimers in distinct cell lines by ^{1}H NMR metabolomics. Experiments were done using CAL-72[173] cells, A2789[174,175], CACO-2[176,177], and NIH 3T3 cell extracts (treated and non-treated cells were analysed). The cancer cell lines were chosen because they represent types of cancers treated with DOX, an anticancer drug with many side effects, which has been the target of nanotechnology strategies to improve its efficiency.[178] NIH 3T3 was used as a non-cancer model. Generation 4 of PAMAM was selected for being able to form stable conjugates with DOX.[179]

1. Cytotoxicity of PAMAM G4NH$_2$ on different cell lines

The antiproliferative effect of PAMAM G4NH$_2$ on four different cell lines was assessed indirectly by resazurin reduction assay to determine the drug concentration for metabolomics studies.

After 24h, the results indicated a clear difference between the cancer cell lines, CAL-72 (osteosarcoma), CACO-2 (colon cancer), and A2780 (ovarian cancer) and non-cancer cells, NIH 3T3 (fibroblast cell).

PAMAM dendrimers are less cytotoxic against non-cancer cells than cancer cells (Figure 18). The IC_{50} of dendrimer on those cell lines decreases following the sequence NIH 3T3> CACO-2>A2780 >CAL-72. The IC_{50} value of PAMAM on the cancer cell lines was 5 times more cytotoxic than "normal" fibroblast. Between the cancer cell lines, there wasn´t a significant difference. Our results are in good agreement with the one published by Mukherjee[131], where cancer cells are more sensitive than non-cancer cells.

These results served as a basis to select two concentrations corresponding to equivalent effects on cell viability: IC_{50} and IC_{25}. The choice to treat cells with the subtoxic concentration was based on the assumption that cell metabolism would respond even in the absence of major toxicity.[56]

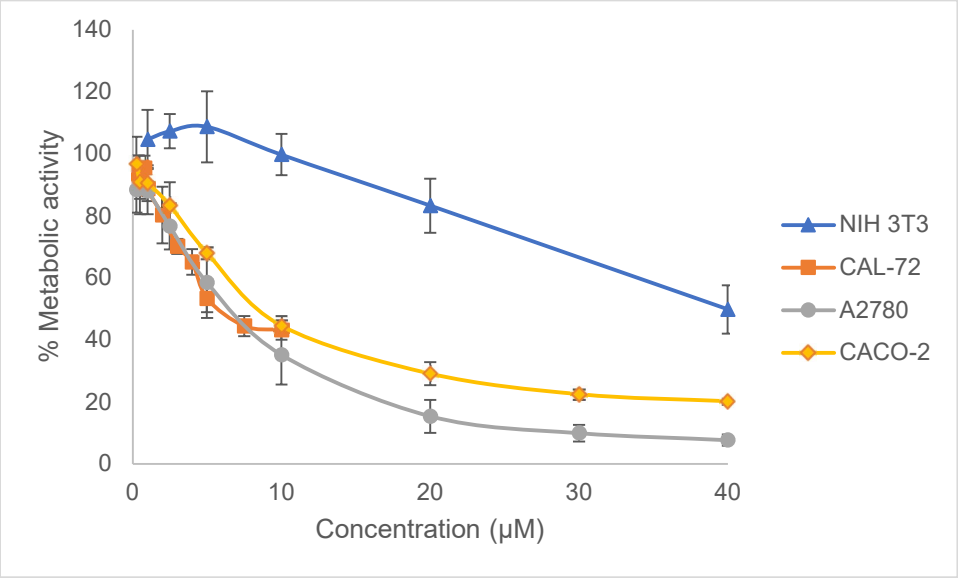

Figure 17. Curve dose-response of CAL-72, NIH 3T3, A2780, and CACO-2 cell lines after 24h of exposure with G4NH2

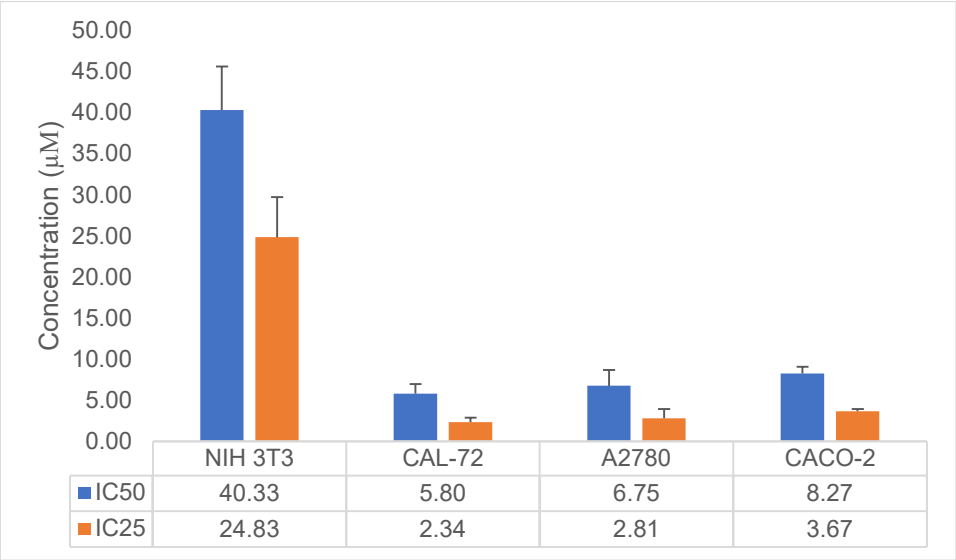

	NIH 3T3	CAL-72	A2780	CACO-2
IC50	40.33	5.80	6.75	8.27
IC25	24.83	2.34	2.81	3.67

Figure 18. Calculated IC_{25} and IC_{50} values measured by the resazurin reduction assay after 24h of exposure with G4NH2 in CAL-72, NIH 3T3, A2780, and CACO-2 cell lines.

2. Metabolite profiling of cultured cells: identification of metabolites

The elucidation of the toxicological effect of PAMAM G4NH$_2$ in four cell lines was analysed, with the assistance of several databases and literature reported previously in chapter 2 (materials and methods), using ^{1}H NMR metabolomics by identifying the endogenous and exogenous metabolites from dendrimers treated and untreated cells..

2D NMR experiment was also performed to assist in the identification of the metabolites that cannot be identified exclusively from database information. The ^{1}H-^{13}C HSQC experiment provides information, like the chemical shifts of the protons and their connected heteroatoms, that improved spectral resolution. The carbon chemical shifts have a much broader dispersion (up to ~ 220 ppm) than the proton spectrum, which assists considerably in analysing the heavily overlapped resonances.[163,180]

2.1.Endometabolome

A representative ^{1}H NMR spectrum of the endometabolome of CAL-72, NIH 3T3, A2780, and CACO-2 is shown in Figure 19, where the detectable metabolites were labelled. The signal assignment allows identifying 37 metabolites based on their chemical shifts. Assignments are presented in Table 1.

Single quantum coherence (HSQC) is a heteronuclear 2D experiments that hold the advantage of the spectral width of carbon assisting the metabolite discrimination and identification. 2D NMR techniques are used as a strategy to overcome the problem of overlapping resonances, aiding in the unambiguous identification of metabolites. Figure 20 shows the ^{1}H-^{13}C HSQC spectrum of the A2780 endometabolome. The spectra analysis confirms, for example, the signal of glycerophosphocholine (H= 3.23 ppm and C= 56.64 ppm).

As expected, the identified metabolites belong to different classes. Sixteen amino acids encoded in the genetic code were found (glutamine, alanine, threonine, etc.). Other classes of compounds like sugars (glucose), energy storage compounds (ATP), organic acids (lactate, succinate, fumarate, etc.), and organic osmolytes (myo-inositol) were also observed.

The most intense metabolite ^{1}H NMR signals were obtained from lactate, glutamate, alanine, glycine, and glucose. Metabolites that were commonly identified in several studies that use metabolomics in mammalian cells[60,181]

With some exceptions, most metabolites are found in all cell lines. Myo-inositol is not detected in CAL-72, aspargine is not found in CAL-72 and NIH 3T3, UMP is not detected in CACO-2, acetoin only is detected in CAL-72, and glutamine only appears in A2780. The relative concentrations of these metabolites vary depending on the cell line.

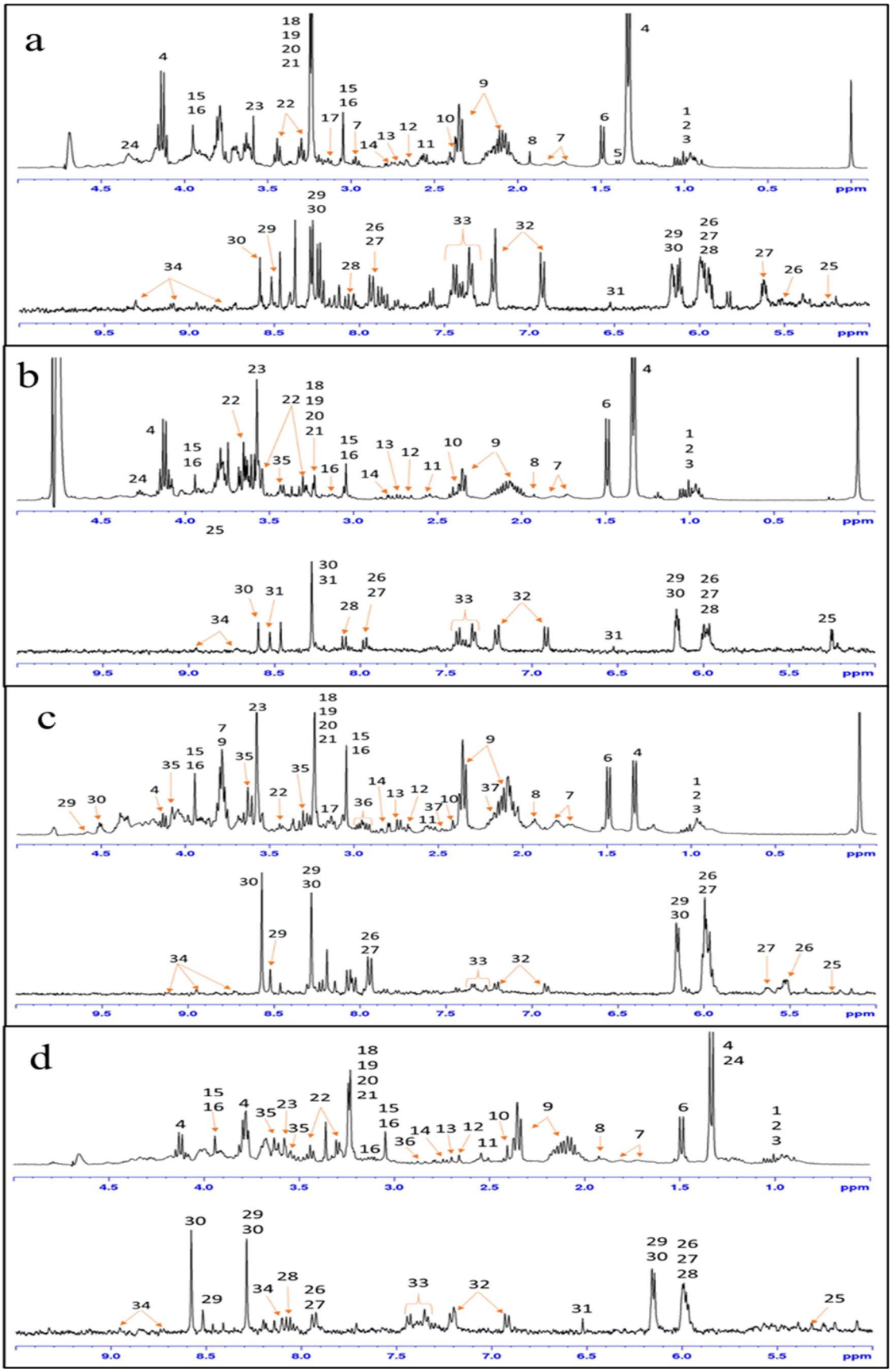

Figure 19. 400 MHz ^{1}H NMR spectrum of endometabolome extracts from a) CAL-72 b) NIH 3T3 c) A2780 d) CACO-2 control cells in D_2O. Signals are numbered accordingly with Table 1.

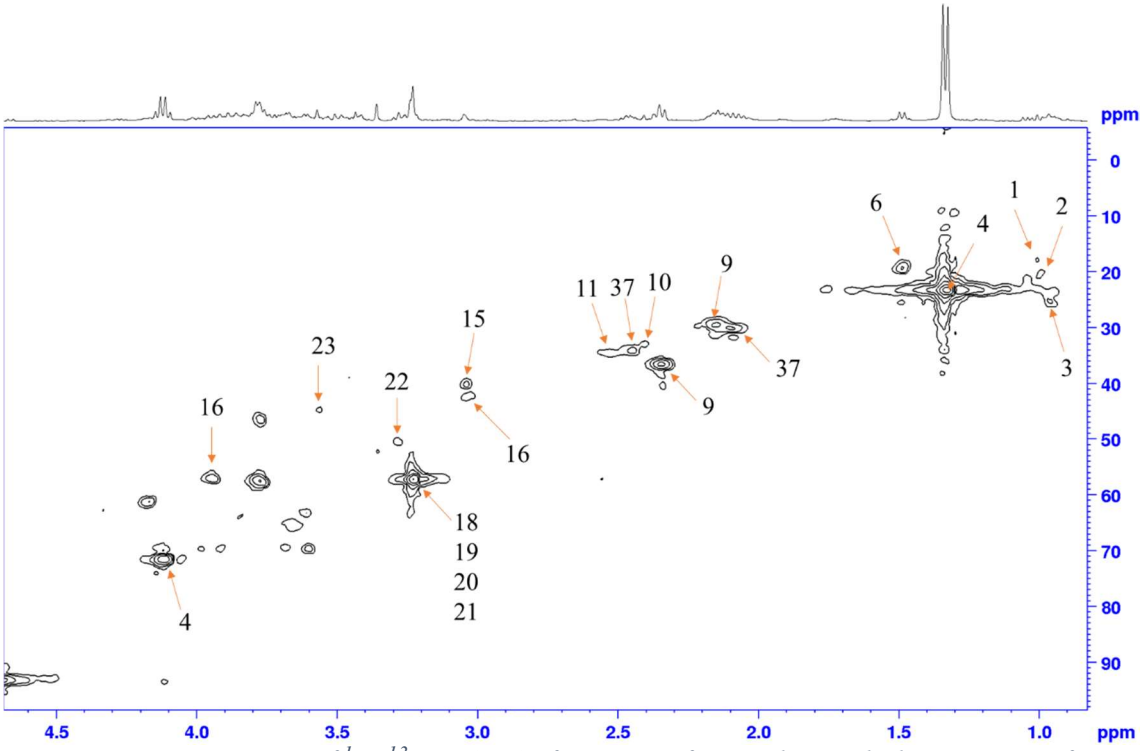

Figure 20. Expansion of ^{1}H-^{13}C HSQC of spectra of an endometabolome extract from A2780 control cells in D_2O. Signals are in accordance with Table 1.

Table 1. Assignment of resonances in the NMR profile of polar extracts from CAL-72, NIH 3T3, CACO-2 and A2780 cells. (s) singlet, (d) doublet (dd) doublet - doublet, (t) triplet, (m) multiplet.

Nº	Compound	^{1}H in ppm (*multiplicity, assignment*)/^{13}C in ppm	CAL-72	NIH 3T3	CACO-2	A2780
1	Leucine	0.95 (d, *3H*), 0.96 (d, 3H) 25.27	√	√	√	√
2	Valine	0.98 (*d, 3H*)/20.52, 1.03 (*d, 3H*)	√	√	√	√
3	Isoleucine	0.93 (*t, 3H*), 1,00 (*d, 3H*)/ 18.20	√	√	√	√
4	Lactate	1.32 (*d, 3H*)/23.53, 4.110 (*q, 1H*)/71.77	√	√	√	√
5	Acetoin	1.40 (*d, 3H*)	√	-	-	-
6	Alanine	1.49 (*d, 3H*)/19.47	√	√	√	√
7	N_α-acetyllysine	1.69 (*m*), 1.81 (*m*), 2.03 (*s*)	√	√	√	√

Nº	Compound	^{1}H in ppm (*multiplicity, assignment*)/^{13}C in ppm	CAL-72	NIH 3T3	CACO-2	A2780
8	Acetate	1.91 (*s*, 3H)	√	√	√	√
9	Glutamate	2.08 (*m, 2H*)/31.42, 2.34 (*m, 2H*)/36.52	√	√	√	√
10	Succinate	2.40 (*s, 4H*)	√	√	√	√
11	β-Alanine	2.54 (*t, 2H*)/34.43, 3.18 (*t, 2H*)	√	√	√	√
12	Methionine	2.63 (*t, 2H*)	√	√	√	√
13	Dimethylamine	2.71 (*s, 6H*)	√	√	√	√
14	Aspartate	2.67 (m, 1H), 2.81 (m, 1H)	√	√	√	√
15	Creatine	3.03 (*s, 2H*)/40.14, 3.92 (*s, 2H*)	√	√	√	√
16	Creatine Phosphate	3.03 (*s, 4H*)/42.23, 3.94 (*s, 1H*)/56.86	√	√	√	√
17	1,3-Diaminopropane	3.11 (*t, 4H*)	√	√	√	√
18	Choline	3.20 (*s, 9H*)	√	√	√	√
19	Acetylcholine	3.22 (*s, 9H*)	√	√	√	√
20	Phosphoscholine	3.22 (*s, 9H*)/57.56	√	√	√	√
21	Glycero phosphocholine	3.23 (*s, 9H*)	√	√	√	√
22	Taurine	3.27 (*t, 2H*)/50.31, 3.43 (*t, 2H*)	√	√	√	√
23	Glycine	3.58 (*s, 2H*)/44.73	√	√	√	√
24	Threonine	4.26 (*m, 1H*)	√	√		
25	Glucose	4.64 (*d, 1H*), 5.23 (*d, 1H*)	√	√	√	√
26	UDP-N-Acetylglucosamine	5.50 (*dd,* 1H), 5.95 (*d,* 1H), 5.97 (*d,* 1H), 7.93 (*d,* 1H), 8.34 (*d,* 1H)	√	√	√	√
27	UDP-Glucose	5.59 (*dd,* 1H), 5.97 (*m,* 1H), 7.93 (*d,* 1H)	√	√	√	√
28	UMP	5.99 (*m,* 2H), 8.07 (*d,* 1H)	√	√	√	

Nº	Compound	^{1}H in ppm (*multiplicity, assignment*)/^{13}C in ppm	CAL-72	NIH 3T3	CACO-2	A2780
29	ATP	8.52 (*s,* 1H)	√	√	√	√
30	AMP	8.58 (*s,* 1H)	√	√	√	√
31	Fumarate	6.51 (*s,* 2H)	√	√	√	
32	Tyrosine	6.92 (*d,* 2H), 7.20 (*d,* 2H)	√	√	√	√
33	Phenylalanine	7.34 (*d,* 2H), 7.39 (*m,* 1H), 7.44 (*m,* 2H)/134.25	√	√	√	√
34	NADP+	8.14 (*s,* 2H), 8.41 (*s,* 2H), 8.83 (*d,* 2H), 9.10 (*d,* 2H), 9.30 (*s,* 2H)	√	√	√	√
35	Myo-inositol	3.28 (*t,* 1H), 4.06 (*t,* 1H)		√	√	√
36	Aspargine	2.87 (*m,*1H), 2.95 (*m,* 1H)			√	√
37	Glutamine	2.11(*m*, 2H)/30.15, 2.45 (*m,* 2H)/34.08			√	

2.2.Exometabolome

The cell culture medium used for CAL-72, NIH 3T3 was DMEM, for A2780 was RPMI and for CACO-2 was MEM. All medium was supplemented with 10% of FBS and 1% of antibiotic/antimicotic. Although in the case of A2780 cells, the medium was further supplemented with 2mM glutamine and, in the case of CACO-2 cells with 1% NEEA, as recommended by the cell line supplier to enhance cell growth.

Figure 21 shows the comparison between the ^{1}H NMR spectra of the media of the 3 culture media used to culture the cell lines under study. The formulation of each cell culture medium is listed in the supplementary material (Table 2).

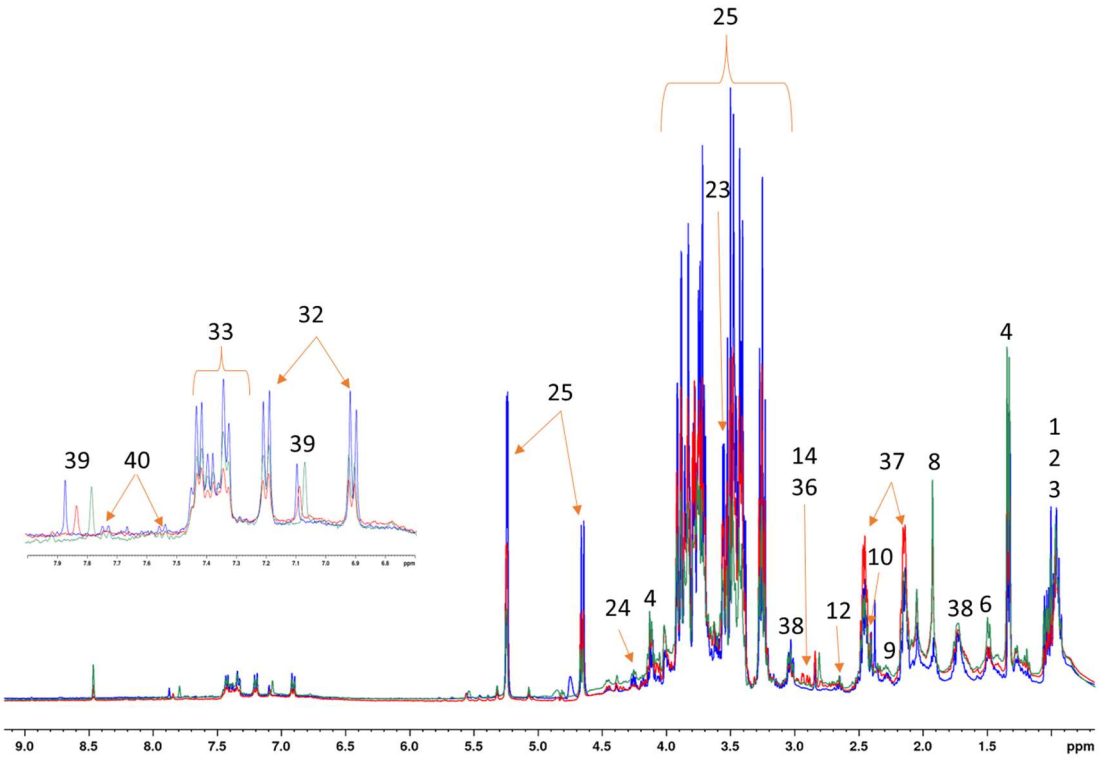

Figure 21. 400 MHZ ^{1}H NMR spectra of DMEM, RPMI, and MEM medium. Signals are in accordance with Table 2.

Typical ^{1}H NMR spectra of the exometabolome of CAL-72, NIH 3T3, A2780, and CACO-2 are shown in Figure 22, where the detectable metabolites were labelled. The signal assignment allows for the identification of 23 metabolites based on their chemical shifts. Assignments are presented in Table 2. The identified metabolites were essentially amino acids and glycolysis players (glucose and lactate).

Exometabolome analysis allows to understand the changes between the use and excretion of metabolites during *in vitro* incubation, which allows us to understand the metabolic activity. Some metabolites were identified after incubation that were not present in the acellular medium, indicating that they were excreted by the cells. These metabolites were: Nα-acetyllysine, Glutamate, Aspartate, Myo-inositol, Aspargine, and Citrate.

As in the endometabolome, the same metabolites are generally identified in all cell lines. In this case, the exceptions are: glutamate and aspargine are not detected in CAL-72 and NIH 3T3, aspartate is only found in A2780, myo-inositol is only found in CACO-2, lysine and tryptophan are not detected in A2780 and citrate is only detected in NIH 3T3 and CACO-2.

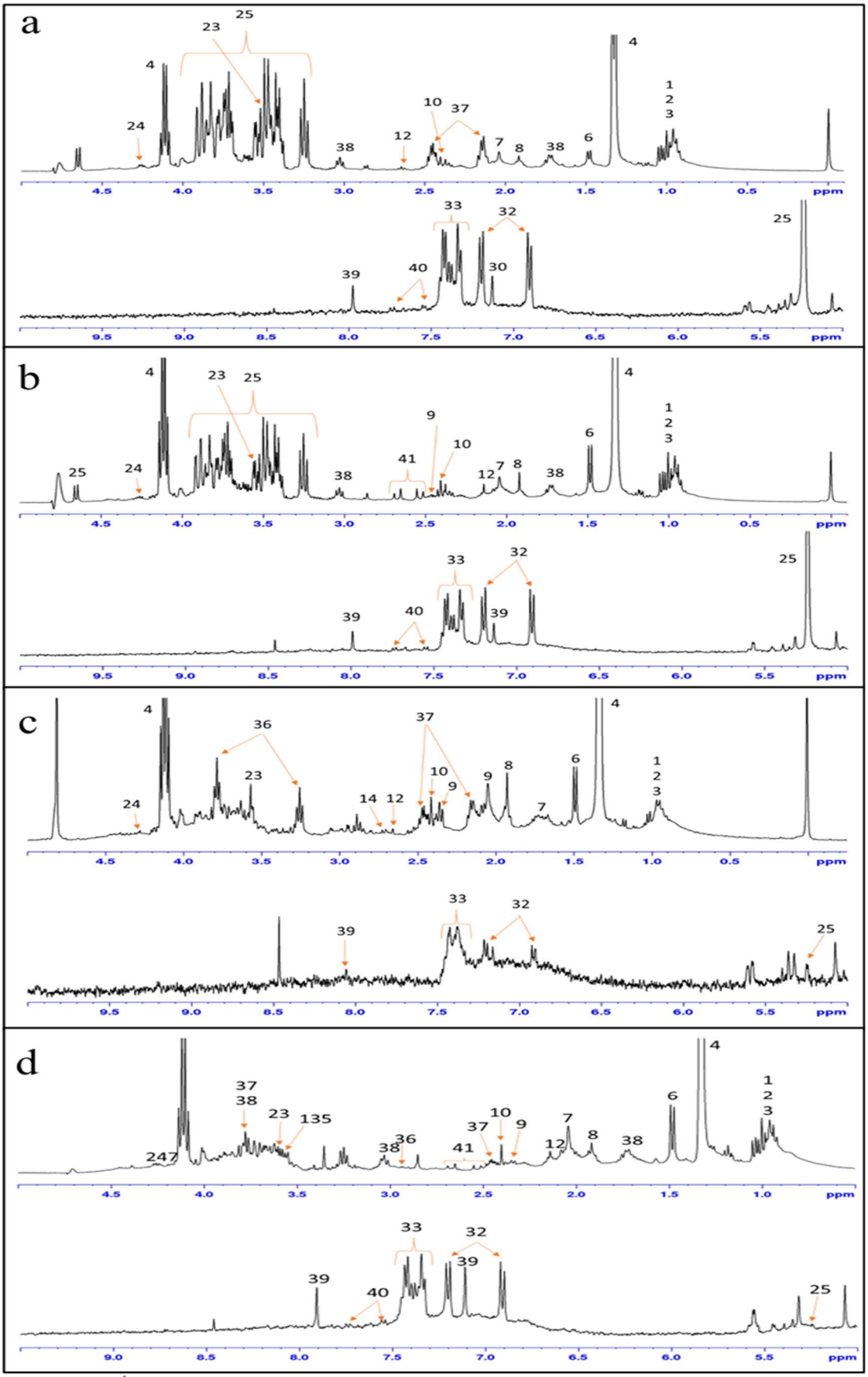

Figure 22. ^{1}H NMR spectrum of CAL-72, NIH 3T3, A2780 and CACO-2 treated with PAMAM G4NH2 exometabolome in D_2O. Signals are numbered accordingly to Table 2.

Table 2. Assignment of resonances in the NMR profile of culture media from CAL-72, NIH 3T3, CACO-2, and A2780. (s) singlet, (d) doublet, (dd) doublet - doublet, (t) triplet, (m) multiplet

Nº Compound	**^{1}H in ppm (*multiplicity, assignment*)**	**CAL-72**	**NIH 3T3**	**CACO-2**	**A2780**
1 Leucine	0.94 (m, 6H)	√	√	√	√
2 Valine	0.97 (*d, 3H*), 1.02 (*d, 3H*)	√	√	√	√
3 Isoleucine	0.92 (*t,* 3H), 0,99 (*d,* 3H)	√	√	√	√
4 Lactate	1.31 (*d, 3H*), 4.09 (*q, 1H*)	√	√	√	√
6 Alanine	1.46 (*d, 3H*)	√	√	√	√
7 N_{α}-acetyllysine	1.69 (*m,* 2H), 1.81 (*m,*1H), 2.03 (*s,*3H)	√	√	√	√
8 Acetate	1.90 (*s*, 3H)	√	√	√	√
9 Glutamate	2.36 (*m, 2H*)			√	√
10 Succinate	2.38 (*s, 4H*)	√	√	√	√
12 Methionine	2.63 (*t, 2H*)	√	√	√	√
14 Aspartate	2.64 (*m,* 1H)			√	
23 Glycine	3.56 (*s, 2H*)	√	√	√	√
24 Threonine	4.26 (*m, 1H*)	√	√	√	√
25 Glucose	3.23 (*t*, 1H), 3.40 (*m*, 1H), 3.47 (*m*, 1H), 3.53 (*dd*, 1H), 3.73 (*m,* 1H), 3.83 (*m,* 1H), 4.63 (*d,* 1H, *β-glucose,*), 5.22 (*d,* 1H, *α-glucose*)	√	√	√	√
32 Tyrosine	6.89 (*d,* 2H), 7.18 (*d,* 2H)	√	√	√	√
33Phenylalanine	7.32 (*d,* 2H), 7.36 (*m,* 1H), 7.41 (*m,* 2H)	√	√	√	√
35 Myo-inositol	3.27 (*t, 1H*), 3.52 (*d*, 2H) 3.61 (*t*, 2H)	-	-	-	√
36 Aspargine	2.85 (*m,1H*), 2.94 (*m, 1H*)	-	-	√	√
37 Glutamine	2.12 (*m*, 2H), 2.44 (*m, 2H*)	√	√	√	√
38 Lysine	1.72 (*m,* 2H), 3.02 (*t,* 2H)	√	√	-	√
39 Histidine	7.07 (*s,* 1H), 7.85 (*s,* 1H)	√	√	√	√

Nº Compound	^{1}H in ppm (*multiplicity, assignment*)	CAL-72	NIH 3T3	CACO-2	A2780
40 Tryptophan	7.53 (*d, 1H*), 7.72 (*d, 1H*)	√	√	-	√
41 Citrate	2.53 (*d, 2H*), 2.69 (*d, 2H*)	-	√	-	√

Based on NMR relative quantitative integration, the exometabolites alterations were assessed by comparing the acellular culture medium and the culture medium after incubation with cells.

The results presented in Table 3 show that despite the cell lines using different culture media, they have a similar metabolic profile. The considered cell lines consume amino acids (except alanine, nα-acetyllysine, and phenylalanine (CACO-2)) and glucose while excreting lactate, succinate, and citrate.

Looking at the high glucose consumption and the scribed lactate metabolite, we can say that all four cell lines have similar glycolytic activity, consistent with the 'Warburg' phenotype of cancer cells.[182]

The glutamine intake also shows that the cells have high glycolytic activity since much of the carbon in cancer cells comes from amino acids that are taken up from the environment or synthesized from some non-essential amino acids.[183]

Alanine increases especially in NIH 3T3 and A2780, which would be expected as the biosynthetic demand correlates with the excretion of metabolites such as alanine and lactate.[183]

These results serve as a basis for establishing the conditions for studying the biological response of dendrimers in the metabolomic environment.

Table 3. Variation in the exometabolome of CAL-72, NIH 3T3, A2780, and CACO-2 cell lines after 24h of incubation. Signals are coloured according to % variation relative to an acellular medium.

		CAL-72	NIH 3T3	A2780	CACO-2
1	**Leucine**	▼*	▼*	▼*	▼*
2	**Valine**	▼*	▼*	▼*	▼*
3	**Isoleucine**	▼*	▼*	▼*	▼*
4	**Lactate**	▲*	▲*	▲*	▲*
6	**Alanine**	▲	▲*	▲*	▲
7	**Nα-acetyllysine**	▲*	▲*	-	▲*
8	**Acetate**	▼*	▼	▼*	▼*
9	**Glutamate**	-	-	▼	▼*
10	**Succinate**	▼*	▼*	▼	▼*
12	**Methionine**	▼*	▼*	▼*	▼*
14	**Aspartate**	-	-	▼*	-
23	**Glycine**	▼*	▼	▼*	▼*
24	**Threonine**	▼*	▼*	▼*	▼*
25	**Glucose**	▼*	▼*	▼*	▼*
32	**Tyrosine**	▼*	▼*	▼*	▼*
33	**Phenylalanine**	▼*	▼*	▼*	▲
35	**Myo-inositol**	-	-	-	▲*
36	**Aspargine**	-	-	▼*	▼*
37	**Glutamine**	▼*	▼*	▼*	▼*
38	**Lysine**	▼*	▼*	▼*	▼*
39	**Histidine**	▼*	▼*	▼*	▼*
40	**Tryptophan**	▼*	▼*	▼*	▼*
41	**Citrate**	-	▲*	▲*	-

3. Metabolomic analysis of different cell lines exposed to PAMAM G4NH2

Each cell line exhibited an undistinguishable NMR profile. Using Chenomx Software (version 8.6), a data matrix was created to obtain relative quantitative information between whole treated cells and control.

The normalized NMR data matrix was analysed by multivariate data analysis to reduce data complexity and visualize if there is intrinsic clustering.

To determine the differences in the metabolic profiles among the four cell lines, principal component analysis (PCA) was performed. Figure 23 and Figure 24 show the projection of the variance between untreated cell samples and those that were treated with IC_{25} and

IC_{50} of dendrimer in two principal components (PC1 and PC2). These PCs correspond to a new coordinate system that mathematically summarizes the measured variables in the dataset. The PCs are projected in a way that PC1 explains the greatest variance in the data matrix, followed by the PC2, PC3, and so on.[184]

It is possible to observe that all cell lines show a trend for separating the groups, indicating that both intracellular and extracellular metabolites were altered in response to the presence of the PAMAM. The cell line with more obvious separation is CAL-72, where both endogenous and exogenous metabolites form 3 well-defined clusters. Endometabolome of CACO-2 also showed a separation between the treat and non-treat cells, but no difference was observed between both dendrimer concentrations tested. The exometabolome does not follow the same tendency. NIH 3T3 shows a tendency to form clusters, but the separation of the groups is unclear. In the A2780 cell line, no separation among the groups was observed in the entire metabolome. In the subsequent loading plots, the metabolites that exhibited more importance/predominance in the variance projection of the samples were roughly the same between all the cell lines. The metabolite that contributed more was lactate, followed by glucose (for the exometabolome), glycerophosphocholine, lysine, glycine, glutamate, alanine, myo-inositol, isoleucine, and threonine.

High lactate concentration is found near many tumours due to the increase in aerobic cellular lactate excretion via the Warburg effect.[185] This lactate induces the migration of cells and cell clusters, promoting various cancers' development and malignant progression.[186] Glucose is an essential metabolic energy source and the main source of lactate production in most solid tumors.[187] Glycerophosphocholine and myo-inositol are osmolytes that are accumulated by cells in response to environmental stresses and present a protective behaviour.[188]

PLS-DA was used to maximize the separation between the groups, especially in cell lines where this separation was not so evident. The PLS-DA (Figure 25 and

Figure 26) confirmed that all the samples have a good tendency to group according to the treatment condition. The metabolites that contributed more to the separation were the same as PCA, adding asparagine and aspartate.

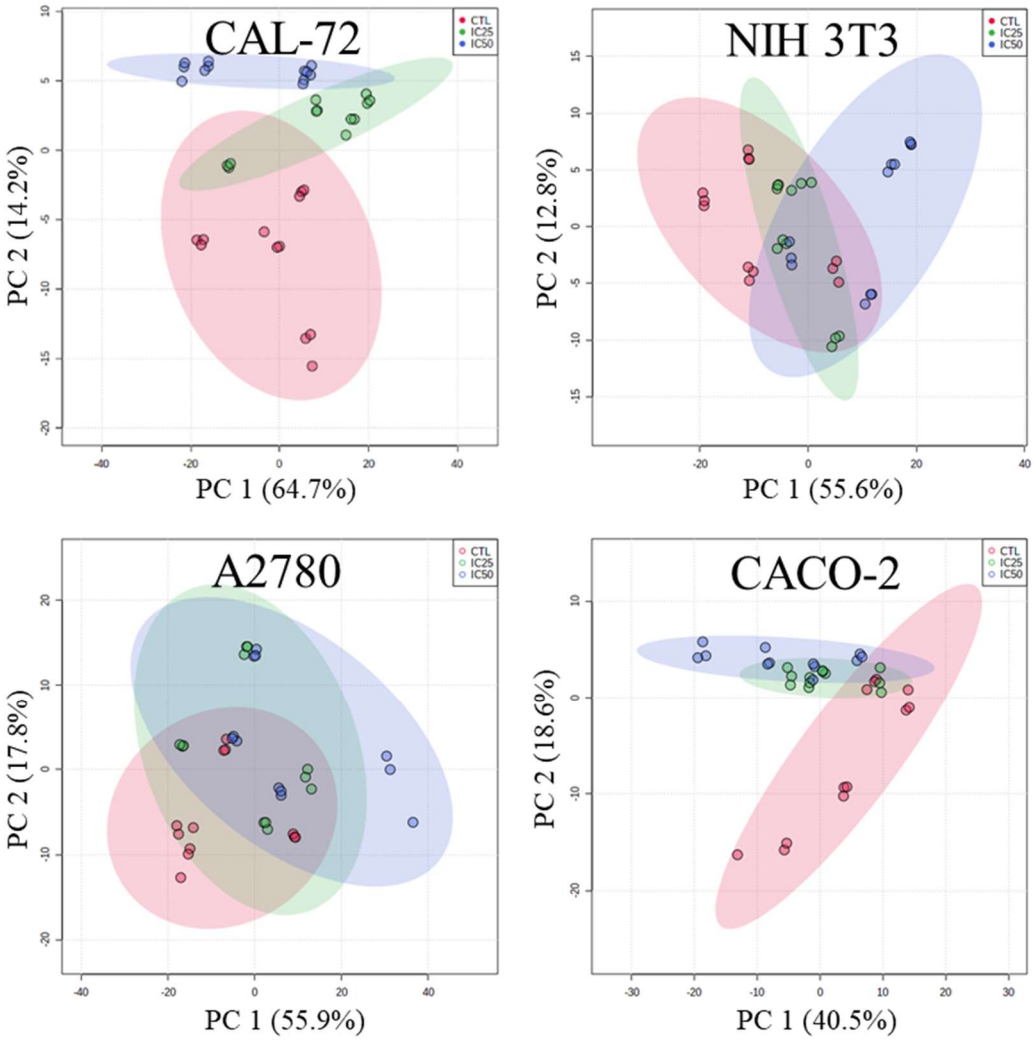

Figure 23. Multivariate analysis PCA of ^{1}H NMR spectra from the CAL-72, NIH 3T3, A2780, and CACO-2 endometabolome.

In addition to the loading plots, the PLS-DA method gives the variable importance in a projection (VIP). In some cases, it only confirms the metabolites already identified as potential biomarkers. In other cases, it reveals new ones, like creatine, beta-alanine, tyrosine, leucine, phenylalanine, taurine, and methionine. The metabolites with VIP values greater than 1 were considered significant.

Statistical analysis reveals that the most represented group of compounds are amino acids. Twelve proteinogenic amino acids show alterations after the treatment with the dendrimer. Creatine participates in several enzymatic reactions, plays an important energy/pH buffer function in tissues, and guarantees the maintenance of its total body pool.[189]

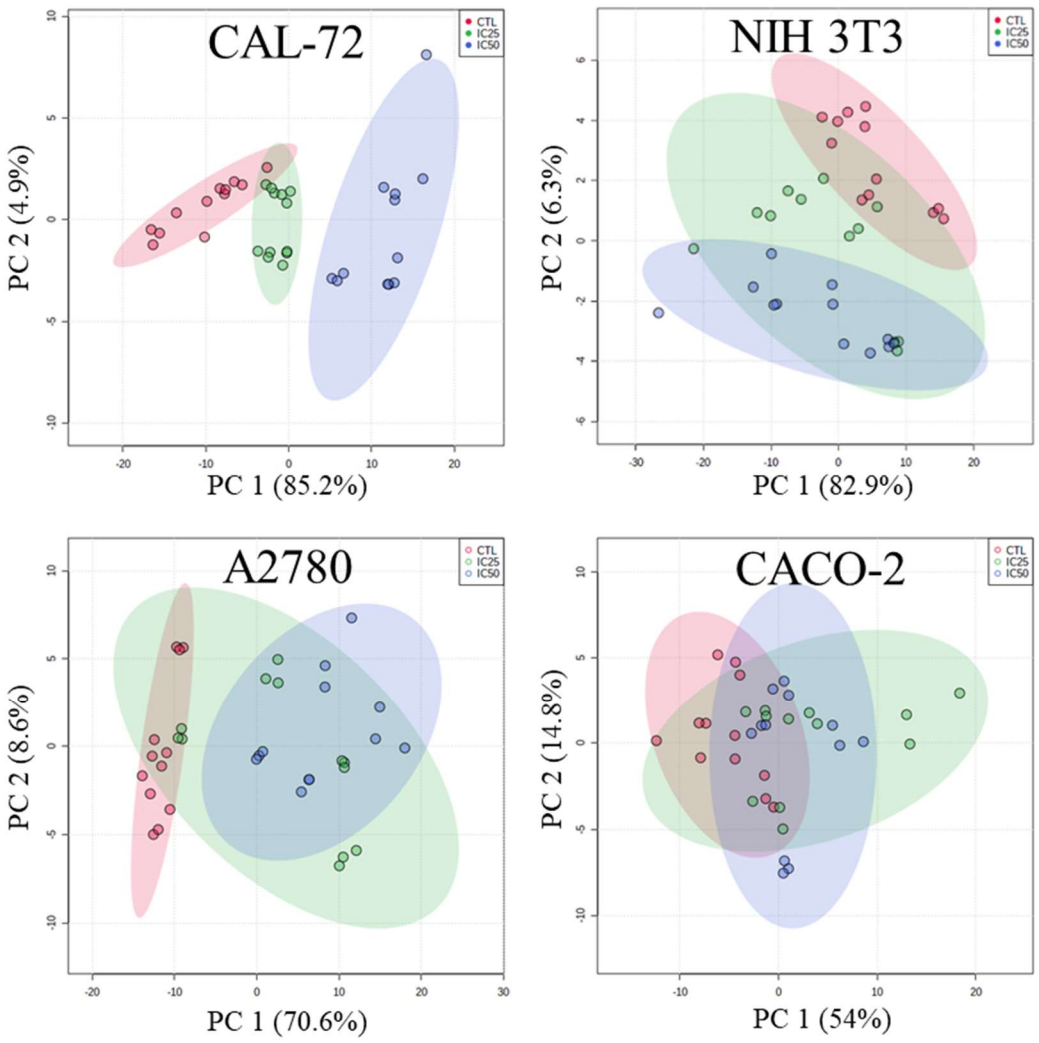

Figure 24. Multivariate analysis PCA of ^{1}H NMR spectra from the CAL-72, NIH 3T3, A2780, and CACO-2 exometabolome.

The robustness of the model was tested using a random permutation test with 2000 permutations (see Supplementary Information). The empirical p-value calculated for all the cell lines was 0.0005 in 2000 permutations, which means that just once in 2000 permutations did the permutated data yield better performance than the original label, indicating that the model is not over-fitted and has a good predictive ability to distinguish between the groups under study.

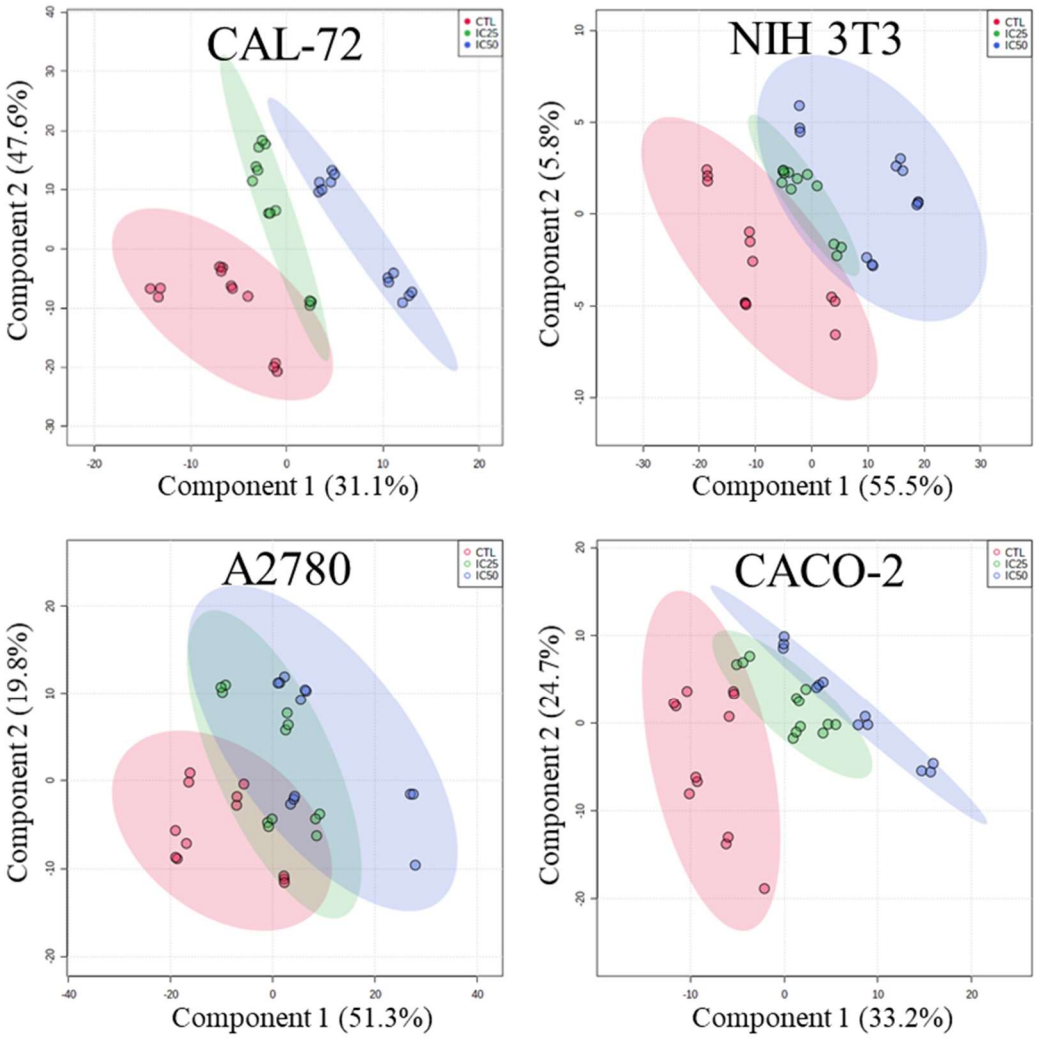

Figure 25. Multivariate analysis PLS-Da of ^{1}H NMR spectra from the CAL-72, NIH 3T3, A2780, and CACO-2 endometabolome.

4. Metabolic variation induced by PAMAM G4NH2

The relative concentrations for the metabolites found were displayed in a heatmap for more precise data visualization. The heatmap transforms a numerical table into a corresponding 2D color map with the hierarchical cluster. The variation in color from "hot" (extremely high) to "cold" (very low) colours indicates data values change and give visual cues about how the data is clustered. Hierarchical clustering uses simple statistical measures to estimate the distance between distinct biological samples, reorganizing the rows/columns with dendrograms plotted on the subsequent side.[190]

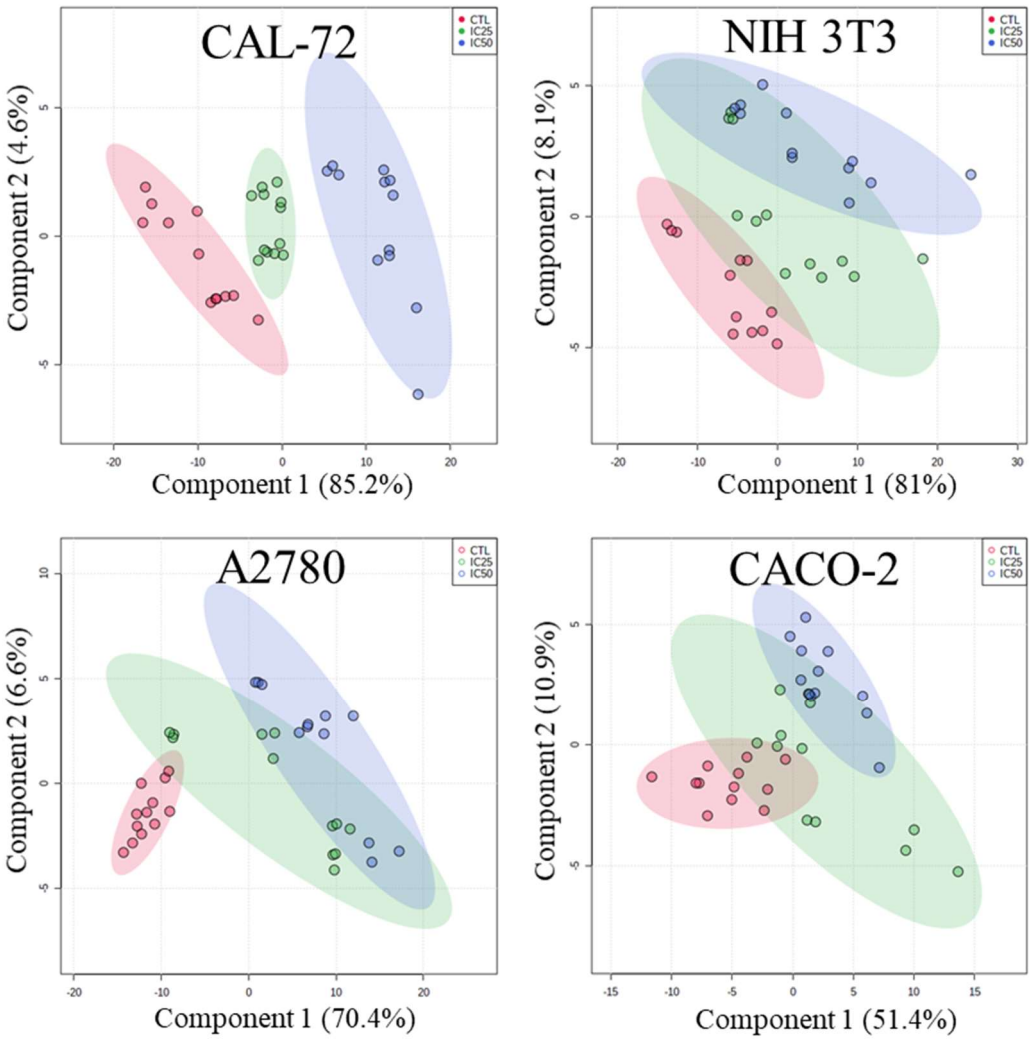

Figure 26. Multivariate analysis PLS-Da of ^{1}H NMR spectra from the CAL-72, NIH 3T3, A2780, and CACO-2 exometabolome.

This heatmap was constructed using Pearson's correlation and Ward algorithm.[191] The hierarchical clustering of our data was performed only on the metabolites (rows), while studies groups (columns) were ordered based on their labels. Each value represents the average of four independent samples.

As noted in Figure 27 and Figure 28, the concentration of all the metabolites exhibited alterations after the treatment with PAMAM dendrimer. These alterations vary with the different cell lines under study. The heatmap shows that the variability of the concentration of some metabolites does not follow a trend when we increase the concentration of dendrimer used. It would be expected that by increasing the dendrimer concentration, these alterations would be more evident, but some metabolites completely reverse the direction of the change.

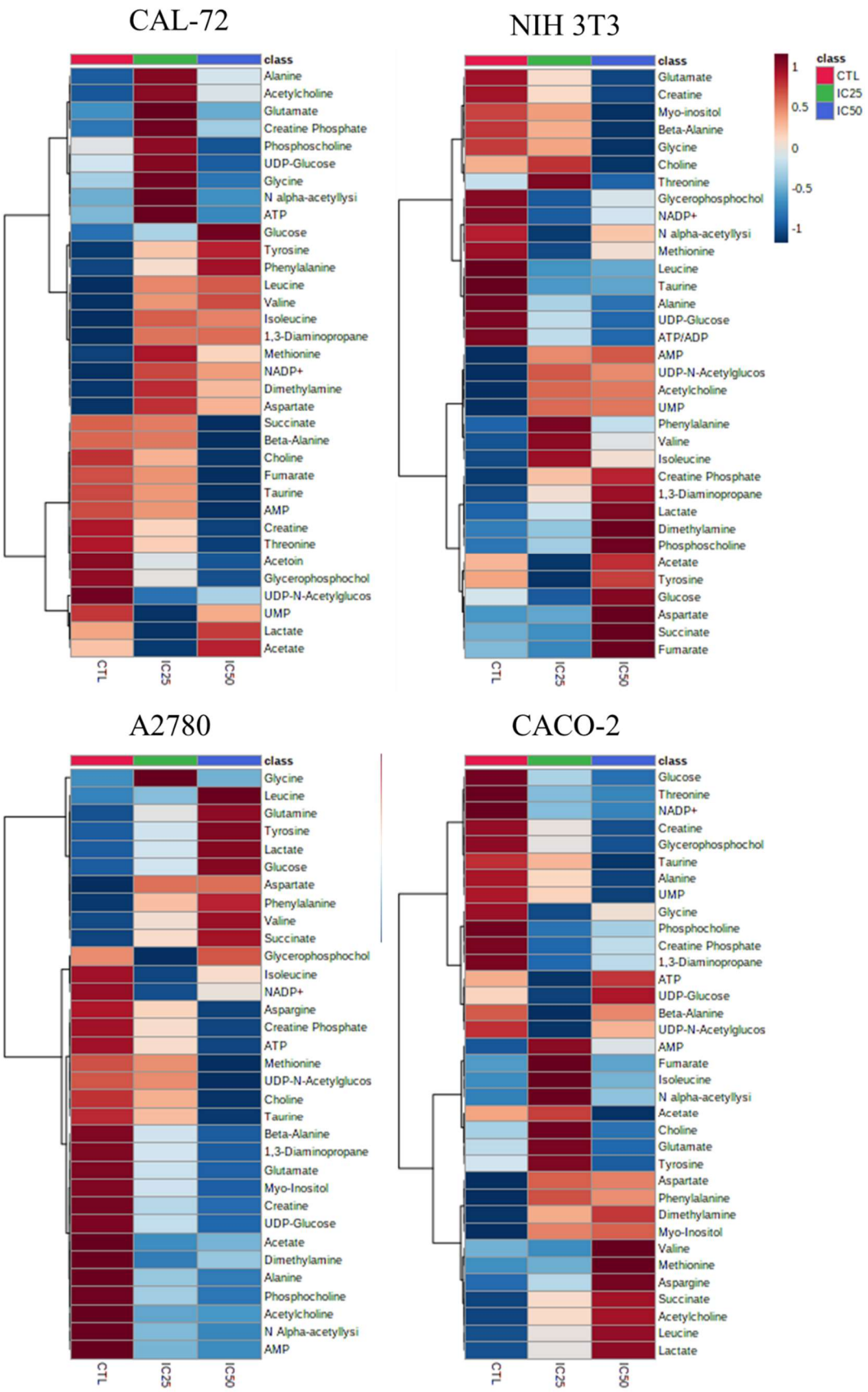

Figure 27. Heat map visualization and hierarchical clustering analysis by Pearson's distance analysis of endometabolome.

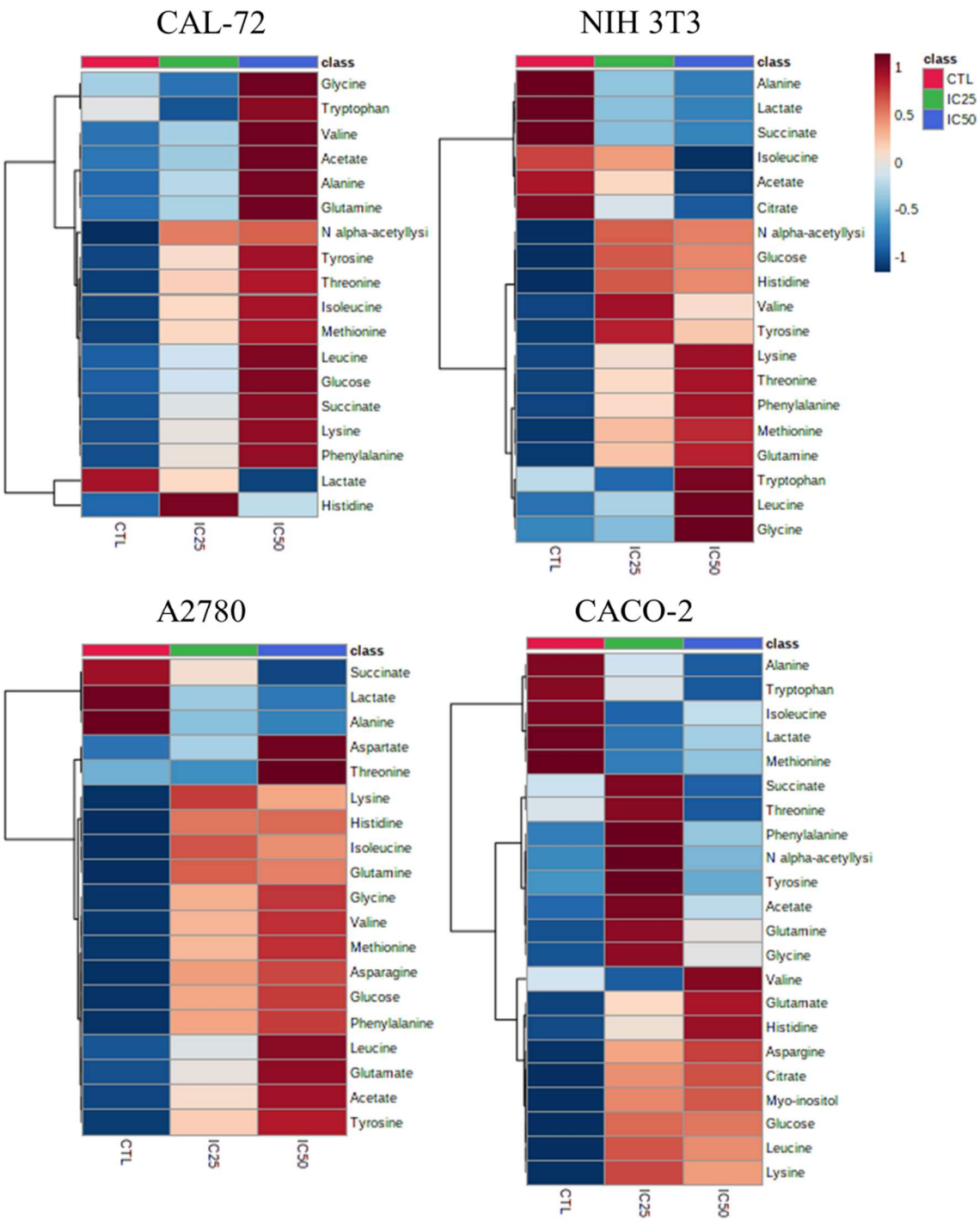

Figure 28. Heat map visualization and hierarchical clustering analysis by Pearson's distance analysis of exometabolome.

The magnitude of the differences for each metabolite in relation to the controls was determined by the percentage of variation and the statistical significance by the ANOVA test to allow a more comprehensive analysis of metabolic variations.

The ANOVA test is used in this context to indicate which cell line was more affected by the treatment with the dendrimer. CAL-72 cell line has 72% metabolites, with a significant difference between the control and the treated cells. In both, endometabolome and exometabolome had the higher percentage of metabolites affected by treatment, followed by A2780 with 46%, CACO-2 with 31%, and NIH 3T3 with 17% of significative affected metabolites. These results are consistent with the cell viability results. Metabolites with significant differences ($p < 0.05$) were considered as potential biomarkers.

The results of the endometabolites and exometabolites affected by the dendrimer were summarized in Table 4 and Table 5, respectively. Only the metabolites with statistical significance were included. In the endometabolome, the affected metabolites belong to the energy-gaining metabolism, glycolysis, and Krebs cycle, amino acids, and phospholipids.

The intracellular metabolites that increased the most in CAL-72 were NADP and glucose, in NIH 3T3 was acetylcholine (the variation was equal in both concentrations of PAMAM), in A2780 was lactate (only when a more toxic concentration was used) and in CACO-2 were N-α-acetyl-lysine and methionite (when used at a more toxic concentration). While those that decreased the most in CAL-72 was glycero phosphocholine, in NIH 3T3 were ATP and alanine, in A2780 was alanine and in CACO-2 was threonine.

The lactate, succinate, glucose, and fumarate metabolites, involved in glycolysis and on the citrate cycle (Krebs cycle), were affected upon exposure of PAMAM G4NH2. Except for the CAL-72 cancer cell line, glucose did not show considerable variations, where the intracellular concentration significantly increased especially after using a higher dendrimer concentration. Lactate metabolite concentration was generally increased except at the lowest PAMAM concentration in CAL-72. The succinate is only significantly affected in A2780 and fumarate when the highest dendrimers concentration is used in NIH 3T3.

Several amino acids altered their concentration significantly upon contact with PAMAM G4NH2. While in the case of n CAL-72 cancer cell line, the amino acids concentration increases, in the case of NIH 3T3, it decreases, except for threonine. This change in amino acid concentration is variable for A2780 and CACO-2 cancer cell lines. Globally, CAL-

72 cell line seems to be more affected than the other cancer cells once intracellular amino acid concentrations increase, which may indicate that the dendrimer causes protein degradation in this cancer cell line.

Table 4. Main metabolite variation in the endometabolome of CAL-72, NIH 3T3, A2780, and CACO-2 cell lines after exposure with different PAMAM G4NH2 concentrations. Signals coloured accordingly with the percentage of variation relative to controls.

		CAL-72		NIH 3T3		A2780		CACO-2	
Concentration		IC_{25}	IC_{50}	IC_{25}	IC_{50}	IC_{25}	IC_{50}	IC_{25}	IC_{50}
Energy generation	Creatine	-	▼*	-	-	▼*	▼*	-	▼*
	Creatine Phosphate	▲*	-	-	-	-	-	-	-
	ATP	▲*	-	▼	▼*	-	-	▲	-
	NADP+	▲*	▲*	-	-	-	-	▼*	▼
Glycolysis and Krebs cycle	Lactate	▼*		▲*	▲*		▲*	▲*	▲*
	Glucose	▲*	▲*	-	-	-	-	-	-
	Succinate	-	-	-	-	▲*	▲	-	-
	Fumarate	-	-	-	▲*	-	-	-	-
Amino acids metabolism	Leucine	▲*	▲*	-	-	-		-	-
	Valine	▲*	▲*	-	-	-	▲*	-	-
	Isoleucine	▲*	▲*	-	-	-		-	-
	Alanine	▲*		▼*	▼*	▼*	▼*	-	-
	Nα-acetyllysine	-	-	▼*	-	-	-	▲*	-
	Glutamate	▲*	-	-	▼*	▼*	▼*	-	-
	β-Alanine		▼*	-	-	▼*	▼*	-	-
	Methionine	▲*	▲*	-	-	-	-	-	▲*
	Aspartate	▲*	▲*	-	-	-	-	-	-
	Taurine	-	-	▼*	▼*	-	-	-	▼*
	Glycine	-	-	-	-	-	-	▼*	▼
	Threonine	-	-	▲*		-	-	▼*	▼*
	Tyrosine	▲*	▲*	-	-	-	-	-	-
	Phenylalanine	▲*	▲*	-	-	▲*	▲*	-	-
Phospholipid metabolism	Acetylcholine	▲*		▲*	▲*	-	-	-	-
	Glycero phosphocholine	▼*	▼*	-	-	-	-	▼*	▼*
Other	1,3-Diaminopropane	-	-	-	-	▼*	▼*	-	-
	UDP-Glucose	▲*	▼*	-	-		▼*	-	-
	Myo-inositol	-	-	-	-	▼*	▼*	-	-

In the case of the exometabolome, the metabolites affected belong mainly to glycolysis and the Krebs cycle, and to amino acid metabolism. The exception is for alanine metabolites which decreased significantly in A2780 cells line, and tryptophan in CACO-

2. In the case of NIH 3T3 cancer cells, only one metabolite shows a significant difference, the lysine.

In general, when compared to the control, PAMAM causes the metabolites to increase in concentration in the extracellular medium. PAMAM-treated cells exhibit a reversal of the metabolite profile when compared to control cells, showing less glucose and amino acid consumption and less lactate metabolite excretion.

In contrast to the intracellular environment, the lactate metabolite concentration decreases in all cell lines compared to the control, but in NIH 3T3 cancer cells, the difference was not so significant. This may mean that PAMAM dendrimers at the concentration studied does interrupt the transport of lactate out of the cells, perhaps by blocking the MTCs.

The glycolytic activity of the cells can be measured by glucose consumption. Our results show that the cells decreased their glycolytic activity after treatment with the dendrimer, mainly in CAL-72 and A2780.

Table 5. Main metabolite variation in the exometabolome of CAL-72, NIH 3T3, A2780 and CACO-2 cell lines after exposure with different PAMAM G4NH2 concentrations. Signals coloured accordingly with the percentage of variation relative to controls.

		CAL-72		NIH 3T3		A2780		CACO-2	
Concentration		IC_{25}	IC_{50}	IC_{25}	IC_{50}	IC_{25}	IC_{50}	IC_{25}	IC_{50}
Glycolisis and Krebs cycle	Lactate	▼*	▼*	-	-	▼*	▼*	▼*	▼*
	Glucose	▲*	▲*	-	-	▲*	▲*	▲	▲
Amino acids metabolism	Leucine	▲*	▲*	-	-		▲*	-	-
	Valine		▲*	-	-	▲*	▲*	-	-
	Isoleucine	▲*	▲*	-	-	▲*	▲*	-	-
	Alanine		▲*	-	-	▼*	▼*	-	-
	Nα-acetyllysine	▲*	▲*	-	-	-	-	▲*	-
	Glutamate	-	-	-	-	▲*	▲*	▲*	▲*
	Methionine	▲*	▲*	-	-	-	-	-	-
	Glycine	-	-	-	-	▲*	▲*	-	-
	Threonine	▲*	▲*	-	-	-	-	-	-
	Tyrosine	-	▲	-	-	▲*	▲*	-	-
	Phenylalanine	▲*	▲*	-	-	▲*	▲*	▲*	-
	Aspargine	-	-	-	-	-	-	▲*	▲*
	Glutamine	▲*	▲*	-	-	▲*	▲*	-	-
	Lysine	-	▲*	▲*	▲*	-	-	▲*	▲*
	Tryptophan	-	-	-	-	-	-	▼	▼*
Other	Acetate	▲*	▲*	-	-	-	-	-	-

5. Pathway analysis by MetaboAnalyst

The impact of the dendrimer was determined by analysis of the metabolic pathways that were possibly disturbed after drug dosage. The MetaboAnalyst 5.0 app web[34] was used to identify the most relevant metabolic pathways involved in the conditions under study. This app offers a variety of tools for metabolomic data interpretation, including metabolite set enrichment analysis and metabolite pathway analysis. The metabolome view map and enrichment overview of CAL-72 endometabolites after treatment with IC_{25} of G4NH$_2$ using KEGG library are shown in Figure 29. The remaining results are in Supplementary Information (Table S2).

Table 2 summarizes the results, where it can be highlighted that the pathway with the highest impact in all cell lines was the phenylalanine, tyrosine, and tryptophan biosynthesis. Despite having selected the database for humans or rats, the algorithm used references metabolomic pathways that are not part of the metabolism of mammals. Animals do not have complete pathways for these three proteogenic aromatic amino acids[192] or any other essential amino acids, which are anabolized only by bacteria, other microorganisms, and plants. However, the results give an idea of what may be happening in the metabolism of cells after treatment with the dendrimer, as they align with the statistical analysis results by highlighting the amino acids and metabolites/metabolisms related to obtaining energy.

Initially, KEGG database was used to carry on the pathway analysis.[35] However, since it was developed before the advent of metabolomics, it is understandable that in this database, the pathway coverage was often insufficient, sometimes incorrect, or occasionally absent, like several key metabolic pathways in mammals (i.e., the malate-aspartate shuttle and electron transfer).[193]

Consequently, a database more specific for pathway elucidation and pathway discovery in clinical metabolomics was employed, SPMDB.[167,193]

The pathway analysis referencing the SMPDB pathway database revealed no metabolic pathways in common between cell lines. Like in the KEGG database, not a specific pathway was shown to be affected by treatment with the dendrimer.

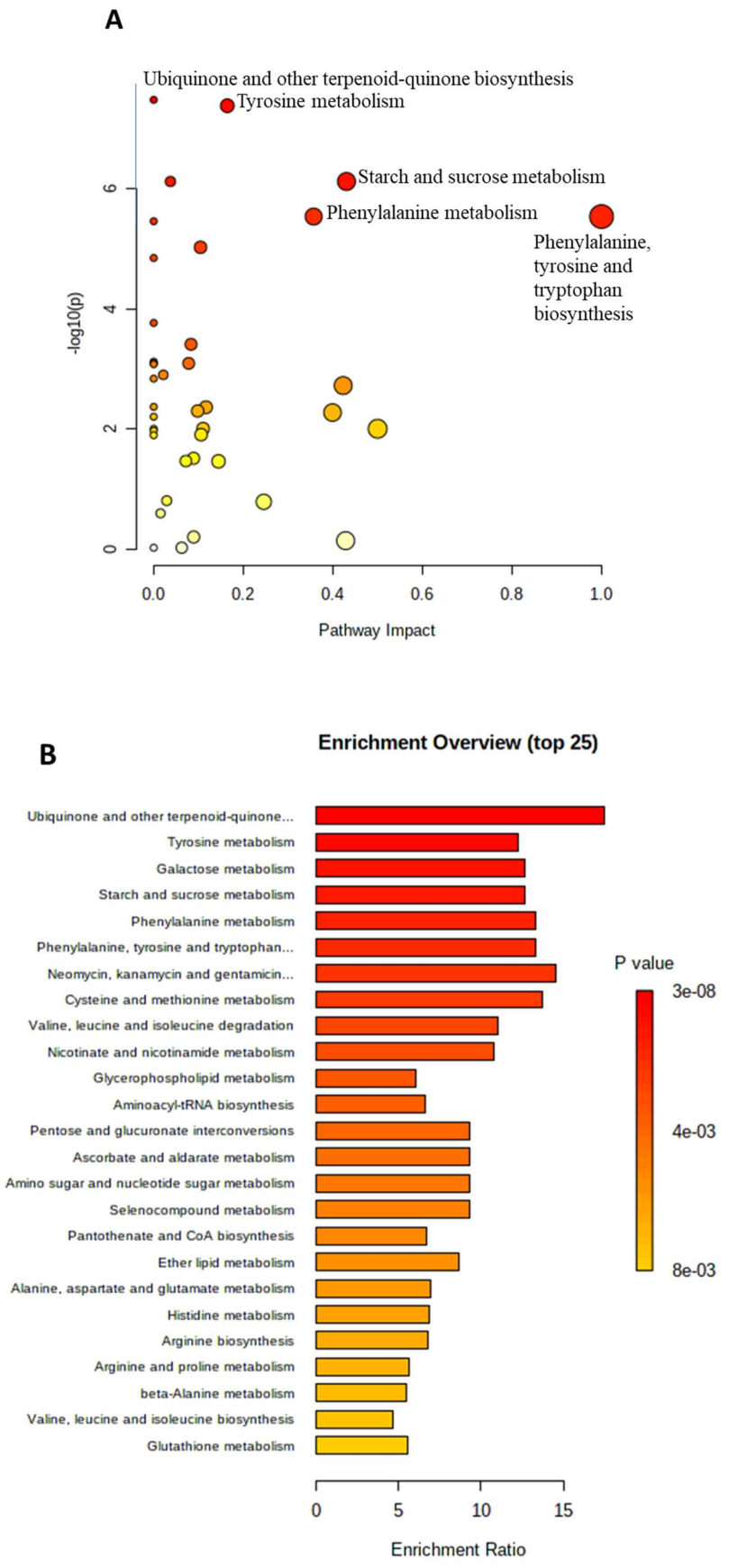

Figure 29. (A) The metabolome view map and (B) enrichment overview of CAL-72 endometabolites after treatment with IC_{25} of G4NH$_2$ using KEGG library.

Table 6. Pathway analysis using Kegg library.

				IC_{25}	IC_{50}
CAL-72	Starch and sucrose metabolism Phenylalanine metabolism Phenylalanine, tyrosine, and tryptophan biosynthesis	Endo	Phenylalanine metabolism Galactose metabolism	Ubiquinone and another terpenoid-quinone biosynthesis Tyrosine metabolism	Valine, leucine and isoleucine degradation Neomicyn, kanamycin, and gentamicin biosynthesis
		Exo	Aminoacyl-tRNA biosynthesis Pyruvate metabolism Phenylalanine metabolism Glycolysis/Gluconeogenesis Valine, leucine, and isoleucine biosynthesis	Galactose metabolism	Pyruvate metabolism Valine, leucine and isoleucine degradation
A2780	Alanine, aspartate and glutamate metabolism Phenylalanine, tyrosine, and tryptophan biosynthesis	Endo	Inositol phosphate metabolism D-glutamine and D-glutamate metabolism Selenocompound metabolism	Propanoate metabolism Glutathione metabolism Porphyrin and chlorophyll metabolism Aminoacyl-tRNA biosynthesis	Arginine and proline metabolism Galactose metabolism Butanoate metabolism Histidine metabolism Arginine biosynthesis Phenylalanine metabolism
		Exo	Glyoxylate and dicarboxylate metabolism D-glutamine and D-glutamate metabolism Starch and sucrose metabolism	Pyruvate metabolism Glycolysis/gluconeogenesis Nitrogen metabolism	Neomycin, kanamycin, and gentamicin biosynthesis Galactose metabolism
NIH 3T3	Phenylalanine, tyrosine, and tryptophan biosynthesis Aminoacyl-tRNA biosynthesis	Endo	Alanine, aspartate and glutamate metabolism Selenocompound metabolism	Taurine and hypotaurine metabolism D-glutamine and D-glutamate metabolism Valine, leucine, and isoleucine biosynthesis	Pyruvate metabolism Glycolysis/gluconeogenesis
		Exo	Biotin metabolism Lysine degradation	Propanoate metabolism Butanoate metabolism	Citrate cycle (TCA cycle) Cysteine and methionine metabolism

				IC_{25}	IC_{50}
CACO-2	Phenylalanine, tyrosine, and tryptophan biosynthesis	Endo	Glycine, serine, and threonine metabolism Valine, leucine, and isoleucine biosynthesis	Aminoacyl-tRNA biosynthesis Primary bile acid biosynthesis Purine metabolism	Taurine and hypotaurine metabolism Ether lipid metabolism Glycolysis/gluconeogenesis Pyruvate metabolism
		Exo	Butanoate metabolism Arginine and proline metabolism Histidine metabolism Alanine, aspartate and glutamate metabolism D-glutamine and D-glutamate metabolism	Glutathione metabolism Porphyrin and chlorophyll metabolism	Arginine biosynthesis

Table 7. Pathway analysis using SMPDB library.

				IC_{25}	IC_{50}
CAL-72	Phenylalanine and Tyrosine Metabolism Valine, Leucine and Isoleucine Degradation	Endo	Phenylalanine and Tyrosine Metabolism Nucleotide Sugars Metabolism Beta-Alanine Metabolism Aspartate Metabolism Transfer of acetyl groups into mitochondria Glycolysis Lactose degradation	Catecholamine Biosynthesis Thyroid hormone synthesis	Valine, Leucine and Isoleucine Degradation Sphingolipid metabolism Galactose degradation
		Exo	Phenylalanine and Tyrosine Metabolism Histidine Metabolism Pyruvate Metabolism Gluconeogenesis Warburg Effect	Threonine and 2-Oxobutanoate Degradation Glucose-alanine cycle	Valine, Leucine and Isoleucine Degradation Ethanol degradation
A2780	Cysteine Metabolism Aspartate Metabolism Pyruvate Metabolism	Endo	Inositol Metabolism Aspartate Metabolism Threonine and 2-Oxobutanoate Degradation Glycine and Serine metabolism	Porphyrin Metabolism Bile Acid Biosynthesis Methionine Metabolism Beta-Alanine Metabolism Carnitine Synthesis	Cysteine Metabolism Inositol Phosphate Metabolism Retinol Metabolism Gluconeogenesis Pyruvate Metabolism

				IC$_{25}$	**IC$_{50}$**
		Exo	Cysteine Metabolism Aspartate Metabolism	Ammonia Recycling Purine Metabolism Pyruvate Metabolism Warburg effect Phenylalanine and Tyrosine Metabolism	Glucose-Alanine Cycle Sphingolipid Metabolism Glycolysis Galactose Metabolism Lactose Synthesis
NIH 3T3		Endo	Bile Acid Biosynthesis Nucleotide Sugars Metabolism Glucose-alanine cycle Tryptophan metabolism Aspartate Metabolism Urea Cycle Selenoamino Acid Metabolism	Taurine and Hypotaurine metabolism	Alanine Metabolism Glutathione Metabolism
		Exo	Biotin Metabolism Lysine degradation Citric Acid Cycle Phenylalanine and Tyrosine Metabolism Carnitine Synthesis Histidine Metabolism	Oxidation of branched chain fatty acids Ketone body metabolism	Betaine metabolism
CACO-2	Aspartate Metabolism	Endo	Glycine and Serine Metabolism Aspartate Metabolism Threonine and 2-Oxobutanoate Degradation	Methionine Metabolism Glutathione Metabolism Carnitine Synthesis Porphyrin Metabolism	Retinol Metabolism Gluconeogenesis Pyruvate Metabolism
		Exo	Cysteine Metabolism Aspartate Metabolism Phenylalanine and Tyrosine Metabolism Citric Acid Cycle Histidine Metabolism Lysine degradation	Folate Metabolism Arachidonic acid Metabolism	Beta-Alanine Metabolism Tryptophan metabolism Inositol Metabolism

However, a trend is observed towards the metabolism of amino acids: phenylalanine, tyrosine, histidine, valine, leucine, isoleucine, glycine, lysine, tryptophan, threonine, and aspartate, indicating that the dendrimer may have an influence in the protein synthesis or could be indicative of protein degradation.

Carbohydrate metabolism also displays alterations in all cell lines but at different phases: glycolysis, gluconeogenesis, Krebs cycle, and galactose metabolism. Even the Warburg effect, where cancer cells convert more glucose into lactic acid than normal cells even in aerobic conditions, shows changes.

6. Discussion of metabolic variations in different cancer cell lines

The integrated analysis of the changes caused by PAMAM G4NH2 mentioned in the previous sections shows the impact on the cellular metabolism of the cell lines studied.

Our results suggest that cells exposed to the dendrimer predominantly affect energy procurement and protein synthesis metabolisms.

Glucose consumption and lactate excretion were considerably affected in treated cells, implying a general impact on glycolytic activity. Intracellular lactate was increased, suggesting that lactic acid fermentation could be enhanced in these cells.

There are different reports about the influence of PAMAM dendrimer on glucose: Owczarek et al.[194] reported that PAMAM dendrimer interacts with insulin is a peptide-hormone involved in the homeostasis of blood glucose levels, Duran-Lara et al.[195] reported that PAMAM G4 presented interaction with glucose present in the blood serum, and Labieniec et al.[196] reports that PAMAM G4 appears to mimic the action of hypoglycaemic agents in reducing plasma hyperglycaemia and long-term markers of poor metabolic control in diabetes. However, until now, no author can precisely the mechanisms underlying carbohydrate metabolism activity.

Another hypothesis could be that the PAMAM dendrimer interacts with FBS and other media components,[131] reducing the effective medium composition and generating a so-called “protein corona” around the dendrimer, as previously reported for nanoparticles in biological media.[197–199] This phenomenon has also been detected in dendrimers.[200–204] The entire metabolism can be compromised because the proteins binding to the dendrimers

are no longer available for their normal functions. Consequently, the energy metabolism would be altered, just as our results show.

Some authors said that the protein-corona effect produced by the serums like FBS[205], BSA[204,206], or HAS[200] was beneficial for use in DDS (Drug Delivery Systems) because it reduces dendrimer toxicity and increases blood circulation time. Nevertheless, later it was found that the interaction with the medium results in an indirect toxicity response by nutrient depletion.[207] Another's study has shown that the supplementation of cell culture medium with serum can influence the metabolism of cells. Due to that, variations in serum can lead to alterations of endometabolites and contamination with exometabolites.[43]

Overall, we can conclude that cells adjust their metabolism even at concentrations that induce minimal changes in cell viability. These changes in metabolites involved in energy and amino acid metabolism (especially Leucine, Isoleucine, and Valine[208]), are consistent with the occurrence of oxidative stress, which is the more common response of the living organism to nanomaterials exposure.[88]

Although the metabolic signatures of PAMAM G4NH2 in the different cell lines have similar characteristics, they have some important differences in how they affect the metabolic network.

7. Conclusion

This study used metabolomics methods to assess the metabolic profile of the PAMAM dendrimer G4NH2 in different cell mammalian lines, using ^{1}H NMR combined with data analysis tools.

Based on statistical analysis results, a successful differentiation and discrimination of samples were achieved between the groups. The PAMAM dendrimer G4NH2 seems to affect human cancer cells more than normal mouse cells, especially in the osteosarcoma cell line.

The metabolic pathway analysis indicated that the discriminatory metabolites potentially originated from energy and protein metabolism. The origin of this effect it's unclear due to the possibility of it being a usual response of the cells to a nanomaterial or a result of the protein-corona phenomena.

These observations are intriguing and may disclose important explanations in more in-depth investigations. Further studies will have to be done to understand the effects of dendrimers in the metabolism using other conditions, such as without FBS, to discharge the possible effect of protein-corona phenomena.

The analysis of the various metabolic profiles demonstrated that NMR metabolomics is a powerful tool for molecular profiling of nanomaterials' effects on cells.

Chapter 4 – CATDEN cinnamic acid terminated PAMAM dendrimers

Our previous results demonstrate that PAMAM dendrimers affect energy-gathering mechanisms such as the carbohydrate and amino acid pathways. One of the most interesting pathways affected by dendrimer is the well-known Warburg effect, where cancer cells reprogram glucose metabolism.[66]

Encapsulating therapeutic agents in nanocarriers increases their efficacy, specificity, and targeting ability since the carrier protects the payload from premature degradation in the biological environment, enhances its bioavailability, and promotes cellular uptake.[209]

Doxorubicin (DOX), one of the most widely used chemotherapeutic drugs for the treatment of cancer, shows insufficient cellular uptake and, in addition, drug resistance.[210] For these reasons, various nanocarrier systems have been developed to deliver DOX efficiently to cancer cells.

Dendrimers can potentially be used as drug vehicles due to their capability to reach solid tumour sites, for example, by active targeting after adequate chemical functionalization.[172,211]

The most studied inhibitor of this effect is the α-cyano-4-hydroxycinnamic acid (ACCA) which was recently used as a vector of nanoparticles for targeted cancer therapy and to avoid oxidative stress. Therefore, it can be used to develop novel drug delivery systems to target cancer cells.[84]

In this work, PAMAM G4NH_2 dendrimer was functionalized with ACCA and studied for the encapsulation of DOX and its subsequent release.

1. Synthesis and characterisation of CATDEN

Systematic synthesis optimization was performed to functionalize the cinnamic acid onto the dendrimer, maintaining the general procedure of the carbodiimide reaction approach. The conditions that were tested are shown in Figure 30.

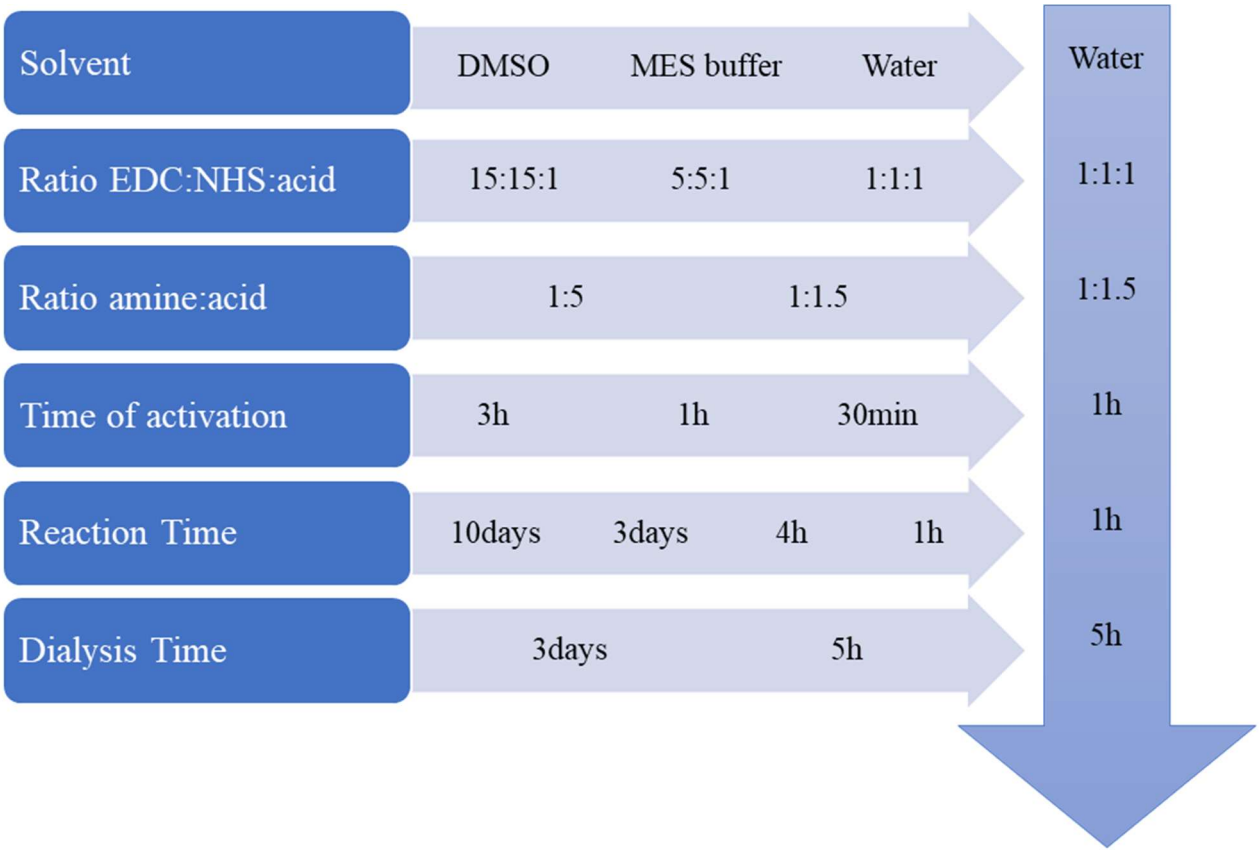

Figure 30. Conditions for reaction optimization.

DMSO was tested because ACCA is poorly soluble in aqueous solutions, but the activation reaction does not occur in this solvent. Following the literature[212], the MES buffer was tested, but it seems to interact with PAMAM (result not shown). When trying the reaction with water, it was noticed that after a few minutes, that ACCA starts to solubilize, and according to the NMR analysis, it binds to EDC.

Regarding the ratio of EDC:NHS, we started with a large ratio to make sure that all the acids were activated, but when following the reaction by NMR, we realized that the EDC was hydrolyzed and the activation reaction did not progress. We decreased the ratio and concluded that 1:1:1 was sufficientfor the reaction to take place. Therefore, we also optimized the ratio EDC:acid to spend fewer initial reagents.

With the ratios optimized, the time variable was the next step to be maximised. As so, we decreased the reaction time, and the best result was obtained in 1h, with the yield increasing close to 100%.

At first, we followed the standard dialysis process of the lab, but to avoid product loss, we tested whether we could remove the reaction intermediates in less time. Our conclusion led us to set a minimum of 5h for the complete clean-up of the reaction intermediates.

To obtain various degrees of functionalization, the proportion of acid versus amines to be functionalized was also optimized. The best ratio is 1.5 acids per 1 amine, where if we want to functionalize the 64 amides of the dendrimer, it is necessary to add 96 acids.

The procedure that achieves an efficient reaction with less amount of reagent and reaction time was followed to obtain different levels of ACCA functionalized dendrimer (Figure 31).

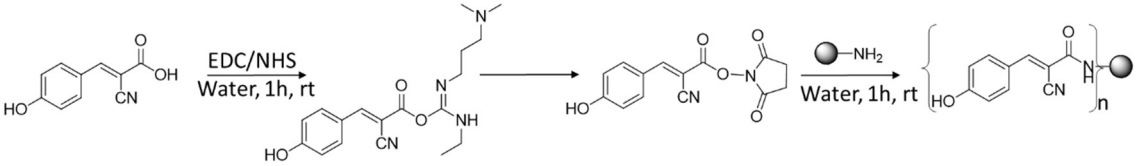

Figure 31. Schematic representation of ACCA functionalization.

The cinnamic acid was activated using a carbodiimide and a hydroxysuccinimide in water at room temperature. After 1h of activation, the PAMAM G4NH_2 (dissolved in water) was added drop by drop to the solution. After 1h more, the reaction was stopped, and the crude was purified by dialysis.

Various degrees of modification were obtained using a different molar ratio of ACCA to amine groups of dendrimers.

The CATDEN dendrimers were characterised by ^{1}H- and ^{13}C-NMR, FTIR, and UV-Vis spectroscopies, mass spectrometry, elementary analysis, and zeta potential techniques.

NMR spectra (Figure 32) of the final products reveal the presence of the characteristic cinnamic acid protons, which were conspicuously absent in the parent PAMAM dendrimers. The changes in the electronic distribution of the dendrimer signals indicate

that the desired product was obtained. The ACCA characteristic signals are shifted to upfield, meaning that the conjugation with the dendrimer shields the nearby protons.

The integration ratio between the protons of PAMAM G4NH$_2$ and the protons of ACCA suggests that dendrimers carried 25, 32, 48, and 64 ACCA groups, respectively. Considering that generation 4 of the PAMAM dendrimer has 64 surface groups: when 25 ACCA are linked to the dendrimer, the functionalization degree represents 39%, if 32 ACCA are linked, 50% of functionalization degree was achieved, 48 ACCA linked to the dendrimer represents 75% of functionalization, and 100% of functionalization degree is obtained when 64 ACCA are linked to the PAMAM dendrimer.

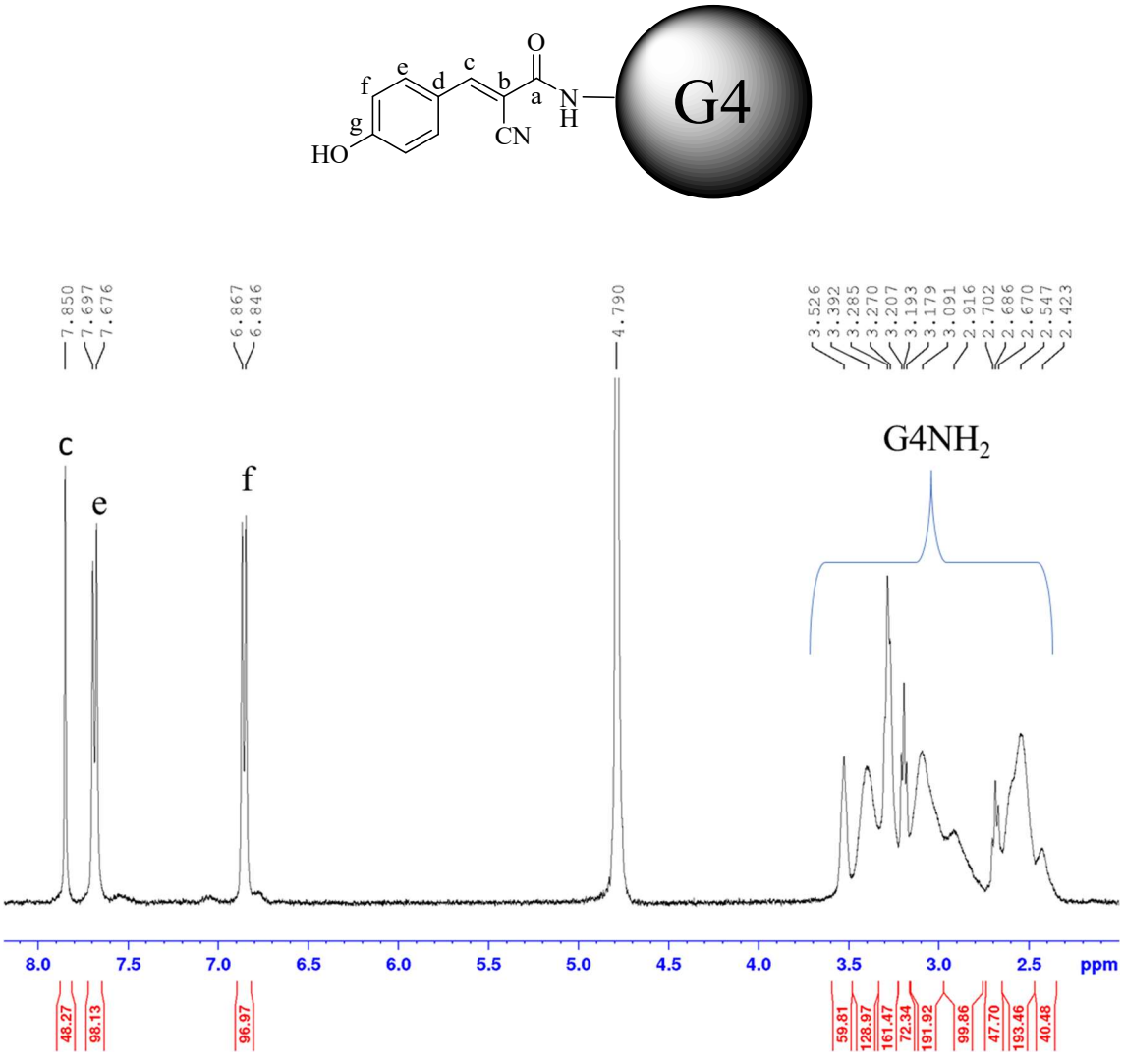

Figure 32. ^{1}H NMR spectrum of G4NH2-48ACCA in D_2O.

In the ^{13}C NMR (Figure 33), it was possible to identify and verify that all the signals of the cinnamic acid appear in the spectrum, and the characteristic signals of PAMAM are slightly shifted to the downfield. 2D HSQC proton-nitrogen was also performed to observe the nitrogen profile of our new dendrimer. When compared with the profile of commercial PAMAM we observed the same 3 signals, but these are shifted.

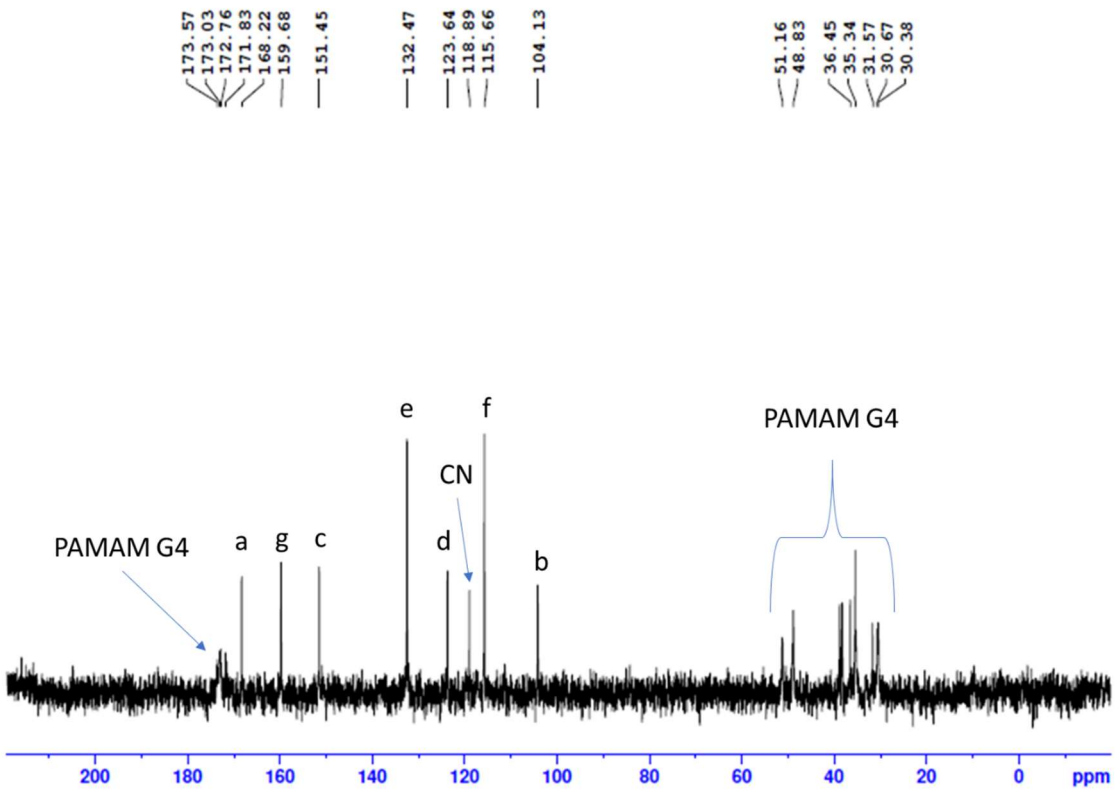

Figure 33. ^{13}C NMR spectrum of G4NH2-48ACCA in D_2O.

The cinnamic acid dendrimers were characterised by MALDI-TOF-MS spectrometry analysis (Figure 34). The average MWs of the CATED determined by MALDI were somewhat different from those calculated from ^{1}H NMR. The difference may be related to the broad signals in the MALDI-TOF spectra, which do not reflect the average absolute molar mass. Unlike the analysis based on NMR, average MWs estimated by MALDI vary slightly depending on the specific conditions applied or by the chemical nature of samples affecting fragmentation patterns.[213–215] However, the major molar mass of each dendrimer sample can be used to compare the starting materials and the functionalized dendrimers. The spectra clearly showed that all dendrimers' major molar mass fraction shifts toward higher m/z ratios after surface modifications with different cinnamic acid groups ratios compared to the starting material.

These results confirm the surface modification, although the degree of the substitution cannot be estimated. Our MALDI-TOF measurements are in agreement with the literature showing broad signals of PAMAM dendrimers in higher generations.[216,217]

The results of the calculated elemental analysis were not the same that the theoretical ones, probably because our entire family of dendrimers is very hygroscopic. The carbon percentage decreases with the decrease of the functionalization level, and the nitrogen percentage increases. Despite the differences observed, the results are consistent between them.

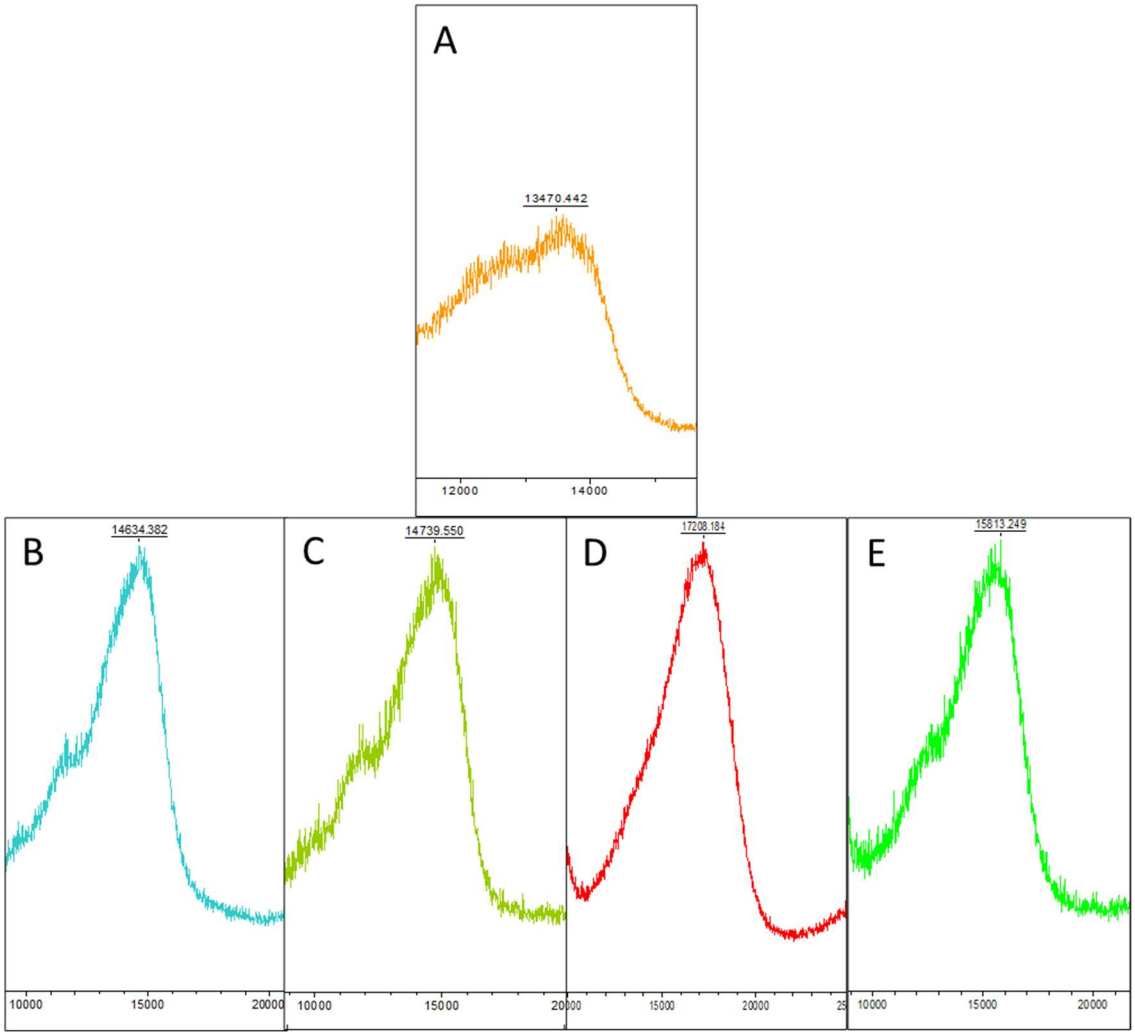

Figure 34. MALDI TOF spectra of CATDEN. A-) native PAMAM dendrimer, B-) G4NH2-25ACCA, C-) G4NH2-32ACCA, D-) G4NH2-48ACCA, E-) G4NH2-64ACCA.

FITR spectroscopy was conducted to characterize and confirm the formation of new functional groups in the cinnamic acid terminated dendrimers (Figure 35). The band corresponding to primary amino groups of PAMAM (3200-3300 cm^{-1}) decreases intensity

as expected due to the amide formation with the cinnamic acid. The dendrimer with more ACCA functionalization shows the lowest intensity of the primary amino band. The C≡N stretching band of the cyano group appears in the functionalized dendrimer (2211 cm^{-1} and 2209 cm^{-1}) and is shifted compared with the commercial ACCA[218] (2230 cm^{-1}). The characteristic absorption bands of amide I and II in the region between 1631 and 1542 cm^{-1} are shifted and merged themselves with the peaks of the carboxylic acid of cinnamic acid, thus confirming the involvement of–COOH of ACCA and $–NH_2$ of G4 PAMAM in the formation of the conjugates.

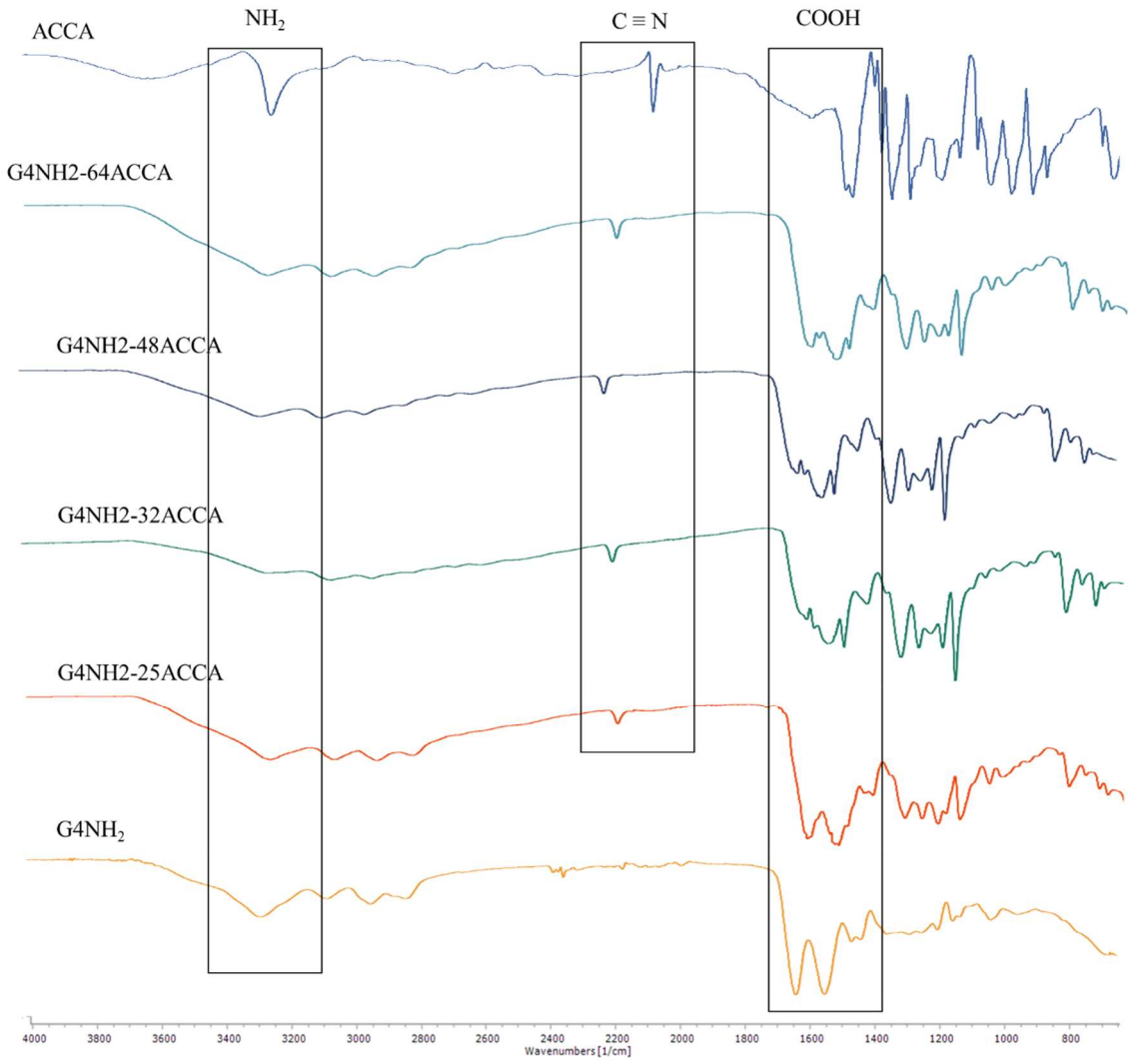

Figure 35. ATR-FTIR of the CATDEN dendrimers family vs. G4NH2 and ACCA.

UV-vis spectroscopy has proven to be a useful tool for studying the effect of functionalization in the electronic characteristics of the dendrimers.[219] Due to the poor

solubility in water of the commercial ACCA, CATDEN (1µM) and the commercial PAMAM G4NH2 (50µM) were dissolved in PBS. Figure 36 shows the absorbance spectrum of the CATDEN and the commercial starting reagents.

The spectra analysis showed that PAMAM dendrimers (G4NH2) have a small shoulder from the native dendrimer that emerges at around 290nm and no prominent absorbance until 1000 nm due to their aliphatic molecular backbones.[220] In contrast with the G4NH2, the CATDEN spectra exhibited 3 strong bands, similar to the commercial ACCA bands. The intensity of these bands appears to increase with the number of ACCA linked, which is additional evidence of the success of the functionalization process.

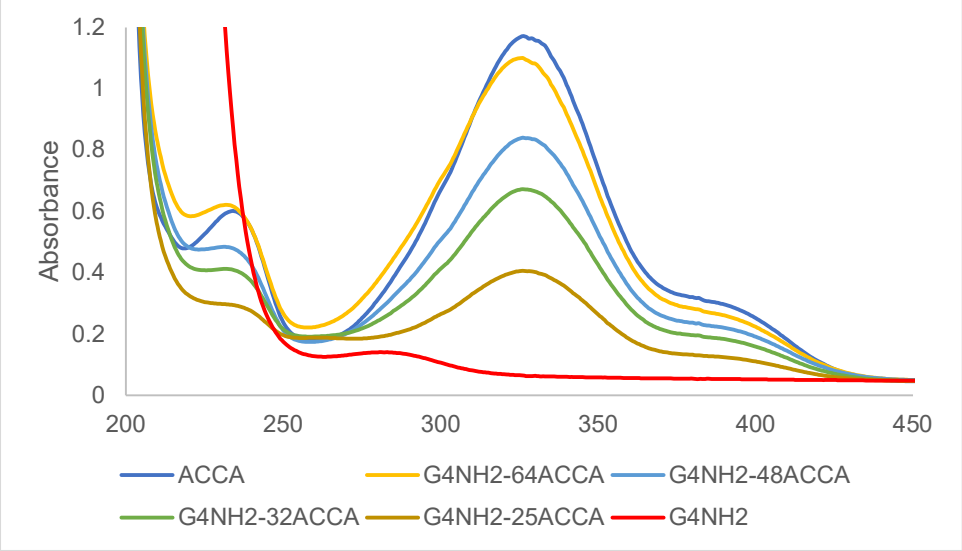

Figure 36. UV-Vis spectra of CATDEN in PBS (1µM and commercial G4NH2 and ACCA at 50µM).

The intrinsic fluorescence of the prepared dendrimers has eevaluated to see if it can be traced without being marked with a fluorescent probe that interferes with their biological properties[221]. Intrinsic fluorescence emission of PAMAM dendrimers was investigated to identify the maximum wavelength optically detectable within cells.[221–224]

Fluorescence spectroscopy was employed to analyse the modifications in the fluorescence profile of the dendrimer with the cinnamic acid functionalization. The CATDEN family of dendrimers was dissolved in PBS at 2µM. Figure 37 and Figure 38 show the excitation

and emission fluorescence spectra of native and CATDEN dendrimers in an aqueous solution.

Dendrimers were excited at 330 nm (characteristic λ_{ex} of ACCA[225]) and 390nm (characteristic λ_{ex} of PAMAM dendrimer[221]). An emission band can be detected for both cases in the blue spectral region between 425 and 450nm, respectively. The fluorescence intensity at 425nm was in inverse proportion to the level of functionalization, while at 450nm it had the opposite behaviour. The functionalization may affect the quenching effects related to the proximity of the ACCA peripheral groups[221]. Another hypothesis is that a FRET (Fluorescence resonance energy transfer) effect may be happening between the ACCA (acting as a donor) and the PAMAM dendrimer (acting as an acceptor), how Lard et al.[226] describe between PAMAM dendrimer and phenanthrene. More studies need to be done to confirm this hypothesis.

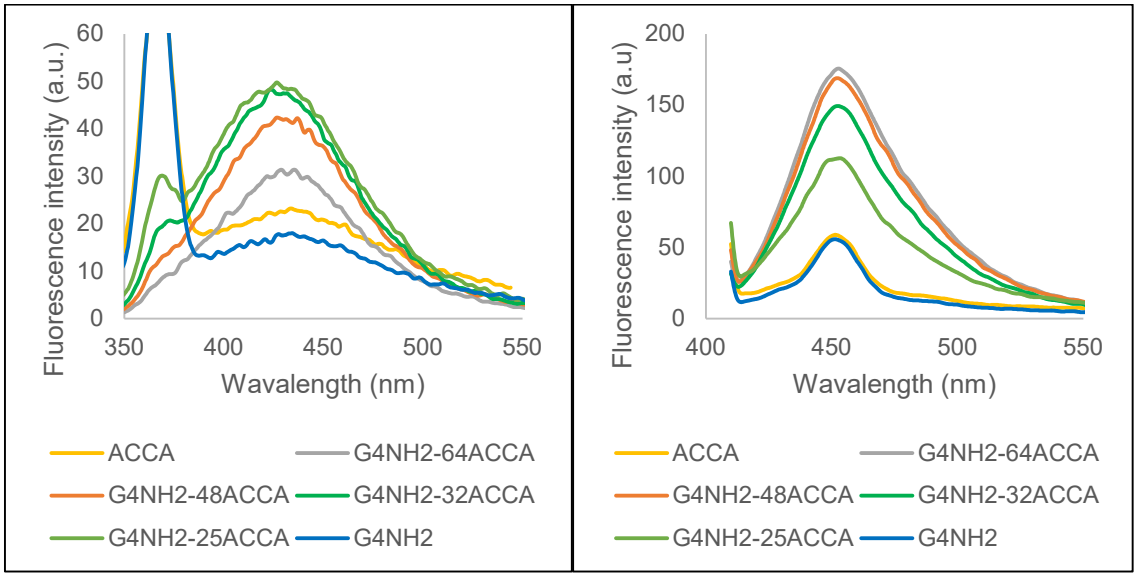

Figure 37. Emission spectra of CATDEN at λ_{ex}330 (left) and λ_{ex}390 (right) in PBS.

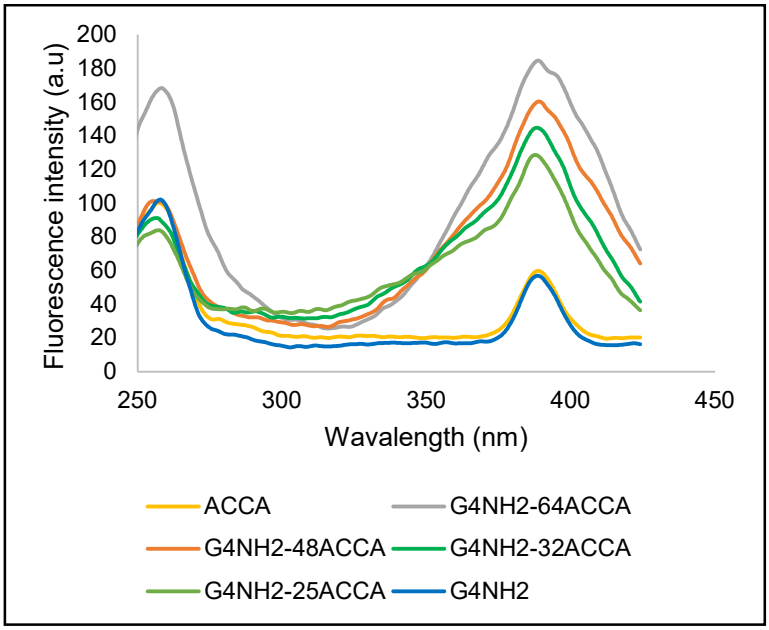

Figure 38. Excitation spectra of CATDEN in PBS.

The zeta potential of CATDEN was measured to determine the electrostatic potential at the surface, which is related to the dendrimer surface charge. The dendrimers were dissolved in 4 different dispersants: water, PBS, DMEM, and RPMI at a concentration of 1mg/ml, and these values are shown in Figure 39.

The observed zeta potential values in the CATDEN family were positive when dispersed in water and negative when dispersed in PBS and cell culture medium. The data indicated that the dispersant influenced the results. Some authors had already described this behaviour with other cell culture mediums.[131,227] Zeta potential is conditional on the particle and dispersant interface, so differences in the zeta potential value in different dispersants are expected.

Kumar et al.[228] related the zeta potential of nanoparticles with the stability of the colloid. Values greater than 30 mV (positive or negative) have high degrees of stability, less than 25mV (absolute values) have incipient instability, and near-zero tends to agglomerate. As so, we can assume that depending on the medium culture media tested, dendrimers tend to interact with the dispersant's components, aggregating when dispersed in PBS, DMEM, and RPMI and being more stable in water.

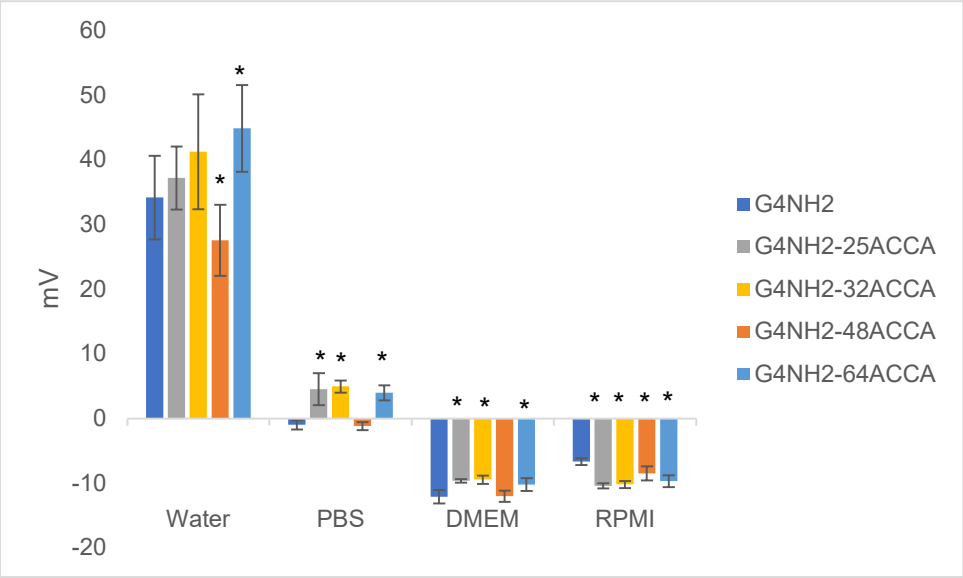

*Figure 39. Zeta potential of CATDEN. * The data represent the mean ± SD of three independent experiments performed in triplicate. *: p<0.05 vs G4NH2.*

2. Mechanistic proposal for the preparation of CATDEN dendrimers family

The direct reaction between an acid and an amine can be achieved at a high temperature, but this is usually incompatible with the presence in the molecule of other functional groups. As so, it is necessary to activate the acid, using a leaving group to the acyl carbon of the acid to allow attack by the amino group.[229] Carbodiimides like dicyclohexyl carbodiimide (DCC), diisopropyl carbodiimide (DIC), and 1-ethyl-3-(3′-dimethylamino)carbodiimide HCl salt (EDC·HCl) are frequently used as coupling reagents for amide bond formation under mild reaction conditions.[229] EDC·HCl has been widely used for conjugation in aqueous media[230] because the resulting urea is water-soluble[229], and thus easily removed by washing or dialysis. However, the reaction is slow in aqueous solutions and the intermediate that does not react with amine results in hydrolysis. To avoid this unstable intermediate, N-hydroxysuccinimide (NHS) was included in EDC coupling protocols to improve efficiency in forming an NHS ester that is considerably more stable and soluble than the O-acylisourea intermediate.[231,232]

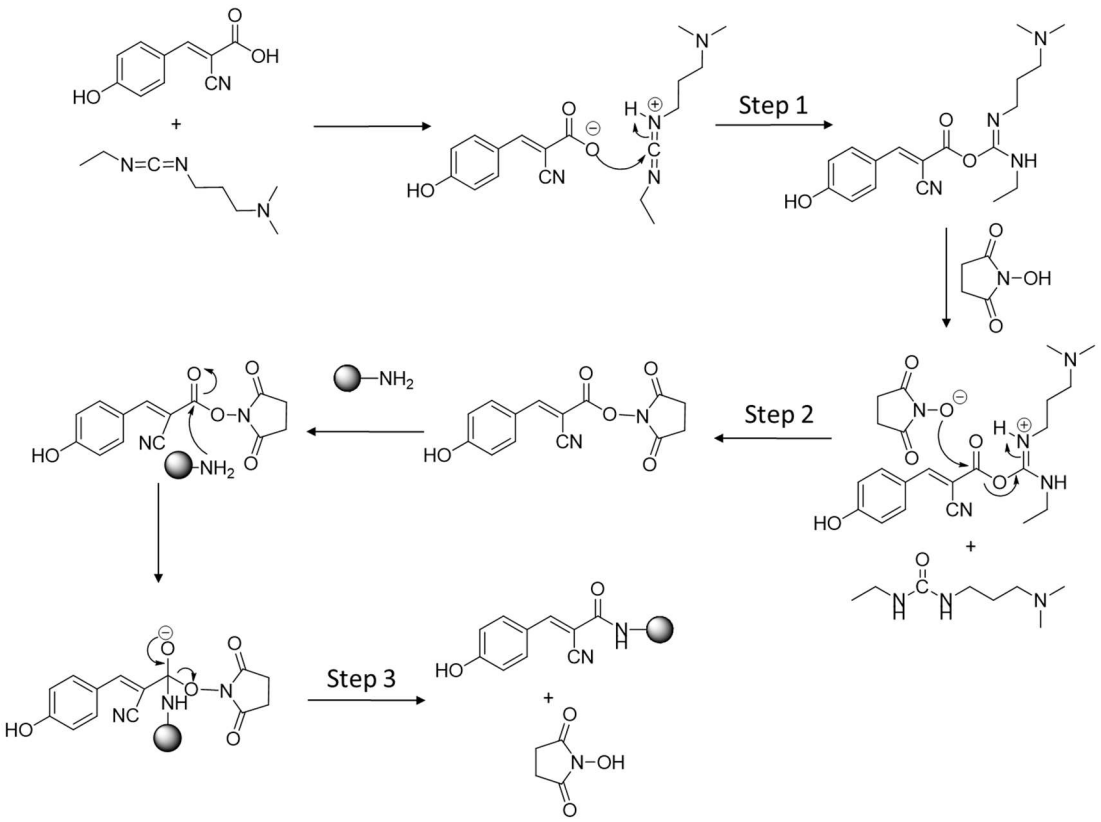

Figure 40. Suggested mechanism for the preparation of CATDEN dendrimers family (adapted [233]).

Arrived at this point, considering the previous characterisation of the new CATDEN dendrimers, based on what is reported in the literature[229,231,232], a mechanism for the reaction of ACCA with PAMAM G4NH2 (Figure 40), leading to the formation of CATDEN (Figure 41) was proposed next.

The ACCA reacts with EDC to form the highly reactive O-acylisourea (Step 1), which then reacts with the NHS to form the NHS ester intermediate (Step 2), which can be viewed as a carboxylic ester with an activated leaving group. This NHS-intermediate is easily displaced by nucleophilic attack from primary amino groups present in the surface dendrimer to give the desired amide bond (Step 3). In the end, the EDC by-product, released as a soluble urea derivative, is the driving force of this reaction.

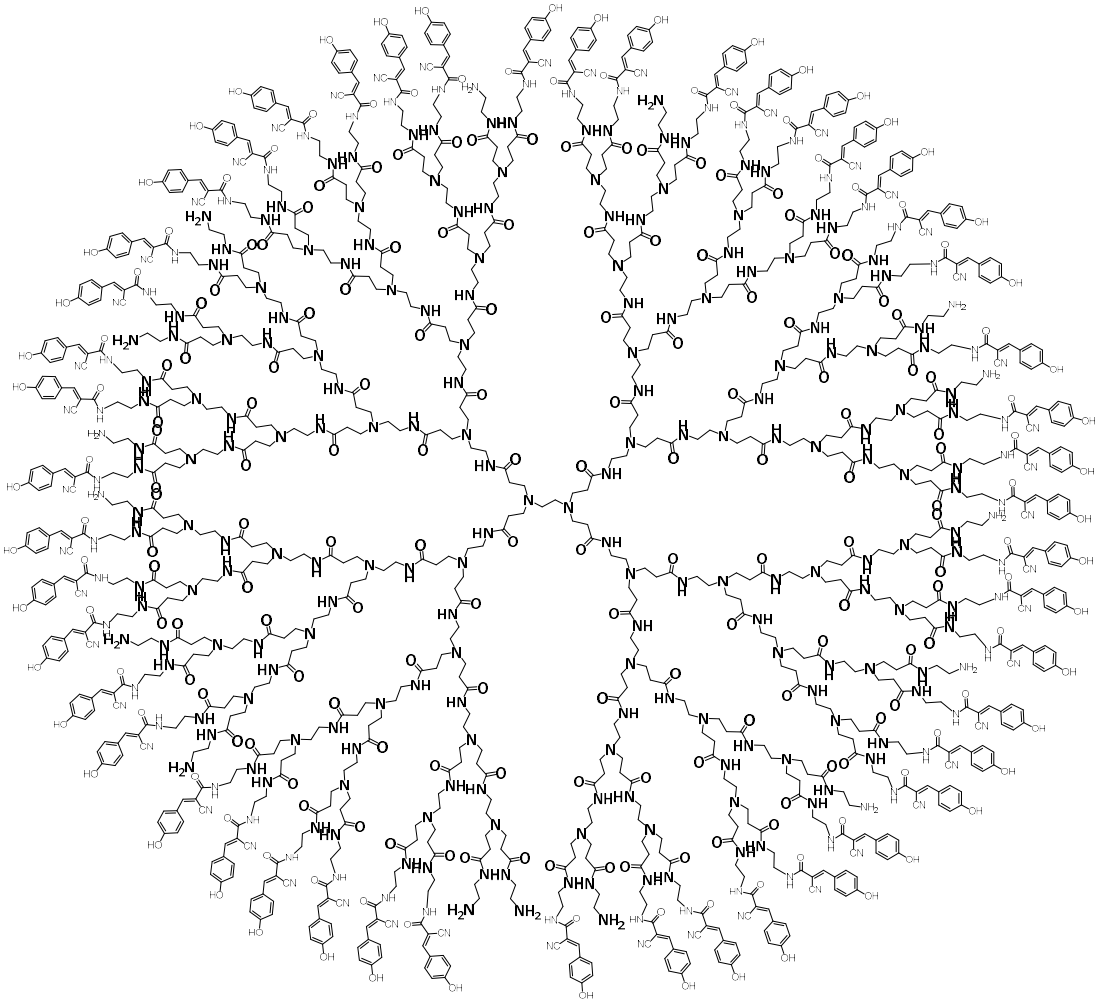

Figure 41. Proposed structure for G4NH$_2$-48ACCA dendrimer.

3. Cytotoxicity of CATDEN dendrimers

The cytotoxicity of dendrimers is a well-debated topic. The positive charges carried out by the primary amino groups on the surface of the cationic dendrimers interact with the negatively charged cell membranes causing adsorption of the dendrimer and leading to the rupture and dissolution of cell membranes.[234,235] Any change in the number of surface amino groups could affect the dendrimer's cytotoxicity. Therefore, the cytotoxicity of PAMAM dendrimers and their derivatives is generation-dependent.

In this study, mitochondrial metabolic activity was measured using the resazurin assay. Human osteosarcoma cell lines (CAL-72), which demonstrated being the most affected by dendrimer in the previous chapter, were treated with PAMAM dendrimer having different ACCA numbers on the surface at different concentrations (Figure 42). Cell

viability is expressed relative to the negative control established by cell exposure only to cell culture medium (values set at 100%).

As expected, results revealed that cytotoxicity increases with dendrimer concentration and, in general, due to the reduction in the number of amino groups on the dendrimer surface, decreases with the increase of the functionalization. This trend is more significant when the number of ACCA on the dendrimer surface is lower (G4NH2-25ACCA) than when its number is higher. For that reason, the differences in terms of cytotoxicity between G4NH2-48ACCA and G4NH2-64ACCA are not relevant.

Synergistic anticancer effect studies were carried out to understand the potential accumulative effect of dendrimer and acid in terms of cytotoxicity. A synergistic effect results from the positive drug's interaction, which combined produce an effect that is greater than when they are used individually. The opposite effect is called antagonism.[236] The combined effect of PAMAM $G4NH_2$ and ACCA against CAL-72 was assessed by using the cell viability assay (resazurin assay).

For this purpose, the concentration of G4NH2 and ACCA was used to induce 50% of cell death, as previously determined. We observed that the treatment combining the determined IC_{50} for $G4NH_2$ and ACCA resulted in higher cytotoxicity than the treatments with isolated drugs (Figure 43). This means that, at this concentration, a synergistic effect exists between the native dendrimer and the ACCA.

Another approach to test the combined effect was using the amount of G4NH2 previously determined to induce 50% of cell death fixed plus the equivalent of ACCA to achieve each functionalized already obtained.

In Figure 44, the results show that the cytotoxicity of G4NH2 was not affected by the addition of the equivalent amount of the ACCA. Also, when they were exposed to the different concentrations of ACCA alone, the cell viability was not significantly affected.

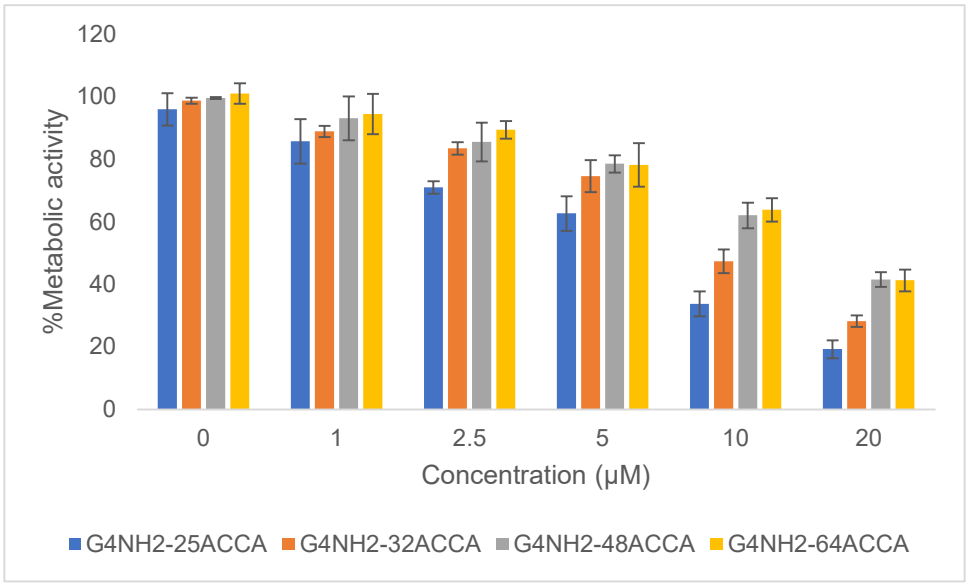

	G4NH2-25ACCA	*G4NH2-32ACCA*	*G4NH2-48ACCA*	*G4NH2-64ACCA*
IC_{50}	7.25±0.90	9.67±1.15	15.67±2.08	16.67±0.76
IC_{25}	2±0.50	4.83±0.76	5.83±1.61	6.08±1.84

Figure 42. Dose-curve of CATDEN dendrimers against CAL-72 cells after 24h of treatment and calculated IC_{50} and IC_{25} values.

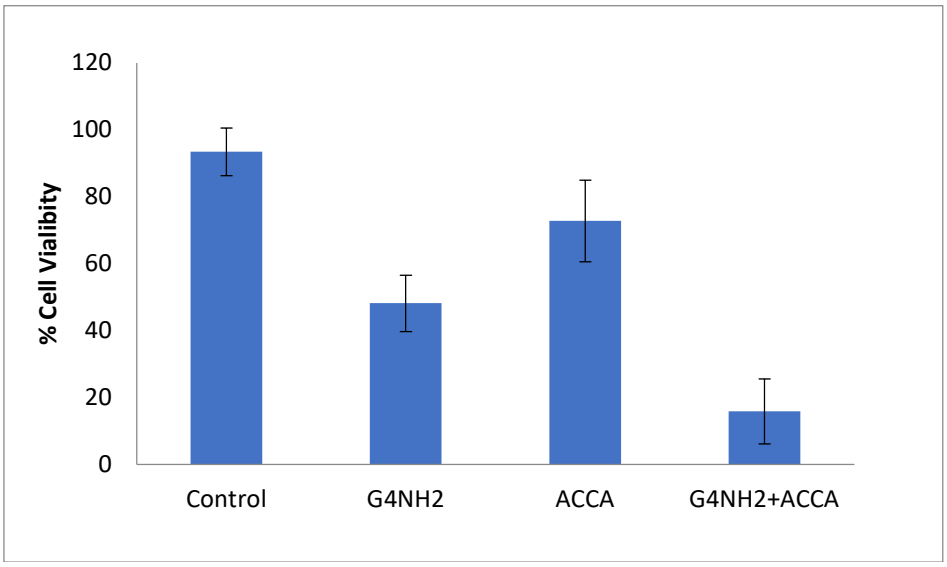

Figure 43. Cytotoxic combined effect using both PAMAM dendrimer and ACCA at IC_{50} previously calculated.

This result confirms that the decrease in the cytotoxicity of CATDEN versus pristine PAMAM dendrimers results from a reduction in the number of surface amines due to covalent functionalization with ACCA and not to the antagonist effect between G4NH2 and ACCA.

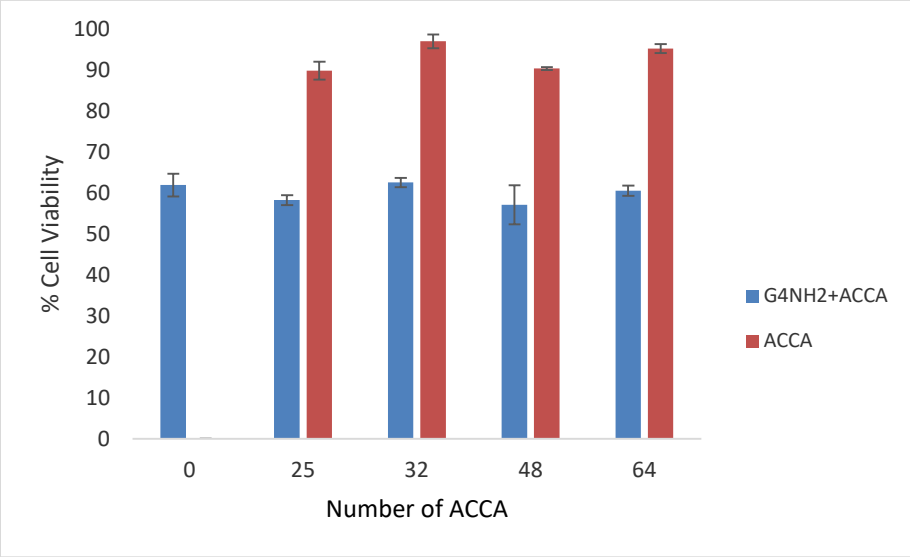

Figure 44. Cytotoxic effect of G4NH2 when added the equivalent of ACCA to achieve each functionalized already obtained.

4. Encapsulation of doxorubicin in PAMAM and CATDEN dendrimer (PAMAM G4NH2-48ACCA)

Based on the characterisation, the dendrimer with 48 bound acids was selected to investigate the drug delivery capacity of the new CATDEN.

Due to its broad spectrum of activity, DOX is one of the most widely used chemotherapeutic drugs as a first-line treatment for various cancer types. However, the use of DOX presents several drawbacks, such as cardiovascular toxicity and dose-dependent myelosuppression being the most relevant.[178]

The encapsulation was accomplished using the methodology followed by our group[152] Commercial G4NH2, or G4NH2-48ACCA dendrimers were dissolved in distilled water and combined with doxorubicin hydrochloride, dissolved in methanol and neutralized with triethylamine. After stirring overnight, the free DOX was precipitated by centrifugation. The free DOX precipitate was analysed by UV-Vis spectroscopy to quantify the non-complexed free DOX.

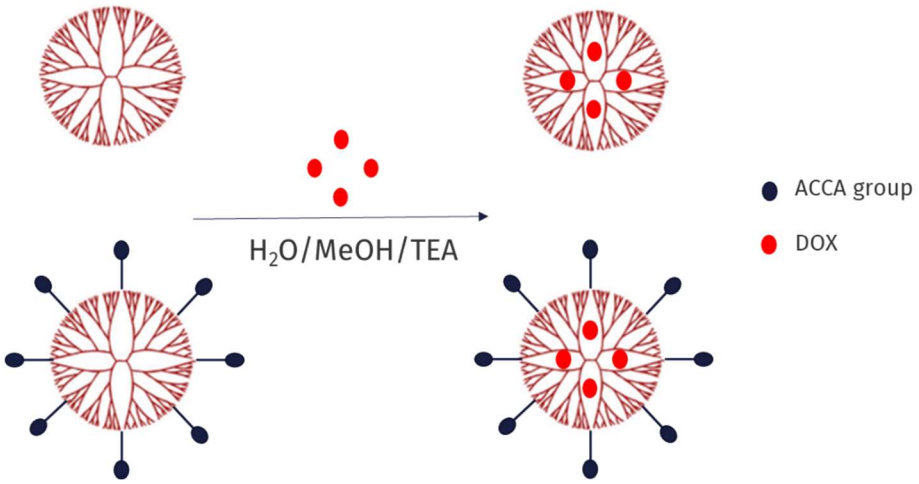

Figure 45. Schematic representation of DOX encapsulation procedure on CATDEN.

This value was used to calculate the Entrapment Efficiency (EE) and the Loading Capacity (LC) (Table 8). The results show that the functionalized dendrimer with 48 ACCA has a lower encapsulation and loading capacity than the commercial dendrimer. This is probably due to the steric hindrance induced by the cinnamic acids on the dendrimers' surface. Steric hindrance is an electron-electron repulsion phenomenon[237] that can be simulated using computational studies.[238]

Table 8. Encapsulation efficiency and loading capacity of DOX-loaded dendrimers.

	$G4NH_2$	*$G4NH_2$-48ACCA*
EE (%)	56.13 ± 4.23	20.03 ± 2.14
LC (μg/mg NPs)	113.20 ± 8.13	26.64 ± 2.78

To be effective as an anticancer drug, DOX encapsulated should be released onto a biological medium in a controllable manner once its release rate is an important variable to decrease the undesirable drug side effects.[239] The release of DOX from native and functionalized dendrimers was studied using free DOX as a control in PBS solution.

Considering the quite acidic environment of the tumour site[240], we also compared the release behaviours of DOX under physiological and acidic conditions. As shown in Figure 46, both G4NH2-DOX and G4NH2-48ACCA-DOX displayed a slower DOX release rate at pH = 5 than at pH = 7.4.

For either pH = 5 or pH = 7.4, DOX is released from both dendrimers in a more sustainable mode than the free DOX drug. Although the CATDEN have no significant difference in the release of DOX than the commercial PAMAM, they may be beneficial

to protect from side effects, as cinnamic acid derivatives show a multidirectional protective effect against DOX-induced DOX cardiotoxicity. [241]

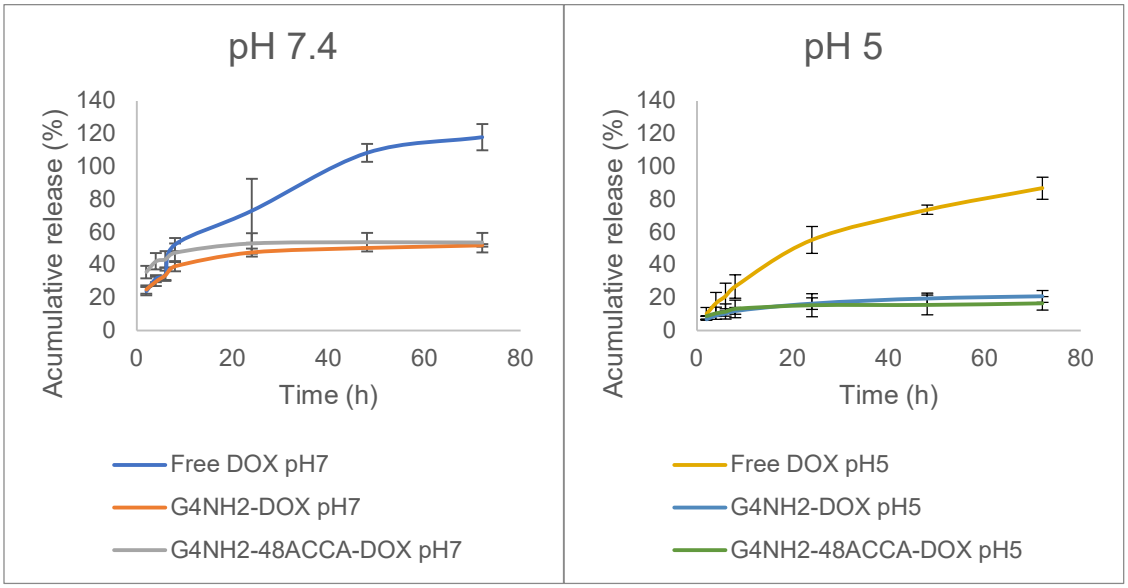

Figure 46. In vitro cumulative release of DOX from G4NH2 and G4NH2-48ACCA in PBS solution at pH 7.4 and 5.

The DOX-encapsulated dendrimers were analysed, in different mediums, by zeta potential (Figure 47). The variation in zeta-potential values for drug-loaded and unloaded nanoparticles indicates DOX loading onto the dendrimer[242]. In all dispersants, the dendrimers which load DOX inside became more positive. This increase is due to the positively charged DOX, indicating that stable DOX-loaded dendrimers could effectively be produced via hydrophobic interactions.[243]

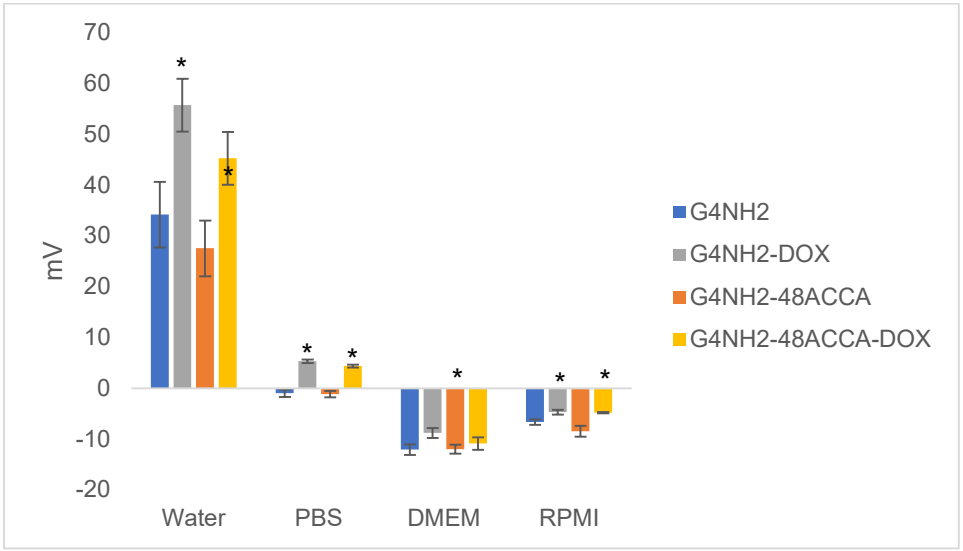

*Figure 47 Zeta potential in several dispersants. The data represent the mean ± SD of three independent experiments performed in triplicate. *: p<0.05 vs. dendrimer before DOX encapsulation.*

A fluorescence study of the DOX-encapsulated dendrimers was performed. The concentration of DOX was established at 10µg/ml. Figure 48 shows excitation and emission fluorescence spectra of DOX and DOX-encapsulated dendrimers. DOX presents an excitation band at 470 nm and an emission band at 595nm. The DOX-encapsulated dendrimers present the same bands, but the intensity decreases 10 times. Chandra et al. [242] point out that this decrease in the fluorescence intensity of DOX results from the intermolecular interaction between the DOX and the dendrimers. This interaction was evident from the prevalent quenching of DOX fluorescence in the presence of both dendrimers.

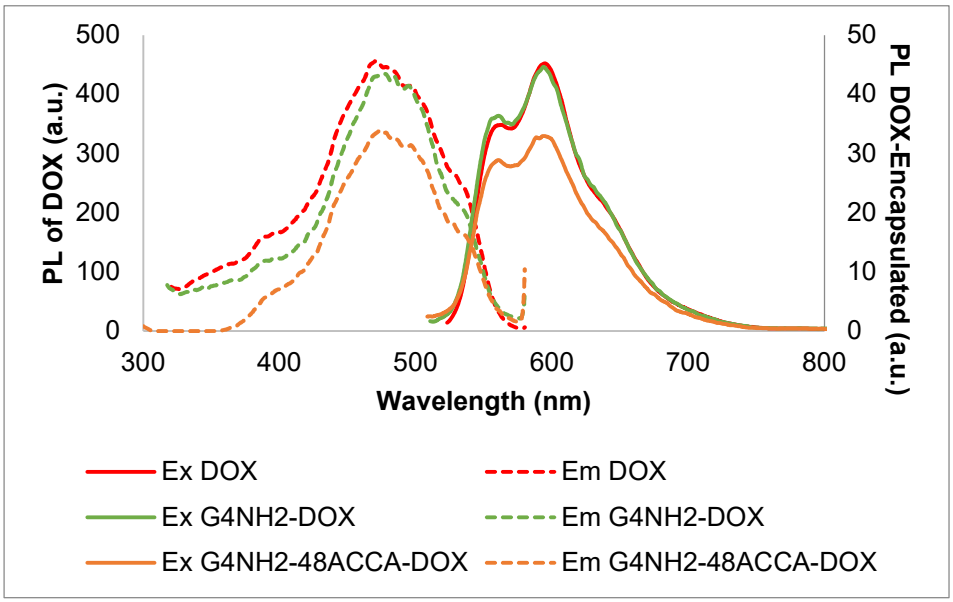

Figure 48. Emission (λ_{ex} = 470 nm) and excitation (λ_{em} = 595 nm) spectra of free doxorubicin and DOX-encapsulated into native and CATDEN dendrimer, in PBS.

To check if the CATDEN could improve the therapeutic efficacy of the DOX drug, the cytotoxicity of the DOX-loaded dendrimer was quantitatively evaluated using CAL-72 cells. As it can be seen in Figure 49, both G4NH2-DOX and G4NH2-48ACCA-DOX displayed improved cytotoxicity toward CAL-72 cells, while free DOX alone had a higher IC_{50} value.

Functionalization with ACCA decreases the cytotoxicity of the PAMAM dendrimer but with equivalent DOX concentrations, the antitumor bioactivity of the DOX is the same. It should be mentioned that both dendrimers alone did not affect cell viability in the concentration used. Consequently, the efficacy is only due to the drug-loaded onto the dendrimers.

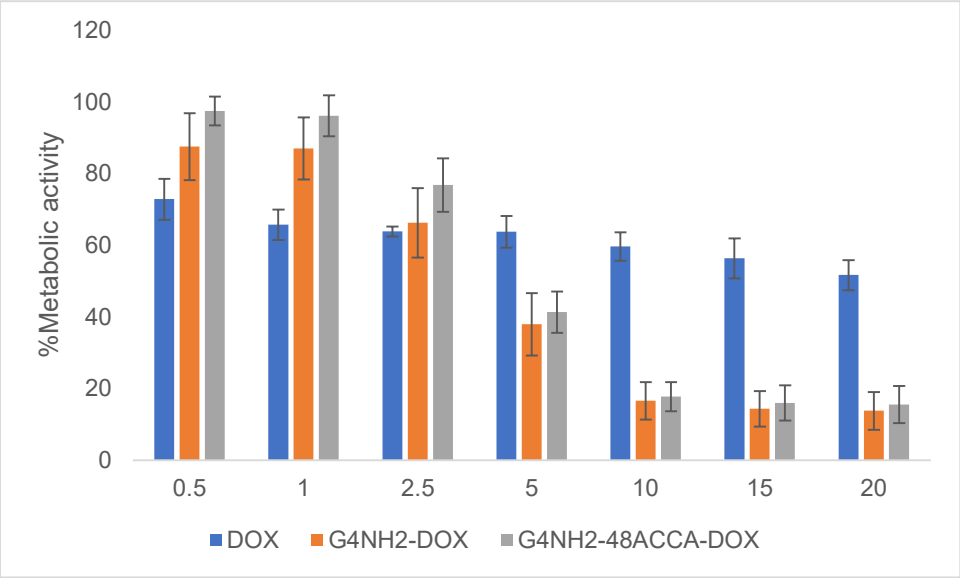

Figure 49. Cell viability of CAL-72 cells after 24h of treatment with DOX-encapsulated dendrimers and free DOX in culture.

Since DOX is a fluorescent molecule, its accumulation in CAL-72 cells can be followed by fluorescence microscopy to verify the intracellular uptake (Figure 50). The results show that DOX is spread in the cytoplasm and the nucleus of cells.

Compared to free DOX experiments, a lower density of red DOX can be seen inside the cells in both dendrimers. However, G4NH2-48ACCA-DOX showed a higher intensity of red dots inside the nucleus of cells.

These observations suggest that the functionalization of the PAMAM dendrimer with ACCA delivers DOX to the nucleus cell more efficiently than commercial PAMAM.

Also, the morphology of the cells treated and untreated present some differences. When treated with free DOX, the cells are more rounded than those treated with the dendrimers. When the cells were treated with the native dendrimer, they presented a healthy morphology than when treated with the CATDEN. At 24h of exposure, all samples presented a combination of fusiform shape (attached cells) and rounded (non-adherent cells) cells, suggesting a moderate level of cytotoxicity. At 48h, the cell morphology indicated an increase in cytotoxicity (Figure 50).

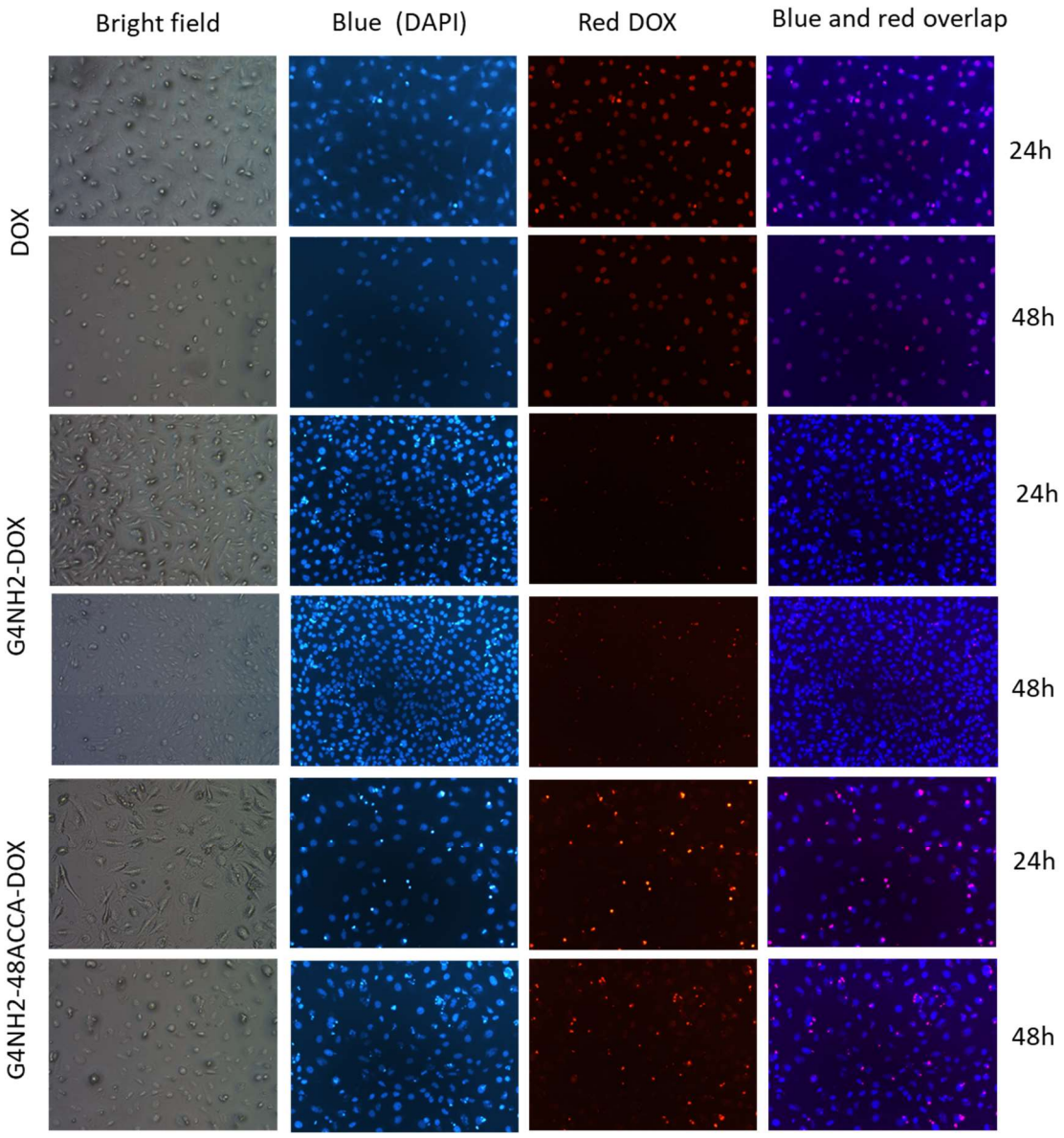

Figure 50. Bright-field and fluorescence microscope images of CAL-72 cells after 24h and 48h culture with DOX-encapsulated dendrimers.

The haemolysis assay was used to evaluate the interaction of the dendrimers, the free DOX, and DOX-encapsulated dendrimers with blood components, specifically by determining its effect on the haemolysis of the erythrocytes. Blood was treated with different concentrations of each compound (5 μM, 10 μM, 25 μM, and 50 μM). The positive and negative control is denoted by C+ and C−, respectively. The results are expressed as mean ± SD of at least three independent experiments performed in triplicate.

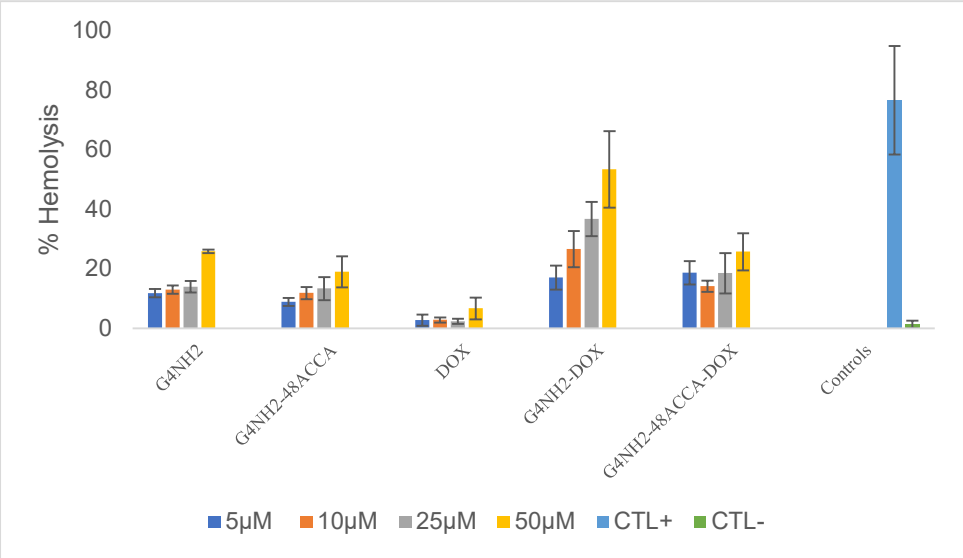

Figure 51. Hemotoxicity of the dendrimers before encapsulation, free DOX, and DOX-encapsulated dendrimers.

The results (Figure 51) show that only when the concentration increases to 50μM some toxicity is observed despite the haemotoxicity increasing with concentration for all situations studied. A very low haemotoxicity level was observed in free DOX when compared with the released haemoglobin with those of the negative control, indicating that DOX does not cause the lysis of the erythrocytes, results on par with those found in the literature.[244]

In the case of DOX-encapsulated dendrimers, haemotoxicity increases compared with the released haemoglobin with those of the dendrimers themselves. However, the value of released haemoglobin is higher in the complex with native dendrimer than CATDEN. This may suggest that the complex dendrimer/DOX interacts with some of the blood constituents, though to a lower extent than DOX by itself.

However, these studies were carried out *in vitro,* and they may not reflect the entirety of events that may occur *in vivo* (such as, among others, selective dendrimers aggregation on atheromatous carotid tissues[245], platelets aggregation[246]) that may have a significant effect on the compatibility of the systems with the blood.

5. Conclusion

In conclusion, we have established an easy synthetic pathway for the preparation of cinnamic acid terminated dendrimers with different degrees of functionalization.

The characterisation of the new CATDEN dendrimers was performed by spectroscopy techniques, like ^{1}H, ^{13}C, MALDI TOF, fluorescence, FITR and UV-Vis, and zeta potential. Although the characterisation does not give the same number of linked acids per dendrimer, it is coherent in demonstrating the tendency to increase functionalisation. Based on the NMR characterisation, the dendrimer with 48 bound acids was selected to be tested for drug delivery capacity. The dendrimer's toxicity decreases with the increase of ACCA on the surface due to the reduction of the exposed number of amino groups on the surface.

The CATDEN dendrimers showed a lower encapsulation and loading capacity for DOX than the pristine dendrimer. Although, there is not a significant difference in the amount of DOX released under physiological conditions. However, the DOX was released from both dendrimers more sustainably than the free DOX drug. The dendrimers' zeta potential that loads DOX inside becomes more positive than the dendrimers themselves, supporting the evidence that the DOX is successfully encapsulated. The cytotoxicity of both $G4NH_2$-DOX and G4NH2-48ACCA-DOX displayed improved cytotoxicity toward CAL-72 cells than the free DOX. The fluorescence microscopy studies revealed a higher intensity of DOX inside the nucleus of cells, suggesting that the functionalization of the PAMAM dendrimer with ACCA delivers DOX to the nucleus more efficiently than commercial PAMAM (generation 4).

Our results demonstrated that the ACCA could be used as a vector since it decreases the potential dendrimers toxicity. Despite the need for further studies to clarify some aspects of our research, our results confirm the potential of the cinnamic acid-based nanomaterials to be more selective against CAL-72 cancer cell lines and be used in novel drug delivery systems.

Chapter 5- ^{1}H NMR metabolomics of CATDEN (PAMAM G4NH2-48 ACCA)

As stated before, cancer is one of the leading causes of death worldwide, affecting the lives of millions of people, having a huge psychological, economic, and social impact on our society. As such, there is a need to develop new and innovative technologies for early detection and treatment.

Emerging evidence supports cancer as a metabolic disease. This conclusion comes from the fact that most cancer cells can reprogram glucose metabolism via the "Warburg effect", in which energy production occurs by aerobic glycolysis only. During this process, cancer cells produce energy by converting excess glucose to lactate in the presence of oxygen[66,247]. The produced lactate is then transported out of the cell by a monocarboxylate transporter (MCTs).[248] MCTs have been investigated for their role in promoting and suppressing osteoclast differentiation and survival on bone.[249] The most studied inhibitor of this effect is the ACCA, which was recently used as a vector of nanoparticles for targeted cancer therapy and to avoid oxidative stress, whereby it can be used to develop novel drug delivery systems to target cancer cells.[84]

For the first time using a ^{1}H NMR metabolomics approach, our previous results (Chapter 3) demonstrated that CAL-72, which seems closer to normal primary osteoblasts than other reported osteosarcomas[250], was the cell line most affected by the treatment with PAMAM dendrimer.

Indeed, dendrimers can target solid tumor sites through the enhanced permeability and retention effect (EPR) and also by active targeting after adequate chemical functionalization.[172]

This chapter aimed to evaluate the new prepared cinnamic acid-terminated dendrimers' influence on cancer metabolism using ^{1}H NMR metabolomics.

1. Identification of metabolites

To investigate the possible metabolic effects of CATDEN, PAMAM G4NH_2-48ACCA was chosen to be applied to the CAL-72 cell line.

NMR analysis was performed on the aqueous cell extracts and metabolized culture media to investigate differences in the endo and exometabolome of treated cells with the new CATDEN (with the IC_{50} and IC_{25} previously determined in Chapter 4).

The comparison between the effect of native dendrimer and the CATDEN in the cell metabolism is presented in Figure 52, where it is possible to distinguish the differences in the metabolite's intensities. The metabolites were already identified in Chapter 3, in Figure 19, and Figure 22, and the assignments are presented in Table 1. The most intense metabolites signals remain as before, from lactate, glutamate, and glycine, with the difference that glucose is more intense when compared to their presence as a result of exposing CAL-72 cancer cells to the native dendrimer.

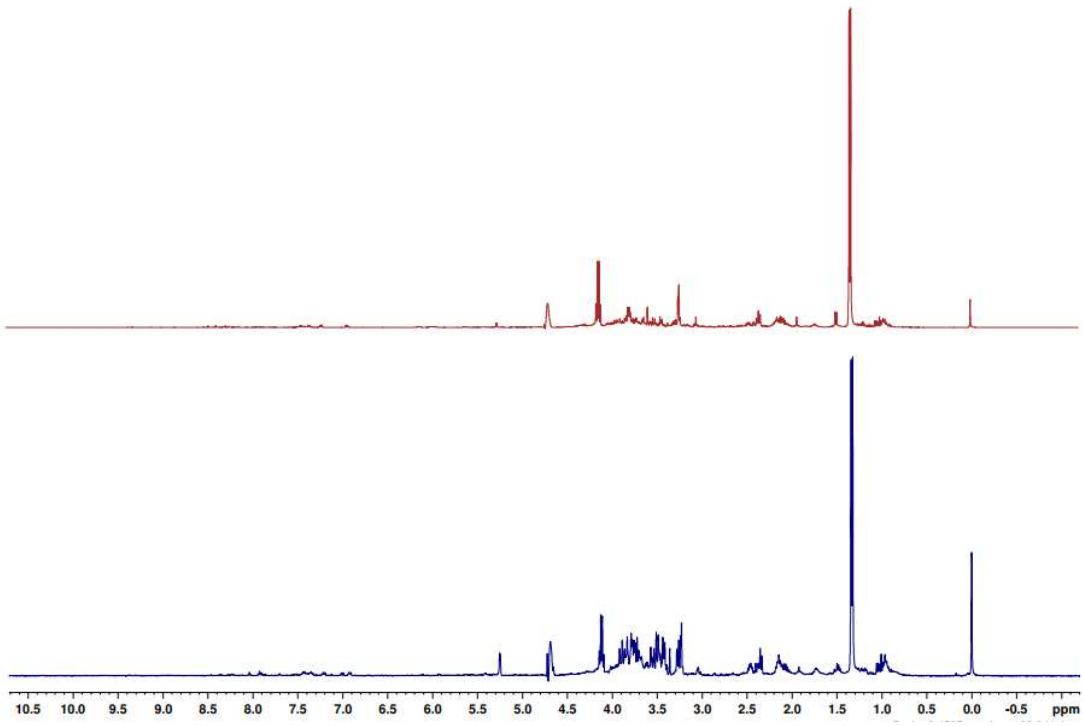

Figure 52. Comparison of ^1H NRM spectrum of CAL-72 endometabolome treated with native PAMAM dendrimer (red) plus treated with CATDEN dendrimer in D_2O.

2. Statistical analysis

To identify similarities and differences in response to the CATDEN dendrimer exposure, a data matrix with the quantitative information of the metabolites was created using Chenomx Software.

The relative concentrations for the metabolites found were displayed in a heatmap (Figure 53), constructed using Pearson's correlation and Ward algorithm for clearer data visualization. The profile of the endometabolome showed that most of the metabolites increase their relative concentration after treatment with the CATDEN. The opposite happens with the exometabolome, where the metabolites decrease their concentration except for lactate. Interestingly, the profile of the exometabolome is exactly the opposite when compared with the behaviour of native dendrimer, in which the only metabolite to decrease the relative concentration was lactate. This observation suggests that the functionalization with ACCA changes the metabolic mechanism pathway of the PAMAM dendrimer.

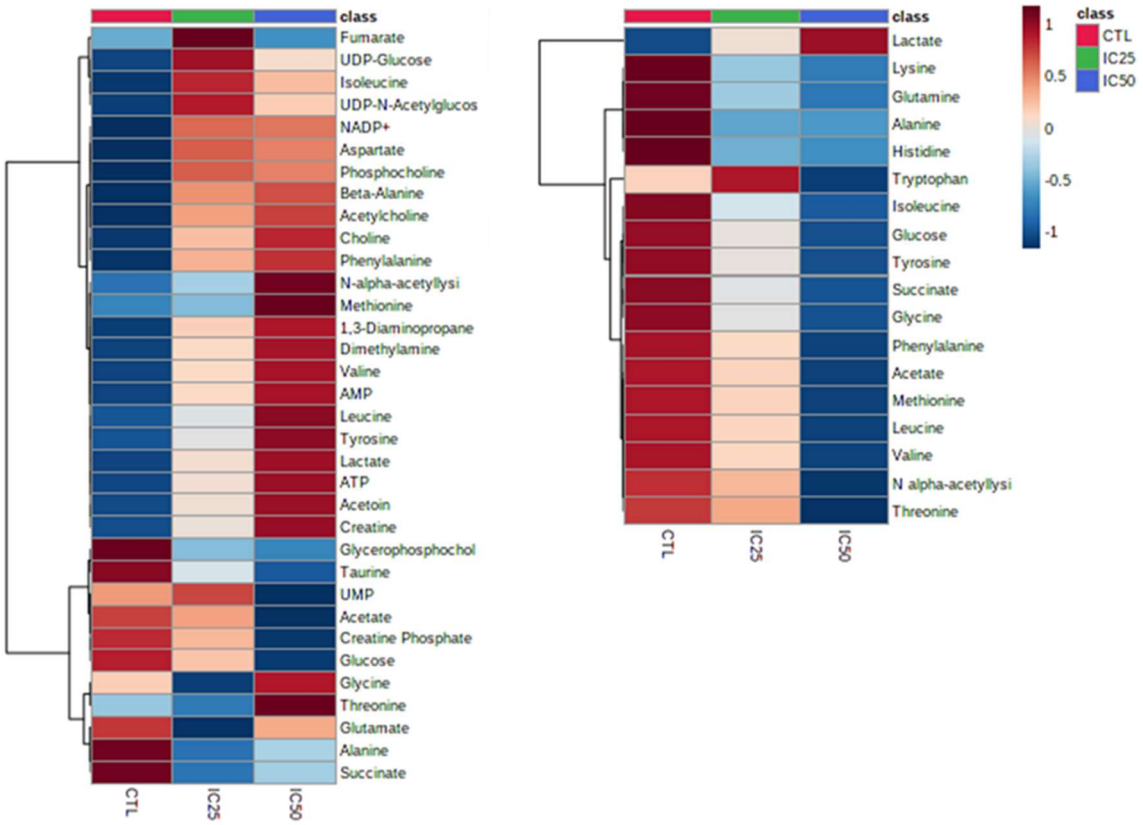

Figure 53. Heat map visualization and hierarchical clustering analysis by Pearson's distance analysis. Left-endometabolome, right- exometabolome.

Multivariate data analysis was performed to reduce data complexity and visualize if there is intrinsic clustering. A PCA (Figure 54) used to retrieve hidden information from the NMR spectra, showing poor discrimination between untreated cell samples and those were treated with IC_{25} and IC_{50} of the dendrimer, especially when compared with the pristine PAMAM dendrimer. The PLS-DA was also performed in an attempt to maximize the separation between groups of metabolites. However, only a little discrimination between the study groups is observed.

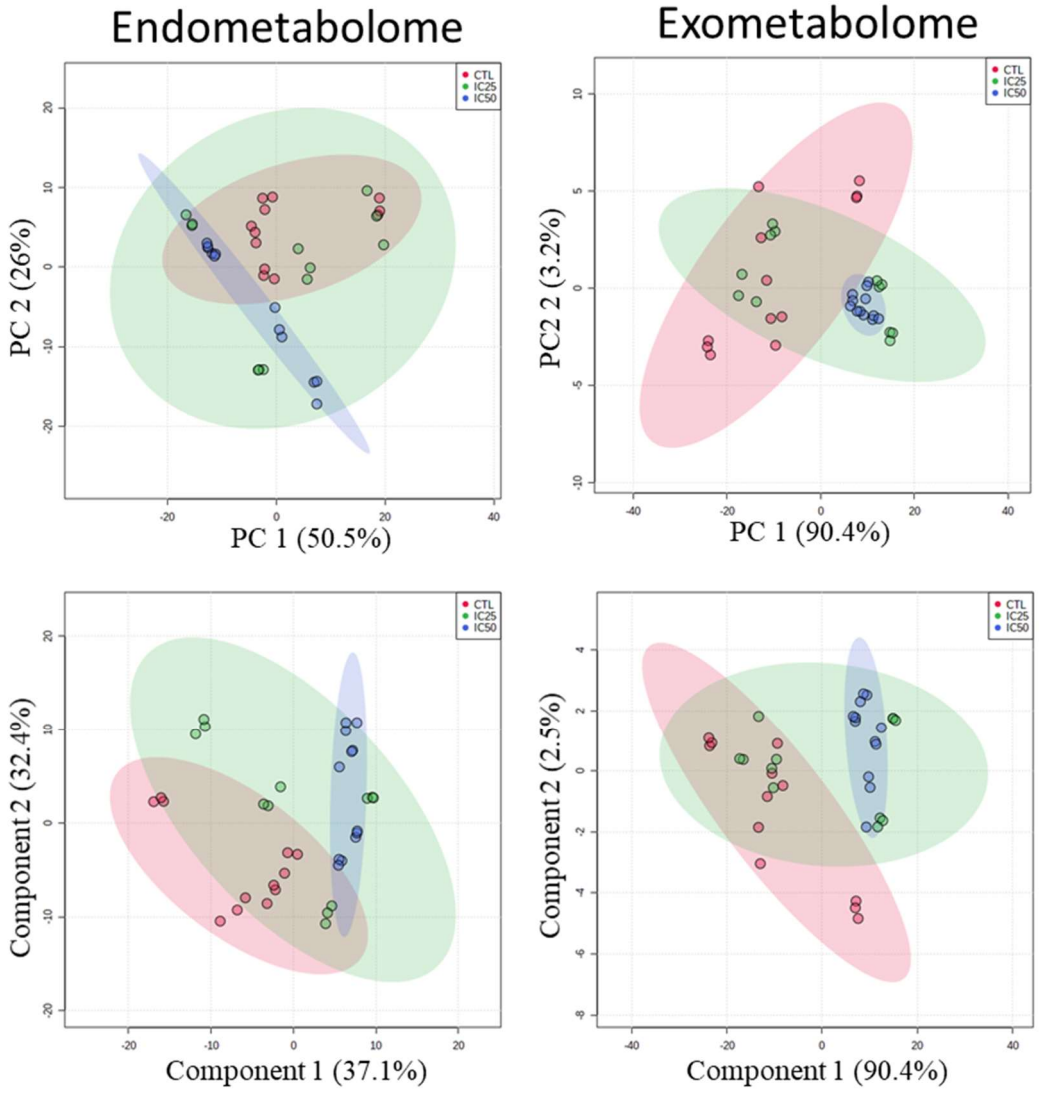

Figure 54. PCA and PLS-Da analysis of CATDEN dendrimer, PAMAM G4NH$_2$-48ACCA.

The metabolites that exhibited more importance/predominance in the variance projection of the samples were roughly the same between endo and exometabolome. The metabolites

that contributed the most were glucose, lactate, taurine, threonine, alanine, and glutamate. Despite the need for complementary *in vivo* studies, these metabolites may be potential biomarkers for the early detection of osteosarcomas.

3. Metabolic variation induced by CATDEM (PAMAM G4NH2-48 ACCA)

The magnitude of variations of each metabolite concerning the controls, was determined by the percentage of variation and the statistical significance usingthe ANOVA test. The ANOVA test shows that the affected metabolites with a statistical significance decrease from 72% of the native PAMAM to 53% of the CATDEN. These results are consistent with the cell viability results, where the CATDEN exhibited less toxicity.

The results of the endometabolites and exometabolites affected by the PAMAM G4NH2-48ACCA dendrimers were summarized in Table 9 and Table 10, respectively. Only the metabolites with statistical significance were included.

As in the case of the commercial dendrimer, the affected endometabolites belong to the energy-gaining metabolism, glycolysis, and Krebs cycle, amino acids, and phospholipids.

Unlike the commercial dendrimer, intracellular lactate and glucose metabolite concentration are not significantly affected. As with the commercial dendrimer, the glycero phosphocholine was the intrametabolite that decreased its concentration most. Amino acids are only affected when a higher concentration is used.

In the case of exometabolome, the profile is completely opposite to that seen in the commercial dendrimer. In this case, the only metabolite that increases significantly is lactate, and amino acids decrease.

CATDEN dendrimer influences the same metabolic pathways as commercial PAMAM but in the opposite direction.

The results in chapter 3 show that the commercial dendrimer alone seems to have some effect on MCTs as it decreases lactate in the extracellular medium and increases it in the intracellular medium. One would expect ACCA bound to the dendrimer to increase the effect, but this is not observed.

The inhibitory effect that ACCA has on MCT's seems to be lost when bound with the dendrimer. This may be happening because of the steric effect, where ACCA cannot fit into the active sites of the transporter to block it.

Table 9. Main metabolite variation in the endometabolome of CAL-72 cell lines after exposure with different PAMAM G4NH2-48ACCA concentrations. Signals coloured accordingly with the percentage of variation relative to controls.

		IC_{25}	**IC_{50}**
Energy generation	Creatine	▲*	▲*
Glycolysis and Krebs cycle	Fumarate	▲*	
Amino acids metabolism	Leucine	▲*	▲*
	Nα-acetyllysine		▲*
	Methionine		▲*
	Taurine		▼*
	Tyrosine		▲*
Other	Dimethylamine	▲*	▲*
	1,3- Diaminopropane	▲*	▲*
Phospholipid metabolism	Glycero phosphocholine	▼*	▼*

Table 10. Main metabolite variation in the exometabolome of CAL-72 cell lines after exposure with different PAMAM G4NH2-48ACCA concentrations. Signals coloured accordingly with the percentage of variation relative to controls.

		IC_{25}	**IC_{50}**
Glycolysis and Krebs cycle	Lactate	▲*	▲*
	Succinate	▼*	▼*
	Glucose	▼*	▼*
Amino acids metabolism	Leucine		▼*
	Alanine	▼*	▼*
	Tyrosine		▼*
	Phenylalanine		▼*
	Glutamine	▼*	▼*
	Lysine	▼*	▼*
Other	Acetate	▼*	▼*

4. Pathway analysis

Pathway analysis was used to identify biologically meaningful patterns that are significantly enriched in quantitative metabolomic data. The analysis was performed between the control *vs.* IC_{25} group and the control *vs.* IC_{50} group. Since the smaller the *p*-value, the more significant the pathway is, the top 5 pathways were chosen for the analysis (Table 7). The entire results are shown in the Supplementary Information.

The pathways affected by CATDEM dendrimer focused on amino acids metabolism and glucose metabolism, similar to the native PAMAM dendrimer (Chapter 3). As PAMAM dendrimer was demonstrated to interact with the medium serum[206], the same may be happening with the CATDEN since cinnamic acids can interact with HSA (human serum albumin).[251]

Other interesting pathways altered were oxidation of branched-chain fatty acids and ketone body metabolism. Ketone bodies result from intense gluconeogenesis, which generates glucose from not fatty acids sources. A normal balanced diet provides sufficient nutrient content to satisfy the glucose requirements. Under these conditions, ketogenesis is negligible. However, the ability to survive periods of food deprivation relies typically on a biochemical interaction that ensures the appropriate interorgan redirection and utilization of main metabolism fuels.[252]

This observation reinforces that the cells probably were deficient in nutrients after being treated with CATDEN. This behavior is similar after treatment with the native PAMAM dendrimer. Our new CATDEN appears to disrupt that mechanism for obtaining energy that cancer cells require to support the higher proliferative rates even in suboptimal environments.

Table 11. Pathway analysis summarized.

		IC_{25}		IC_{50}	
		Pathway	**Enrichment**	**Pathway**	**Enrichment**
KEGG	Endo	Ubiquinone and other terpenoid-quinone biosynthesis Tyrosine metabolism Starch and sucrose metabolism Phenylalanine metabolism Phenylalanine, tyrosine, and tryptophan biosynthesis	Ubiquinone and other terpenoid-quinone biosynthesis Tyrosine metabolism Galactose metabolism Starch and sucrose metabolism Phenylalanine metabolism	Valine, leucine and isoleucine degradation Starch and sucrose metabolism Phenylalanine metabolism Phenylalanine, tyrosine, and tryptophan biosynthesis	Valine, leucine and isoleucine degradation Neomycin, kanamycin, and gentamicin biosynthesis Galactose metabolism Starch and sucrose metabolism Phenylalanine metabolism
	Exo	Aminoacyl-tRNA biosynthesis Pyruvate metabolism Starch and sucrose metabolism Phenylalanine metabolism Phenylalanine, tyrosine, and tryptophan biosynthesis	Aminoacyl-tRNA biosynthesis Glycolysis/Gluconeogenesis Pyruvate metabolism Valine, leucine, and isoleucine biosynthesis Galactose metabolism	Aminoacyl-tRNA biosynthesis Pyruvate metabolism Starch and sucrose metabolism Phenylalanine metabolism Phenylalanine, tyrosine, and tryptophan biosynthesis	Aminoacyl-tRNA biosynthesis Glycolysis/Gluconeogenesis Pyruvate metabolism Valine, leucine and isoleucine degradation Valine, leucine, and isoleucine biosynthesis

		IC_{25}		IC_{50}	
		Pathway	**Enrichment**	**Pathway**	**Enrichment**
SMPDB	Endo	Retinol Metabolism Beta-Alanine Metabolism Aspartate Metabolism Nucleotide Sugars Metabolism	Retinol Metabolism Pterin biosynthesis Fatty acid elongation in mitochondria Ubiquinone biosynthesis Androgen and estrogen metabolism	Retinol Metabolism Beta-Alanine Metabolism Aspartate Metabolism Nucleotide Sugars Metabolisms	Retinol Metabolism Betaine metabolism Spermide and Spermine biosynthesis Gluconeogenesis Taurine and hypotaurine metabolism
	Exo	Phytanic Acid Peroxisomal Oxidation Warburg Effect Citric Acid Cycle Phenylalanine and Tyrosine Metabolism Histidine Metabolism	Selenoamino acid metabolism Tryptophan metabolism Urea Cycle Oxidation of branched-chain fatty acids Citric Acid Cycle	Phytanic Acid Peroxisomal Oxidation Warburg Effect Citric Acid Cycle Phenylalanine and Tyrosine Metabolism Histidine Metabolism	Oxidation of branched-chain fatty acids Citric Acid Cycle Ketone Body metabolism Butyrate metabolism Mitochondrial electron transport chain

5. Lactate and glucose quantification

The quantification of lactate and glucose metabolites using a colorimetric kit was evaluated to understand if the effect observed by NMR is comparable to that published in the literature.[253,254]

Lactate and glucose were quantified in the treated cells compared to the control, to which 1% DMSO was added as ACCA is insoluble in water. In general, cancer cells consume more glucose than normal cells and simultaneously produce more lactate. When ACCA inhibits these cells, they exhibit a decrease in lactate production.[254,255]

To determine the effect of the dendrimers on glucose consumption and lactate transport on cancer cells. CAL-72 cells were cultured to obtain $5x10^6$ cells, to be treated with the concentration corresponding to the IC_{50} value for 24h.

The results of the quantification of lactate and glucose by NMR are shown in Figure 55. In the exometabolome, the medium without cells presented, as expected, more glucose than lactate metabolite. The opposite was observed in the control sample, where was more lactate than glucose due to cells consumption of glucose and production of lactate. In the samples with ACCA, there was more glucose than lactate, showing that ACCA influences lactate production. This result is consistent with the reported literature.[256] In cells treated with G4NH2, the lactate production is less affected than when treated with ACCA. In cells treated with G4NH2-48ACCA, the lactate metabolite is less affected than observed with the commercial dendrimer.

The metabolomics results show that the extracellular lactate concentration after incubation with PAMAM G4NH2-48ACCA is higher than that quantified after incubation with the native dendrimer and even with the control.The slightly different result shown in the metabolomics, probably is due to the difference in the cells used in the study ($5x10^6$ *vis*. $15x10^6$). However, it is important to note that in both studies, the cells produced more lactate after treatment with ACCA functionalized dendrimer than with the native dendrimer.

The endometabolome shows a behaviour similar to the exometabolome, where glucose does not show a significant variation in the metabolite concentration, while lactate is affected after treatment with the different compounds under study.

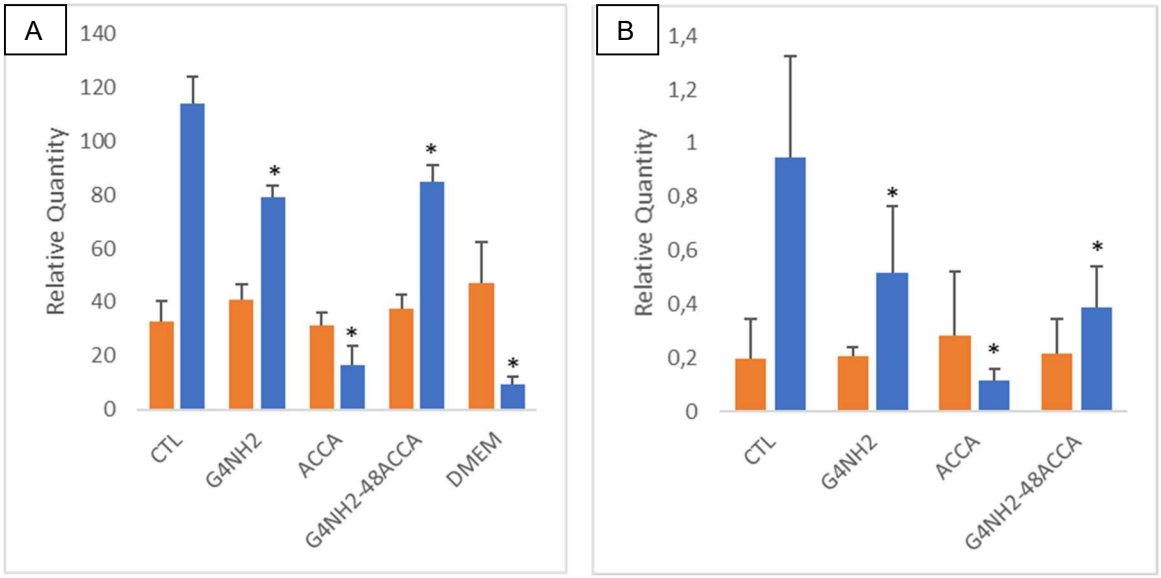

Figure 55. Quantification of lactate and glucose by NMR A) Exometabolome B) Endometabolome. (Blue-lactate, Orange- glucose).

The results of the quantification of lactate and glucose by colorimetric kits are shown in Figure 56 and Figure 57. In the exometabolome, coherent behaviour was found between the medium without cells (high concentration of glucose, less concentration of lactate) and the control sample (opposite from the observed on the medium). Both dendrimers do not show significant lactate production or glucose consumption compared with the control. As previously reported, the only sample with a statistically significant difference was ACC.[256,257] The endometabolome, in contrast with the NMR data, shows that most compounds generally do not present statistically significant differences concerning the control.

When comparing the two methods used to quantify glucose and lactate metabolites, the data show that both methods have consistent results for the exometabolome, but for the endometabolome the NMR shows advantages in quantifying metabolites intracellularly.

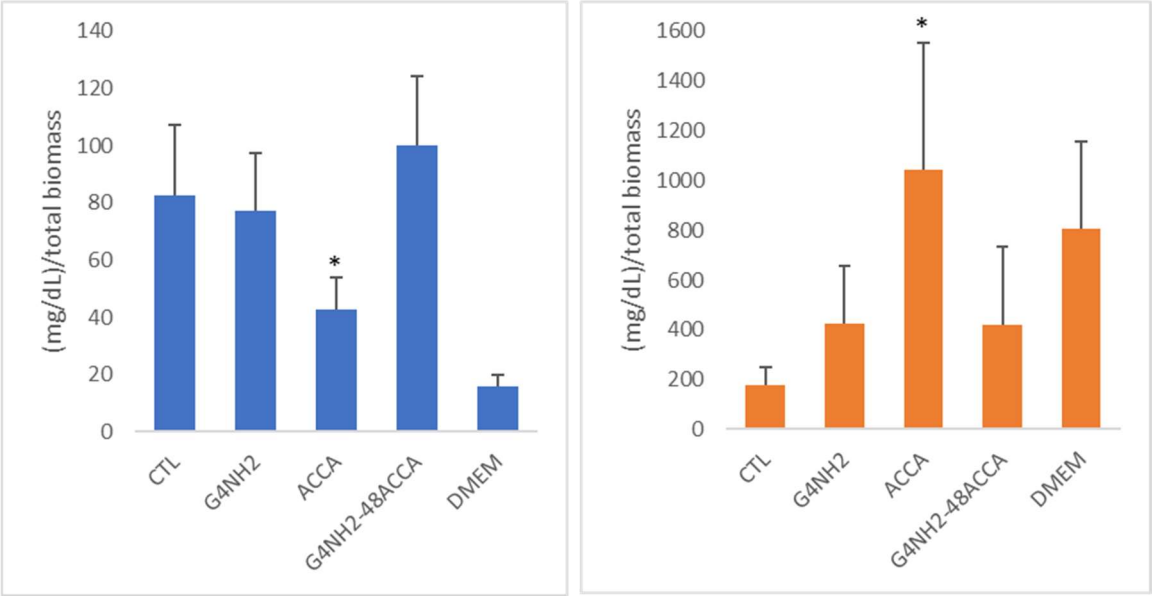

Figure 56. Quantification of lactate and glucose in the exometabolome by colorimetric kit. (Blue-lactate, Orange- glucose).

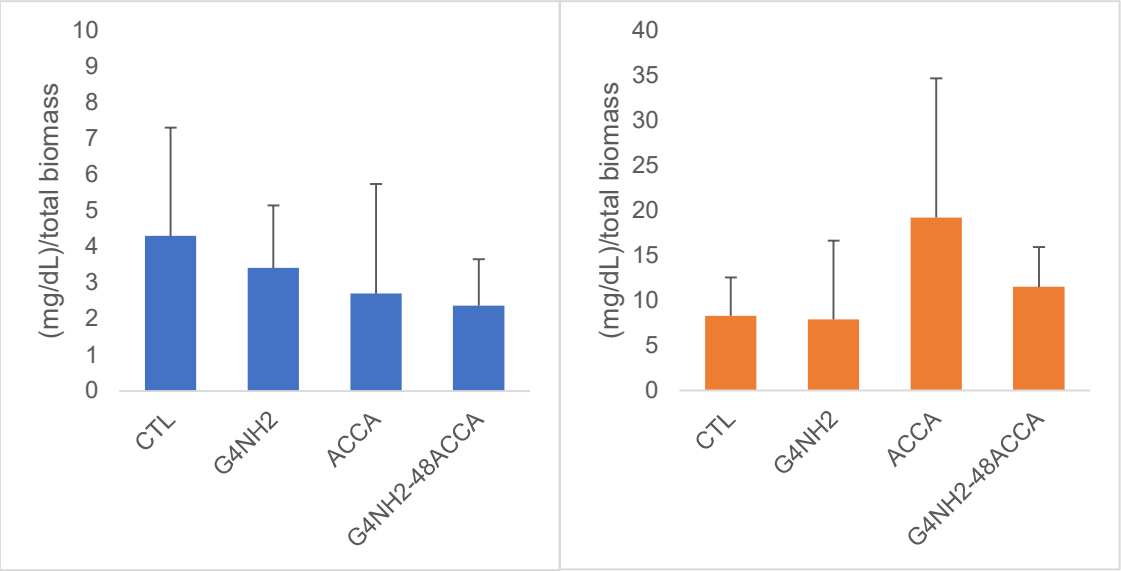

Figure 57. Quantification of lactate and glucose endometabolome by colorimetric kit. (Blue-lactate, Orange- glucose).

1. Conclusions

The metabolic changes induced by CATDEN dendrimer on cells cultured *in vitro* were monitored by ^{1}H NMR metabolomics, and the results were compared between treated and untreated cells.

Analyses were performed on complete spectral data and quantified metabolic data in intracellular and extracellular media, leading to the determination of the most significantly affected metabolites.

Statistical analysis showed that assays with commercial dendrimers exhibited higher discrimination between treated and non-treated cells than the functionalized ones.

The results of the statistic analysis and the metabolic pathways showed that CADTEN dendrimer alters metabolites and metabolisms differently from the commercial PAMAM dendrimer but that it belongs to the same main metabolic pathways, such as starch-acid metabolism and glycolysis. These metabolic pathways are part of energy metabolism.

CATDEN dendrimer shows a different behaviour to the native PAMAM dendrimer. Despite having ACCA on the surface, lactate production is less affected than in the native dendrimer itself. In fact, it even seems to enhance glycolysis.

Quantification of glucose and lactate was performed using NMR and a colorimetric kit. The results of the colorimetric kit quantification in comparison with the NMR quantification results show consistent outputs, demonstrating that the ^{1}H NMR proved to be a useful tool for quantifying metabolites on treated and non-treated cells, especially intracellular ones.

Chapter 6 – General conclusions and future perspectives

The general objective of this Ph.D. project was to synthesise and characterise a new family of cinnamic acid-terminated dendrimers, study their influence on cancer by NMR metabolomics, and explore their potential application as vehicles for the transport of cancer drugs. From the overall work, some conclusions can be drawn, and some comments can be made:

- The ^{1}H NMR metabolomics methods were successfully used to study the metabolic profile of the PAMAM dendrimer G4NH2 in different cell mammalian lines.
- Statistical analysis results successfully differentiated and discriminated samples between the metabolite groups. The pristine PAMAM dendrimer affects human cancer cells more than normal mouse cells.
- The metabolic analysis demonstrated that the pathways affected in native PAMAM dendrimer were essentially the aminoacids (valine, leucine, and isoleucine, phenylalanine, tyrosine, threonine, histidine) and glucose metabolism (Glycolysis/Gluconeogenesis, pyruvate, Warburg Effect). These results indicate that the discriminatory metabolites potentially originated from energy and protein metabolism. The origin of this effect is unclear because it could be a normal response of the dendrimers or a result of the protein-corona phenomena.
- The novel cinnamic acid-terminated PAMAM dendrimers (CATDEN) were successfully synthesised. The characterisation showed four different levels of functionalization (25, 32, 48, and 64 ACCA).
- CATDEN dendrimer toxicity decreases with the increase of ACCA terminal functionalisation due to the reduction in the exposure/number of amino groups on the surface.
- The native PAMAM and PAMAM G4NH$_2$-48ACCA dendrimer were chosen as scaffolds to encapsulate the anticancer drug model DOX. CATDEN dendrimer showed lower DOX encapsulation and loading capacity than the commercial dendrimer, but the release from both dendrimers is more sustainable when compared to the free DOX drug. The cytotoxicity of both dendrimers exhibited an improvement toward CAL-72 cells than free DOX.

- The fluorescence microscopy studies revealed a higher intensity of DOX inside the nucleus of cells, suggesting that the functionalization of PAMAM G4NH2 with ACCA delivers DOX to the nucleus more efficiently than commercial PAMAM dendrimer.
- CATDEN dendrimer shows a different behavior to the native PAMAM dendrimer. Lactate production is less affected than in the native dendrimer itself, despite having ACCA on the surface. In fact, it even seems to enhance glycolysis.

Metabolomic technologies are well-suited for evaluating the effects of any nanomaterial because any metabolic change associated with a response to treatment may be an early biomarker of sensitivity or resistance to a drug. Targeting lactate metabolism and transport can represent a promising approach to counteract cancer growth and progression. The power of NMR metabolomics as an easy tool for cellular and molecular profiling and for studying nanomaterials' effects on cells was demonstrated.

These observations may trigger important explanations resulting in additional future studies. In terms of working perspectives, we can highlight the following:

- The gene expression of MCT in osteosarcoma cell lines must be studied to correlate with the obtained results.
- The cell viability study of CATDEN´s in the presence of MCT inhibitors must be evaluated to determine the carriers' involvement in dendrimer activity.
- It would be of great interest to functionalize the PAMAM dendrimers with other cinnamic acids to further analyse their biological potential.
- NMR evaluation of the effect of the different cinnamic acid-functionalized dendrimers prepared on different cancer cells that overexpress MCTs.
- More studies will have to be done to understand the effects of dendrimers in the metabolism using other conditions, for example, without FBS.
- FRET studies of CATDEN to understand the electronic interaction between the dendrimer and the cinnamic acid could also be helpful in understanding the effect of ACCA on the intrinsic fluorescence of the PAMAM dendrimer.
- Since nanomaterials, in general, are known to produce ROS, detecting ROS after treatment with CATDEN dendrimers could help understand their mechanism of action.

- Diffusion-ordered nuclear magnetic resonance spectroscopy (DOSY) can be employed to measure the self-diffusion coefficients and corresponding hydrodynamic radii of CATDEN as a function of dendrimer size (i.e., molecular weight) and tertiary structure (i.e., generational or oligomeric nature).

Bibliography

(1) Human Genome Project http://www.ornl.gov/hgmis (accessed Nov 20, 2021).

(2) Vailati-Riboni, M.; Palombo, V.; Loor, J. J. What Are Omics Sciences? In *Periparturient Diseases of Dairy Cows: A Systems Biology Approach*; Ametaj, B. N., Ed.; Springer International Publishing: Cham, 2017; pp 1–7. https://doi.org/10.1007/978-3-319-43033-1_1.

(3) Oliver, S. Systematic Functional Analysis of the Yeast Genome. *Trends Biotechnol.* **1998**, *16*, 373–378. https://doi.org/10.1016/S0167-7799(98)01214-1.

(4) Oliver, S. G. Functional Genomics: Lessons from Yeast. In *Philosophical Transactions of the Royal Society B: Biological Sciences*; 2002; Vol. 357, pp 17–23. https://doi.org/10.1098/rstb.2001.1049.

(5) Nicholson, J. K.; Lindon, J. C.; Holmes, E. "Metabonomics": Understanding the Metabolic Responses of Living Systems to Pathophysiological Stimuli via Multivariate Statistical Analysis of Biological NMR Spectroscopic Data. *Xenobiotica* **1999**, *29*, 1181–1189. https://doi.org/10.1080/004982599238047.

(6) Fiehn, O. Metabolomics - The Link between Genotypes and Phenotypes. *Plant Mol. Biol.* **2002**, *48*, 155–171. https://doi.org/10.1023/A:1013713905833.

(7) Keurentjes, J. J. Genetical Metabolomics: Closing in on Phenotypes. *Curr. Opin. Plant Biol.* **2009**, *12*, 223–230. https://doi.org/10.1016/J.PBI.2008.12.003.

(8) Markley, J. L.; Brüschweiler, R.; Edison, A. S.; Eghbalnia, H. R.; Powers, R.; Raftery, D.; Wishart, D. S. The Future of NMR-Based Metabolomics. *Curr. Opin. Biotechnol.* **2017**, *43*, 34–40. https://doi.org/10.1016/j.copbio.2016.08.001.

(9) Wishart, D. S. Wishart Research Group https://www.wishartlab.com/about (accessed Nov 18, 2021).

(10) Wishart, D. S. Proteomics and the Human Metabolome Project. *Expert Rev. Proteomics* **2007**, *4*, 333–335. https://doi.org/10.1586/14789450.4.3.333.

(11) Wishart, D. S.; Tzur, D.; Knox, C.; Eisner, R.; Guo, A. C.; Young, N.; Cheng, D.; Jewell, K.; Arndt, D.; Sawhney, S.; Fung, C.; Nikolai, L.; Lewis, M.; Coutouly, M. A.; Forsythe, I.; Tang, P.; Shrivastava, S.; Jeroncic, K.; Stothard, P.; Amegbey, G.; Block, D.; Hau, D. D.; Wagner, J.; Miniaci, J.; Clements, M.; Gebremedhin, M.; Guo, N.; Zhang, Y.; Duggan, G. E.; MacInnis, G. D.; Weljie, A. M.; Dowlatabadi, R.; Bamforth, F.; Clive, D.; Greiner, R.; Li, L.; Marrie, T.; Sykes, B. D.; Vogel, H. J.; Querengesser, L. HMDB: The Human Metabolome Database. *Nucleic Acids Res.* **2007**, *35*, 521–526. https://doi.org/10.1093/nar/gkl923.

(12) Viant, M. R.; Kurland, I. J.; Jones, M. R.; Dunn, W. B. How Close Are We to

Complete Annotation of Metabolomes? *Curr. Opin. Chem. Biol.* **2017**, *36*, 64–69. https://doi.org/10.1016/j.cbpa.2017.01.001.

(13) Vuckovic, D.; Vuckovic, D. Current Trends and Challenges in Sample Preparation for Global Metabolomics Using Liquid Chromatography-Mass Spectrometry. *Anal Bioanal Chem* **2012**, *403*, 1523–1548. https://doi.org/10.1007/s00216-012-6039-y.

(14) Johnson, C. H.; Ivanisevic, J.; Siuzdak, G. Metabolomics: Beyond Biomarkers and towards Mechanisms. *Nat. Rev. Mol. Cell Biol.* **2016**, *17*, 451–459. https://doi.org/10.1038/nrm.2016.25.

(15) Álvarez-Sánchez, B.; Priego-Capote, F.; de Castro, L. Metabolomics Analysis I. Selection of Biological Samples and Practical Aspects Preceding Sample Preparation. *Trends Anal. Chem. 29*, 111–119. https://doi.org/10.1016/j.trac.2009.12.003.

(16) Kuehnbaum, N. L.; Britz-McKibbin, P. New Advances in Separation Science for Metabolomics: Resolving Chemical Diversity in a Post-Genomic Era. *Chem. Rev.* **2013**, *113*, 2437–2468. https://doi.org/10.1021/cr300484s.

(17) Villas-Bôas, S. G.; Bruheim, P. The Potential of Metabolomics Tools in Bioremediation Studies. *Omi. A J. Integr. Biol.* **2007**, *11*, 305–313. https://doi.org/10.1089/omi.2007.0005.

(18) Beckonert, O.; Keun, H. C.; Ebbels, T. M. D.; Bundy, J.; Holmes, E.; Lindon, J. C.; Nicholson, J. K. Metabolic Profiling, Metabolomic and Metabonomic Procedures for NMR Spectroscopy of Urine, Plasma, Serum and Tissue Extracts. *Nat. Protoc.* **2007**, *2* (11), 2692–2703. https://doi.org/10.1038/nprot.2007.376.

(19) Ludwig, C.; Viant, M. R. Two-Dimensional J -Resolved NMR Spectroscopy: Review of a Key Methodology in the Metabolomics Toolbox. *Phytochem. Anal.* **2010**, *21*, 22–32. https://doi.org/10.1002/pca.1186.

(20) Dettmer, K.; Aronov, P. A.; Hammock, B. D. Mass Spectrometry-Based Metabolomics. *Mass Spectrom. Rev.* **2007**, *26*, 51–78. https://doi.org/10.1002/mas.20108.

(21) Dunn, W. B.; Ellis, D. I. Metabolomics: Current Analytical Platforms and Methodologies. *TrAC - Trends Anal. Chem.* **2005**, *24*, 285–294. https://doi.org/10.1016/j.trac.2004.11.021.

(22) Han, J.; Danell, R. M.; Patel, J. R.; Gumerov, D. R.; Scarlett, C. O.; Speir, J. P.; Parker, C. E.; Rusyn, I.; Zeisel, S.; Borchers, C. H. Towards High-Throughput

Metabolomics Using Ultrahigh-Field Fourier Transform Ion Cyclotron Resonance Mass Spectrometry. *Metabolomics* **2008**, *4*, 128–140. https://doi.org/10.1007/s11306-008-0104-8.

(23) Mirnezami, R.; Spagou, K.; Vorkas, P. A.; Lewis, M. R.; Kinross, J.; Want, E.; Shion, H.; Goldin, R. D.; Darzi, A.; Takats, Z.; Holmes, E.; Cloarec, O.; Nicholson, J. K. Chemical Mapping of the Colorectal Cancer Microenvironment via MALDI Imaging Mass Spectrometry (MALDI-MSI) Reveals Novel Cancer-Associated Field Effects. *Mol. Oncol.* **2014**, *8*, 39–49. https://doi.org/10.1016/j.molonc.2013.08.010.

(24) Fan, T. W.-M.; Lane, A. N. Applications of NMR Spectroscopy to Systems Biochemistry. *Prog. Nucl. Magn. Reson. Spectrosc.* **2016**, *92–93*, 18–53. https://doi.org/10.1016/j.pnmrs.2016.01.005.

(25) Emwas, A.-H.; Roy, R.; McKay, R. T.; Tenori, L.; Saccenti, E.; Gowda, G. A. N.; Raftery, D.; Alahmari, F.; Jaremko, L.; Jaremko, M.; Wishart, D. S. NMR Spectroscopy for Metabolomics Research. *Metabolites* **2019**, *9* (7), 123. https://doi.org/10.3390/metabo9070123.

(26) Nicholson, J. K.; Lindon, J. C. Metabonomics. *Nature* **2008**, *455*, 1054–1056. https://doi.org/10.1038/4551054a.

(27) Crook, A. A.; Powers, R. Quantitative NMR-Based Biomedical Metabolomics: Current Status and Applications. *Molecules* **2020**, *25*, 1–33. https://doi.org/10.3390/molecules25215128.

(28) Putri, S. P.; Yamamoto, S.; Tsugawa, H.; Fukusaki, E. Current Metabolomics: Technological Advances. *J. Biosci. Bioeng.* **2013**, *116* (1), 9–16. https://doi.org/10.1016/j.jbiosc.2013.01.004.

(29) Lenz, E. M.; Wilson, I. D. Analytical Strategies in Metabonomics. *J. Proteome Res.* **2007**, *6* (2), 443–458. https://doi.org/10.1021/pr0605217.

(30) Diserens, G.; Vermathen, M.; Gjuroski, I.; Eggimann, S.; Precht, C.; Boesch, C.; Vermathen, P. Direct Determination of Phosphate Sugars in Biological Material by 1H High-Resolution Magic-Angle-Spinning NMR Spectroscopy. *Anal. Bioanal. Chem.* **2016**, *408* (20), 5651–5656. https://doi.org/10.1007/s00216-016-9671-0.

(31) Lindon, J. C.; Holmes, E.; Nicholson, J. K. Pattern Recognition Methods and Applications in Biomedical Magnetic Resonance. *Prog. Nucl. Magn. Reson. Spectrosc.* **2001**, *39*, 1–40. https://doi.org/10.1016/S0079-6565(00)00036-4.

(32) Sugimoto, M.; Kawakami, M.; Robert, M.; Soga, T.; Tomita, M. *Bioinformatics Tools for Mass Spectroscopy-Based Metabolomic Data Processing and Analysis*; 2012; Vol. 7.

(33) Djoumbou-Feunang, Y.; Fiamoncini, J.; Gil-de-la-Fuente, A.; Greiner, R.; Manach, C.; Wishart, D. S. BioTransformer: A Comprehensive Computational Tool for Small Molecule Metabolism Prediction and Metabolite Identification. *J. Cheminform.* **2019**, *11* (1), 2. https://doi.org/10.1186/s13321-018-0324-5.

(34) Chong, J.; Wishart, D. S.; Xia, J. Using MetaboAnalyst 4.0 for Comprehensive and Integrative Metabolomics Data Analysis. *Curr. Protoc. Bioinforma.* **2019**, *68*, 1–128. https://doi.org/10.1002/cpbi.86.

(35) Kanehisa, M. KEGG: Kyoto Encyclopedia of Genes and Genomes. *Nucleic Acids Res.* **2000**, *28*, 27–30. https://doi.org/10.1093/nar/28.1.27.

(36) Haug, K.; Cochrane, K.; Nainala, V. C.; Williams, M.; Chang, J.; Jayaseelan, K. V.; O'Donovan, C. MetaboLights: A Resource Evolving in Response to the Needs of Its Scientific Community. *Nucleic Acids Res.* **2020**, *48*, 440–444. https://doi.org/10.1093/nar/gkz1019.

(37) Lindon, J. C.; Nicholson, J. K.; Everett, J. R. NMR Spectroscopy of Biofluids. *Annu. Reports NMR Spectrosc.* **1999**, *38* (C), 1–88. https://doi.org/10.1016/S0066-4103(08)60035-6.

(38) Gil, Victor M.S., Geraldes, C. F. G. C. *Ressonância Magnética Nuclear – Fundamentos e Aplicações*; Gulbenkian, F. C., Ed.; Lisboa, 1987.

(39) Morrison, R.; Boyd, R. *Química Orgânica*, 16th ed.; Gulbenkian, F. C., Ed.; Lisboa, 2011.

(40) Cullen, C. H.; Ray, G. J.; Szabo, C. M. A Comparison of Quantitative Nuclear Magnetic Resonance Methods: Internal, External, and Electronic Referencing. *Magn. Reson. Chem.* **2013**, *51*, 705–713. https://doi.org/10.1002/mrc.4004.

(41) Rundlöf, T.; Mathiasson, M.; Bekiroglu, S.; Hakkarainen, B.; Bowden, T.; Arvidsson, T. Survey and Qualification of Internal Standards for Quantification by 1H NMR Spectroscopy. *J. Pharm. Biomed. Anal.* **2010**, *52*, 645–651. https://doi.org/10.1016/j.jpba.2010.02.007.

(42) Bharti, S. K.; Roy, R. Quantitative 1H NMR Spectroscopy. *TrAC Trends Anal. Chem.* **2012**, *35*, 5–26. https://doi.org/10.1016/j.trac.2012.02.007.

(43) Čuperlović-Culf, M.; Barnett, D. A.; Culf, A. S.; Chute, I. Cell Culture Metabolomics: Applications and Future Directions. *Drug Discov. Today* **2010**, *15*,

610–621. https://doi.org/10.1016/j.drudis.2010.06.012.

(44) Kim, S. J.; Kim, S. H.; Kim, J. H.; Hwang, S.; Yoo, H. J. Understanding Metabolomics in Biomedical Research. *Endocrinol. Metab.* **2016**, *31*, 7. https://doi.org/10.3803/EnM.2016.31.1.7.

(45) Duarte, I. F.; Lamego, I.; Rocha, C.; Gil, A. M. NMR Metabonomics for Mammalian Cell Metabolism Studies. *Bioanalysis* **2009**, *1*, 1597–1614. https://doi.org/10.4155/bio.09.151.

(46) Teng, Q.; Huang, W.; Collette, T. W.; Ekman, D. R.; Tan, C. A Direct Cell Quenching Method for Cell-Culture Based Metabolomics. *Metabolomics* **2009**, *5*, 199–208. https://doi.org/10.1007/s11306-008-0137-z.

(47) Dietmair, S.; Timmins, N. E.; Gray, P. P.; Nielsen, L. K.; Krömer, J. O. Towards Quantitative Metabolomics of Mammalian Cells: Development of a Metabolite Extraction Protocol. *Anal. Biochem.* **2010**, *404*, 155–164. https://doi.org/10.1016/j.ab.2010.04.031.

(48) Zhang, K.; Zhang, X.; Bai, Y.; Yang, L.; Wu, T.; Zhang, J.; Li, L.; Zhang, H.; Wang, H. Optimization of the Sample Preparation Method for Adherent Cell Metabolomics Based on Ultra-Performance Liquid Chromatography Coupled to Mass Spectrometry. *Anal. Methods* **2019**, *11*, 3678–3686. https://doi.org/10.1039/c9ay00326f.

(49) Martineau, E.; Tea, I.; Loaëc, G.; Giraudeau, P.; Akoka, S. Strategy for Choosing Extraction Procedures for NMR-Based Metabolomic Analysis of Mammalian Cells. *Anal. Bioanal. Chem.* **2011**, *401*, 2133–2142. https://doi.org/10.1007/s00216-011-5310-y.

(50) Bi, H.; Krausz, K. W.; Manna, S. K.; Li, F.; Johnson, C. H.; Gonzalez, F. J. Optimization of Harvesting, Extraction, and Analytical Protocols for UPLC-ESI-MS-Based Metabolomic Analysis of Adherent Mammalian Cancer Cells. *Anal. Bioanal. Chem.* **2013**, *405*, 5279–5289. https://doi.org/10.1007/s00216-013-6927-9.

(51) Aranibar, N.; Reily, M. D. NMR Methods for Metabolomics of Mammalian Cell Culture Bioreactors. In *Animal Cell Biotechnology*; Pörtner, R., Ed.; Methods in Molecular Biology; Humana Press: Totowa, NJ, 2014; Vol. 1104, pp 223–236. https://doi.org/10.1007/978-1-62703-733-4_15.

(52) Aranibar, N.; Borys, M.; Mackin, N. A.; Ly, V.; Abu-Absi, N.; Abu-Absi, S.; Niemitz, M.; Schilling, B.; Li, Z. J.; Brock, B.; Russell, R. J.; Tymiak, A.; Reily,

M. D. NMR-Based Metabolomics of Mammalian Cell and Tissue Cultures. *J. Biomol. NMR* **2011**, *49*, 195–206. https://doi.org/10.1007/s10858-011-9490-8.

(53) Hayton, S.; Maker, G. L.; Mullaney, I.; Trengove, R. D. Untargeted Metabolomics of Neuronal Cell Culture: A Model System for the Toxicity Testing of Insecticide Chemical Exposure. *J. Appl. Toxicol.* **2017**, *37* (12), 1481–1492. https://doi.org/10.1002/jat.3498.

(54) Balcerczyk, A.; Damblon, C.; Elena-Herrmann, B.; Panthu, B.; Rautureau, G. J. P. Metabolomic Approaches to Study Chemical Exposure-Related Metabolism Alterations in Mammalian Cell Cultures. *Int. J. Mol. Sci.* **2020**, *21* (18), 6843. https://doi.org/10.3390/ijms21186843.

(55) Dubuis, S.; Ortmayr, K.; Zampieri, M. A Framework for Large-Scale Metabolome Drug Profiling Links Coenzyme A Metabolism to the Toxicity of Anti-Cancer Drug Dichloroacetate. *Commun. Biol.* **2018**, *1*, 1–11. https://doi.org/10.1038/s42003-018-0111-x.

(56) Carrola, J.; Pinto, R. J. B.; Nasirpour, M.; Freire, C. S. R.; Gil, A. M.; Santos, C.; Oliveira, H.; Duarte, I. F. NMR Metabolomics Reveals Metabolism-Mediated Protective Effects in Liver (HepG2) Cells Exposed to Subtoxic Levels of Silver Nanoparticles. *J. Proteome Res.* **2018**, *17*, 1636–1646. https://doi.org/10.1021/acs.jproteome.7b00905.

(57) Tsai, I.-L.; Kuo, T.-C.; Ho, T.-J.; Harn, Y.-C.; Wang, S.-Y.; Fu, W.-M.; Kuo, C.-H.; Tseng, Y. Metabolomic Dynamic Analysis of Hypoxia in MDA-MB-231 and the Comparison with Inferred Metabolites from Transcriptomics Data. *Cancers (Basel).* **2013**, *5*, 491–510. https://doi.org/10.3390/cancers5020491.

(58) Bayet-Robert, M.; Lim, S.; Barthomeuf, C.; Morvan, D. Biochemical Disorders Induced by Cytotoxic Marine Natural Products in Breast Cancer Cells as Revealed by Proton NMR Spectroscopy-Based Metabolomics. *Biochem. Pharmacol.* **2010**, *80* (8), 1170–1179. https://doi.org/10.1016/j.bcp.2010.07.007.

(59) Ferretti, A.; Knijn, A.; Iorio, E.; Pulciani, S.; Giambenedetti, M.; Molinari, A.; Meschini, S.; Stringaro, A.; Calcabrini, A.; Freitas, I.; Strom, R.; Arancia, G.; Podo, F. Biophysical and Structural Characterization of 1H-NMR-Detectable Mobile Lipid Domains in NIH-3T3 Fibroblasts. *Biochim. Biophys. Acta - Mol. Cell Biol. Lipids* **1999**, *1438*, 329–348. https://doi.org/10.1016/S1388-1981(99)00071-2.

(60) Vilasi, A.; Vilasi, S.; Romano, R.; Acernese, F.; Barone, F.; Balestrieri, M. L.;

Maritato, R.; Irace, G.; Sirangelo, I. Unraveling Amyloid Toxicity Pathway in NIH3T3 Cells by a Combined Proteomic and 1 H-NMR Metabonomic Approach. *J. Cell. Physiol.* **2013**, *228*, 1359–1367. https://doi.org/10.1002/jcp.24294.

(61) Liu, S.; Wang, W.; Zhou, X.; Gu, R.; Ding, Z. Dose Responsive Effects of Cisplatin in L02 Cells Using NMR-Based Metabolomics. *Environ. Toxicol. Pharmacol.* **2014**, *37*, 150–157. https://doi.org/10.1016/j.etap.2013.11.016.

(62) Bradley, S. A.; Ouyang, A.; Purdie, J.; Smitka, T. A.; Wang, T.; Kaerner, A. Fermentanomics: Monitoring Mammalian Cell Cultures with NMR Spectroscopy. *J. Am. Chem. Soc.* **2010**, *132*, 9531–9533. https://doi.org/10.1021/ja101962c.

(63) Wagstaff, J. L.; Masterton, R. J.; Povey, J. F.; Smales, C. M.; Howard, M. J. 1H NMR Spectroscopy Profiling of Metabolic Reprogramming of Chinese Hamster Ovary Cells upon a Temperature Shift during Culture. *PLoS One* **2013**, *8*, 2–11. https://doi.org/10.1371/journal.pone.0077195.

(64) Miceli, M. V.; Kan, L. S.; Newsome, D. A. Phosphorus-31 NMR Spectroscopy of Cultured Human Retinal Pigmented Epithelial Cells. *Investig. Ophthalmol. Vis. Sci.* **1987**, *28* (1), 70–75.

(65) Hanahan, D.; Weinberg, R. A. The Hallmarks of Cancer. *Cell* **2000**, *100*, 57–70. https://doi.org/10.1016/S0092-8674(00)81683-9.

(66) Hanahan, D.; Weinberg, R. A. Hallmarks of Cancer: The Next Generation. *Cell* **2011**, *144*, 646–674. https://doi.org/10.1016/j.cell.2011.02.013.

(67) Halestrap, A. P.; Price, N. T. The Proton-Linked Monocarboxylate Transporter (MCT) Family: Structure, Function and Regulation. *Biochem. J.* **1999**, *299*, 281–299.

(68) Dimmer, K. S.; Friedrich, B.; Lang, F.; Deitmer, J. W.; Bröer, S. The Low-Affinity Monocarboxylate Transporter MCT4 Is Adapted to the Export of Lactate in Highly Glycolytic Cells. *Biochem. J.* **2000**, *350*, 219–227.

(69) Meredith, D.; Christian, H. C. The SLC16 Monocaboxylate Transporter Family. *Xenobiotica* **2008**, *38*, 1072–1106. https://doi.org/10.1080/00498250802010868.

(70) Vaupel, P.; Schmidberger, H.; Mayer, A. The Warburg Effect: Essential Part of Metabolic Reprogramming and Central Contributor to Cancer Progression. *Int. J. Radiat. Biol.* **2019**, *95*, 912–919. https://doi.org/10.1080/09553002.2019.1589653.

(71) Ward, C.; Meehan, J.; Gray, M. E.; Murray, A. F.; Argyle, D. J.; Kunkler, I. H.; Langdon, S. P. The Impact of Tumour PH on Cancer Progression: Strategies for Clinical Intervention. *Explor. Target. Anti-tumor Ther.* **2020**, *1*, 71–100.

https://doi.org/10.37349/etat.2020.00005.

(72) Pelicano, H.; Martin, D. S.; Xu, R.-H.; Huang, P. Glycolysis Inhibition for Anticancer Treatment. *Oncogene* **2006**, *25*, 4633–4646. https://doi.org/10.1038/sj.onc.1209597.

(73) Halestrap, A. P.; Meredith, D. The SLC16 Gene Family?From Monocarboxylate Transporters (MCTs) to Aromatic Amino Acid Transporters and Beyond. *Pflugers Arch. Eur. J. Physiol.* **2004**, *447*, 619–628. https://doi.org/10.1007/s00424-003-1067-2.

(74) Poole, R. C.; Sansom, C. E.; Halestrap, A. P. Studies of the Membrane Topology of the Rat Erythrocyte H+/Lactate Cotransporter (MCT1). *Biochem. J.* **1996**, *320* (3), 817–824. https://doi.org/10.1042/bj3200817.

(75) Wu, P.; Zhou, Y.; Guo, Y.; Zhang, S.-L.; Tam, K. Y. Recent Developments of Human Monocarboxylate Transporter (HMCT) Inhibitors as Anticancer Agents. *Drug Discov. Today* **2021**, *26*. https://doi.org/10.1016/j.drudis.2021.01.003.

(76) Halestrap, A. P. The Monocarboxylate Transporter Family-Structure and Functional Characterization. *IUBMB Life* **2012**, *64*, 1–9. https://doi.org/10.1002/iub.573.

(77) Pinheiro, C.; Longatto-Filho, A.; Scapulatempo, C.; Ferreira, L.; Martins, S.; Pellerin, L.; Rodrigues, M.; Alves, V. A. F.; Schmitt, F.; Baltazar, F. Increased Expression of Monocarboxylate Transporters 1, 2, and 4 in Colorectal Carcinomas. *Virchows Arch.* **2008**, *452*, 139–146. https://doi.org/10.1007/s00428-007-0558-5.

(78) Payen, V. L.; Mina, E.; Van Hée, V. F.; Porporato, P. E.; Sonveaux, P. Monocarboxylate Transporters in Cancer. *Mol. Metab.* **2020**, *33*, 48–66. https://doi.org/10.1016/j.molmet.2019.07.006.

(79) Fox, J. E. M.; Meredith, D.; Halestrap, A. P. Characterisation of Human Monocarboxylate Transporter 4 Substantiates Its Role in Lactic Acid Efflux from Skeletal Muscle. *J. Physiol.* **2000**, *529* (2), 285–293. https://doi.org/10.1111/j.1469-7793.2000.00285.x.

(80) Sonveaux, P.; Végran, F.; Schroeder, T.; Wergin, M. C.; Verrax, J.; Rabbani, Z. N.; De Saedeleer, C. J.; Kennedy, K. M.; Diepart, C.; Jordan, B. F.; Kelley, M. J.; Gallez, B.; Wahl, M. L.; Feron, O.; Dewhirst, M. W.; Saedeleer, C. J. De; Kennedy, K. M.; Diepart, C.; Jordan, B. F.; Kelley, M. J.; Gallez, B.; Wahl, M. L.; Feron, O.; Dewhirst, M. W. Targeting Lactate-Fueled Respiration Selectively Kills Hypoxic Tumor Cells in Mice. *J. Clin. Invest.* **2008**, *118*, 3930–3942.

https://doi.org/10.1172/JCI36843.however.

(81) Todenhöfer, T.; Seiler, R.; Stewart, C.; Moskalev, I.; Gao, J.; Ladhar, S.; Kamjabi, A.; Al Nakouzi, N.; Hayashi, T.; Choi, S.; Wang, Y.; Frees, S.; Daugaard, M.; Oo, H. Z.; Fisel, P.; Schwab, M.; Schaeffeler, E.; Douglas, J.; Hennenlotter, J.; Bedke, J.; Gibb, E. A.; Fazli, L.; Stenzl, A.; Black, P. C. Selective Inhibition of the Lactate Transporter MCT4 Reduces Growth of Invasive Bladder Cancer. *Mol. Cancer Ther.* **2018**, *17*, 2746–2755. https://doi.org/10.1158/1535-7163.MCT-18-0107.

(82) Beloueche-Babari, M.; Casals Galobart, T.; Delgado-Goni, T.; Wantuch, S.; Parkes, H. G.; Tandy, D.; Harker, J. A.; Leach, M. O. Monocarboxylate Transporter 1 Blockade with AZD3965 Inhibits Lipid Biosynthesis and Increases Tumour Immune Cell Infiltration. *Br. J. Cancer* **2020**, *122*, 895–903. https://doi.org/10.1038/s41416-019-0717-x.

(83) Wu, P.; Zhou, Y.; Guo, Y.; Zhang, S.-L.; Tam, K. Y. Recent Developments of Human Monocarboxylate Transporter (HMCT) Inhibitors as Anticancer Agents. *Drug Discov. Today* **2021**, *26* (3), 836–844. https://doi.org/10.1016/j.drudis.2021.01.003.

(84) Calori, I. R.; Piva, H. L.; Tedesco, A. C. Targeted Cancer Therapy Using Alpha-Cyano-4-Hydroxycinnamic Acid as a Novel Vector Molecule: A Proof-of-Concept Study. *J. Drug Deliv. Sci. Technol.* **2020**, *57*, 1–9. https://doi.org/10.1016/j.jddst.2020.101633.

(85) Sattler, B.; Kranz, M.; Wenzel, B.; Jain, N. T.; Moldovan, R.-P.; Toussaint, M.; Deuther-Conrad, W.; Ludwig, F.-A.; Teodoro, R.; Sattler, T.; Sadeghzadeh, M.; Sabri, O.; Brust, P. Preclinical Incorporation Dosimetry of [18F]FACH—A Novel 18F-Labeled MCT1/MCT4 Lactate Transporter Inhibitor for Imaging Cancer Metabolism with PET. *Molecules* **2020**, *25*, 2024. https://doi.org/10.3390/molecules25092024.

(86) Jonnalagadda, S.; Jonnalagadda, S. K.; Ronayne, C. T.; Nelson, G. L.; Solano, L. N.; Rumbley, J.; Holy, J.; Mereddy, V. R.; Drewes, L. R. Novel N,N-Dialkyl Cyanocinnamic Acids as Monocarboxylate Transporter 1 and 4 Inhibitors. *Oncotarget* **2019**, *10*, 2355–2368. https://doi.org/10.18632/oncotarget.26760.

(87) Mabrouk, M.; Das, D. B.; Salem, Z. A.; Beherei, H. H. Nanomaterials for Biomedical Applications: Production, Characterisations, Recent Trends and Difficulties. *Molecules* **2021**, *26*, 1–27. https://doi.org/10.3390/molecules26041077.

(88) Schnackenberg, L. K.; Sun, J.; Beger, R. D. Metabolomics Techniques in Nanotoxicology Studies. In *Nanomedicine for Inflammatory Diseases*; CRC Press, 2012; pp 141–156. https://doi.org/10.1007/978-1-62703-002-1_10.

(89) Oberdörster, G. Safety Assessment for Nanotechnology and Nanomedicine: Concepts of Nanotoxicology. *J. Intern. Med.* **2010**, *267*, 89–105. https://doi.org/10.1111/j.1365-2796.2009.02187.x.

(90) Savage, D. T.; Hilt, J. Z.; Dziubla, T. D. In Vitro Methods for Assessing Nanoparticle Toxicity; 2019; pp 1–29. https://doi.org/10.1007/978-1-4939-8916-4_1.

(91) Kumar, V.; Sharma, N.; Maitra, S. S. In Vitro and in Vivo Toxicity Assessment of Nanoparticles. *Int. Nano Lett.* **2017**, *7* (4), 243–256. https://doi.org/10.1007/s40089-017-0221-3.

(92) Shin, T. H.; Nithiyanandam, S.; Lee, D. Y.; Kwon, D. H.; Hwang, J. S.; Kim, S. G.; Jang, Y. E.; Basith, S.; Park, S.; Mo, J.-S.; Lee, G. Analysis of Nanotoxicity with Integrated Omics and Mechanobiology. *Nanomaterials* **2021**, *11* (9), 2385. https://doi.org/10.3390/nano11092385.

(93) Lv, M.; Huang, W.; Chen, Z.; Jiang, H.; Chen, J.; Tian, Y.; Zhang, Z.; Xu, F. Metabolomics Techniques for Nanotoxicity Investigations. *Bioanalysis* **2015**, *7*, 1527–1544. https://doi.org/10.4155/bio.15.83.

(94) Olsson, L. Development of an in Vitro Assay for Analysis of Cellular Uptake of Nanoparticles, 2013.

(95) Lu, X.; Tian, Y.; Zhao, Q.; Jin, T.; Xiao, S.; Fan, X. Integrated Metabonomics Analysis of the Size-Response Relationship of Silica Nanoparticles-Induced Toxicity in Mice. *Nanotechnology* **2011**, *22* (5), 055101. https://doi.org/10.1088/0957-4484/22/5/055101.

(96) Gioria, S.; Lobo Vicente, J.; Barboro, P.; La Spina, R.; Tomasi, G.; Urbán, P.; Kinsner-Ovaskainen, A.; François, R.; Chassaigne, H. A Combined Proteomics and Metabolomics Approach to Assess the Effects of Gold Nanoparticles in Vitro. *Nanotoxicology* **2016**, *10*, 736–748. https://doi.org/10.3109/17435390.2015.1121412.

(97) Lindeque, J. Z.; Matthyser, A.; Mason, S.; Louw, R.; Taute, C. J. F. Metabolomics Reveals the Depletion of Intracellular Metabolites in HepG2 Cells after Treatment with Gold Nanoparticles. *Nanotoxicology* **2018**, *12*, 251–262. https://doi.org/10.1080/17435390.2018.1432779.

(98) Li, Q.; Liao, J.; Lei, C.; Shi, J.; Zhang, H.; Han, Q.; Guo, J.; Hu, L.; Li, Y.; Pan, J.; Tang, Z. Metabolomics Analysis Reveals the Effect of Copper on Autophagy in Myocardia of Pigs. *Ecotoxicol. Environ. Saf.* **2021**, *213*, 112040. https://doi.org/10.1016/j.ecoenv.2021.112040.

(99) Lee, S.-H.; Wang, T.-Y.; Hong, J.-H.; Cheng, T.-J.; Lin, C.-Y. NMR-Based Metabolomics to Determine Acute Inhalation Effects of Nano- and Fine-Sized ZnO Particles in the Rat Lung. *Nanotoxicology* **2016**, *10* (7), 924–934. https://doi.org/10.3109/17435390.2016.1144825.

(100) Zhang, W.; Zhao, Y.; Li, F.; Li, L.; Feng, Y.; Min, L.; Ma, D.; Yu, S.; Liu, J.; Zhang, H.; Shi, T.; Li, F.; Shen, W. Zinc Oxide Nanoparticle Caused Plasma Metabolomic Perturbations Correlate with Hepatic Steatosis. *Front. Pharmacol.* **2018**, *9*, 57. https://doi.org/10.3389/fphar.2018.00057.

(101) Raja, G.; Selvaraj, V.; Suk, M.; Suk, K. T.; Kim, T.-J. Metabolic Phenotyping Analysis of Graphene Oxide Nanosheets Exposures in Breast Cancer Cells: Metabolomics Profiling Techniques. *Process Biochem.* **2021**, *104*, 39–45. https://doi.org/10.1016/j.procbio.2021.02.016.

(102) Lykogianni, M.; Papadopoulou, E.-A.; Sapalidis, A.; Tsiourvas, D.; Sideratou, Z.; Aliferis, K. A. Metabolomics Reveals Differential Mechanisms of Toxicity of Hyperbranched Poly(Ethyleneimine)-Derived Nanoparticles to the Soil-Borne Fungus Verticillium Dahliae Kleb. *Pestic. Biochem. Physiol.* **2020**, No. 165, 1–14. https://doi.org/10.1016/j.pestbp.2020.02.001.

(103) Elmi, T.; Shafiee Ardestani, M.; Hajialiani, F.; Motevalian, M.; Mohamadi, M.; Sadeghi, S.; Zamani, Z.; Tabatabaie, F. Novel Chloroquine Loaded Curcumin Based Anionic Linear Globular Dendrimer G2: A Metabolomics Study on Plasmodium Falciparum in Vitro Using 1 H NMR Spectroscopy. *Parasitology* **2020**, 1–13. https://doi.org/10.1017/S0031182020000372.

(104) Jain, K.; Kesharwani, P.; Gupta, U.; Jain, N. K. Dendrimer Toxicity: Let's Meet the Challenge. *Int. J. Pharm.* **2010**, *394*, 122–142. https://doi.org/10.1016/j.ijpharm.2010.04.027.

(105) Duncan, R.; Izzo, L. Dendrimer Biocompatibility and Toxicity. *Adv. Drug Deliv. Rev.* **2005**, *57* (15), 2215–2237. https://doi.org/10.1016/j.addr.2005.09.019.

(106) Gillies, E. R.; Fréchet, J. M. J. Dendrimers and Dendritic Polymers in Drug Delivery. *Drug Discov. Today* **2005**, *10* (1), 35–43. https://doi.org/10.1016/S1359-6446(04)03276-3.

(107) Buhleier, E.; Wehner, W.; Vögtle, F. “Cascade”- and “Nonskid-Chain-like” Syntheses of Molecular Cavity Topologies. *Synthesis (Stuttg).* **1978**, *1978* (02), 155–158. https://doi.org/10.1055/s-1978-24702.

(108) Kesharwani, P.; Jain, K.; Jain, N. K. Dendrimer as Nanocarrier for Drug Delivery. *Prog. Polym. Sci.* **2014**, *39* (2), 268–307. https://doi.org/10.1016/j.progpolymsci.2013.07.005.

(109) Mignani, S.; Rodrigues, J.; Tomas, H.; Zablocka, M.; Shi, X.; Caminade, A.-M.; Majoral, J.-P. Dendrimers in Combination with Natural Products and Analogues as Anti-Cancer Agents. *Chem. Soc. Rev.* **2018**, *47* (2), 514–532. https://doi.org/10.1039/C7CS00550D.

(110) Kateb, B.; Chiu, K.; Black, K. L.; Yamamoto, V.; Khalsa, B.; Ljubimova, J. Y.; Ding, H.; Patil, R.; Portilla-Arias, J. A.; Modo, M.; Moore, D. F.; Farahani, K.; Okun, M. S.; Prakash, N.; Neman, J.; Ahdoot, D.; Grundfest, W.; Nikzad, S.; Heiss, J. D. Nanoplatforms for Constructing New Approaches to Cancer Treatment, Imaging, and Drug Delivery: What Should Be the Policy? *Neuroimage* **2011**, *54* (SUPPL. 1), S106–S124. https://doi.org/10.1016/j.neuroimage.2010.01.105.

(111) Esfand, R.; Tomalia, D. A. Poly(Amidoamine) (PAMAM) Dendrimers: From Biomimicry to Drug Delivery and Biomedical Applications. *Drug Discov. Today* **2001**, *6* (8), 427–436. https://doi.org/10.1016/S1359-6446(01)01757-3.

(112) Wang, X.; Yang, L.; Chen, Z.; Shin, D. M. Application of Nanotechnology in Cancer Therapy and Imaging. *CA. Cancer J. Clin.* **2008**, *58* (2), 97–110. https://doi.org/10.3322/CA.2007.0003.

(113) Vergaro, V.; Scarlino, F.; Bellomo, C.; Rinaldi, R.; Vergara, D.; Maffia, M.; Baldassarre, F.; Giannelli, G.; Zhang, X.; Lvov, Y. M.; Leporatti, S. Drug-Loaded Polyelectrolyte Microcapsules for Sustained Targeting of Cancer Cells. *Adv. Drug Deliv. Rev.* **2011**, *63* (9), 847–864. https://doi.org/10.1016/j.addr.2011.05.007.

(114) D’Emanuele, A.; Attwood, D. Dendrimer–Drug Interactions. *Adv. Drug Deliv. Rev.* **2005**, *57* (15), 2147–2162. https://doi.org/10.1016/j.addr.2005.09.012.

(115) Augustus, E. N.; Allen, E. T.; Nimibofa, A.; Donbebe, W. A Review of Synthesis, Characterization and Applications of Functionalized Dendrimers. *Am. J. Polym. Sci.* **2017**, *7* (1), 8–14. https://doi.org/10.5923/j.ajps.20170701.02.

(116) Liu, M.; Fréchet, J. M. J. Designing Dendrimers for Drug Delivery. *Pharm. Sci. Technolo. Today* **1999**, *2* (10), 393–401. https://doi.org/10.1016/S1461-

5347(99)00203-5.

(117) Gupta, V.; Nayak, S. Dendrimers: A Review on Synthetic Approaches. *J. Appl. Pharm. Sci.* **2015**, *5* (3), 117–122. https://doi.org/10.7324/JAPS.2015.50321.

(118) Grayson, S. M.; Fréchet, J. M. J. Convergent Dendrons and Dendrimers: From Synthesis to Applications. *Chem. Rev.* **2001**, *101* (12), 3819–3868. https://doi.org/10.1021/cr990116h.

(119) Idris, A. O.; Mamba, B.; Feleni, U. Poly (Propylene Imine) Dendrimer: A Potential Nanomaterial for Electrochemical Application. *Mater. Chem. Phys.* **2020**, *244*, 1–9. https://doi.org/10.1016/j.matchemphys.2020.122641.

(120) Mousavifar, L.; Roy, R. Design, Synthetic Strategies, and Therapeutic Applications of Heterofunctional Glycodendrimers. *Molecules* **2021**, *26* (9), 2428. https://doi.org/10.3390/molecules26092428.

(121) Rodrigues, J.; Jardim, M. G.; Figueira, J.; Gouveia, M.; Tomás, H.; Rissanen, K. Poly(Alkylidenamines) Dendrimers as Scaffolds for the Preparation of Low-Generation Ruthenium Based Metallodendrimers. *New J. Chem.* **2011**, *35* (10), 1938. https://doi.org/10.1039/c1nj20364a.

(122) El Kazzouli, S.; El Brahmi, N.; Mignani, S.; Bousmina, M.; Zablocka, M.; -P. Majoral, J. From Metallodrugs to Metallodendrimers for Nanotherapy in Oncology: A Concise Overview. *Curr. Med. Chem.* **2012**, *19* (29), 4995–5010. https://doi.org/10.2174/092986731120902499 5.

(123) Ramírez-Crescencio, F.; Enciso, A.; Hasan, M.; da Costa, V.; Annunziata, O.; Redón, R.; Coffer, J.; Simanek, E. Thermoregulated Coacervation, Metal-Encapsulation and Nanoparticle Synthesis in Novel Triazine Dendrimers. *Molecules* **2016**, *21*, 599. https://doi.org/10.3390/molecules21050599.

(124) Caminade, A.-M.; Servin, P.; Laurent, R.; Majoral, J.-P. Dendrimeric Phosphines in Asymmetric Catalysis. *Chem. Soc. Rev.* **2008**, *37*, 56–67. https://doi.org/10.1039/B606569B.

(125) Caminade, A.-M.; Majoral, J.-P. Bifunctional Phosphorus Dendrimers and Their Properties. *Molecules* **2016**, *21*, 538. https://doi.org/10.3390/molecules21040538.

(126) Maciel, D.; Guerrero-Beltrán, C.; Ceña-Diez, R.; Tomás, H.; Muñoz-Fernández, M. Á.; Rodrigues, J. New Anionic Poly(Alkylideneamine) Dendrimers as Microbicide Agents against HIV-1 Infection. *Nanoscale* **2019**, *11* (19), 9679–9690. https://doi.org/10.1039/C9NR00303G.

(127) Svenson, S.; Tomalia, D. Dendrimers in Biomedical Applications—Reflections on

the Field. *Adv. Drug Deliv. Rev.* **2005**, *57*, 2106–2129. https://doi.org/10.1016/j.addr.2005.09.018.

(128) Kesharwani, P.; Banerjee, S.; Gupta, U.; Mohd Amin, M. C. I.; Padhye, S.; Sarkar, F. H.; Iyer, A. K. PAMAM Dendrimers as Promising Nanocarriers for RNAi Therapeutics. *Mater. Today* **2015**, *18* (10), 565–572. https://doi.org/10.1016/j.mattod.2015.06.003.

(129) Gupta, U.; Agashe, H. B.; Asthana, A.; Jain, N. K. Dendrimers: Novel Polymeric Nanoarchitectures for Solubility Enhancement. *Biomacromolecules* **2006**, *7* (3), 649–658. https://doi.org/10.1021/bm050802s.

(130) Mukherjee, S. P.; Lyng, F. M.; Garcia, A.; Davoren, M.; Byrne, H. J. Mechanistic Studies of in Vitro Cytotoxicity of Poly(Amidoamine) Dendrimers in Mammalian Cells. *Toxicol. Appl. Pharmacol.* **2010**, *248* (3), 259–268. https://doi.org/10.1016/j.taap.2010.08.016.

(131) Mukherjee, S. P.; Davoren, M.; Byrne, H. J. In Vitro Mammalian Cytotoxicological Study of PAMAM Dendrimers – Towards Quantitative Structure Activity Relationships. *Toxicol. Vitr.* **2010**, *24* (1), 169–177. https://doi.org/10.1016/j.tiv.2009.09.014.

(132) Naha, P.; Mukherjee, S.; Byrne, H. Toxicology of Engineered Nanoparticles: Focus on Poly(Amidoamine) Dendrimers. *Int. J. Environ. Res. Public Health* **2018**, *15* (2), 338. https://doi.org/10.3390/ijerph15020338.

(133) Janaszewska; Lazniewska; Trzepiński; Marcinkowska; Klajnert-Maculewicz. Cytotoxicity of Dendrimers. *Biomolecules* **2019**, *9* (8), 330. https://doi.org/10.3390/biom9080330.

(134) Navath, R. S.; Menjoge, A. R.; Wang, B.; Romero, R.; Kannan, S.; Kannan, R. M. Amino Acid-Functionalized Dendrimers with Heterobifunctional Chemoselective Peripheral Groups for Drug Delivery Applications. *Biomacromolecules* **2010**, *11* (6), 1544–1563. https://doi.org/10.1021/bm100186b.

(135) Santos, J. L.; Oliveira, H.; Pandita, D.; Rodrigues, J.; Pêgo, A. P.; Granja, P. L.; Tomás, H. Functionalization of Poly(Amidoamine) Dendrimers with Hydrophobic Chains for Improved Gene Delivery in Mesenchymal Stem Cells. *J. Control. Release* **2010**, *144* (1), 55–64. https://doi.org/10.1016/j.jconrel.2010.01.034.

(136) Fu, F.-F.; Zhou, B.-Q.; Ouyang, Z.-J.; Wu, Y.-L.; Zhu, J.-Y.; Shen, M.-W.; Xia, J.-D.; Shi, X.-Y. Multifunctional Cholesterol-Modified Dendrimers for Targeted Drug Delivery to Cancer Cells Expressing Folate Receptors. *Chinese J. Polym. Sci.*

2019, *37* (2), 129–135. https://doi.org/10.1007/s10118-019-2172-9.

(137) Qian, W.; Song, T.; Ye, M.; Huang, X.; Li, Y.; Hao, B. Au-Covered Nanographene Oxide/PEG/PAMAM for Surface-Enhanced Raman Scattering Detection. *Compos. Commun.* **2021**, *23* (December 2020), 100598. https://doi.org/10.1016/j.coco.2020.100598.

(138) Santos, S. D.; Xavier, M.; Leite, D. M.; Moreira, D. A.; Custódio, B.; Torrado, M.; Castro, R.; Leiro, V.; Rodrigues, J.; Tomás, H.; Pêgo, A. P. PAMAM Dendrimers: Blood-Brain Barrier Transport and Neuronal Uptake after Focal Brain Ischemia. *J. Control. Release* **2018**, *291*, 65–79. https://doi.org/10.1016/j.jconrel.2018.10.006.

(139) Kasprzak, A.; Dabrowski, B.; Zuchowska, A. A Biocompatible Poly(Amidoamine) (PAMAM) Dendrimer Octa-Substituted with α-Cyclodextrin towards the Controlled Release of Doxorubicin Hydrochloride from Its Ferrocenyl Prodrug. *RSC Adv.* **2020**, *10* (39), 23440–23445. https://doi.org/10.1039/D0RA03694C.

(140) Triulzi, R. C.; Micic, M.; Giordani, S.; Serry, M.; Chiou, W.-A.; Leblanc, R. M. Immunoasssay Based on the Antibody-Conjugated PAMAM-Dendrimer–Gold Quantum Dot Complex. *Chem. Commun.* **2006**, No. 48, 5068–5070. https://doi.org/10.1039/B611278A.

(141) Wolfenden, M. L.; Cloninger, M. J. Mannose/Glucose-Functionalized Dendrimers To Investigate the Predictable Tunability of Multivalent Interactions. *J. Am. Chem. Soc.* **2005**, *127* (35), 12168–12169. https://doi.org/10.1021/ja053008n.

(142) Sztandera, K.; Działak, P.; Marcinkowska, M.; Stańczyk, M.; Gorzkiewicz, M.; Janaszewska, A.; Klajnert-Maculewicz, B. Sugar Modification Enhances Cytotoxic Activity of PAMAM-Doxorubicin Conjugate in Glucose-Deprived MCF-7 Cells – Possible Role of GLUT1 Transporter. *Pharm. Res.* **2019**, *36* (10), 140. https://doi.org/10.1007/s11095-019-2673-9.

(143) Biswas, S.; Deshpande, P. P.; Navarro, G.; Dodwadkar, N. S.; Torchilin, V. P. Lipid Modified Triblock PAMAM-Based Nanocarriers for SiRNA Drug Co-Delivery. *Biomaterials* **2013**, *34* (4), 1289–1301. https://doi.org/10.1016/j.biomaterials.2012.10.024.

(144) Jang, W.-D.; Kamruzzaman Selim, K. M.; Lee, C.-H.; Kang, I.-K. Bioinspired Application of Dendrimers: From Bio-Mimicry to Biomedical Applications. *Prog. Polym. Sci.* **2009**, *34*, 1–23. https://doi.org/10.1016/j.progpolymsci.2008.08.003.

(145) Kolhe, P. Drug Complexation, in Vitro Release and Cellular Entry of Dendrimers

and Hyperbranched Polymers. *Int. J. Pharm.* **2003**, *259* (1–2), 143–160. https://doi.org/10.1016/S0378-5173(03)00225-4.

(146) McNerny, D. Q.; Leroueil, P. R.; Baker, J. R. Understanding Specific and Nonspecific Toxicities: A Requirement for the Development of Dendrimer-Based Pharmaceuticals. *Wiley Interdiscip. Rev. Nanomedicine Nanobiotechnology* **2010**, *2* (3), 249–259. https://doi.org/10.1002/wnan.79.

(147) Han, Y.-L.; Kim, S.-Y.; Kim, T.; Kim, K.-H.; Park, J.-W. The Role of Terminal Groups in Dendrimer Systems for the Treatment of Organic Contaminants in Aqueous Environments. *J. Clean. Prod.* **2020**, *250*, 119494. https://doi.org/10.1016/j.jclepro.2019.119494.

(148) Mustapha Kamil, Y.; Al-Rekabi, S. H.; Yaacob, M. H.; Syahir, A.; Chee, H. Y.; Mahdi, M. A.; Abu Bakar, M. H. Detection of Dengue Using PAMAM Dendrimer Integrated Tapered Optical Fiber Sensor. *Sci. Rep.* **2019**, *9* (1), 13483. https://doi.org/10.1038/s41598-019-49891-7.

(149) Andrés, R.; de Jesús, E.; Flores, J. C. Catalysts Based on Palladium Dendrimers. *New J. Chem.* **2007**, *31* (7), 1161. https://doi.org/10.1039/b615761k.

(150) Araújo, R.; Santos, S.; Igne Ferreira, E.; Giarolla, J. New Advances in General Biomedical Applications of PAMAM Dendrimers. *Molecules* **2018**, *23* (11), 2849. https://doi.org/10.3390/molecules23112849.

(151) He, H.; Li, Y.; Jia, X.-R.; Du, J.; Ying, X.; Lu, W.-L.; Lou, J.-N.; Wei, Y. PEGylated Poly(Amidoamine) Dendrimer-Based Dual-Targeting Carrier for Treating Brain Tumors. *Biomaterials* **2011**, *32* (2), 478–487. https://doi.org/10.1016/j.biomaterials.2010.09.002.

(152) He, X.; Alves, C. S.; Oliveira, N.; Rodrigues, J.; Zhu, J.; Bányai, I.; Tomás, H.; Shi, X. RGD Peptide-Modified Multifunctional Dendrimer Platform for Drug Encapsulation and Targeted Inhibition of Cancer Cells. *Colloids Surfaces B Biointerfaces* **2015**, *125*, 82–89. https://doi.org/10.1016/j.colsurfb.2014.11.004.

(153) Vandamme, T. F.; Brobeck, L. Poly(Amidoamine) Dendrimers as Ophthalmic Vehicles for Ocular Delivery of Pilocarpine Nitrate and Tropicamide. *J. Control. Release* **2005**, *102* (1), 23–38. https://doi.org/10.1016/j.jconrel.2004.09.015.

(154) Shi, X.; Sun, K.; Balogh, L. P.; Baker, J. R. Synthesis, Characterization, and Manipulation of Dendrimer-Stabilized Iron Sulfide Nanoparticles. *Nanotechnology* **2006**, *17* (18), 4554–4560. https://doi.org/10.1088/0957-4484/17/18/005.

(155) Aliannejadi, S.; Hassani, A. H.; Panahi, H. A.; Borghei, S. M. Fabrication and Characterization of High-Branched Recyclable PAMAM Dendrimer Polymers on the Modified Magnetic Nanoparticles for Removing Naphthalene from Aqueous Solutions. *Microchem. J.* **2019**, *145*, 767–777. https://doi.org/10.1016/j.microc.2018.11.043.

(156) Hou, C.; Zhu, H.; Wu, D.; Li, Y.; Hou, K.; Jiang, Y.; Li, Y. Immobilized Lipase on Macroporous Polystyrene Modified by PAMAM-Dendrimer and Their Enzymatic Hydrolysis. *Process Biochem.* **2014**, *49* (2), 244–249. https://doi.org/10.1016/j.procbio.2013.10.019.

(157) Caminade, A.-M. Dendrimers, an Emerging Opportunity in Personalized Medicine? *J. Pers. Med.* **2022**, *12* (8), 1334. https://doi.org/10.3390/jpm12081334.

(158) Price, C. F.; Tyssen, D.; Sonza, S.; Davie, A.; Evans, S.; Lewis, G. R.; Xia, S.; Spelman, T.; Hodsman, P.; Moench, T. R.; Humberstone, A.; Paull, J. R. A.; Tachedjian, G. SPL7013 Gel (VivaGel®) Retains Potent HIV-1 and HSV-2 Inhibitory Activity Following Vaginal Administration in Humans. *PLoS One* **2011**, *6* (9), e24095. https://doi.org/10.1371/journal.pone.0024095.

(159) León, Z.; García-Cañaveras, J. C.; Donato, M. T.; Lahoz, A. Mammalian Cell Metabolomics: Experimental Design and Sample Preparation. *Electrophoresis* **2013**, *34* (19), 2762–2775. https://doi.org/10.1002/elps.201200605.

(160) Bligh, E. G.; Dyer, W. J. A Rapid Method of Total Lipid Extraction and Purification. *Can. J. Biochem. Physiol.* **1959**, *37* (8), 911–917. https://doi.org/10.1139/o59-099.

(161) Lauri, I.; Savorani, F.; Iaccarino, N.; Zizza, P.; Pavone, L. M.; Novellino, E.; Engelsen, S. B.; Randazzo, A. Development of an Optimized Protocol for NMR Metabolomics Studies of Human Colon Cancer Cell Lines and First Insight from Testing of the Protocol Using DNA G-Quadruplex Ligands as Novel Anti-Cancer Drugs. *Metabolites* **2016**, *6* (1), 1–14. https://doi.org/10.3390/metabo6010004.

(162) Dona, A. C.; Kyriakides, M.; Scott, F.; Shephard, E. A.; Varshavi, D.; Veselkov, K.; Everett, J. R. A Guide to the Identification of Metabolites in NMR-Based Metabonomics/Metabolomics Experiments. *Comput. Struct. Biotechnol. J.* **2016**, *14*, 135–153. https://doi.org/10.1016/j.csbj.2016.02.005.

(163) Kostidis, S.; Addie, R. D.; Morreau, H.; Mayboroda, O. A.; Giera, M. Quantitative NMR Analysis of Intra- and Extracellular Metabolism of Mammalian Cells: A Tutorial. *Anal. Chim. Acta* **2017**, *980*, 1–24.

https://doi.org/10.1016/j.aca.2017.05.011.

(164) Pang, Z.; Chong, J.; Zhou, G.; de Lima Morais, D. A.; Chang, L.; Barrette, M.; Gauthier, C.; Jacques, P.-É.; Li, S.; Xia, J. MetaboAnalyst 5.0: Narrowing the Gap between Raw Spectra and Functional Insights. *Nucleic Acids Res.* **2021**, *49* (W1), W388–W396. https://doi.org/10.1093/nar/gkab382.

(165) van den Berg, R. A.; Hoefsloot, H. C. J.; Westerhuis, J. A.; Smilde, A. K.; van der Werf, M. J. Centering, Scaling, and Transformations: Improving the Biological Information Content of Metabolomics Data. *BMC Genomics* **2006**, *7* (1), 142. https://doi.org/10.1186/1471-2164-7-142.

(166) Weljie, A. M.; Newton, J.; Mercier, P.; Carlson, E.; Slupsky, C. M. Targeted Profiling: Quantitative Analysis of 1 H NMR Metabolomics Data. *Anal. Chem.* **2006**, *78* (13), 4430–4442. https://doi.org/10.1021/ac060209g.

(167) Jewison, T.; Su, Y.; Disfany, F. M.; Liang, Y.; Knox, C.; Maciejewski, A.; Poelzer, J.; Huynh, J.; Zhou, Y.; Arndt, D.; Djoumbou, Y.; Liu, Y.; Deng, L.; Guo, A. C.; Han, B.; Pon, A.; Wilson, M.; Rafatnia, S.; Liu, P.; Wishart, D. S. SMPDB 2.0: Big Improvements to the Small Molecule Pathway Database. *Nucleic Acids Res.* **2014**, *42* (D1), D478–D484. https://doi.org/10.1093/nar/gkt1067.

(168) Goeman, J. J.; van de Geer, S. A.; de Kort, F.; van Houwelingen, H. C. A Global Test for Groups of Genes: Testing Association with a Clinical Outcome. *Bioinformatics* **2004**, *20* (1), 93–99. https://doi.org/10.1093/bioinformatics/btg382.

(169) Bull, B.; Houwen, B.; Koepke, J.; Simson, E. *Reference and Selected Procedures for the Quantitative Determination of Hemoglobin in Blood*, 3rd editio.; NCCLS: Wayne, Pa, 2000.

(170) Standard Practice for Assessment of Hemolytic Properties of Materials, ASTM International. In *ASTM F756-17*; ASTM International: West Conshohocken, PA, 2017.

(171) Astaldi, G.; Sirtori, C.; Vanzetti Fondazione Carlo Erba, G. International Committee for Standardization in Haematology. Recommendations for Reference Method for Haemoglobinometry in Human Blood (ICSH Standard EP 6/2: 1977) and Specifications for International Haemiglobincyanide Reference Preparation (ICSH Standard. *J. Clin. Pathol.* **1978**, *31* (2), 139–143. https://doi.org/10.1136/jcp.31.2.139.

(172) Leiro, V.; Garcia, J. P.; Tomás, H.; Pêgo, A. P. The Present and the Future of

Degradable Dendrimers and Derivatives in Theranostics. *Bioconjug. Chem.* **2015**, *26* (7), 1185–1197. https://doi.org/10.1021/bc5006224.

(173) Yu, D.; Zhang, S.; Feng, A.; Xu, D.; Zhu, Q.; Mao, Y.; Zhao, Y.; Lv, Y.; Han, C.; Liu, R.; Tian, Y. Methotrexate, Doxorubicin, and Cisplatinum Regimen Is Still the Preferred Option for Osteosarcoma Chemotherapy. *Medicine (Baltimore).* **2019**, *98* (19), e15582. https://doi.org/10.1097/MD.0000000000015582.

(174) Schmid, B. C.; Oehler, M. K. New Perspectives in Ovarian Cancer Treatment. *Maturitas* **2014**, *77* (2), 128–136. https://doi.org/10.1016/j.maturitas.2013.11.009.

(175) Yuan, Z.; Zhang, Y.; Cao, D.; Shen, K.; Li, Q.; Zhang, G.; Wu, X.; Cui, M.; Yue, Y.; Cheng, W.; Wang, L.; Qu, P.; Tao, G.; Hou, J.; Sun, L.; Meng, Y.; Li, G.; Li, C.; Shi, H.; Chen, Y. Pegylated Liposomal Doxorubicin in Patients with Epithelial Ovarian Cancer. *J. Ovarian Res.* **2021**, *14* (1), 12. https://doi.org/10.1186/s13048-020-00736-2.

(176) Pan, D. C.; Krishnan, V.; Salinas, A. K.; Kim, J.; Sun, T.; Ravid, S.; Peng, K.; Wu, D.; Nurunnabi, M.; Nelson, J. A.; Niziolek, Z.; Guo, J.; Mitragotri, S. Hyaluronic Acid–Doxorubicin Nanoparticles for Targeted Treatment of Colorectal Cancer. *Bioeng. Transl. Med.* **2021**, *6* (1), 1–14. https://doi.org/10.1002/btm2.10166.

(177) Xiong, S.; Xiao, G. Reverting Doxorubicin Resistance in Colon Cancer by Targeting a Key Signaling Protein, Steroid Receptor Coactivator. *Exp. Ther. Med.* **2018**, *15* (4), 3751–3758. https://doi.org/10.3892/etm.2018.5912.

(178) Gonçalves, M.; Mignani, S.; Rodrigues, J.; Tomás, H. A Glance over Doxorubicin Based-Nanotherapeutics: From Proof-of-Concept Studies to Solutions in the Market. *J. Control. Release* **2020**, *317*, 347–374. https://doi.org/10.1016/j.jconrel.2019.11.016.

(179) Chanphai, P.; Bekale, L.; Sanyakamdhorn, S.; Agudelo, D.; Bérubé, G.; Thomas, T. J.; Tajmir-Riahi, H. A. PAMAM Dendrimers in Drug Delivery: Loading Efficacy and Polymer Morphology. *Can. J. Chem.* **2017**, *95* (9), 891–896. https://doi.org/10.1139/cjc-2017-0115.

(180) Yang, W.; Wang, Y.; Zhou, Q.; Tang, H. Analysis of Human Urine Metabolites Using SPE and NMR Spectroscopy. *Sci. China Ser. B Chem.* **2008**, *51* (3), 218–225. https://doi.org/10.1007/s11426-008-0031-6.

(181) Lee, I. J.; Hom, K.; Bai, G.; Shapiro, M. NMR Metabolomic Analysis of Caco-2 Cell Differentiation. *J. Proteome Res.* **2009**, *8* (8), 4104–4108. https://doi.org/10.1021/pr8010759.

(182) Zielinski, D. C.; Jamshidi, N.; Corbett, A. J.; Bordbar, A.; Thomas, A.; Palsson, B. O. Systems Biology Analysis of Drivers Underlying Hallmarks of Cancer Cell Metabolism. *Sci. Rep.* **2017**, *7* (1), 41241. https://doi.org/10.1038/srep41241.

(183) Nilsson, A.; Haanstra, J. R.; Engqvist, M.; Gerding, A.; Bakker, B. M.; Klingmüller, U.; Teusink, B.; Nielsen, J. Quantitative Analysis of Amino Acid Metabolism in Liver Cancer Links Glutamate Excretion to Nucleotide Synthesis. *Proc. Natl. Acad. Sci.* **2020**, *117* (19), 10294–10304. https://doi.org/10.1073/pnas.1919250117.

(184) Lamichhane, S.; Sen, P.; Dickens, A. M.; Hyötyläinen, T.; Orešič, M. An Overview of Metabolomics Data Analysis: Current Tools and Future Perspectives; 2018; pp 387–413. https://doi.org/10.1016/bs.coac.2018.07.001.

(185) Walenta, S.; Schroeder, T.; Mueller-Klieser, W. Lactate in Solid Malignant Tumors: Potential Basis of a Metabolic Classification in Clinical Oncology. *Curr. Med. Chem.* **2004**, *11* (16), 2195–2204. https://doi.org/10.2174/0929867043364711.

(186) Hirschhaeuser, F.; Sattler, U. G. a; Mueller-Klieser, W. Lactate: A Metabolic Key Player in Cancer. *Cancer Res.* **2011**, *71* (22), 6921–6925. https://doi.org/10.1158/0008-5472.CAN-11-1457.

(187) de la Cruz-López, K. G.; Castro-Muñoz, L. J.; Reyes-Hernández, D. O.; García-Carrancá, A.; Manzo-Merino, J. Lactate in the Regulation of Tumor Microenvironment and Therapeutic Approaches. *Front. Oncol.* **2019**, *9*, 1143. https://doi.org/10.3389/fonc.2019.01143.

(188) Wlodarczyk, S. R.; Costa-Silva, T. A.; Pessoa-Jr, A.; Madeira, P.; Monteiro, G. Effect of Osmolytes on the Activity of Anti-Cancer Enzyme L-Asparaginase II from Erwinia Chrysanthemi. *Process Biochem.* **2019**, *81*, 123–131. https://doi.org/10.1016/j.procbio.2019.03.009.

(189) Barcelos, R. P.; Stefanello, S. T.; Mauriz, J. L.; Gonzalez-Gallego, J.; Soares, F. A. A. Creatine and the Liver: Metabolism and Possible Interactions. *Mini-Reviews Med. Chem.* **2015**, *16* (1), 12–18. https://doi.org/10.2174/1389557515666150722102613.

(190) Xia, J.; Wishart, D. S. Using MetaboAnalyst 3.0 for Comprehensive Metabolomics Data Analysis. *Curr. Protoc. Bioinforma.* **2016**, *55* (1), 14.10.1-14.10.91. https://doi.org/10.1002/cpbi.11.

(191) Ward, J. H. Hierarchical Grouping to Optimize an Objective Function. *J. Am. Stat.*

Assoc. **1963**, *58* (301), 236–244. https://doi.org/10.1080/01621459.1963.10500845.

(192) Parthasarathy, A.; Cross, P. J.; Dobson, R. C. J.; Adams, L. E.; Savka, M. A.; Hudson, A. O. A Three-Ring Circus: Metabolism of the Three Proteogenic Aromatic Amino Acids and Their Role in the Health of Plants and Animals. *Front. Mol. Biosci.* **2018**, *5*, 29. https://doi.org/10.3389/fmolb.2018.00029.

(193) Frolkis, A.; Knox, C.; Lim, E.; Jewison, T.; Law, V.; Hau, D. D.; Liu, P.; Gautam, B.; Ly, S.; Guo, A. C.; Xia, J.; Liang, Y.; Shrivastava, S.; Wishart, D. S. SMPDB: The Small Molecule Pathway Database. *Nucleic Acids Res.* **2010**, *38* (suppl_1), D480–D487. https://doi.org/10.1093/nar/gkp1002.

(194) Owczarek, K.; Nowacka, O.; Klajnert, B.; Kujawa, J.; Bryszewska, M. Interaction between Polyamidoamine (PAMAM) Dendrimers and Bovine Insulin. *Neuro Endocrinol. Lett.* **2013**, *34* (6), 573–578.

(195) Durán-Lara, E.; Guzmán, L.; John, A.; Fuentes, E.; Alarcón, M.; Palomo, I.; Santos, L. S. PAMAM Dendrimer Derivatives as a Potential Drug for Antithrombotic Therapy. *Eur. J. Med. Chem.* **2013**, *69*, 601–608. https://doi.org/10.1016/j.ejmech.2013.08.047.

(196) Labieniec, M.; Ulicna, O.; Vancova, O.; Glowacki, R.; Sebekova, K.; Bald, E.; Gabryelak, T.; Watala, C. PAMAM G4 Dendrimers Lower High Glucose but Do Not Improve Reduced Survival in Diabetic Rats. *Int. J. Pharm.* **2008**, *364* (1), 142–149. https://doi.org/10.1016/j.ijpharm.2008.08.001.

(197) Cedervall, T.; Lynch, I.; Lindman, S.; Berggard, T.; Thulin, E.; Nilsson, H.; Dawson, K. A.; Linse, S. Understanding the Nanoparticle-Protein Corona Using Methods to Quantify Exchange Rates and Affinities of Proteins for Nanoparticles. *Proc. Natl. Acad. Sci.* **2007**, *104* (7), 2050–2055. https://doi.org/10.1073/pnas.0608582104.

(198) Lundqvist, M.; Stigler, J.; Elia, G.; Lynch, I.; Cedervall, T.; Dawson, K. A. Nanoparticle Size and Surface Properties Determine the Protein Corona with Possible Implications for Biological Impacts. *Proc. Natl. Acad. Sci.* **2008**, *105* (38), 14265–14270. https://doi.org/10.1073/pnas.0805135105.

(199) Ghosh, G.; Panicker, L. Protein–Nanoparticle Interactions and a New Insight. *Soft Matter* **2021**, *17* (14), 3855–3875. https://doi.org/10.1039/D0SM02050H.

(200) Klajnert, B.; Pikala, S.; Bryszewska, M. Haemolytic Activity of Polyamidoamine Dendrimers and the Protective Role of Human Serum Albumin. *Proc. R. Soc. A*

Math. Phys. Eng. Sci. **2010**, *466* (2117), 1527–1534. https://doi.org/10.1098/rspa.2009.0050.

(201) Åkesson, A.; Cárdenas, M.; Elia, G.; Monopoli, M. P.; Dawson, K. A. The Protein Corona of Dendrimers: PAMAM Binds and Activates Complement Proteins in Human Plasma in a Generation Dependent Manner. *RSC Adv.* **2012**, *2* (30), 11245. https://doi.org/10.1039/c2ra21866f.

(202) Chen, J.; Banaszak Holl, M. M. Dendrimer and Dendrimer–Conjugate Protein Complexes and Protein Coronas. *Can. J. Chem.* **2017**, *95* (9), 903–906. https://doi.org/10.1139/cjc-2017-0198.

(203) Shcharbin, D.; Ionov, M.; Abashkin, V.; Loznikova, S.; Dzmitruk, V.; Shcharbina, N.; Matusevich, L.; Milowska, K.; Gałęcki, K.; Wysocki, S.; Bryszewska, M. Nanoparticle Corona for Proteins: Mechanisms of Interaction between Dendrimers and Proteins. *Colloids Surfaces B Biointerfaces* **2015**, *134*, 377–383. https://doi.org/10.1016/j.colsurfb.2015.07.017.

(204) Rae, J. M.; Jachimska, B. Analysis of Dendrimer-Protein Interactions and Their Implications on Potential Applications of Dendrimers in Nanomedicine. *Nanoscale* **2021**, *13* (4), 2703–2713. https://doi.org/10.1039/D0NR07607D.

(205) Casey, A.; Davoren, M.; Herzog, E.; Lyng, F. M.; Byrne, H. J.; Chambers, G. Probing the Interaction of Single Walled Carbon Nanotubes within Cell Culture Medium as a Precursor to Toxicity Testing. *Carbon N. Y.* **2007**, *45* (1), 34–40. https://doi.org/10.1016/j.carbon.2006.08.009.

(206) Klajnert, B.; Stanisławska, L.; Bryszewska, M.; Pałecz, B. Interactions between PAMAM Dendrimers and Bovine Serum Albumin. *Biochim. Biophys. Acta - Proteins Proteomics* **2003**, *1648* (1–2), 115–126. https://doi.org/10.1016/S1570-9639(03)00117-1.

(207) Casey, A.; Herzog, E.; Lyng, F. M.; Byrne, H. J.; Chambers, G.; Davoren, M. Single Walled Carbon Nanotubes Induce Indirect Cytotoxicity by Medium Depletion in A549 Lung Cells. *Toxicol. Lett.* **2008**, *179* (2), 78–84. https://doi.org/10.1016/j.toxlet.2008.04.006.

(208) Zhenyukh, O.; Civantos, E.; Ruiz-Ortega, M.; Sánchez, M. S.; Vázquez, C.; Peiró, C.; Egido, J.; Mas, S. High Concentration of Branched-Chain Amino Acids Promotes Oxidative Stress, Inflammation and Migration of Human Peripheral Blood Mononuclear Cells via MTORC1 Activation. *Free Radic. Biol. Med.* **2017**, *104* (January), 165–177. https://doi.org/10.1016/j.freeradbiomed.2017.01.009.

(209) Kumari, A.; Yadav, S. K.; Yadav, S. C. Biodegradable Polymeric Nanoparticles Based Drug Delivery Systems. *Colloids Surfaces B Biointerfaces* **2010**, *75* (1), 1–18. https://doi.org/10.1016/j.colsurfb.2009.09.001.

(210) Minchinton, A. I.; Tannock, I. F. Drug Penetration in Solid Tumours. *Nat. Rev. Cancer* **2006**, *6* (8), 583–592. https://doi.org/10.1038/nrc1893.

(211) Wang, Y.; Cao, X.; Guo, R.; Shen, M.; Zhang, M.; Zhu, M.; Shi, X. Targeted Delivery of Doxorubicin into Cancer Cells Using a Folic Acid–Dendrimer Conjugate. *Polym. Chem.* **2011**, *2* (8), 1754. https://doi.org/10.1039/c1py00179e.

(212) Sehgal, D.; Vijay, I. K. A Method for the High Efficiency of Water-Soluble Carbodiimide-Mediated Amidation. *Anal. Biochem.* **1994**, *218* (1), 87–91. https://doi.org/10.1006/abio.1994.1144.

(213) Kim, Y.; Klutz, A. M.; Jacobson, K. A. Systematic Investigation of Polyamidoamine Dendrimers Surface-Modified with Poly(Ethylene Glycol) for Drug Delivery Applications: Synthesis, Characterization, and Evaluation of Cytotoxicity. *Bioconjug. Chem.* **2008**, *19* (8), 1660–1672. https://doi.org/10.1021/bc700483s.

(214) Flores-Mejía, R.; Fragoso-Vázquez, M. J.; Pérez-Blas, L. G.; Parra-Barrera, A.; Hernández-Castro, S. S.; Estrada-Pérez, A. R.; Rodrígues, J.; Lara-Padilla, E.; Ortiz-Morales, A.; Correa-Basurto, J. Chemical Characterization (LC–MS–ESI), Cytotoxic Activity and Intracellular Localization of PAMAM G4 in Leukemia Cells. *Sci. Rep.* **2021**, *11* (1), 8210. https://doi.org/10.1038/s41598-021-87560-w.

(215) Subbi, J.; Aguraiuja, R.; Tanner, R.; Allikmaa, V.; Lopp, M. Fragmentation of Poly(Amidoamine) Dendrimers in Matrix-Assisted Laser Desorption. *Eur. Polym. J.* **2005**, *41* (11), 2552–2558. https://doi.org/10.1016/j.eurpolymj.2005.05.031.

(216) Shi, X.; Lesniak, W.; Islam, M. T.; MuÑiz, M. C.; Balogh, L. P.; Baker, J. R. Comprehensive Characterization of Surface-Functionalized Poly(Amidoamine) Dendrimers with Acetamide, Hydroxyl, and Carboxyl Groups. *Colloids Surfaces A Physicochem. Eng. Asp.* **2006**, *272* (1–2), 139–150. https://doi.org/10.1016/j.colsurfa.2005.07.031.

(217) Peterson, J.; Allikmaa, V.; Subbi, J.; Pehk, T.; Lopp, M. Structural Deviations in Poly(Amidoamine) Dendrimers: A MALDI-TOF MS Analysis. *Eur. Polym. J.* **2003**, *39* (1), 33–42. https://doi.org/10.1016/S0014-3057(02)00188-X.

(218) Dembereldorj, U.; Joo, S.-W. Infrared Spectroscopic Study of α-Cyano-4-Hydroxycinnamic Acid on Nanocrystalline TiO 2 Surfaces: Anchoring of Metal-

Free Organic Dyes at Photoanodes in Dye-Sensitized Solar Cells. *Bull. Korean Chem. Soc.* **2010**, *31* (1), 116–119. https://doi.org/10.5012/bkcs.2010.31.01.116.

(219) Pande, S.; Crooks, R. M. Analysis of Poly(Amidoamine) Dendrimer Structure by UV–Vis Spectroscopy. *Langmuir* **2011**, *27* (15), 9609–9613. https://doi.org/10.1021/la201882t.

(220) Shi, X.; Ganser, T. R.; Sun, K.; Balogh, L. P.; Baker, J. R. Characterization of Crystalline Dendrimer-Stabilized Gold Nanoparticles. *Nanotechnology* **2006**, *17* (4), 1072–1078. https://doi.org/10.1088/0957-4484/17/4/038.

(221) Camacho, C. S.; Urgellés, M.; Tomás, H.; Lahoz, F.; Rodrigues, J. New Insights into the Blue Intrinsic Fluorescence of Oxidized PAMAM Dendrimers Considering Their Use as Bionanomaterials. *J. Mater. Chem. B* **2020**, *8* (45), 10314–10326. https://doi.org/10.1039/D0TB01871F.

(222) Konopka, M.; Janaszewska, A.; Klajnert-Maculewicz, B. Intrinsic Fluorescence of PAMAM Dendrimers—Quenching Studies. *Polymers (Basel).* **2018**, *10* (5), 540. https://doi.org/10.3390/polym10050540.

(223) Wang, D.; Imae, T. Fluorescence Emission from Dendrimers and Its PH Dependence. *J. Am. Chem. Soc.* **2004**, *126* (41), 13204–13205. https://doi.org/10.1021/ja0454992.

(224) Wang, D.; Imae, T.; Miki, M. Fluorescence Emission from PAMAM and PPI Dendrimers. *J. Colloid Interface Sci.* **2007**, *306* (2), 222–227. https://doi.org/10.1016/j.jcis.2006.10.025.

(225) Hoyer, T.; Tuszynski, W.; Lienau, C. Ultrafast Photodimerization Dynamics in α-Cyano-4-Hydroxycinnamic and Sinapinic Acid Crystals. *Chem. Phys. Lett.* **2007**, *443* (1–3), 107–112. https://doi.org/10.1016/j.cplett.2007.06.038.

(226) Lard, M.; Kim, S. H.; Lin, S.; Bhattacharya, P.; Ke, P. C.; Lamm, M. H. Fluorescence Resonance Energy Transfer between Phenanthrene and PAMAM Dendrimers. *Phys. Chem. Chem. Phys.* **2010**, *12* (32), 9285. https://doi.org/10.1039/b924522g.

(227) Zeng, Y.; Kurokawa, Y.; Win-Shwe, T.-T.; Zeng, Q.; Hirano, S.; Zhang, Z.; Sone, H. Effects of PAMAM Dendrimers with Various Surface Functional Groups and Multiple Generations on Cytotoxicity and Neuronal Differentiation Using Human Neural Progenitor Cells. *J. Toxicol. Sci.* **2016**, *41* (3), 351–370. https://doi.org/10.2131/jts.41.351.

(228) Kumar, A.; Dixit, C. K. Methods for Characterization of Nanoparticles. In

Advances in Nanomedicine for the Delivery of Therapeutic Nucleic Acids; Elsevier, 2017; pp 43–58. https://doi.org/10.1016/B978-0-08-100557-6.00003-1.

(229) Montalbetti, C. A. G. N.; Falque, V. Amide Bond Formation and Peptide Coupling. *Tetrahedron* **2005**, *61* (46), 10827–10852. https://doi.org/10.1016/j.tet.2005.08.031.

(230) Nakajima, N.; Ikada, Y. Mechanism of Amide Formation by Carbodiimide for Bioconjugation in Aqueous Media. *Bioconjug. Chem.* **1995**, *6* (1), 123–130. https://doi.org/10.1021/bc00031a015.

(231) Yan, Q.; Zheng, H.-N.; Jiang, C.; Li, K.; Xiao, S.-J. EDC/NHS Activation Mechanism of Polymethacrylic Acid: Anhydride versus NHS-Ester. *RSC Adv.* **2015**, *5* (86), 69939–69947. https://doi.org/10.1039/C5RA13844B.

(232) Iwasawa, T.; Wash, P.; Gibson, C.; Rebek, J. Reaction of an Introverted Carboxylic Acid with Carbodiimide. *Tetrahedron* **2007**, *63* (28), 6506–6511. https://doi.org/10.1016/j.tet.2007.03.075.

(233) Hermanson, G. T. Zero-Length Crosslinkers. In *Bioconjugate Techniques*; Elsevier, 2013; pp 259–273. https://doi.org/10.1016/B978-0-12-382239-0.00004-2.

(234) Fox, L. J.; Richardson, R. M.; Briscoe, W. H. PAMAM Dendrimer - Cell Membrane Interactions. *Adv. Colloid Interface Sci.* **2018**, *257*, 1–18. https://doi.org/10.1016/j.cis.2018.06.005.

(235) Lombardo, D.; Calandra, P.; Bellocco, E.; Laganà, G.; Barreca, D.; Magazù, S.; Wanderlingh, U.; Kiselev, M. A. Effect of Anionic and Cationic Polyamidoamine (PAMAM) Dendrimers on a Model Lipid Membrane. *Biochim. Biophys. Acta* **2016**, *1858* (11), 2769–2777. https://doi.org/10.1016/j.bbamem.2016.08.001.

(236) Roell, K. R.; Reif, D. M.; Motsinger-Reif, A. A. An Introduction to Terminology and Methodology of Chemical Synergy—Perspectives from Across Disciplines. *Front. Pharmacol.* **2017**, *8*, 158. https://doi.org/10.3389/fphar.2017.00158.

(237) Yamazaki, Y.; Naganuma, J.; Gotoh, H. A Theoretical, Dynamical Evaluation Method of the Steric Hindrance in Nitroxide Radicals Using Transition States of Model Reactions. https://doi.org/10.1038/s41598-019-56342-w.

(238) Wu, X.-M.; Chang, B. K.; Hsieh, C.-M. Computational Study on the Effect of Steric Hindrance in Functionalised Zr-Based Metal-Organic Frameworks on Hydrocarbon Storage and Separation. *Mol. Simul.* **2021**, *47* (7), 565–574. https://doi.org/10.1080/08927022.2021.1895433.

(239) Papagiannaros, A.; Dimas, K.; Papaioannou, G. T.; Demetzos, C. Doxorubicin–PAMAM Dendrimer Complex Attached to Liposomes: Cytotoxic Studies against Human Cancer Cell Lines. *Int. J. Pharm.* **2005**, *302* (1–2), 29–38. https://doi.org/10.1016/j.ijpharm.2005.05.039.

(240) Griffiths, J. Are Cancer Cells Acidic? *Br. J. Cancer* **1991**, *64* (3), 425–427. https://doi.org/10.1038/bjc.1991.326.

(241) Koczurkiewicz-Adamczyk, P.; Kla´skla´s, K.; Gunia-Krzy˙ Zak, A.; Piska, K.; Andrysiak, K.; St¸ Epniewski, J.; Lasota, S.; Wójcik-Pszczoła, K.; Dulak, J.; Madeja, Z.; Zbieta, E.; Ekala, P. Cinnamic Acid Derivatives as Cardioprotective Agents against Oxidative and Structural Damage Induced by Doxorubicin. *Int. J. Mol. Sci. Artic. J. Mol. Sci* **2021**. https://doi.org/10.3390/ijms22126217.

(242) Chandra, S.; Dietrich, S.; Lang, H.; Bahadur, D. Dendrimer–Doxorubicin Conjugate for Enhanced Therapeutic Effects for Cancer. *J. Mater. Chem.* **2011**, *21* (15), 5729. https://doi.org/10.1039/c0jm04198j.

(243) Almuqbil, R. M.; Heyder, R. S.; Bielski, E. R.; Durymanov, M.; Reineke, J. J.; da Rocha, S. R. P. Dendrimer Conjugation Enhances Tumor Penetration and Efficacy of Doxorubicin in Extracellular Matrix-Expressing 3D Lung Cancer Models. *Mol. Pharm.* **2020**, *17* (5), 1648–1662. https://doi.org/10.1021/acs.molpharmaceut.0c00083.

(244) Dalmark, M. Characteristics of Doxorubicin Transport in Human Red Blood Cells. *Scand. J. Clin. Lab. Invest.* **1981**, *41* (7), 633–639. https://doi.org/10.3109/00365518109090508.

(245) Spyropoulos-Antonakakis, N.; Sarantopoulou, E.; Trohopoulos, P. N.; Stefi, A. L.; Kollia, Z.; Gavriil, V. E.; Bourkoula, A.; Petrou, P. S.; Kakabakos, S.; Semashko, V. V; Nizamutdinov, A. S.; Cefalas, A.-C. Selective Aggregation of PAMAM Dendrimer Nanocarriers and PAMAM/ZnPc Nanodrugs on Human Atheromatous Carotid Tissues: A Photodynamic Therapy for Atherosclerosis. *Nanoscale Res. Lett.* **2015**, *10* (1), 210. https://doi.org/10.1186/s11671-015-0904-5.

(246) Enciso, A.; Neun, B.; Rodriguez, J.; Ranjan, A.; Dobrovolskaia, M.; Simanek, E. Nanoparticle Effects on Human Platelets in Vitro: A Comparison between PAMAM and Triazine Dendrimers. *Molecules* **2016**, *21* (4), 428. https://doi.org/10.3390/molecules21040428.

(247) Seyfried, T. N.; Flores, R. E.; Poff, A. M.; D'agostino, D. P. Cancer as a Metabolic Disease: Implications for Novel Therapeutics. *Carcinogenesis* **2014**, *35* (3), 515–

527. https://doi.org/10.1093/carcin/bgt480.

(248) Gurrapu, S.; Jonnalagadda, S. K.; Alam, M. A.; Nelson, G. L.; Sneve, M. G.; Drewes, L. R.; Mereddy, V. R. Monocarboxylate Transporter 1 Inhibitors as Potential Anticancer Agents. *ACS Med. Chem. Lett.* **2015**, *6*, 558–561. https://doi.org/10.1021/acsmedchemlett.5b00049.

(249) Imai, H.; Yoshimura, K.; Miyamoto, Y.; Sasa, K.; Sugano, M.; Chatani, M.; Takami, M.; Yamamoto, M.; Kamijo, R. Roles of Monocarboxylate Transporter Subtypes in Promotion and Suppression of Osteoclast Differentiation and Survival on Bone. *Sci. Rep.* **2019**, *9* (1), 15608. https://doi.org/10.1038/s41598-019-52128-2.

(250) Rochet, N.; Dubousset, J.; Mazeau, C.; Zanghellini, E.; Farges, M.-F.; Stora de Novion, H.; Chompret, A.; Delpech, B.; Cattan, N.; Frenay, M.; Gioanni, J. Establishment, Characterisation and Partial Cytokine Expression Profile of a New Human Osteosarcoma Cell Line (CAL 72). *Int. J. Cancer* **1999**, *82* (2), 282–285. https://doi.org/10.1002/(SICI)1097-0215(19990719)82:2<282::AID-IJC20>3.0.CO;2-R.

(251) Min, J.; Meng-Xia, X.; Dong, Z.; Yuan, L.; Xiao-Yu, L.; Xing, C. Spectroscopic Studies on the Interaction of Cinnamic Acid and Its Hydroxyl Derivatives with Human Serum Albumin. *J. Mol. Struct.* **2004**, *692* (1–3), 71–80. https://doi.org/10.1016/j.molstruc.2004.01.003.

(252) Barnett, C. R.; Barnett, Y. A. Ketone Bodies. In *Encyclopedia of Food Sciences and Nutrition*; Elsevier, 2003; pp 3421–3425. https://doi.org/10.1016/B0-12-227055-X/00663-5.

(253) Vilaça, N.; Amorim, R.; Martinho, O.; Reis, R. M.; Baltazar, F.; Fonseca, A. M.; Neves, I. C. Encapsulation of α-Cyano-4-Hydroxycinnamic Acid into a NaY Zeolite. *J. Mater. Sci.* **2011**, *46* (23), 7511–7516. https://doi.org/10.1007/s10853-011-5722-2.

(254) Amorim, R.; Pinheiro, C.; Miranda-Gonçalves, V.; Pereira, H.; Moyer, M. P.; Preto, A.; Baltazar, F. Monocarboxylate Transport Inhibition Potentiates the Cytotoxic Effect of 5-Fluorouracil in Colorectal Cancer Cells. *Cancer Lett.* **2015**, *365* (1), 68–78. https://doi.org/10.1016/j.canlet.2015.05.015.

(255) Fujiwara, S.; Wada, N.; Kawano, Y.; Okuno, Y.; Kikukawa, Y.; Endo, S.; Nishimura, N.; Ueno, N.; Mitsuya, H.; Hata, H. Lactate, a Putative Survival Factor for Myeloma Cells, Is Incorporated by Myeloma Cells through Monocarboxylate

Transporters 1. *Exp. Hematol. Oncol.* **2015**, *4* (1), 12. https://doi.org/10.1186/s40164-015-0008-z.

(256) Guan, X.; Morris, M. E. In Vitro and In Vivo Efficacy of AZD3965 and Alpha-Cyano-4-Hydroxycinnamic Acid in the Murine 4T1 Breast Tumor Model. *AAPS J.* **2020**, *22* (4), 84. https://doi.org/10.1208/s12248-020-00466-9.

(257) Ferreira, N. N.; Granja, S.; Boni, F. I.; Ferreira, L. M. B.; Reis, R. M.; Baltazar, F.; Gremião, M. P. D. A Novel Strategy for Glioblastoma Treatment Combining Alpha-Cyano-4-Hydroxycinnamic Acid with Cetuximab Using Nanotechnology-Based Delivery Systems. *Drug Deliv. Transl. Res.* **2020**. https://doi.org/10.1007/s13346-020-00713-8.

Supplementary Information

Index(Supplementary information)

Index of Figures

Index of tables

Chapter 3 - ^{1}H NMR Metabolomics of PAMAM G4NH$_2$

Table S 1. Dulbecco's Modified Eagle Medium (DMEM) formulation, from GIBCO®

Components	Molecular Weight	Concentration (mg/L)	mM
Amino Acids			
Glycine	75.0	30.0	0.4
L-Arginine hydrochloride	211.0	84.0	0.39
L-Cystine 2HCl	313.0	63.0	0.20
L-Glutamine	146.0	584.0	4.0
L-Histidine hydrochloride-H_2O	210.0	42.0	0.2
L-Isoleucine	131.0	105.0	0.80
L-Leucine	131.0	105.0	0.8
L-Lysine hydrochloride	183.0	146.0	0.79
L-Methionine	149.0	30.0	0.20
L-Phenylalanine	165.0	66.0	0.4
L-Serine	105.0	42.0	0.4
L-Threonine	119.0	95.0	0.7
L-Tryptophan	204.0	16.0	0.07
L-Tyrosine disodium salt dihydrate	261.0	104.0	0.3
L-Valine	117.0	94.0	0.80
Vitamins			
Choline chloride	140.0	4.0	0.02
D-Calcium pantothenate	477.0	4.0	0.008
Folic Acid	441.0	4.0	0.01
Niacinamide	122.0	4.0	0.03
Pyridoxine hydrochloride	206.0	4.0	0.01
Riboflavin	376.0	0.4	0.001
Thiamine hydrochloride	337.0	4.0	0.0
i-Inositol	180.0	7.2	0.04
Inorganic Salts			
Calcium Chloride ($CaCl_2$) (anhyd.)	111.0	200.0	1.8
Ferric Nitrate ($Fe(NO_3)_3 \cdot 9H_2O$)	404.0	0.1	2.47E-4
Magnesium Sulfate ($MgSO_4$) (anhyd.)	120.0	97.67	0.81

Potassium Chloride (KCl)	75.0	400.0	5.34
Sodium Chloride (NaCl)	58.0	6400.0	110.34
Sodium Phosphate monobasic ($NaH_2PO_4 \cdot H_2O$)	138.0	125.0	0.90
Other Components			
D-Glucose (Dextrose)	180.0	4500.0	25.0
Phenol Red	376.4	15.0	0.04
Sodium Pyruvate	110.0	110.0	1.0

Table S 2. Roswell Park Memorial Institute (RPMI) formulation, from GIBCO®

Components	Molecular Weight	Concentration (mg/L)	mM
Amino Acids			
Glycine	75	10	0.13
L-Arginine	174	200	1.14
L-Asparagine	132	50	0.37
L-Aspartic acid	133	20	0.15
L-Cystine 2HCl	313	65.15	0.20
L-Glutamic Acid	147	20	0.13
L-Glutamine	146	300	2.05
L-Histidine	155	15	0.09
L-Hydroxyproline	131	20	0.15
L-Isoleucine	131	50	0.38
L-Leucine	131	50	0.38
L-Lysine hydrochloride	146	40	0.27
L-Methionine	149	15	0.10
L-Phenylalanine	165	15	0.09
L-Proline	115	20	0.17
L-Serine	105	30	0.28
L-Threonine	119	20	0.16
L-Tryptophan	204	5	0.02
L-Tyrosine disodium salt	225	28.94	0.12
L-Valine	117	20	0.17
Vitamins			
Biotin	244	0.2	8.2E-04
Choline chloride	140	3	0.02
D-Calcium pantothenate	477	0.25	5.2E-04
Folic Acid	441	1	0.002
Niacinamide	122	1	0.008
Para-Aminobenzoic Acid	137	1	0.007
Pyridoxine hydrochloride	206	1	0.005
Riboflavin	376	0.2	5.3E-04
Thiamine hydrochloride	337	1	0.003
Vitamin B12	1355	0.005	3.6E-06
i-Inositol	180	35	0.19
Inorganic Salts			

Calcium nitrate ($Ca(NO_3)_2 \cdot 4H_2O$)	236	100	0.423
Magnesium Sulfate ($MgSO_4$) (anhyd.)	120	48.84	0.40
Potassium Chloride (KCl)	75	400	5.33
Sodium Chloride (NaCl)	58	6000	103.44
Sodium Phosphate dibasic (Na_2HPO_4) anhydrous	142	800	5.63
Other Components			
D-Glucose (Dextrose)	180	2000	11.11
Glutathione (reduced)	307	1	0.003
Phenol Red	376.4	5	0.01

Table S 3. Minimum Essential Media (MEM) formulation, from GIBCO®

Components	Molecular Weight	Concentration (mg/L)	mM
Amino Acids			
L-Arginine hydrochloride	211.0	126.64	0.60
L-Cystine 2HCl	313.0	31.0	0.09
L-Glutamine	146.0	292.0	2.0
L-Histidine hydrochloride-H_2O	210.0	42.0	0.2
L-Isoleucine	131.0	52.0	0.39
L-Leucine	131.0	52.0	0.39
L-Lysine hydrochloride	183.0	72.5	0.39
L-Methionine	149.0	15.0	0.10
L-Phenylalanine	165.0	32.0	0.19
L-Threonine	119.0	48.0	0.40
L-Tryptophan	204.0	10.0	0.04
L-Tyrosine disodium salt	225.0	52.0	0.23
L-Valine	117.0	46.0	0.39
Vitamins			
Choline chloride	140.0	1.0	0.007
D-Calcium pantothenate	477.0	1.0	0.002
Folic Acid	441.0	1.0	0.002
Niacinamide	122.0	1.0	0.008
Pyridoxal hydrochloride	204.0	1.0	0.004
Riboflavin	376.0	0.1	2.65E-4
Thiamine hydrochloride	337.0	1.0	0.002
i-Inositol	180.0	2.0	0.011
Inorganic Salts			
Calcium Chloride ($CaCl_2$) (anhyd.)	111.0	200.0	1.80
Magnesium Sulfate ($MgSO_4$) (anhyd.)	120.0	97.67	0.81
Potassium Chloride (KCl)	75.0	400.0	5.33
Sodium Chloride (NaCl)	58.0	6800.0	117.24
Sodium Phosphate monobasic (NaH_2PO_4-H_2O)	138.0	140.0	1.014

Other Components			
D-Glucose (Dextrose)	180.0	1000.0	5.55
Phenol Red	376.4	10.0	0.02

Table S 4. Main exometabolite variations in cell culture media of CAL-72, NIH 3T3, A2780, and CACO-2 cells in relation to control cells medium, expressed as percentage of variation.

		DMEM		RPMI	MEM
		CAL-72	**NIH 3T3**	**A2780**	**CACO-2**
Leucine	%Var	-204.19	-147.90	-246.95	-92.04
	±	48.10	46.66	54.75	4.55
Valine	%Var	-239.89	-183.63	-123.76	-24.8
	±	73.05	38.49	11.96	4.86
Isoleucine	%Var	-205.77	-155.95	-143.99	-73.03
	±	31.46	60.98	52.50	12.19
Lactate	%Var	88.61	88.27	85.83	77.19
	±	1.35	1.65	0.78	2.14
Alanine	%Var	13.01	48.08	21.83	0.89
	±	15.68	11.60	26.87	3.00
Nα-acetyllysine	%Var	54.72	67.57		74.89
	±	11.86	20.57		6.83
Acetate	%Var	-145.21	0.50	-258.42	-496.57
	±	44.89	30.46	56.12	96.01
Glutamate	%Var			0.35	-65.72
	±			18.18	20.75
Succinate	%Var	-194.14	-103.84	-15.25	-27.10
	±	18.91	32.27	35.37	6.77
Methionine	%Var	-264.66	-201.16	-102.81	-133.66
	±	54.97	81.66	126.39	21.25
Aspartate	%Var			-85.75	
	±			40.60	
Glycine	%Var	-179.60	-69.81	-261.78	-204.28
	±	193.96	10.46	158.23	36.73
Threonine	%Var	-116.61	-128.04	-42.94	-47.70
	±	16.59	12.90	30.59	8.29
Glucose	%Var	-458.10	-444.34	-4310.55	-2042.71
	±	109.40	120.07	1735.69	778.83
Tyrosine	%Var	-198.38	-152.64	-44.04	-82.20
	±	36.99	50.21	9.41	11.66
Phenylalanine	%Var	-214.30	-160.15	-144.95	1.77
	±	45.51	47.52	48.64	5.86
Myo-inositol	%Var				70.26
	±				3.30
Aspargine	%Var			-69.61	-42.80
	±			18.61	4.053
Glutamine	%Var	-253.64	-1082.35	-211.02	-220.02
	±	42.19	568.33	40.13	27.04
Lysine	%Var	-187.11	-166.52	-121.61	-58.45
	±	33.61	48.59	50.36	12.40
Histidine	%Var	-518.95	-170.41	-142.78	58.29
	±v	628.64	23.49	117.66	9.63
Tryptophan	%Var	-196.87	-154.53	-757.67	-34.92
	±	179.49	133.46	270.45	49.87
Citrate	%Var		72.68		73.02
	±		10.39		4.37

Table S 5. Main endometabolite variations in cell culture media of CAL-72, NIH 3T3, A2780 and CACO-2 cells exposed to IC_{25} and IC_{50} of PAMAM G4NH2 in relation to control cells, expressed as percentage of variation.

		CAL-72		NIH 3T3		A2780		CACO-2	
		IC_{25}	IC_{50}	IC_{25}	IC_{50}	IC_{25}	IC_{50}	IC_{25}	IC_{50}
Leucine	%Var	40.94	42.56	-7.03	-6.69	2.54	16.23	1.49	2.94
	±	42.03	21.48	0.87	7.67	10.48	8.27	10.08	13.32
Valine	%Var	24.29	29.30	3.02	1.97	27.62	40.89	-1.03	5.21
	±	6.20	6.64	5.35	10.44	37.82	17.78	16.69	15.11
Isoleucine	%Var	22.28	20.54	8.15	4.84	-5.74	-1.25	7.23	0.17
	±	15.33	10.83	11.51	16.67	9.83	16.51	5.65	11.88
Lactate	%Var	-17.98	5.91	16.67	43.65	73.19	126.44	25.95	43.78
	±	13.30	26.58	12.99	39.15	121.69	99.60	41.23	26.06
Acetoin	%Var	-18.38	-28.91						
	±	14.63	45.03						
Alanine	%Var	36.89	14.04	-23.66	-31.11	-31.80	-37.26	-2.60	-8.20
	±	34.02	11.42	15.37	9.76	10.17	10.86	8.77	7.98
Nα-acetyllysine	%Var	26.62	-2.59	-20.21	-6.53	-7.56	-10.16	30.24	6.63
	±	73.13	14.42	8.54	12.85	10.51	9.93	34.54	13.20
Acetate	%Var	-26.20	34.14	-8.61	21.52	-4.26	-5.61	4.10	-8.07
	±	22.68	110.84	21.75	42.26	30.59	36.42	14.28	44.37
Glutamate	%Var	24.69	3.96	-5.88	-14.78	-16.09	-25.79	5.08	-2.43
	±	23.14	15.73	13.09	18.65	7.92	5.67	14.58	5.62
Succinate	%Var	3.65	-26.55	-1.13	5.56	14.38	24.93	4.42	8.05
	±	27.21	23.07	19.01	15.03	16.79	17.95	4.07	8.27
β-Alanine	%Var	-1.75	-39.17	-3.49	-13.35	-10.69	-18.59	1.52	4.18
	±	14.66	27.69	10.39	25.84	14.93	25.66	32.11	26.39
Methionine	%Var	53.32	29.39	-4.38	-3.17	-0.92	-15.10	4.56	50.87
	±	41.98	17.84	16.37	21.96	36.43	23.59	28.41	55.51
Dimethylamine	%Var	67.76	49.46	0.70	11.01	0.18	3.90	17.86	19.17
	±	29.32	75.39	15.36	19.14	21.37	21.87	12.90	20.79
Aspartate	%Var	83.59	52.11	2.52	13.20	21.03	16.76	15.12	9.84
	±	51.35	41.44	23.08	32.19	26.02	28.39	26.02	18.21
Creatine	%Var	-19.05	-46.22	-10.57	-24.80	-21.62	-31.09	-10.46	-22.09
	±	14.79	22.60	13.02	18.08	11.39	21.65	8.53	8.14
Creatine Phosphate	%Var	72.09	28.23	27.66	38.36	-13.07	-27.33	-5.35	7.68
	±	79.00	64.16	14.74	32.46	11.94	16.11	26.32	90.10
1,3-Diaminopropane	%Var	30.68	37.70	18.91	32.92	-11.47	-19.94	-11.60	-7.17
	±	22.84	50.69	63.32	56.84	18.95	13.25	33.69	26.34
Choline	%Var	-9.52	-32.52	10.63	-16.83	8.79	-4.66	45.01	15.18
	±	26.46	35.53	41.56	33.65	56.07	40.73	108.10	58.28
Acetylcholine	%Var	54.88	37.72	88.69	83.58	0.17	-20.33	18.97	41.91
	±	57.25	89.25	130.41	83.94	76.90	62.92	40.00	76.56
Phosphoscholine	%Var	36.56	-24.80	9.90	44.76	-13.80	-4.76	-10.08	-7.11
	±	38.20	13.61	34.05	24.39	36.49	44.16	8.53	6.62
Glycero phosphocholine	%Var	-28.59	-55.34	-23.95	-9.74	-15.21	9.09	-9.17	-19.25
	±	5.32	12.23	32.50	15.23	12.01	37.88	13.39	9.97
Taurine	%Var	2.33	-14.90	-19.69	-17.89	-2.81	-12.54	-2.35	-10.58
	±	26.66	45.54	23.47	31.38	19.87	17.32	13.65	8.32
Glycine	%Var	15.97	-3.75	-2.55	-27.16	23.75	-0.44	-20.99	-7.69
	±	13.15	17.09	22.39	20.05	27.38	30.47	31.18	33.32

		CAL-72		NIH 3T3		A2780		CACO-2	
		IC_{25}	IC_{50}	IC_{25}	IC_{50}	IC_{25}	IC_{50}	IC_{25}	IC_{50}
Threonine	%Var	-5.29	-12.04	40.71	-17.92			-39.54	-49.74
	±	22.98	70.00	65.95	25.72			39.01	39.35
Glucose	%Var	118.23	403.52	-3.55	51.65	42.06	103.11	-14.01	-22.00
	±	51.76	148.33	75.06	134.92	103.33	110.91	32.89	25.33
UDP-N-Acetylglucosamine	%Var	2.35	42.97	12.07	5.71	-5.50	-44.29	-6.60	-2.05
	±	58.93	86.36	52.32	16.82	16.10	22.53	29.59	29.19
UDP-Glucose	%Var	50.15	-30.10	-20.40	-29.54	-9.79	-6.92	1.54	1.15
	±	19.93	33.82	24.19	16.13	31.76	17.60	19.01	8.42
UMP	%Var	-9.06	62.78	14.08	8.80			-4.11	-20.93
	±	58.80	165.03	31.79	20.39			54.35	77.53
ATP	%Var	39.13	-7.37	-27.63	-29.35	-5.69	-26.48	-4.15	4.58
	±	44.02	36.49	23.08	36.71	24.06	16.99	23.72	16.61
AMP	%Var	28.91	-24.40	11.72	15.31	-26.08	-22.40	36.52	21.50
	±	85.42	47.03	16.91	34.27	12.15	16.08	64.78	53.59
Fumarate	%Var	1.29	-26.83	-5.68	26.79			5.81	0.66
	±	28.59	40.58	35.65	18.69			11.77	6.93
Tyrosine	%Var	48.17	66.81	-0.18	0.02	5.64	16.84	7.77	-2.78
	±	28.49	19.21	4.42	5.12	16.28	15.14	15.15	14.15
Phenylalanine	%Var	40.23	61.86	5.17	2.02	29.09	46.08	6.68	5.71
	±	47.32	23.92	7.99	10.34	24.59	24.79	14.40	8.78
NADP+	%Var	120.10	90.97	-10.77	1.13	-13.53	-6.95	-12.99	-15.58
	±	75.24	38.33	11.61	53.96	20.79	22.48	17.74	26.15
Myo-inositol	%Var			1.00	-15.60	-13.74	-23.58	16.01	16.18
	±			21.92	21.13	10.09	9.25	46.51	41.71
Aspargine	%Var					-8.94	-28.13	19.28	25.32
	±					10.23	26.07	64.12	29.54
Glutamine	%Var					18.04	47.42		
	±					24.20	28.52		

Table S 6. Main exometabolite variations in cell culture media of CAL-72, NIH 3T3, A2780 and CACO-2 cells exposed to IC_{25} and IC_{50} of PAMAM G4NH2 in relation to the control cells medium, expressed as % variation.

		CAL-72		NIH 3T3		A2780		CACO-2	
		IC_{25}	IC_{50}	IC_{25}	IC_{50}	IC_{25}	IC_{50}	IC_{25}	IC_{50}
Leucine	%Var	14.52	36.09	5.14	16.67	20.28	45.43	5.26	4.74
	±	11.06	7.37	8.90	11.8	10.53	27.7	5.51	3.89
Valine	%Var	12.10	35.92	3.18	1.70	41.13	55.63	-2.11	3.26
	±	27.23	21.7	3.5	3.9	29.99	25.86	11.16	6.93
Isoleucine	%Var	20.64	33.79	-2.86	-13.67	16.19	14.84	-2.87	-1.85
	±	13.11	11.98	13.49	4.17	19.50	17.51	10.78	9.90
Lactate	%Var	-5.72	-14.36	-4.88	-5.88	-11.21	-14.81	-5.36	-3.97
	±	3.34	1.02	3.6	5.15	8.56	6.64	5.37	3.65
Alanine	%Var	2.59	7.18	-5.48	-6.92	-17.69	-20.55	-1.23	-2.07
	±	6.89	7.73	6.34	4.59	9.70	15.76	2.95	9.11
Nα-acetyllysine	%Var	25.47	26.55	34.77	31.54			23.94	4.45
	±	27.54	14.46	47.84	33.46			15.52	26.17
Acetate	%Var	10.25	43.31	-4.70	-10.39	12.47	20.96	33.19	10.96
	±	3.69	11.39	21.20	11.83	34.67	35.76	53.88	29.89
Glutamate	%Var					17.61	35.49	21.49	35.67
	±					5.81	4.89	5.82	7.65
Succinate	%Var	8.93	12.66	-12.03	-15.33	-4.01	-9.63	4.01	-2.09
	±	32.69	21.37	10.67	12.71	14.22	24.87	9.08	3.57
Methionine	%Var	54.28	84.42	14.06	19.11	20.75	24.13	-5.16	-4.32
	±	38.77	28.08	7.5	2.65	18.56	32.75	9.27	8.65
Aspartate	%Var					1.46	2.95		
	±					13.49	28.98		
Glycine	%Var	17.03	21.42	5.69	23.94	39.71	60.06	14.60	7.50
	±	77.96	57.12	28.47	39.01	2.51	34.86	23.34	17.38
Threonine	%Var	15.69	24.42	10.70	18.19	2.16	11.70	4.00	-3.04
	±	8.09	10.97	8.00	17.46	21.62	25.56	7.25	7.56
Glucose	%Var	31.56	74.51	23.92	22.66	541.67	690.39	40.06	49.09
	±	21.73	13.73	14.22	18.03	376.42	257.95	42.72	98.31
Tyrosine	%Var	12.51	19.38	12.41	8.99	17.81	26.79	12.95	1.42
	±	14.12	3.98	15.81	19.87	22.53	18.09	18.93	10.51
Phenylalanine	%Var	22.73	42.51	8.13	14.69	23.35	29.85	9.81	2.04
	±	17.68	14.93	7.17	10.19	18.23	19.9	9.05	5.09
Myo-inositol	%Var							17.93	19.96
	±							28.58	20.57
Aspargine	%Var					14.71	18.30	12.31	15.36
	±					4.35	9.8	10.1	13.84
Glutamine	%Var	10.63	36.34	11.56	15.09	36.72	36.32	8.92	4.59
	±	6.07	12.64	22.12	17.9	18.71	25.60	6.80	11.8
Lysine	%Var	16.70	34.28	58.66	103.11	5.31	3.97	10.99	9.02
	±	5.58	20.86	21.59	30.04	11.17	13.33	10.04	4.30
Histidine	%Var	133.40	23.71	8.50	8.59	16.26	15.34	3.51	8.44
	±	303.53	66.04	13.09	23.18	32.17	27.14	7.65	9.72
Tryptophan	%Var	0.58	21.67	0.73	53.11			-18.11	-32.51
	±	39.46	36.64	42.68	68.26			20.84	9.30

		CAL-72		NIH 3T3		A2780		CACO-2	
		IC_{25}	IC_{50}	IC_{25}	IC_{50}	IC_{25}	IC_{50}	IC_{25}	IC_{50}
Citrate	%Var			-9.05	-15.63			14.47	14.02
	±			10.54	12.99			41.06	19.5

1. Endometabolome of CAL-72 treated with PAMAM G4NH$_2$

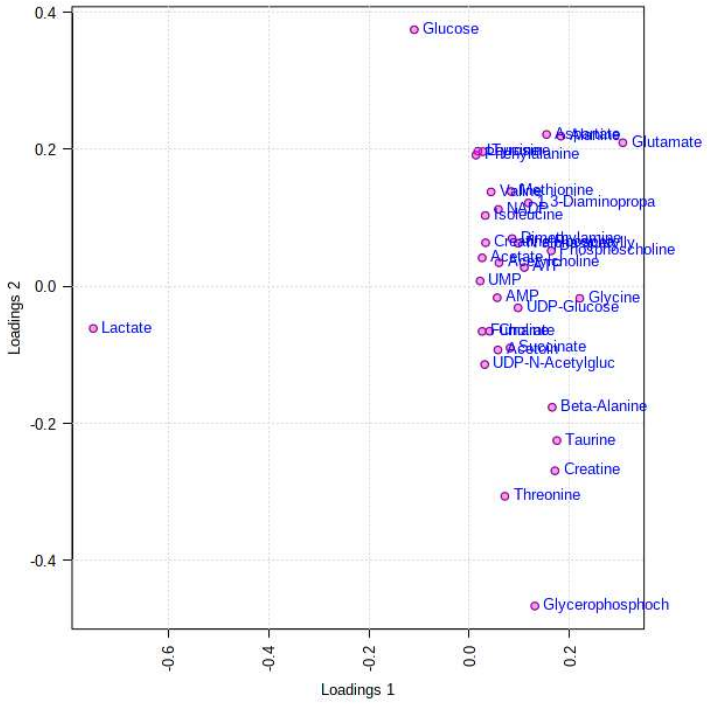

Figure S 1. PCA loading of CAL-72 endometabolites.

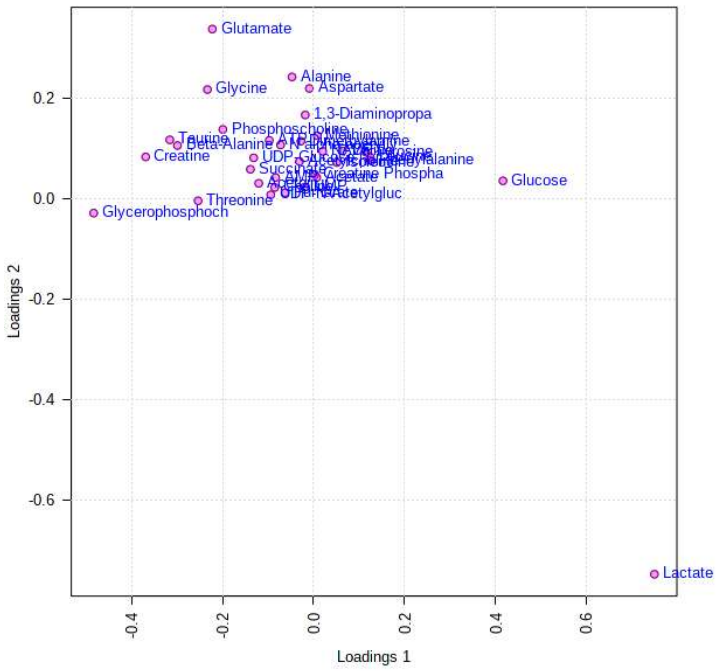

Figure S 2. PLS-DA loadings of CAL-72 endometabolites.

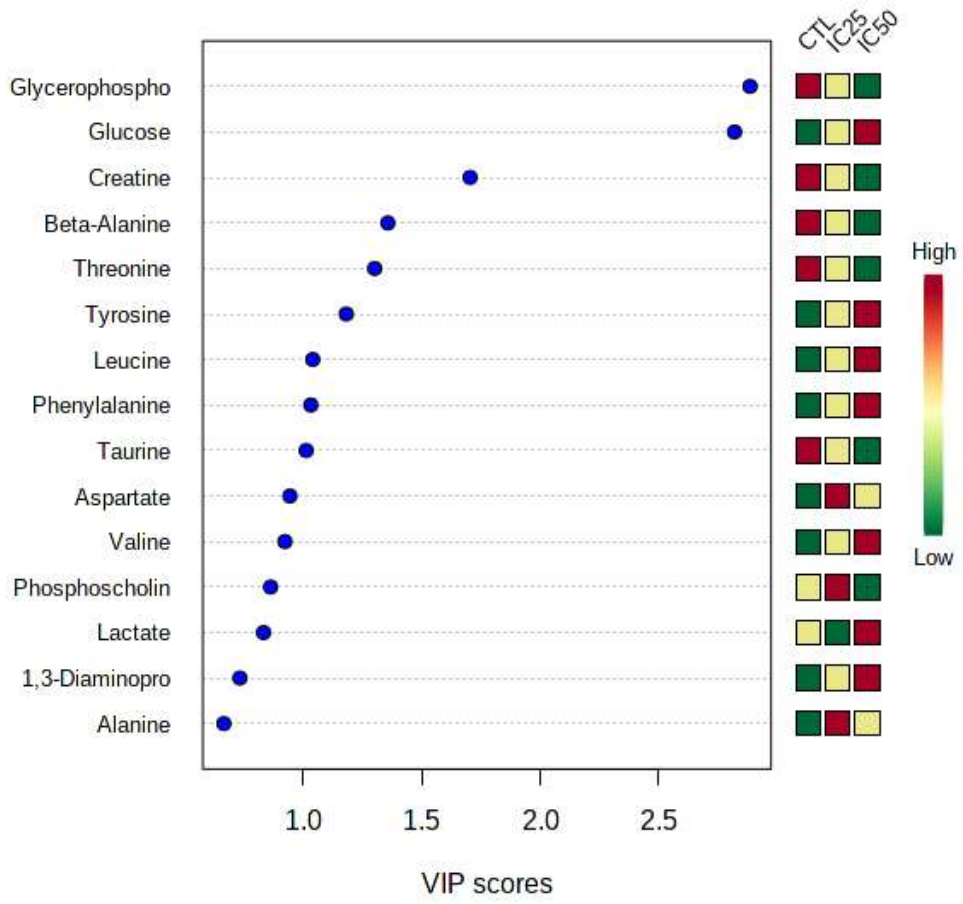

Figure S 3. VIP scores of CAL-72 endometabolites.

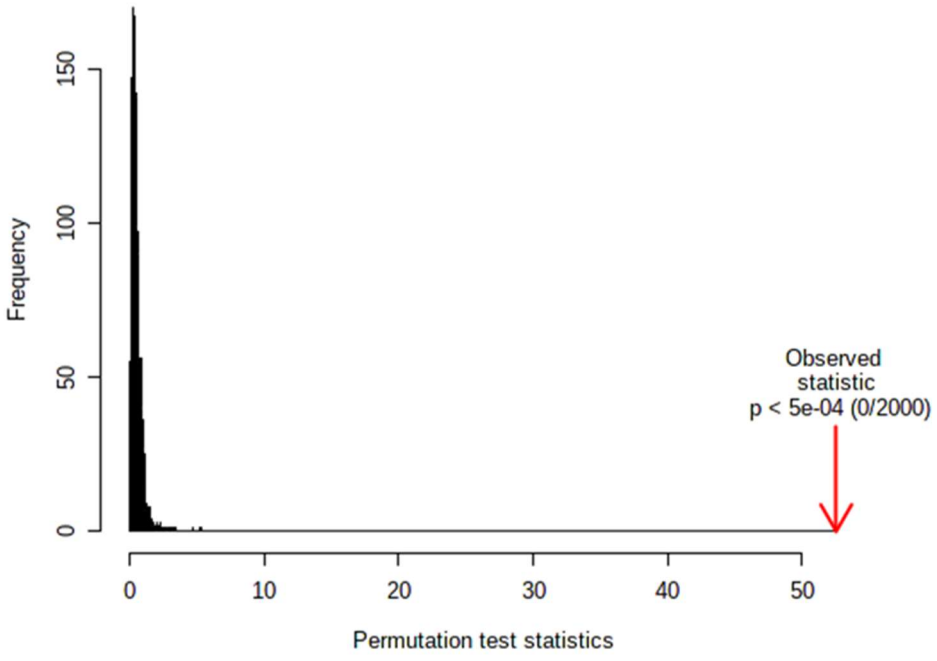

Figure S 4 Model validation by the permutation of CAL-72 endometabolites.

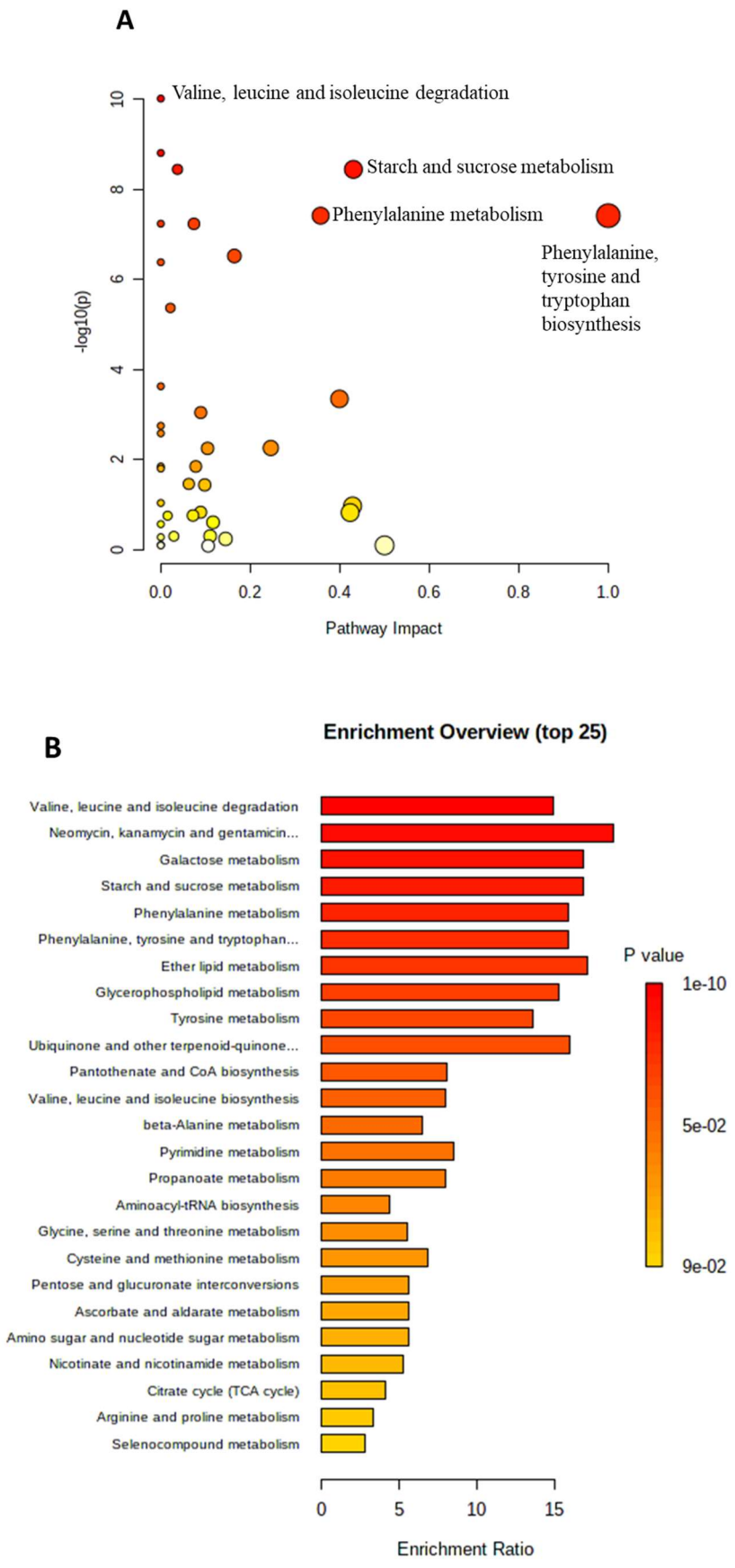

Figure S 5 (A) The metabolome view map and (B) enrichment overview of CAL-72 endometabolites after treatment with IC_{50} of PAMAM G4NH$_2$ using KEGG library.

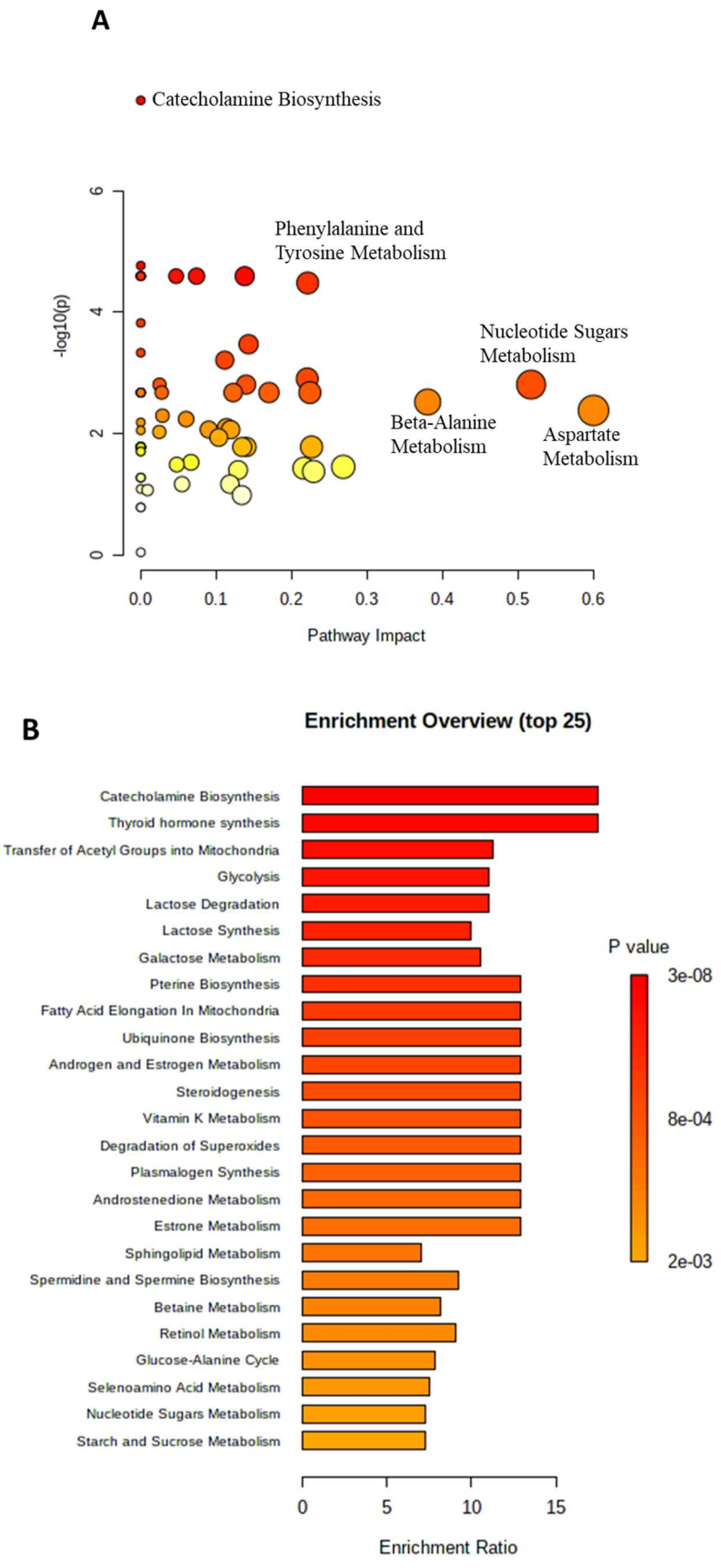

Figure S 6 (A) The metabolome view map and (B) enrichment overview of CAL-72 endometabolites after treatment with IC_{25} of PAMAM G4NH$_2$ using SMPDB library.

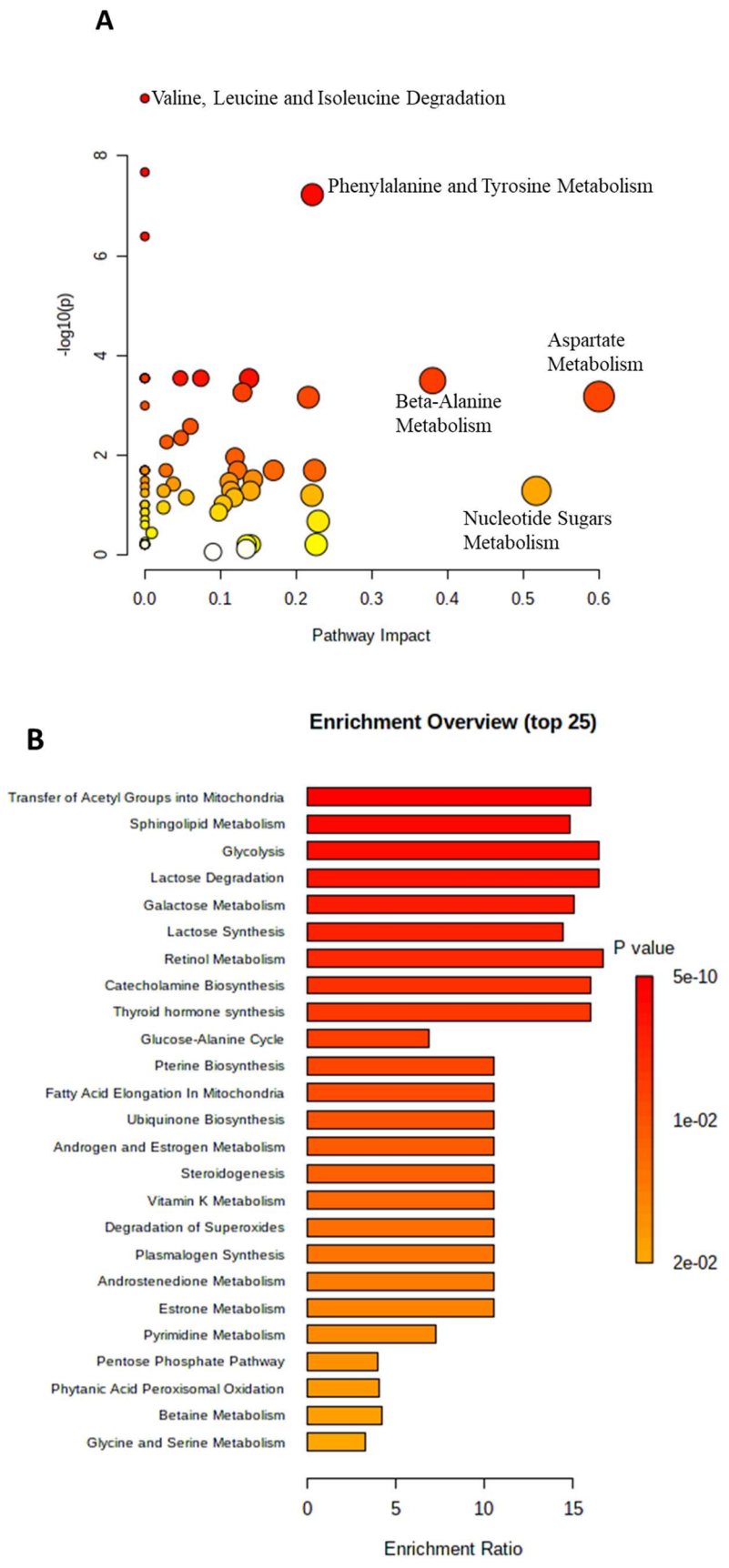

Figure S 7 (A) The metabolome view map and (B) enrichment overview of CAL-72 endometabolites after treatment with IC_{50} of PAMAM G4NH$_2$ using SMPDB library.

2. Exometabolome CAL-72 after treatment with PAMAM G4NH$_2$

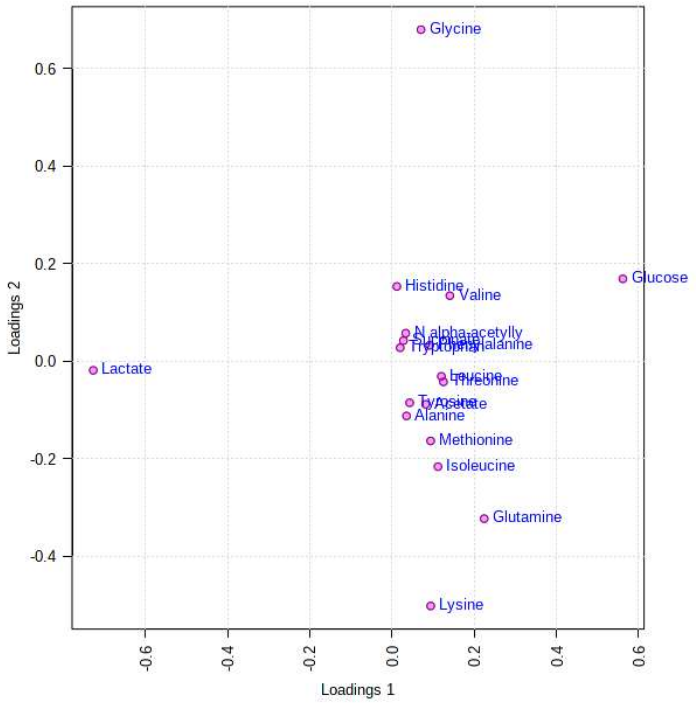

Figure S 8 PCA loadings of CAL-72 exometabolites.

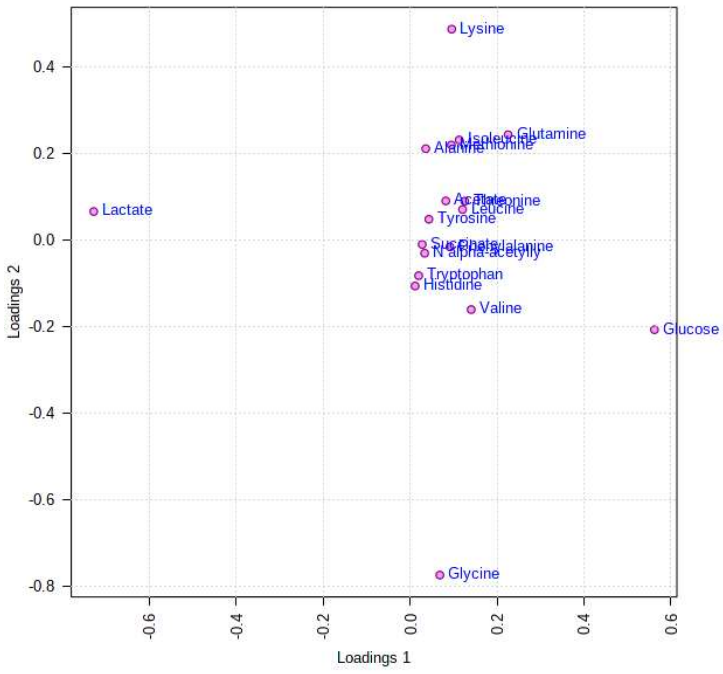

Figure S 9 PLS-DA loadings of CAL-72 exometabolites.

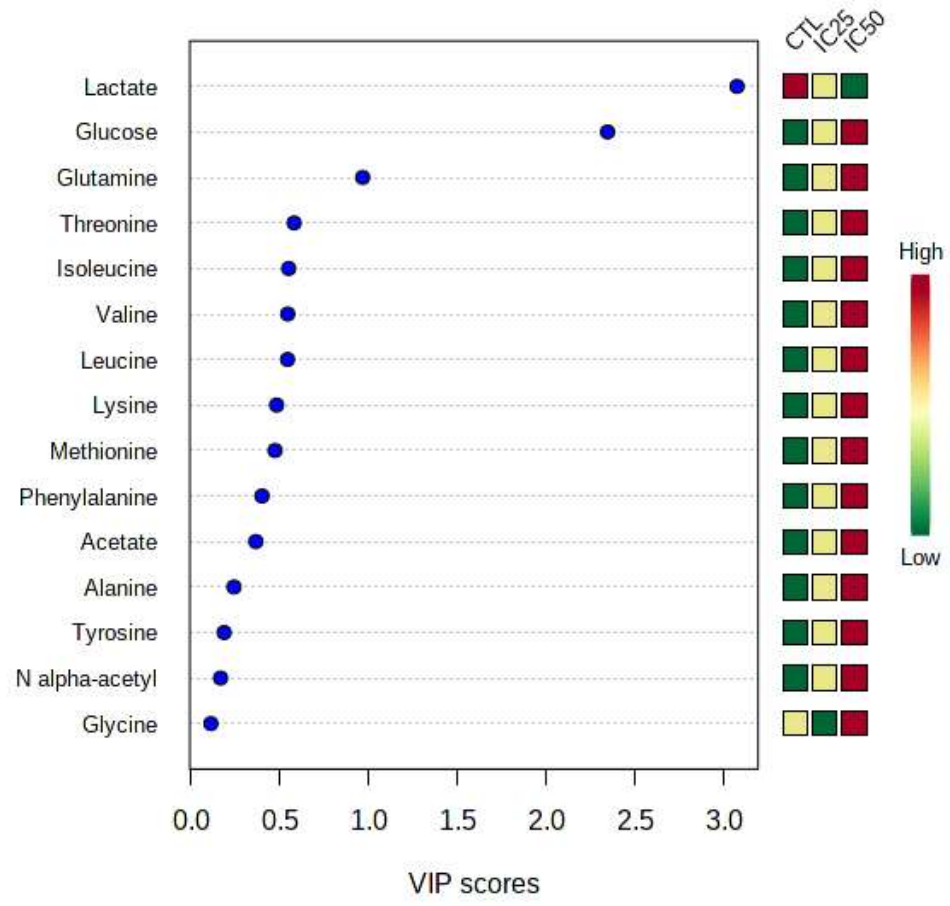

Figure S 10 VIP scores of CAL-72 exometabolites.

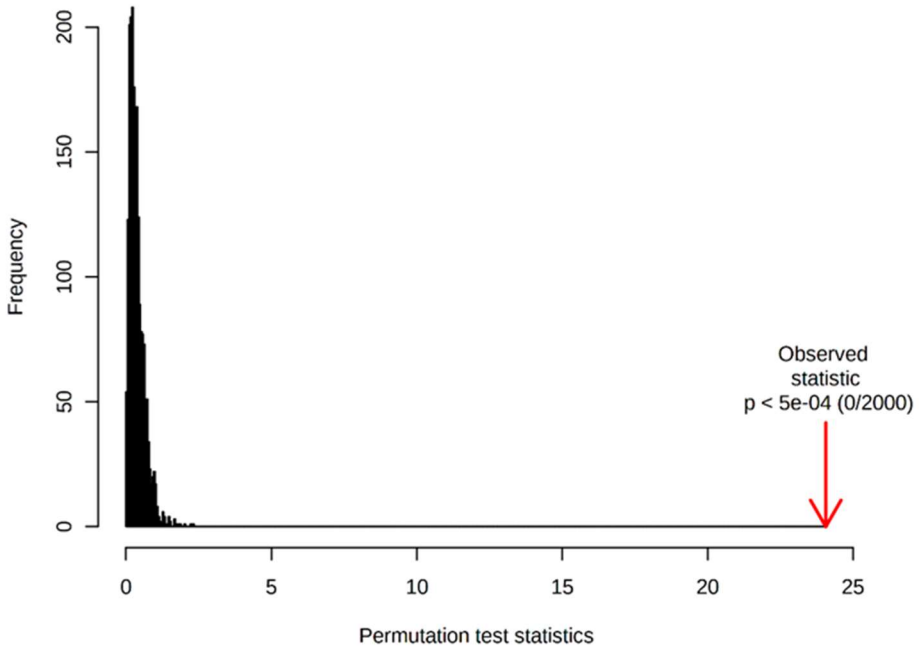

Figure S 11 Model validation by the permutation of CAL-72 exometabolites.

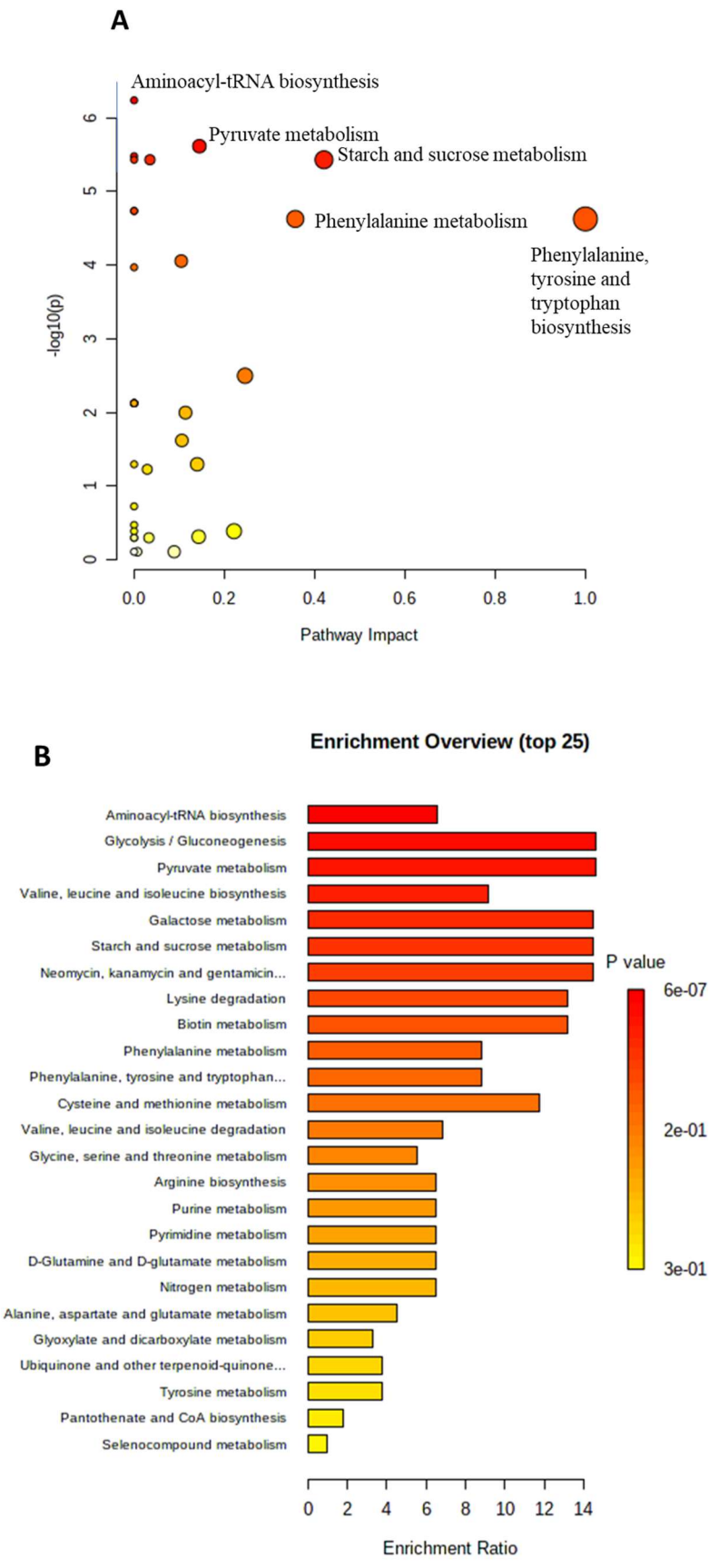

Figure S 12 (A) The metabolome view map and (B) enrichment overview of CAL-72 exometabolites after treatment with IC_{25} of PAMAM G4NH$_2$ using KEGG library.

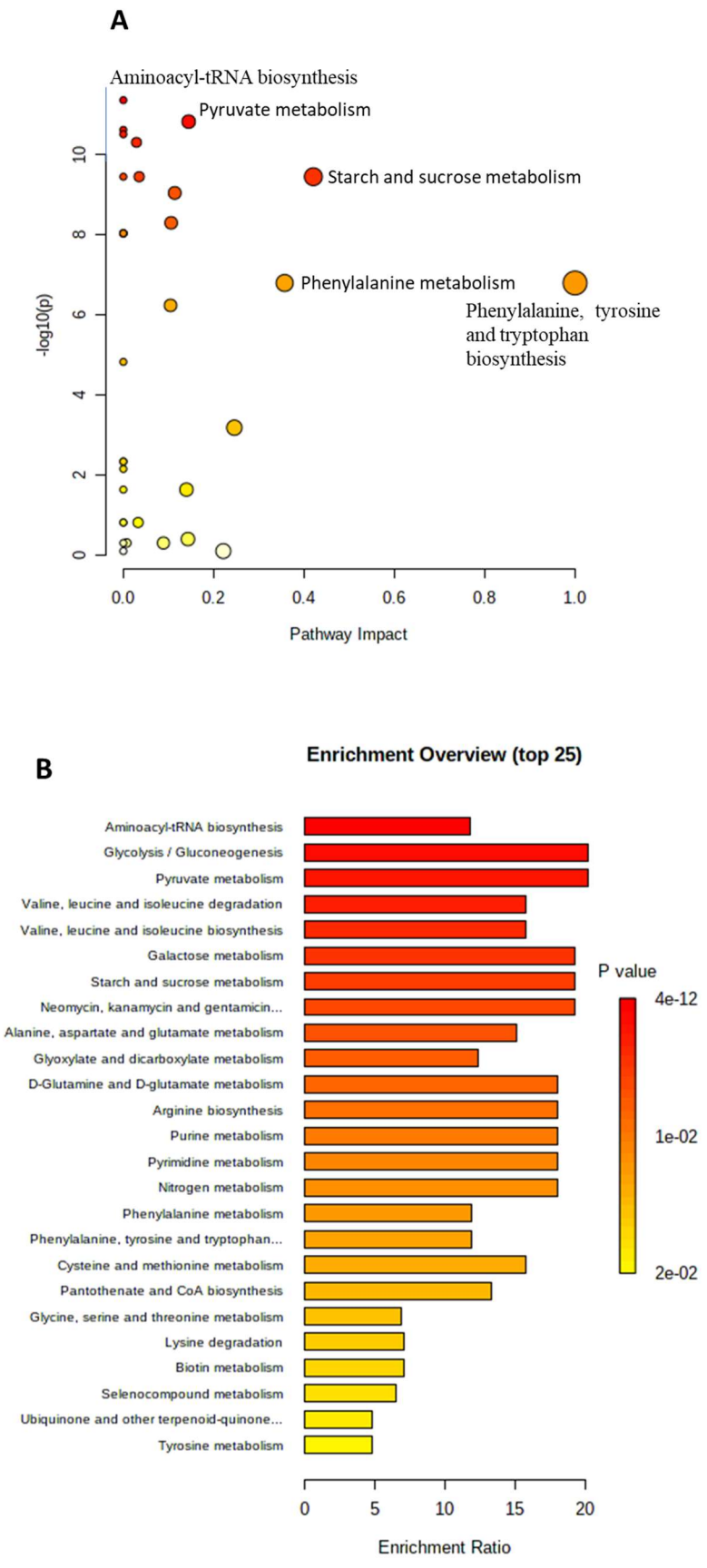

Figure S 13 (A) The metabolome view map and (B) enrichment overview of CAL-72 exometabolites after treatment with IC_{50} of PAMAM G4NH$_2$ using KEGG library.

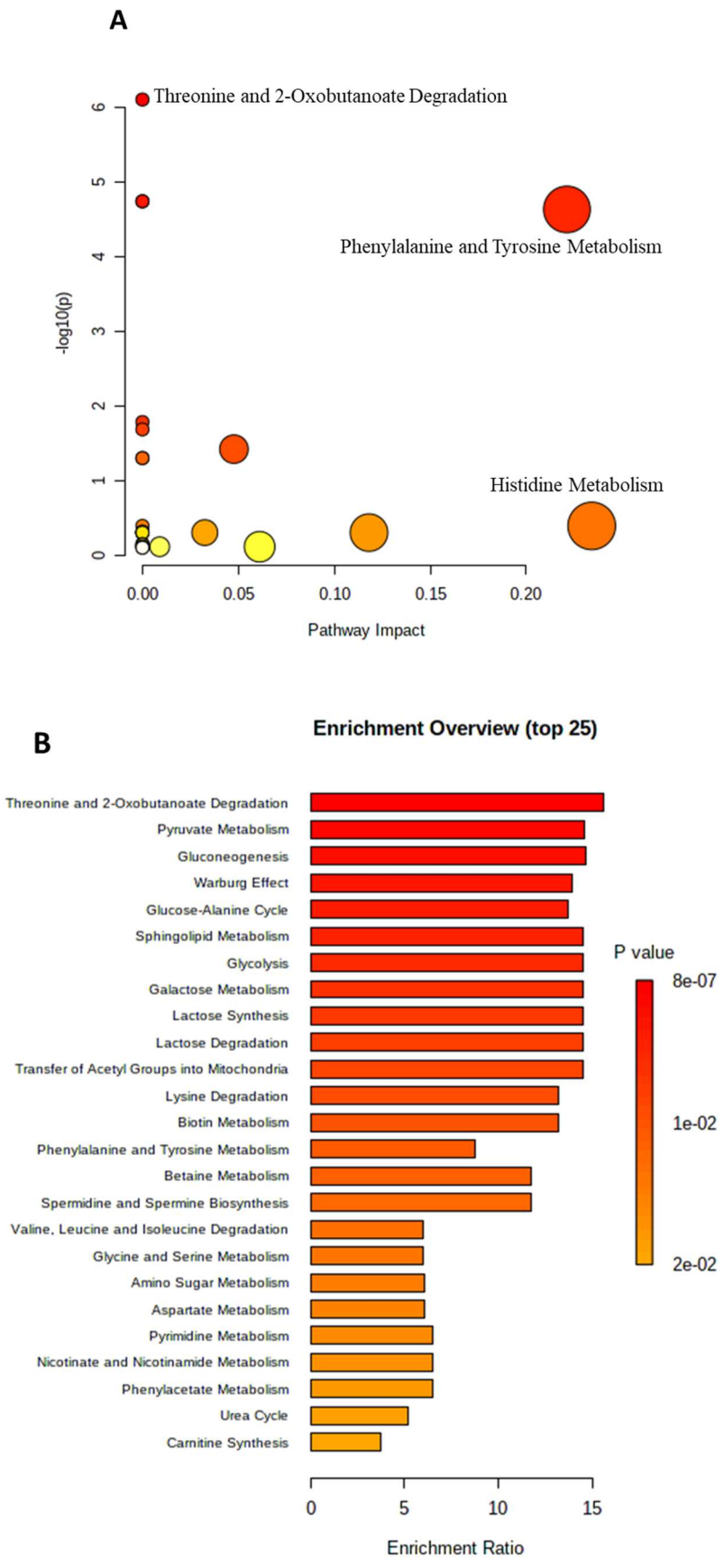

Figure S 14 (A) The metabolome view map and (B) enrichment overview of CAL-72 exometabolites after treatment with IC_{25} of PAMAM G4NH$_2$ using SMPDB library.

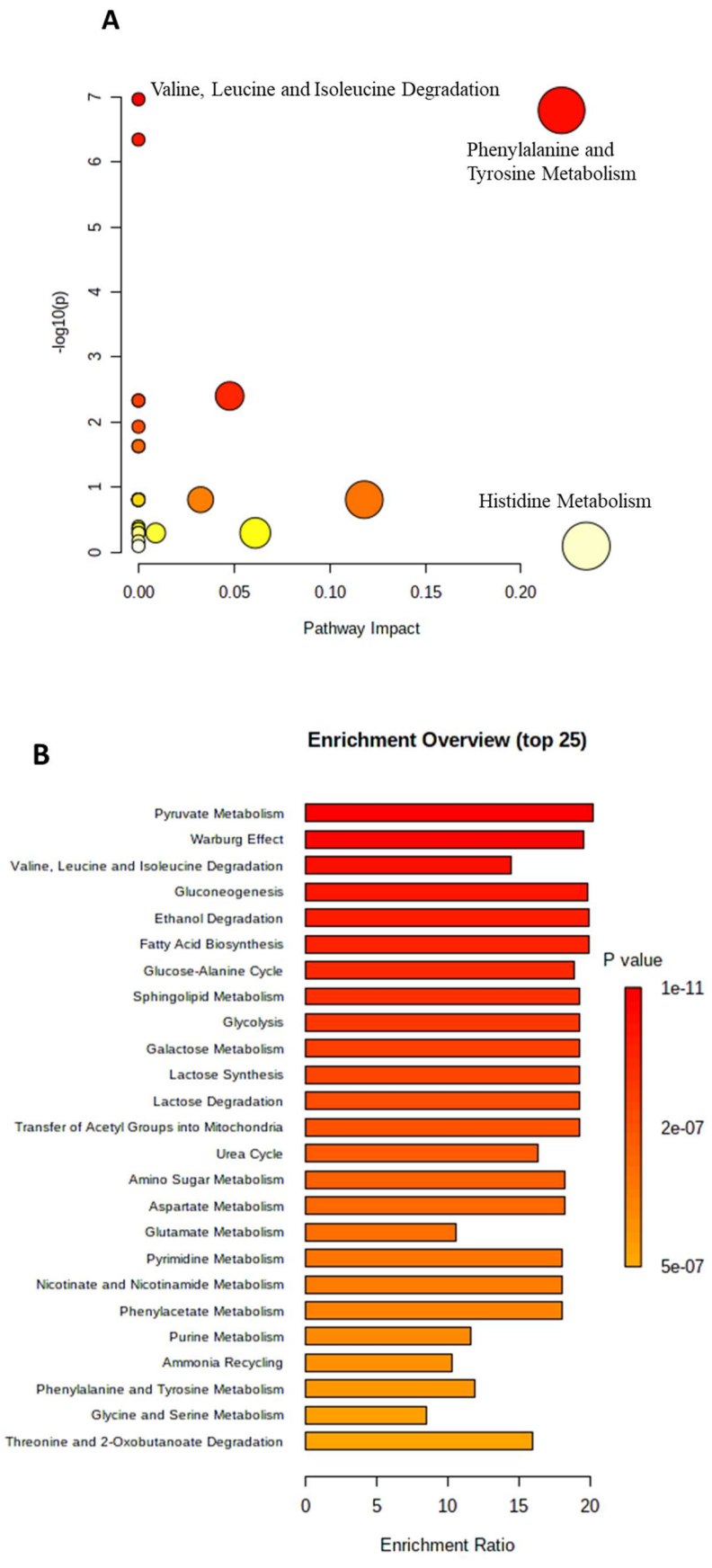

Figure S 15 (A) The metabolome view map and (B) enrichment overview of CAL-72 exometabolites after treatment with IC_{50} of PAMAM G4NH_2 using SMPDB library.

3. Endometabolome NIH 3T3 after treatment with PAMAM G4NH2

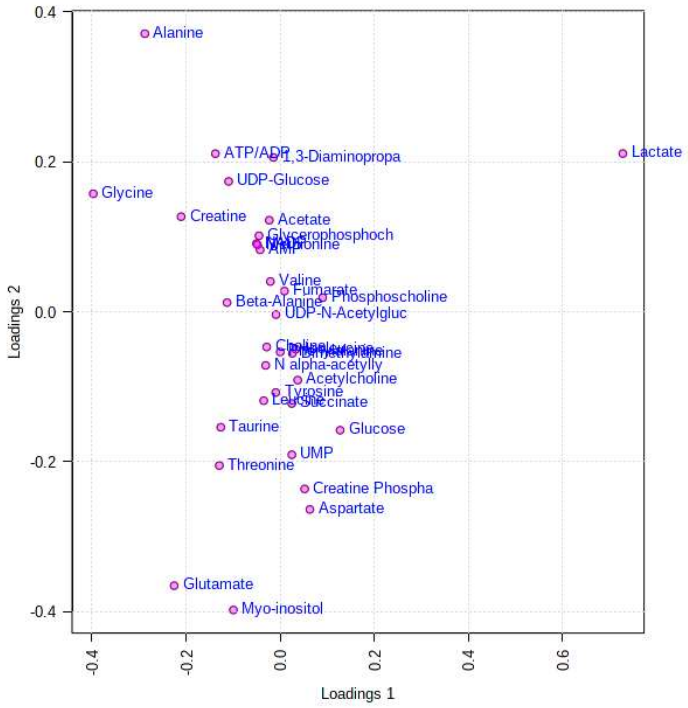

Figure S 16 PCA loadings of NIH 3T3 endometabolites.

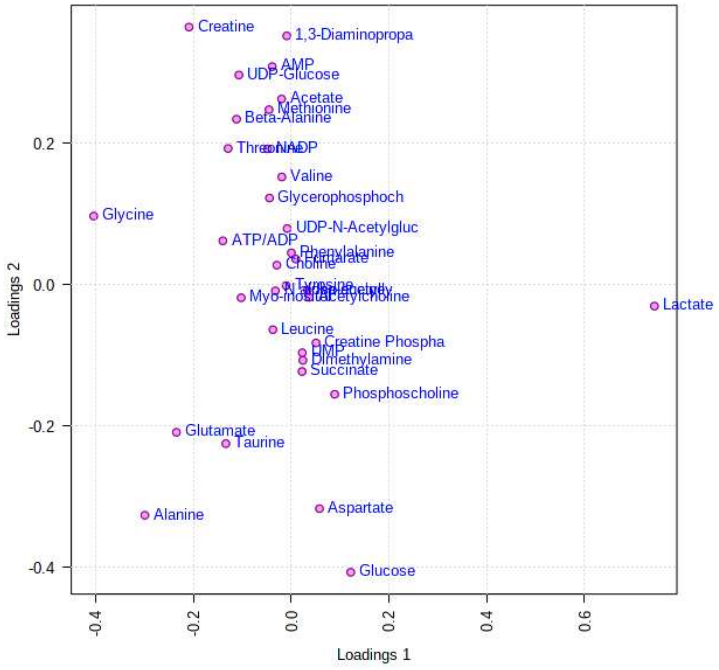

Figure S 17 PLS-DA loadings of NIH 3T3 endometabolites.

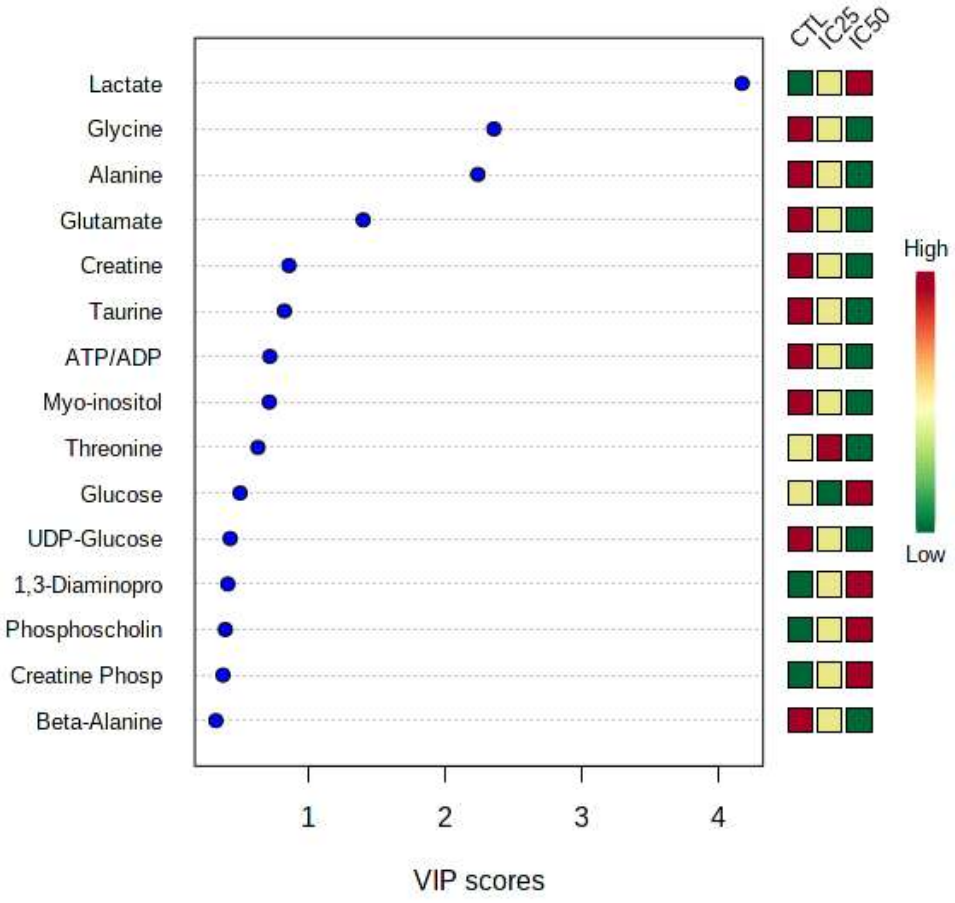

Figure S 18 VIP scores of NIH 3T3 endometabolites.

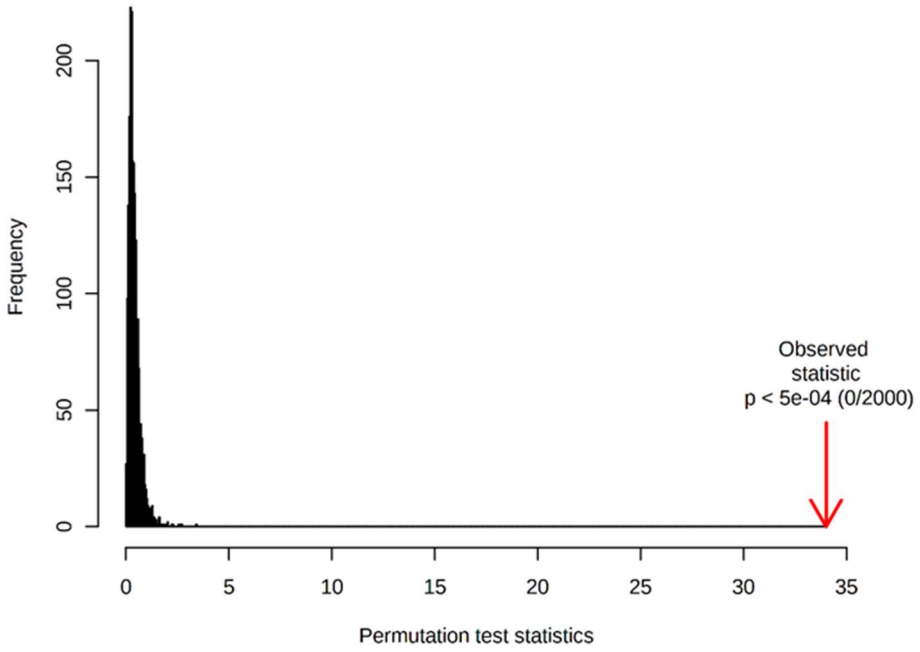

Figure S 19 Model validation by the permutation of NIH 3T3 endometabolites.

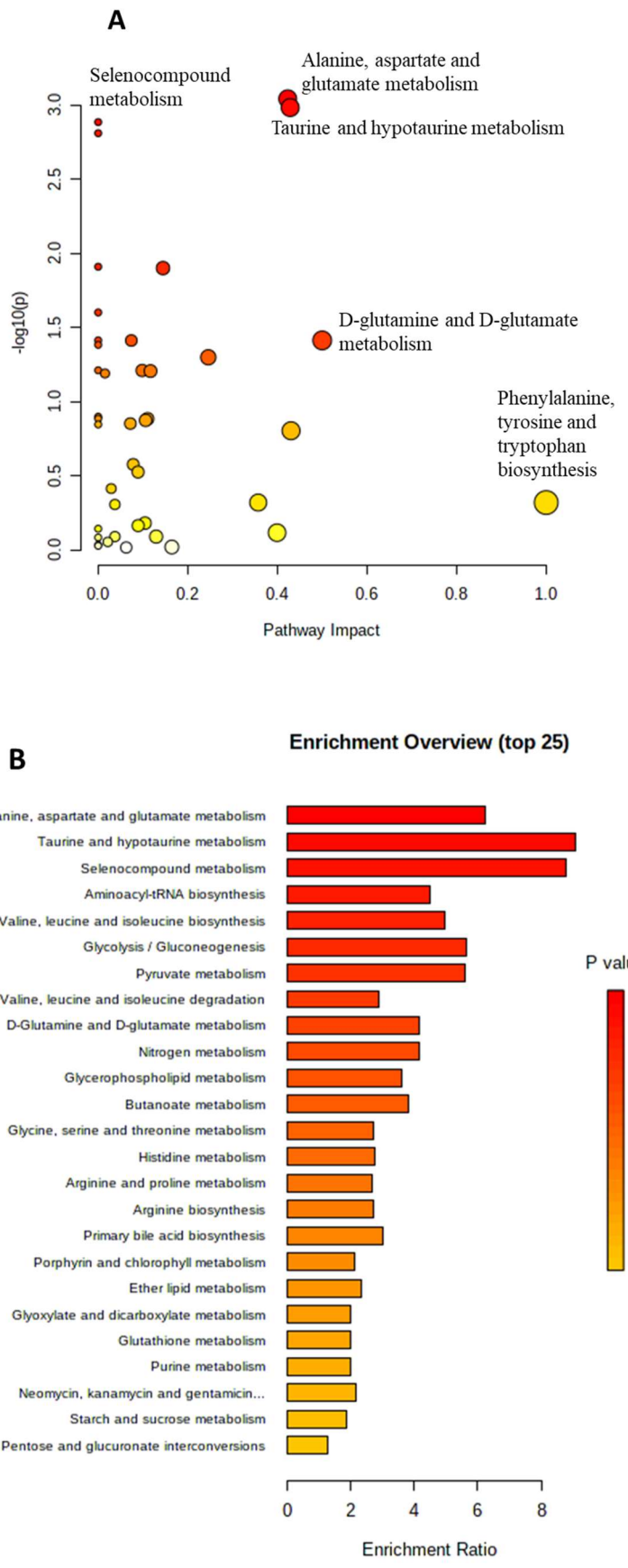

Figure S 20 (A) The metabolome view map and (B) enrichment overview of NIH 3T3 endometabolites after treatment with IC_{25} of PAMAM G4NH$_2$ using KEGG library.

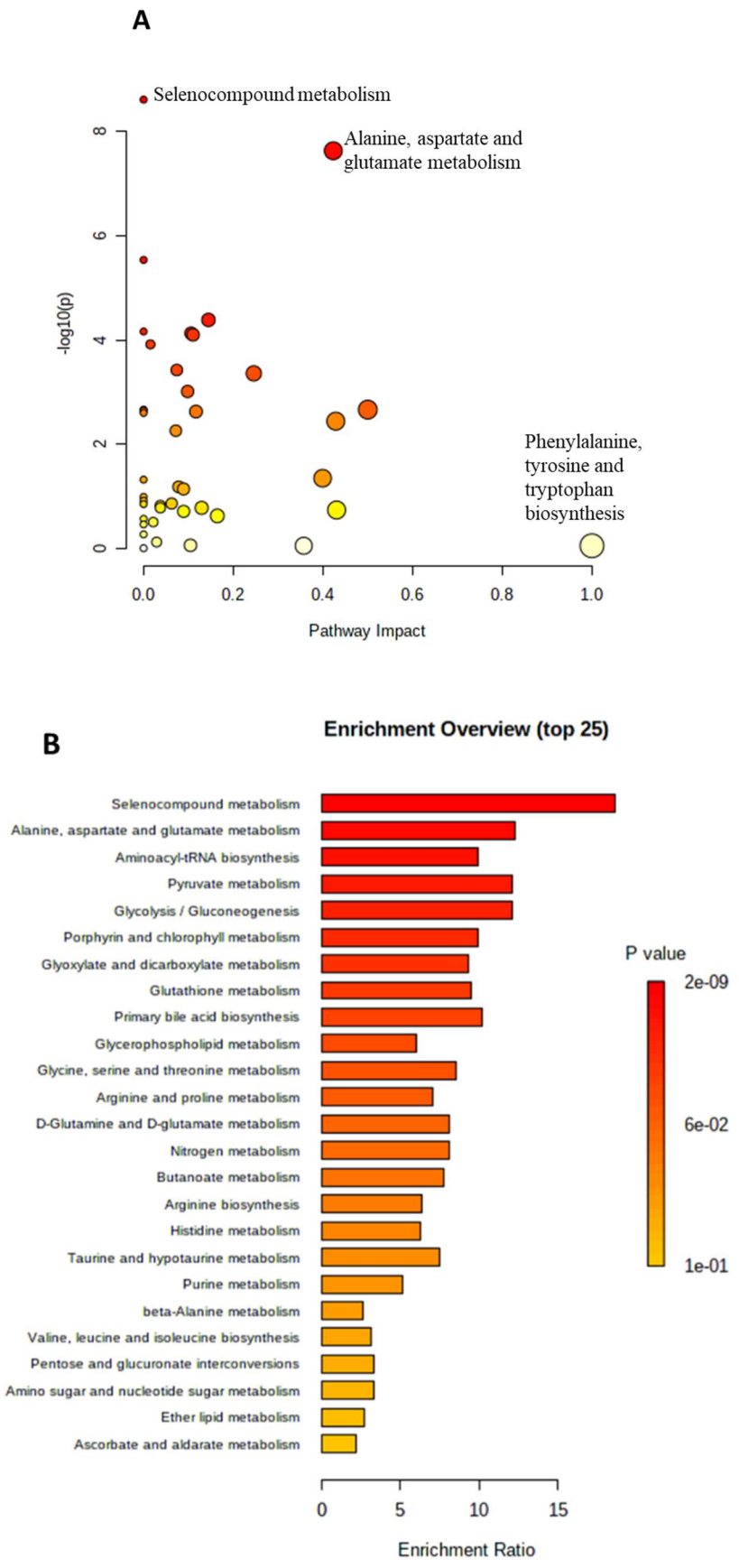

Figure S 21 (A) The metabolome view map and (B) enrichment overview of NIH 3T3 endometabolites after treatment with IC_{50} of PAMAM G4NH_2 using KEGG library.

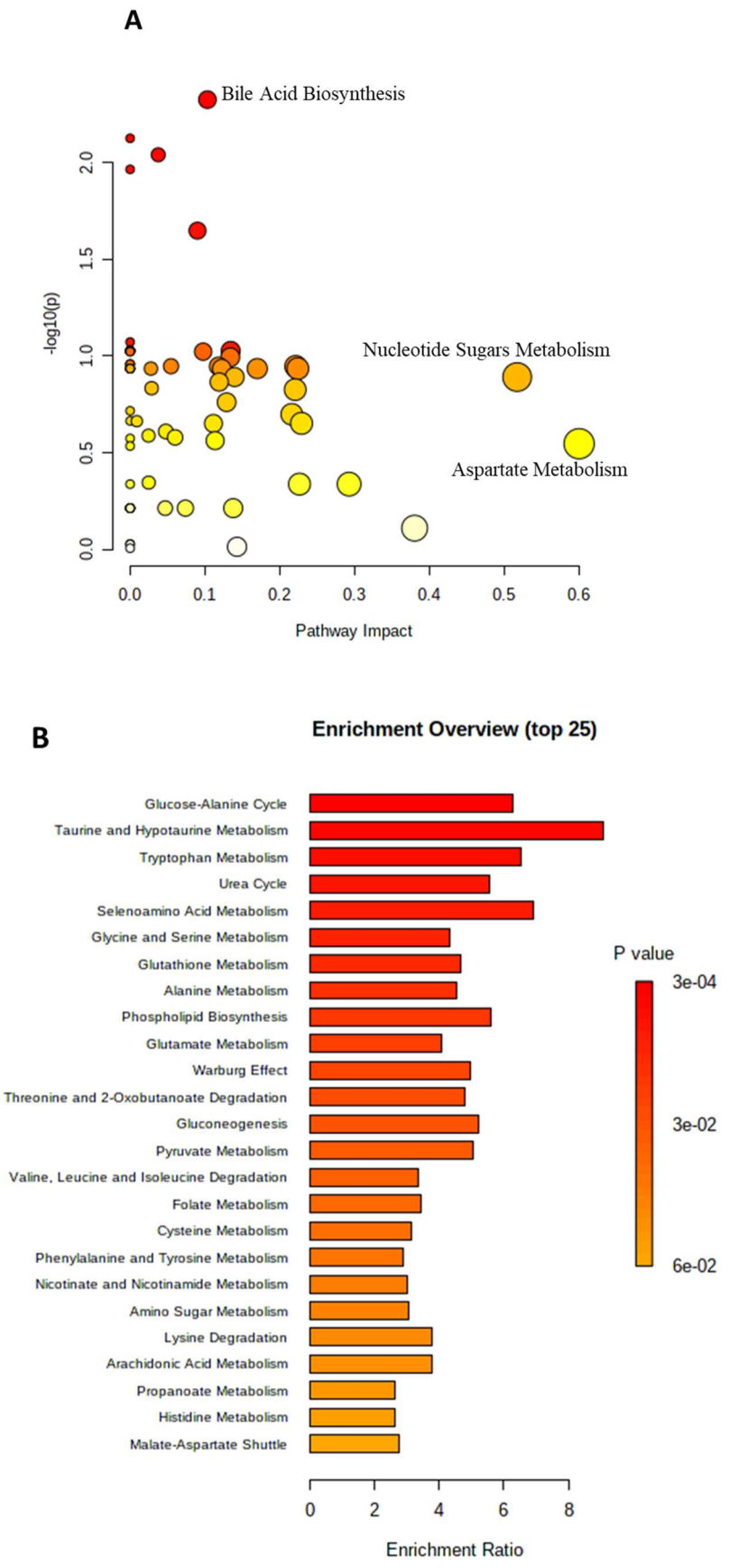

Figure S 22 (A) The metabolome view map and (B) enrichment overview of NIH 3T3 endometabolites after treatment with IC_{25} of PAMAM G4NH$_2$ using SMPDB library.

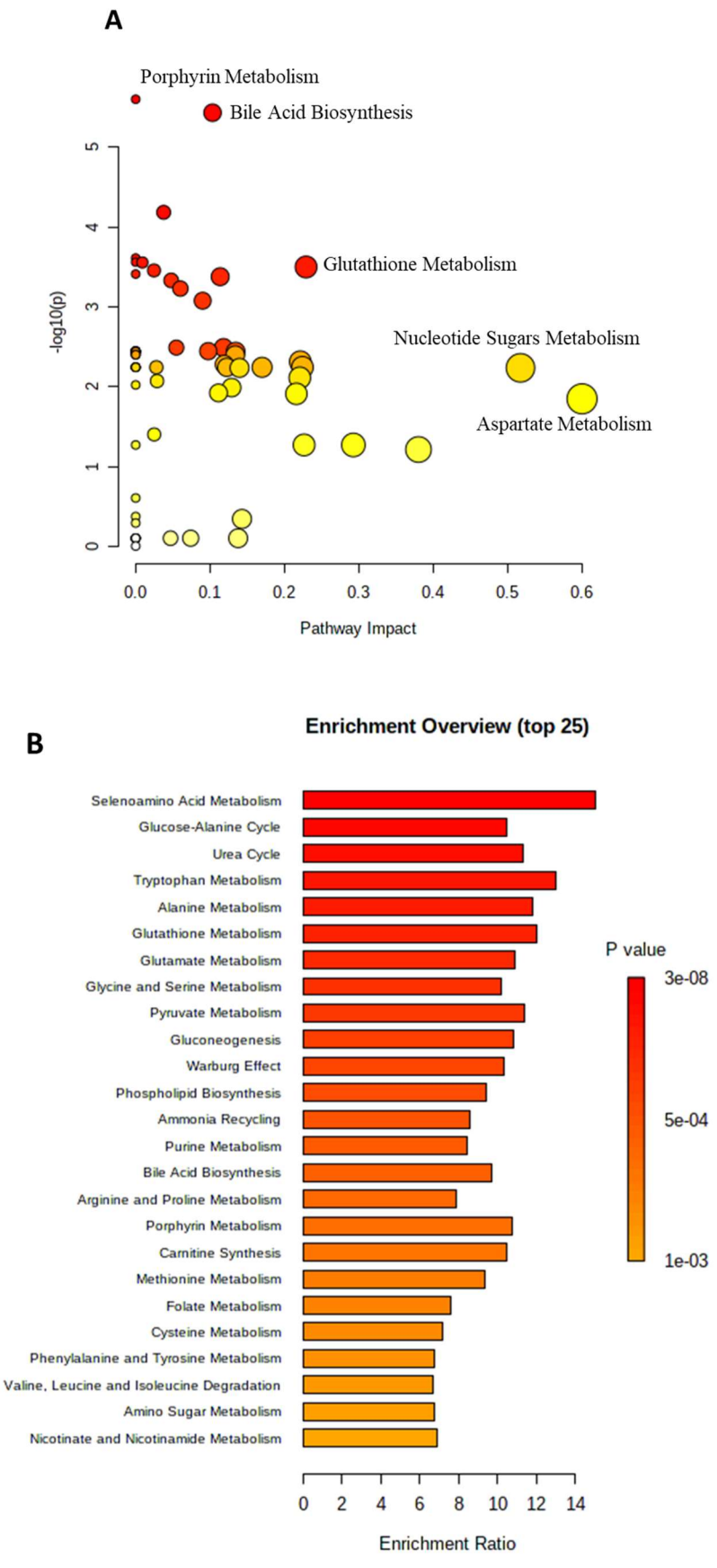

Figure S 23 (A) The metabolome view map and (B) enrichment overview of NIH 3T3 endometabolites after treatment with IC_{50} of PAMAM G4NH$_2$ using SMPDB library.

4. Exometabolome NIH 3T3 after treatment with PAMAM G4NH2

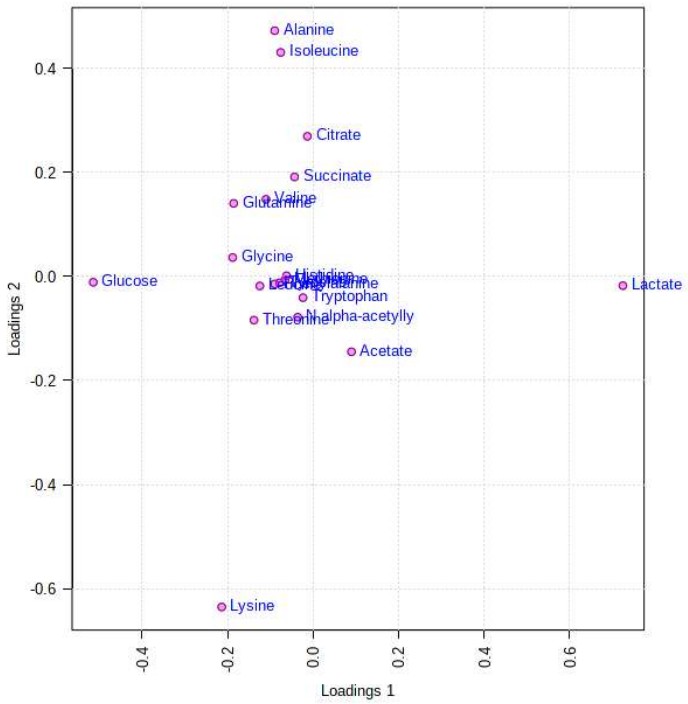

Figure S 24 PCA loadings of NIH 3T3 exometabolites.

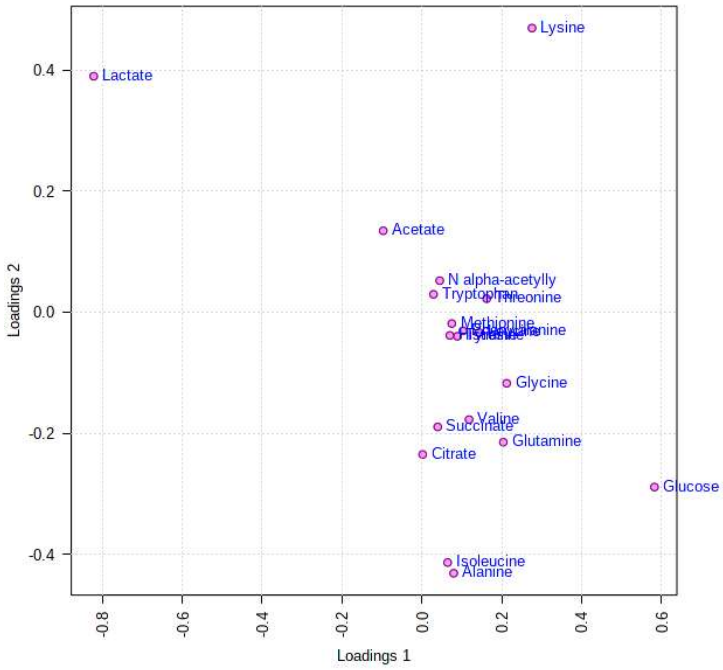

Figure S 25 PLS-DA loadings of NIH 3T3 exometabolites.

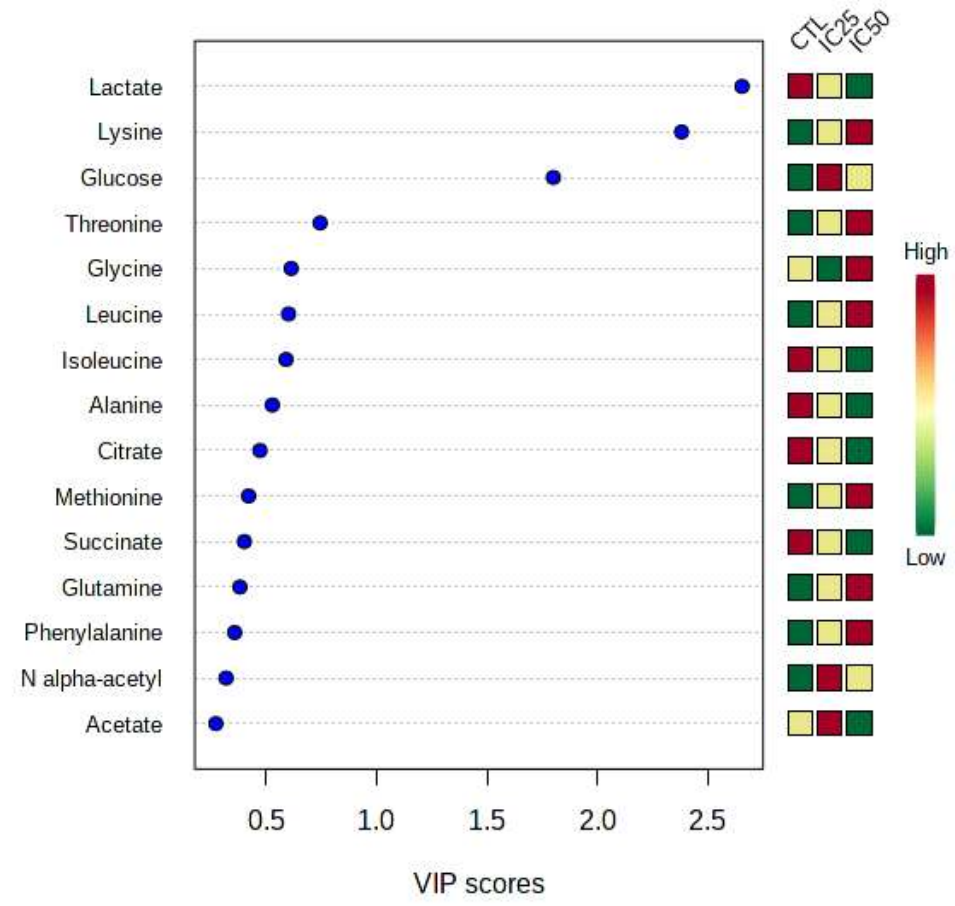

Figure S 26 VIP scores of NIH 3T3 exometabolites.

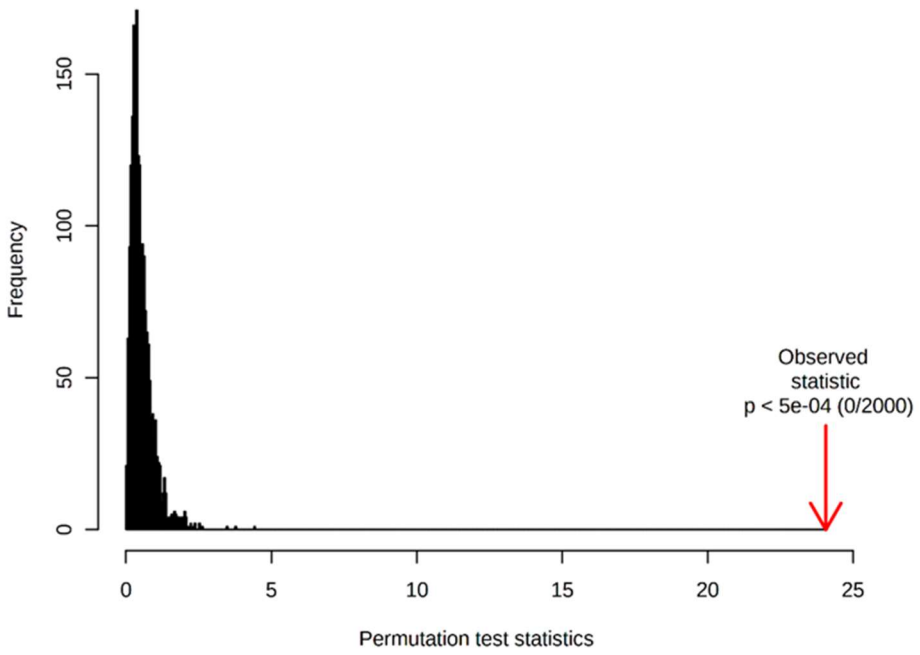

Figure S 27 Model validation by the permutation of NIH 3T3 exometabolites.

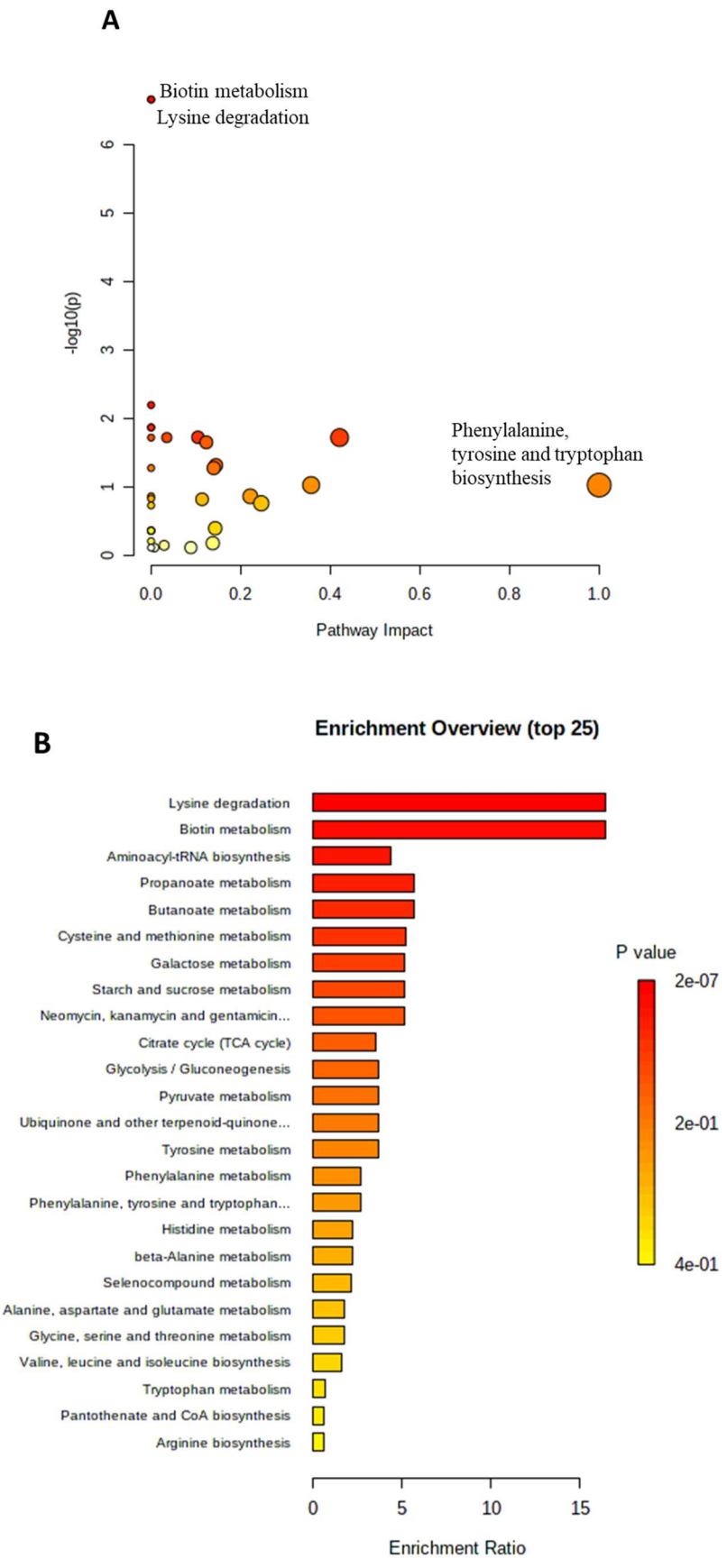

Figure S 28 (A) The metabolome view map and (B) enrichment overview of NIH 3T3 exometabolites after treatment with IC_{25} of PAMAM G4NH$_2$ using KEGG library.

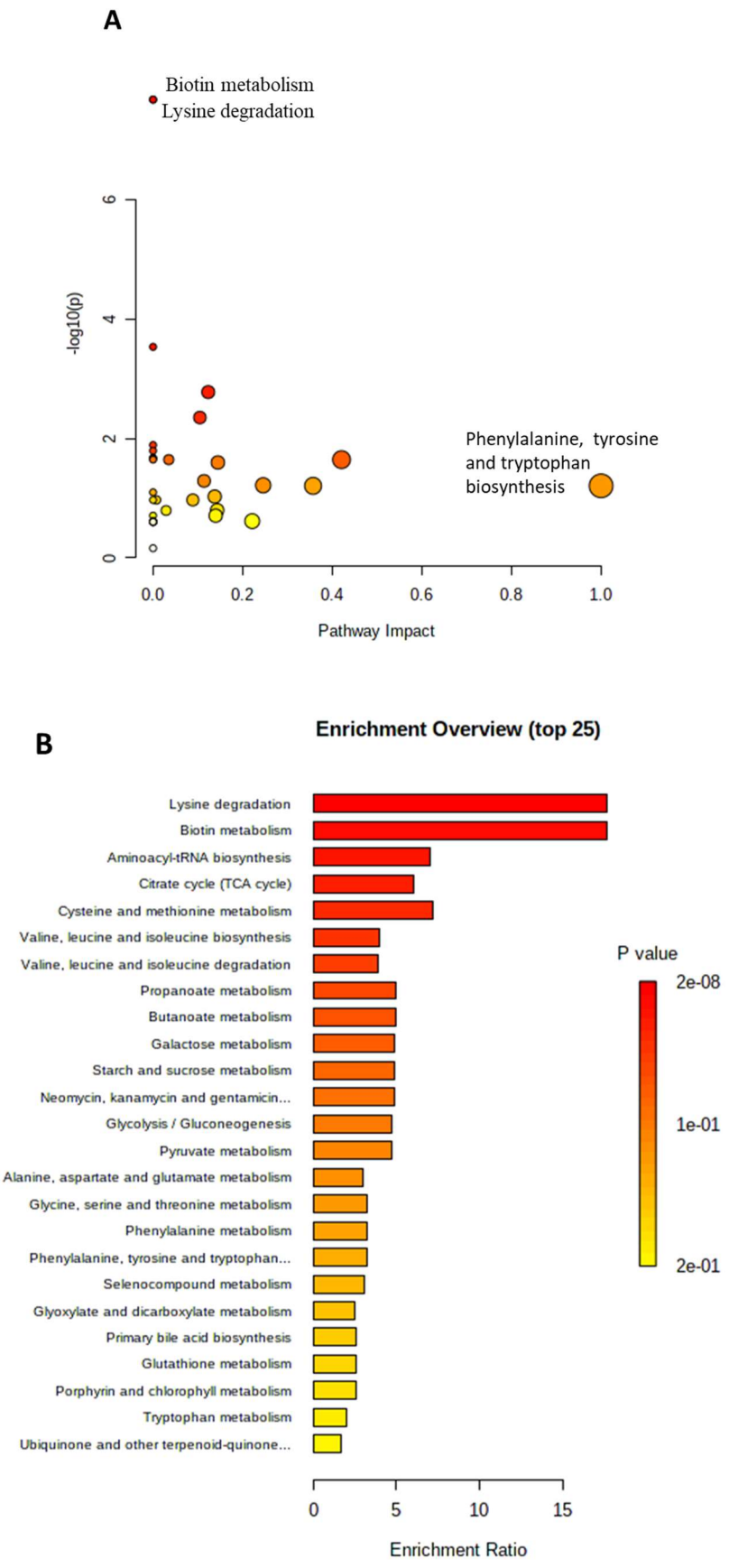

Figure S 29 (A) The metabolome view map and (B) enrichment overview of NIH 3T3 exometabolites after treatment with IC_{50} of PAMAM G4NH$_2$ using KEGG library.

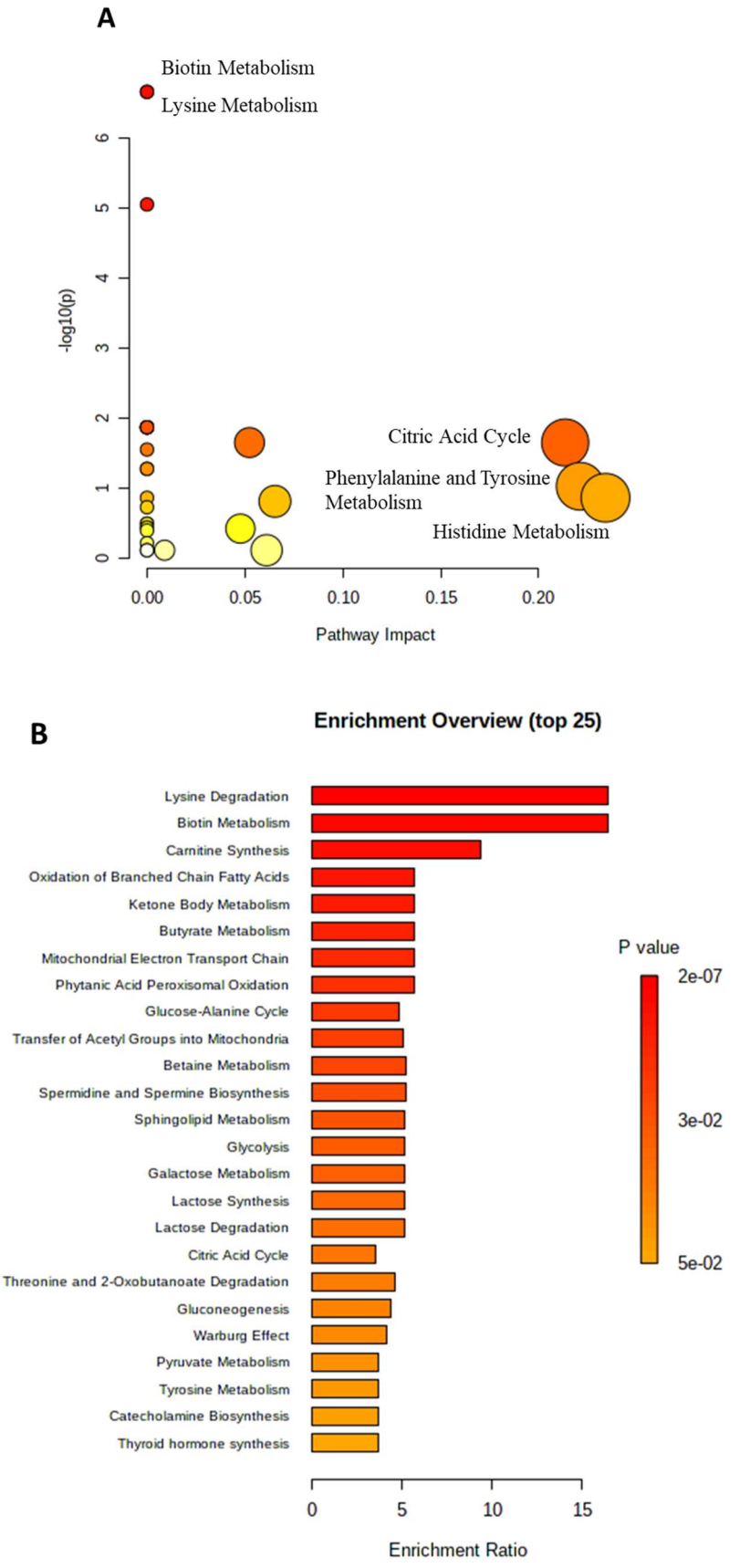

Figure S 30 (A) The metabolome view map and (B) enrichment overview of NIH 3T3 exometabolites after treatment with IC_{25} of PAMAM G4NH$_2$ using SMPDB library.

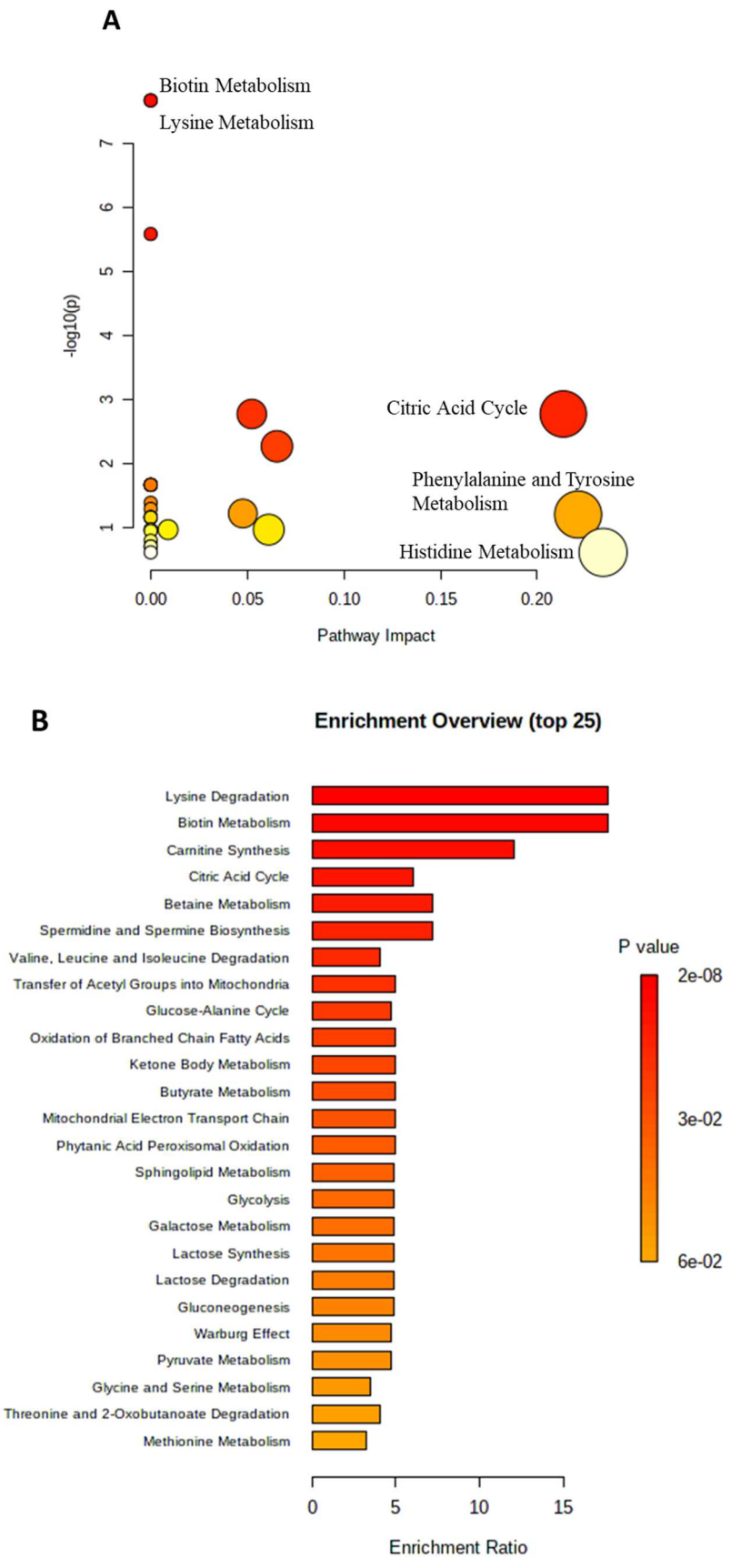

Figure S 31 (A) The metabolome view map and (B) enrichment overview of NIH 3T3 exometabolites after treatment with IC_{50} of PAMAM G4NH_2 using SMPDB library.

5. Endometabolome A2780 after treatment with PAMAM G4NH2

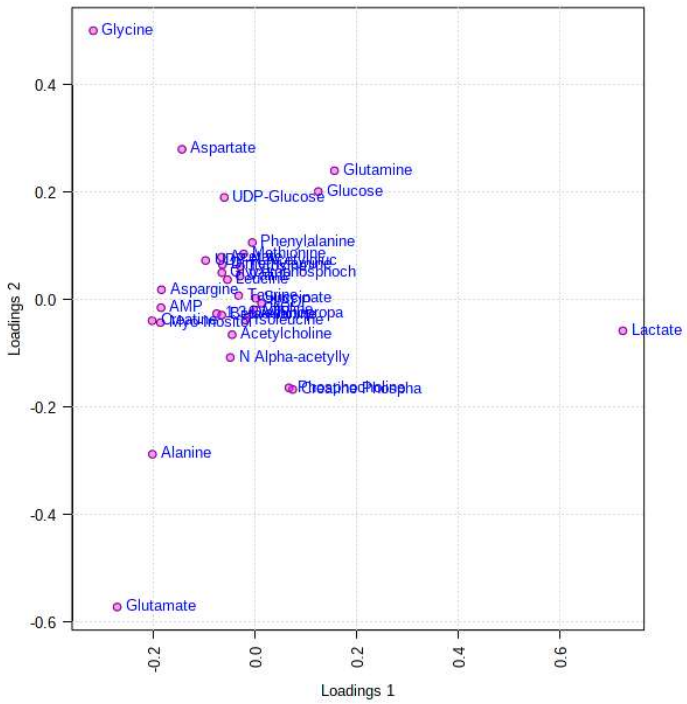

Figure S 32 PCA loading of A2780 endometabolites.

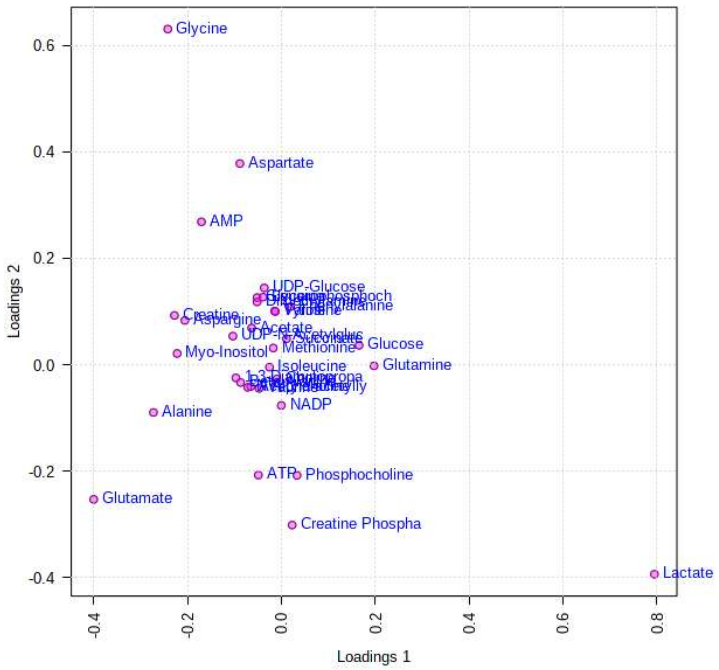

Figure S 33 PLS-DA of A2780 endometabolites.

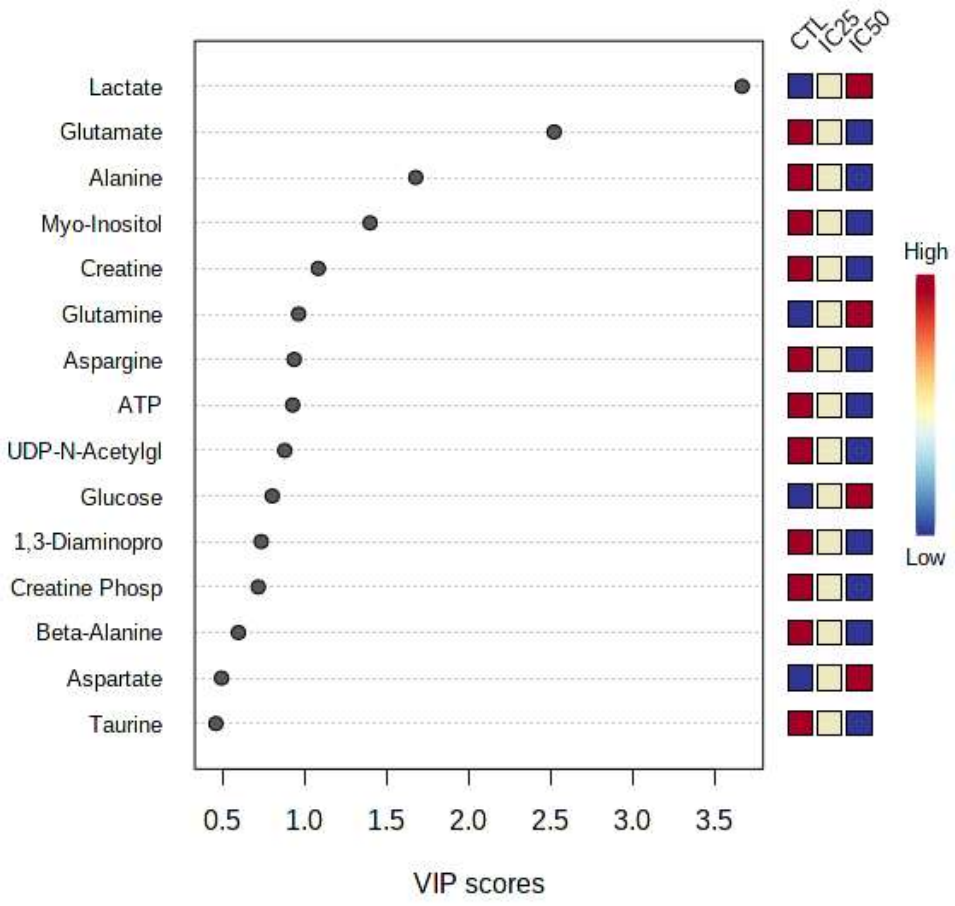

Figure S 34 VIP scores of A2780 endometabolites.

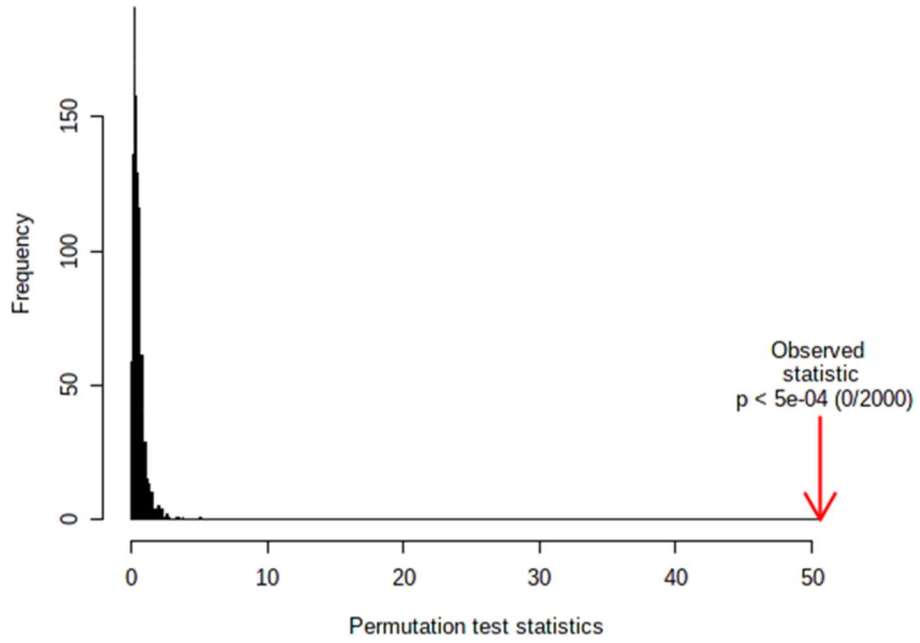

Figure S 35 Model validation by the permutation of A2780 endometabolites.

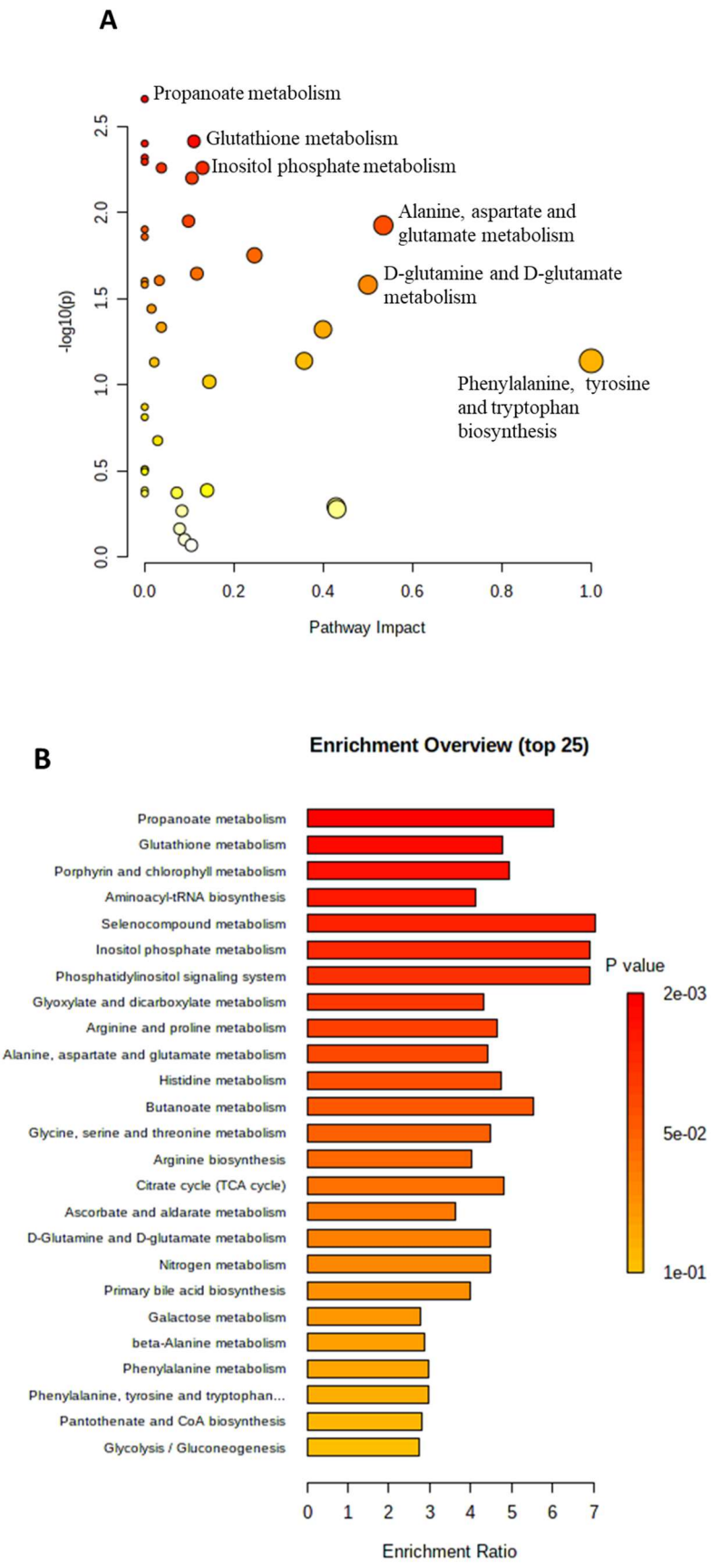

Figure S 36 (A) The metabolome view map and (B) enrichment overview of A2780 endometabolites after treatment with IC_{25} of PAMAM G4NH$_2$ using KEGG library.

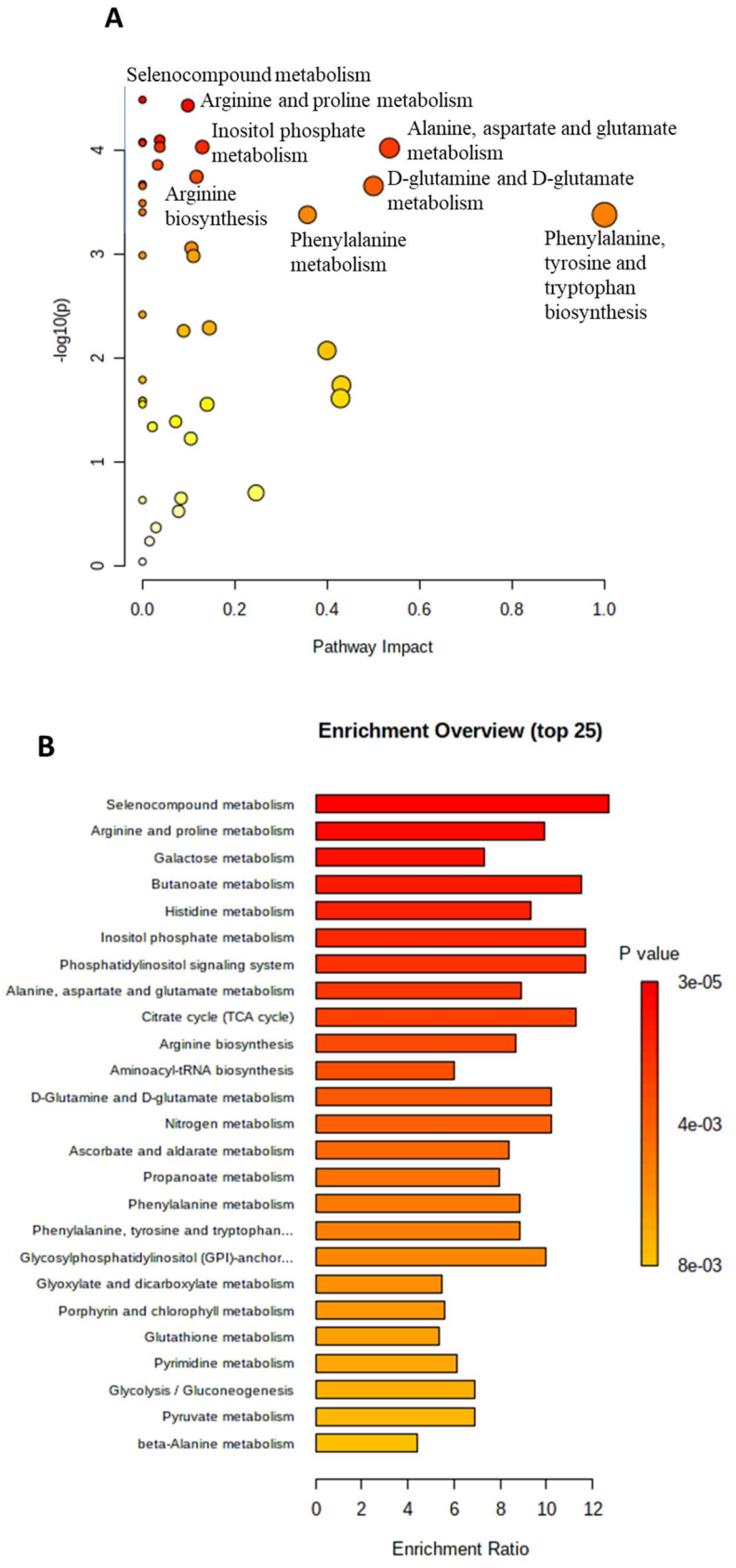

Figure S 37 (A) The metabolome view map and (B) enrichment overview of A2780 endometabolites after treatment with IC_{50} of PAMAM G4NH$_2$ using KEGG library.

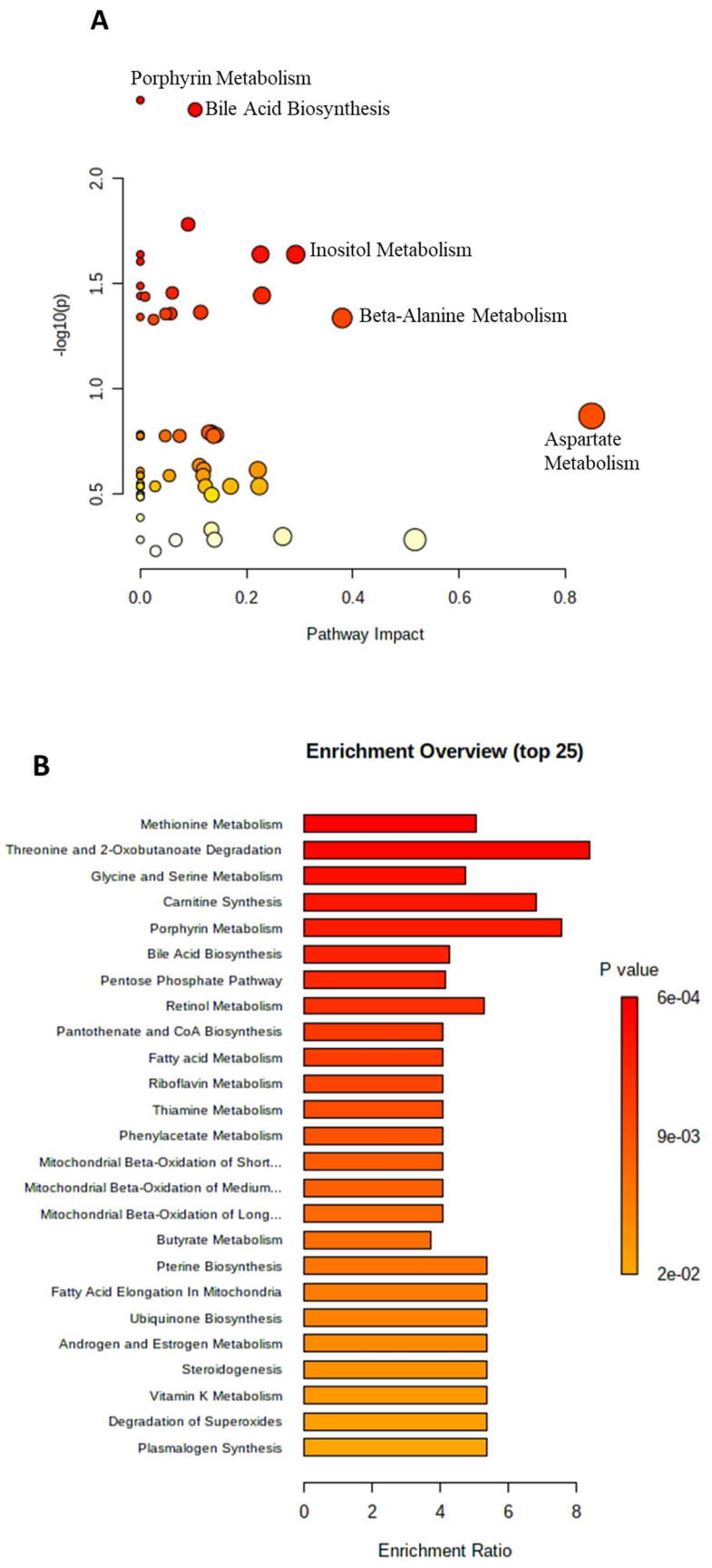

Figure S 38 (A) The metabolome view map and (B) enrichment overview of A2780 endometabolites after treatment with IC_{25} of PAMAM G4NH$_2$ using SMPDB library.

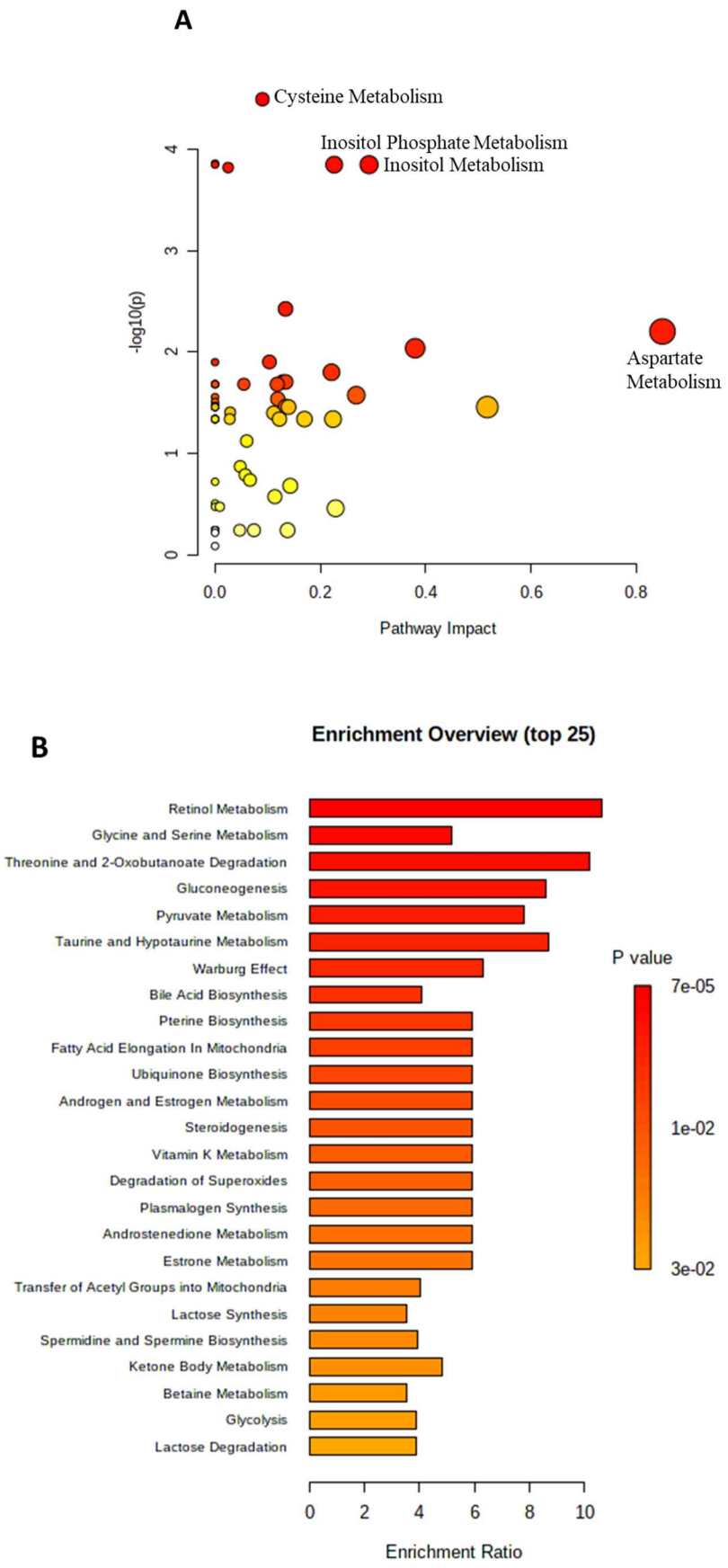

Figure S 39 (A) The metabolome view map and (B) enrichment overview of A2780 endometabolites after treatment with IC_{50} of PAMAM G4NH$_2$ using SMPDB library.

6. Exometabolome A2780 after treatment with PAMAM G4NH2

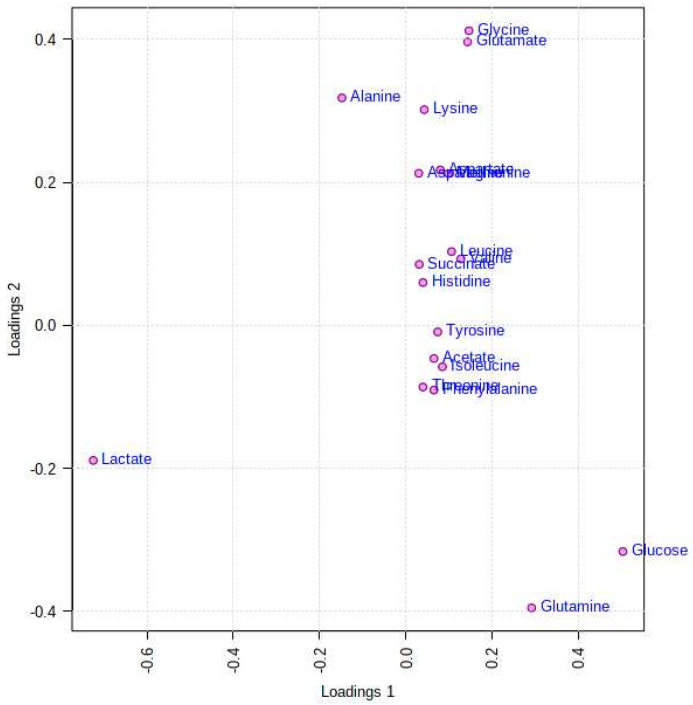

Figure S 40 PCA loading of A2780 exometabolites.

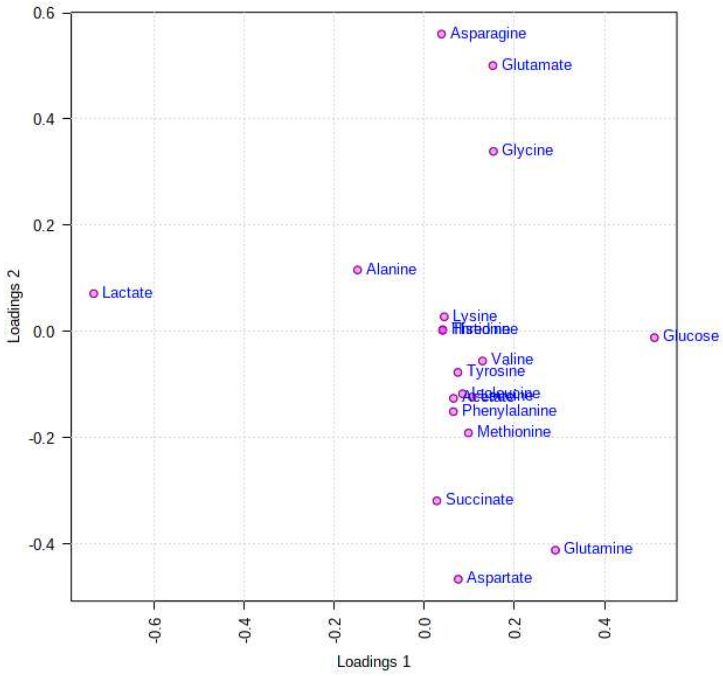

Figure S 41 PLS-DA of A2780 exometabolites.

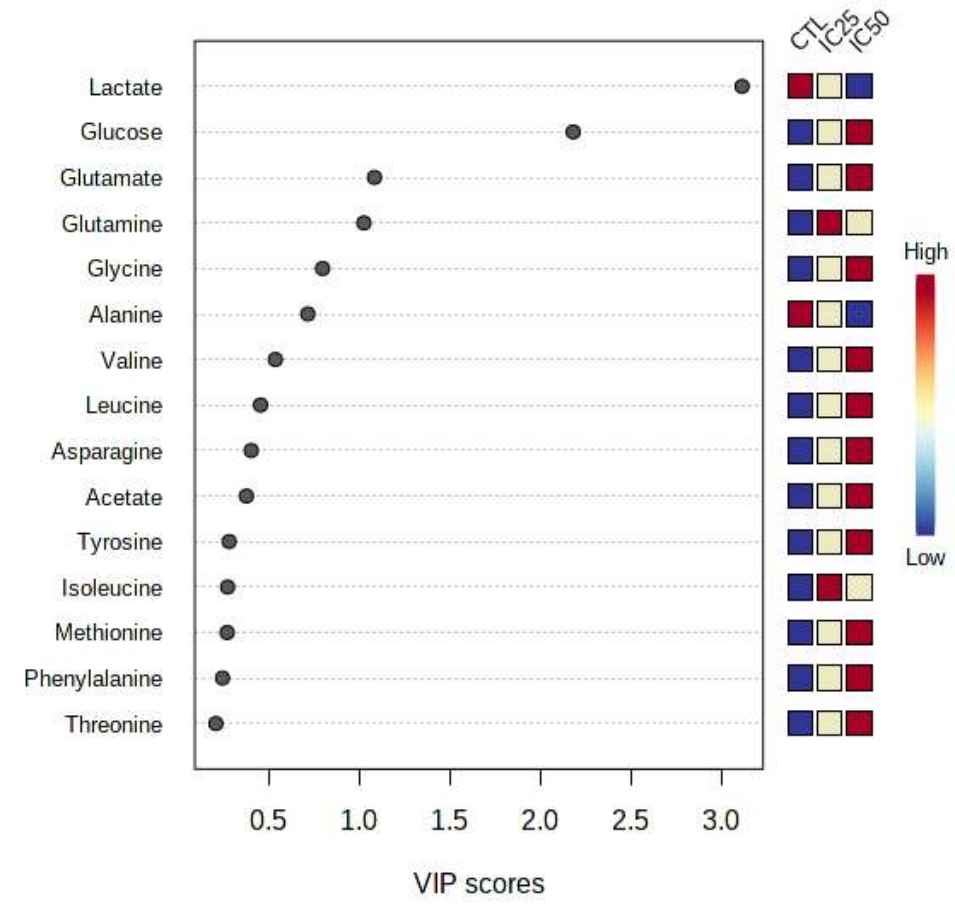

Figure S 42 VIP scores of A2780 exometabolites.

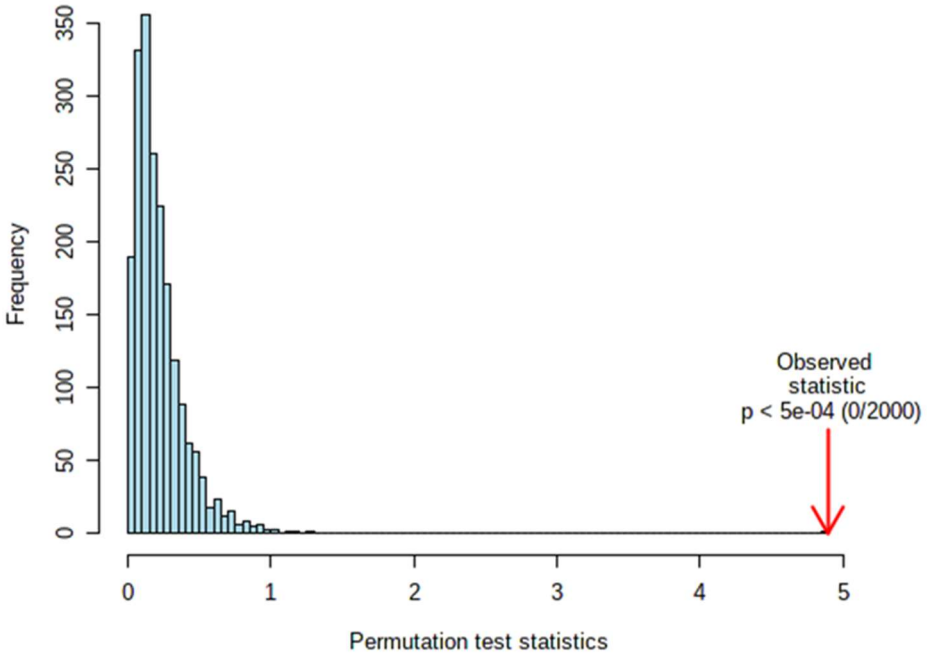

Figure S 43 Model validation by the permutation of A2780 exometabolites.

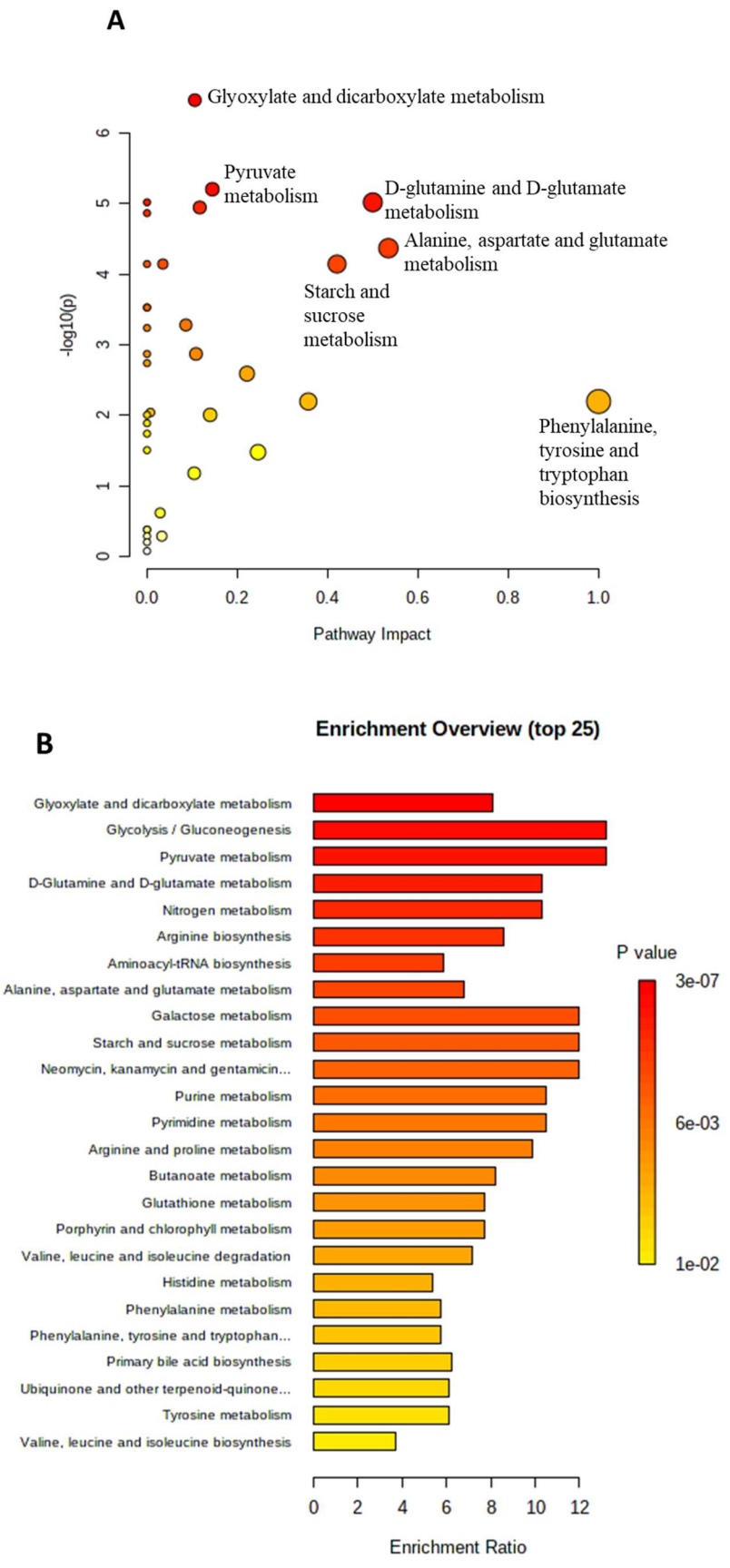

Figure S 44 (A) The metabolome view map and (B) enrichment overview of A2780 exometabolites after treatment with IC_{25} of PAMAM G4NH$_2$ using KEGG library.

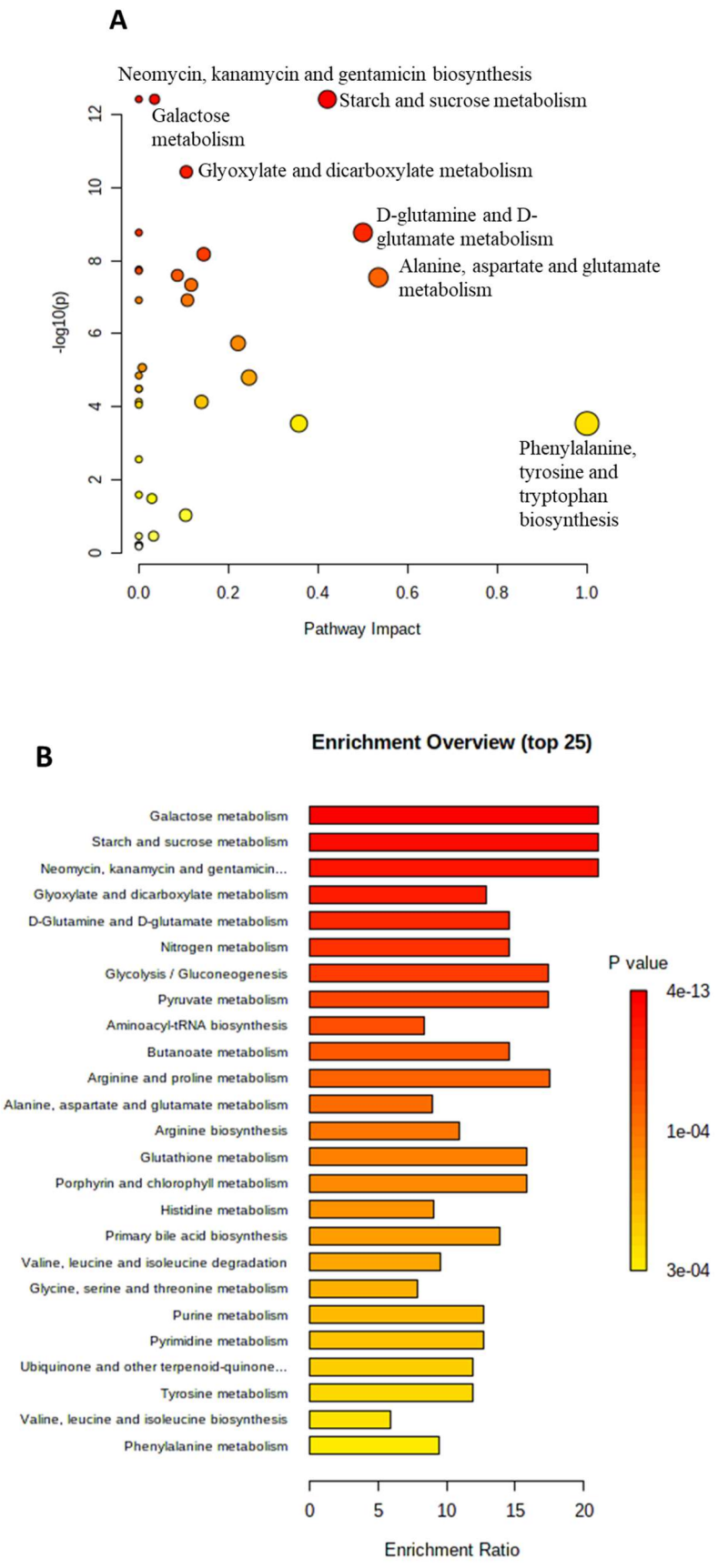

Figure S 45 (A) The metabolome view map and (B) enrichment overview of A2780 exometabolites after treatment with IC_{50} of PAMAM G4NH_2 using KEGG library.

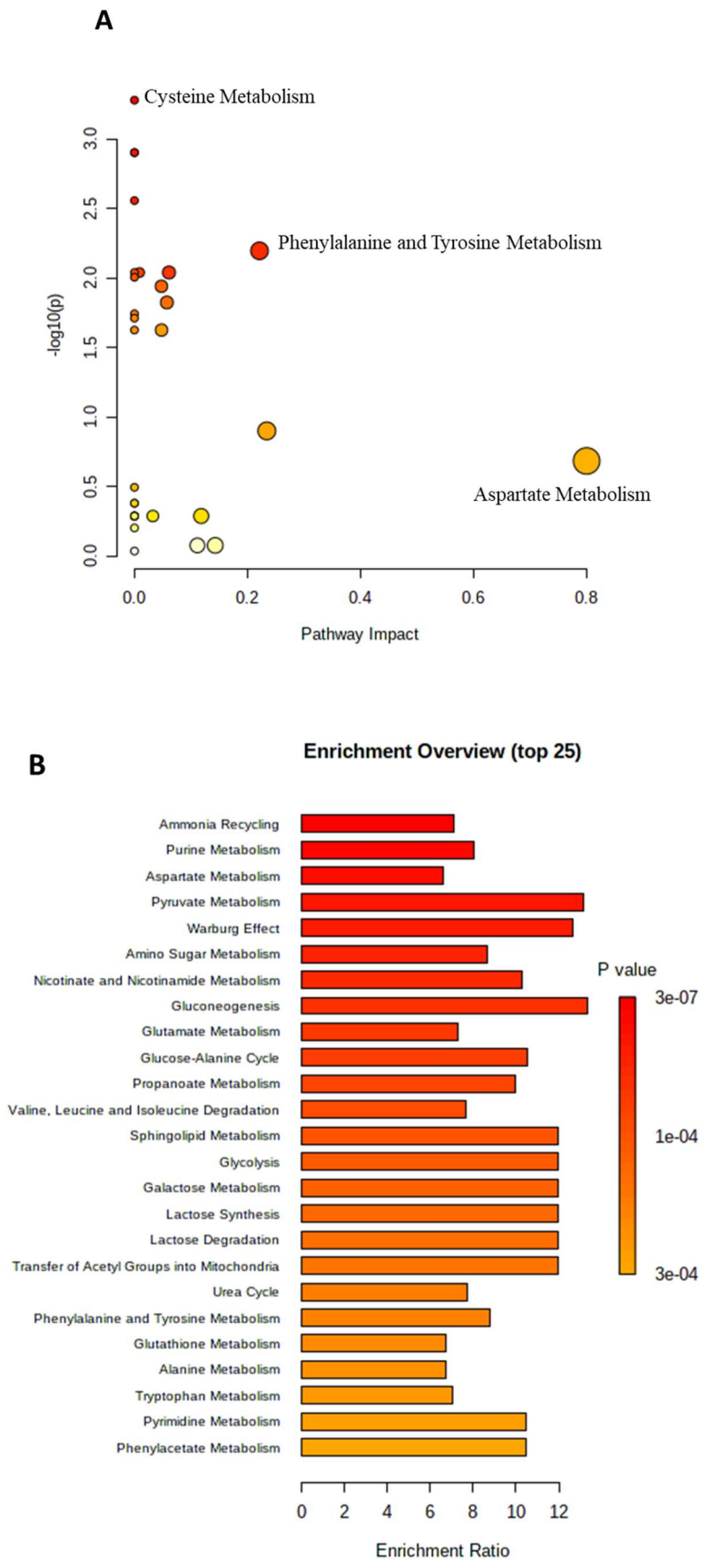

Figure S 46 (A) The metabolome view map and (B) enrichment overview of A2780 exometabolites after treatment with IC_{25} of PAMAM G4NH$_2$ using SMPDB library.

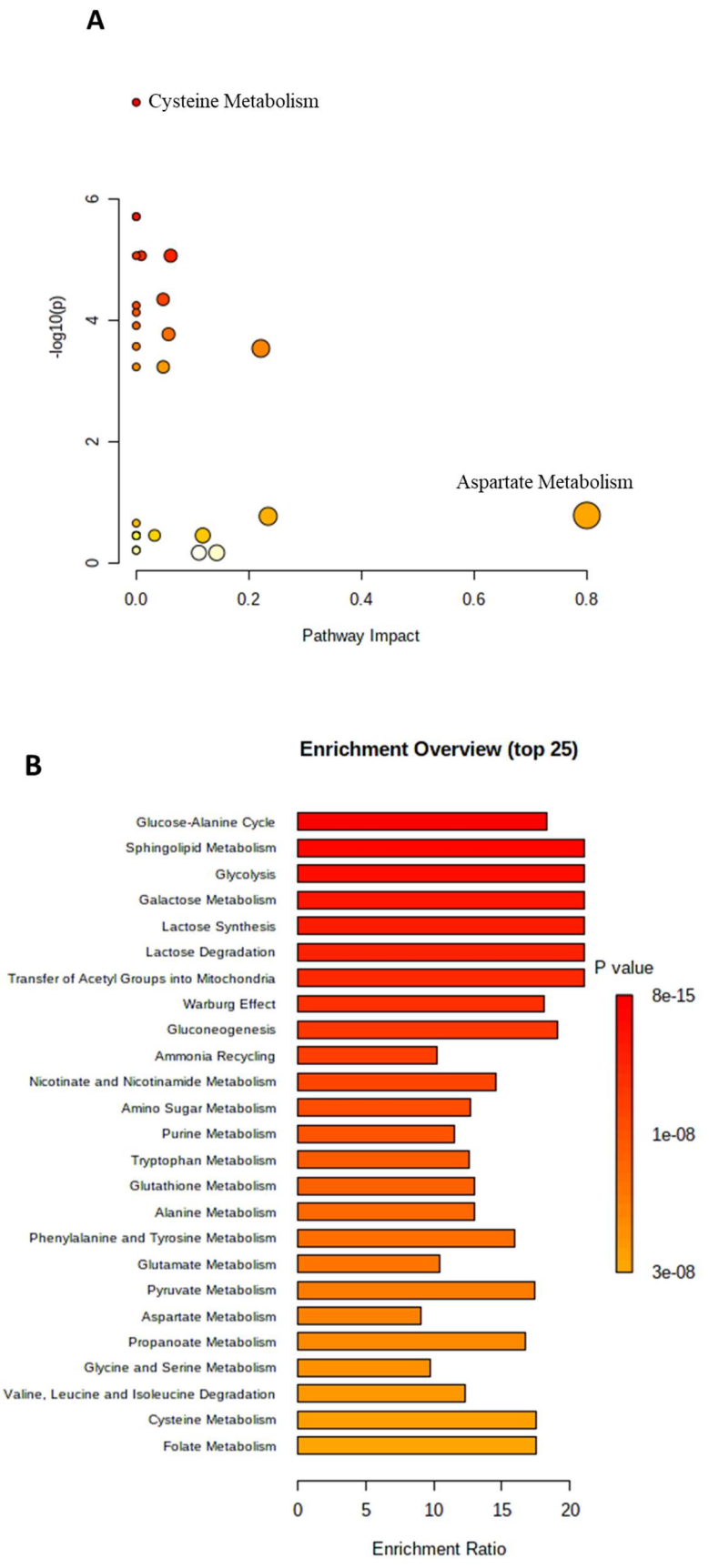

Figure S 47 (A) The metabolome view map and (B) enrichment overview of A2780 exometabolites after treatment with IC_{50} of PAMAM G4NH$_2$ using SMPDB library.

7. Endometabolome CACO-2 after treatment with PAMAM G4NH2

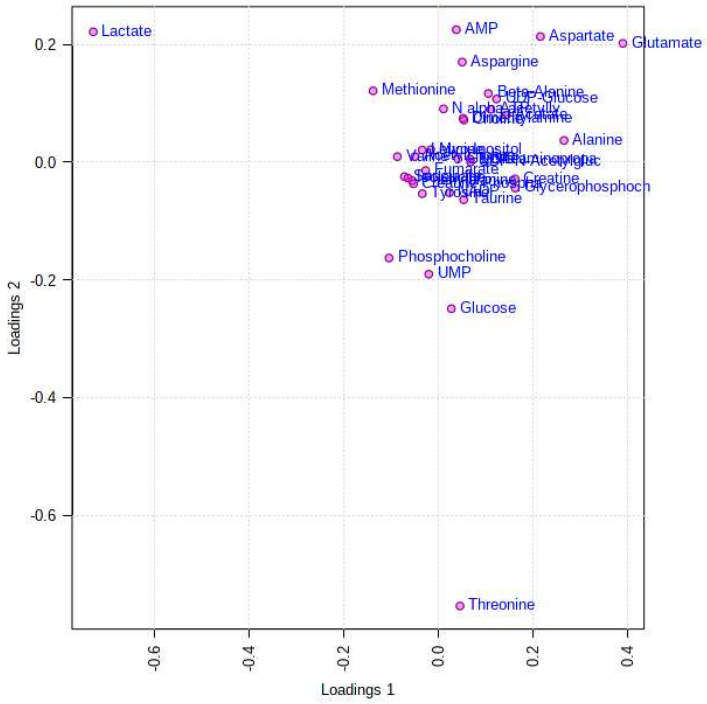

Figure S 48 PCA loading of CACO-2 endometabolites.

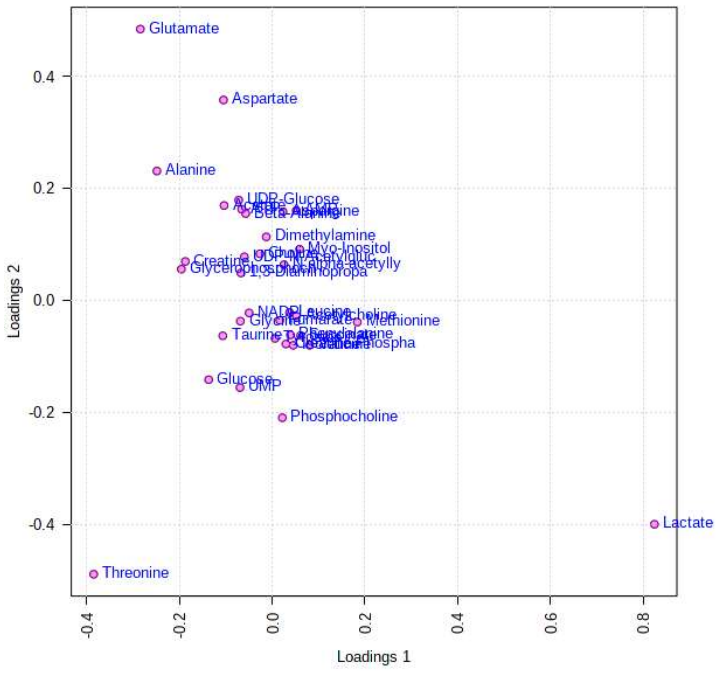

Figure S 49 PLS-DA loading of CACO-2 endometabolites.

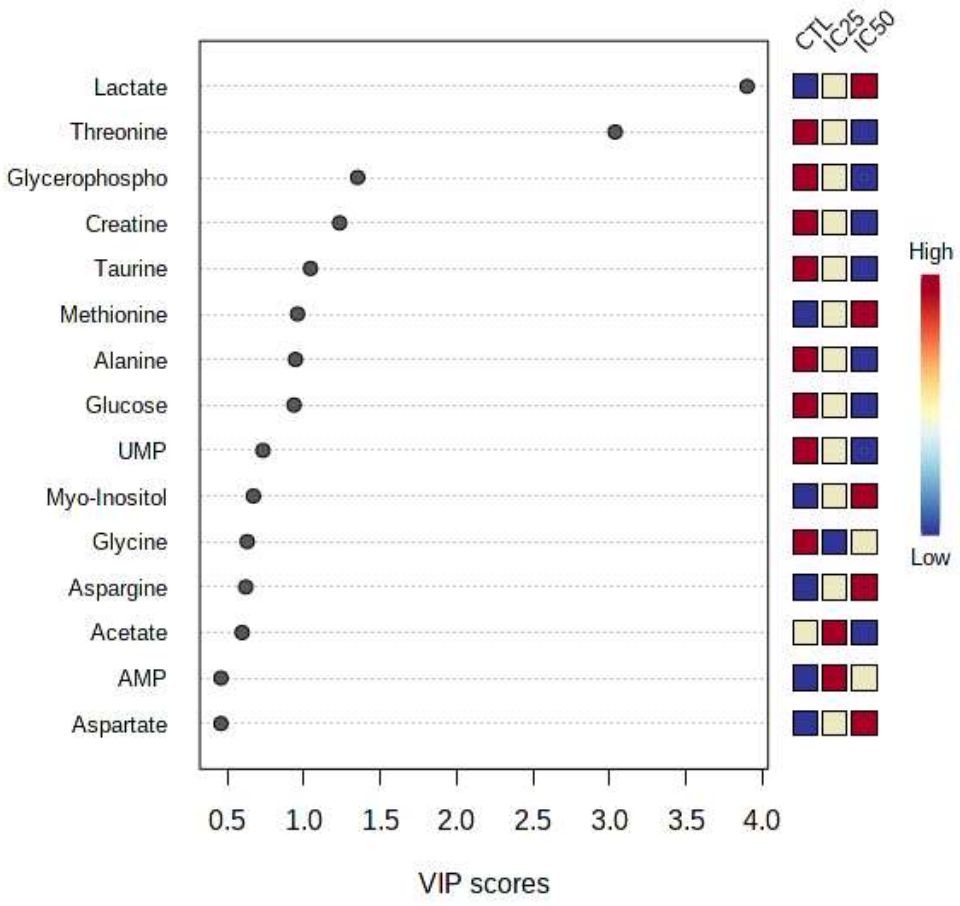

Figure S 50 VIP scores of CACO-2 endometabolites.

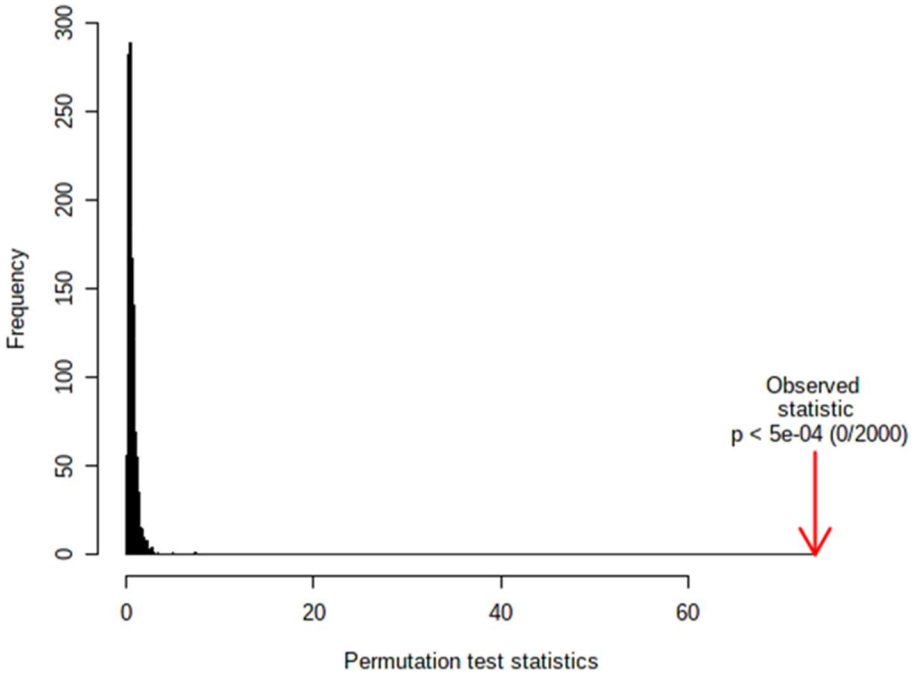

Figure S 51 model validation by the permutation of CACO-2 endometabolites.

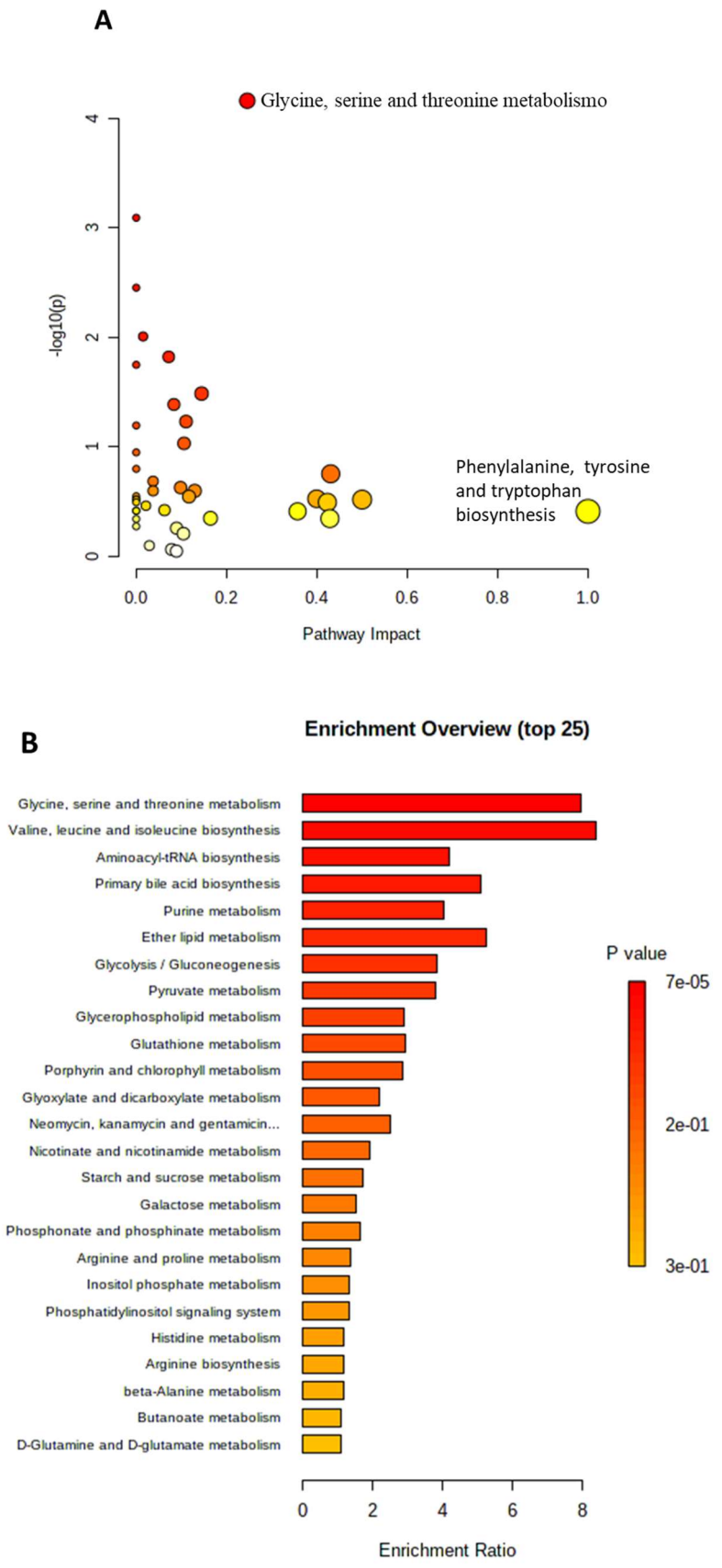

Figure S 52 (A) The metabolome view map and (B) enrichment overview of CACO-2 endometabolites after treatment with IC_{25} of PAMAM G4NH$_2$ using KEGG library.

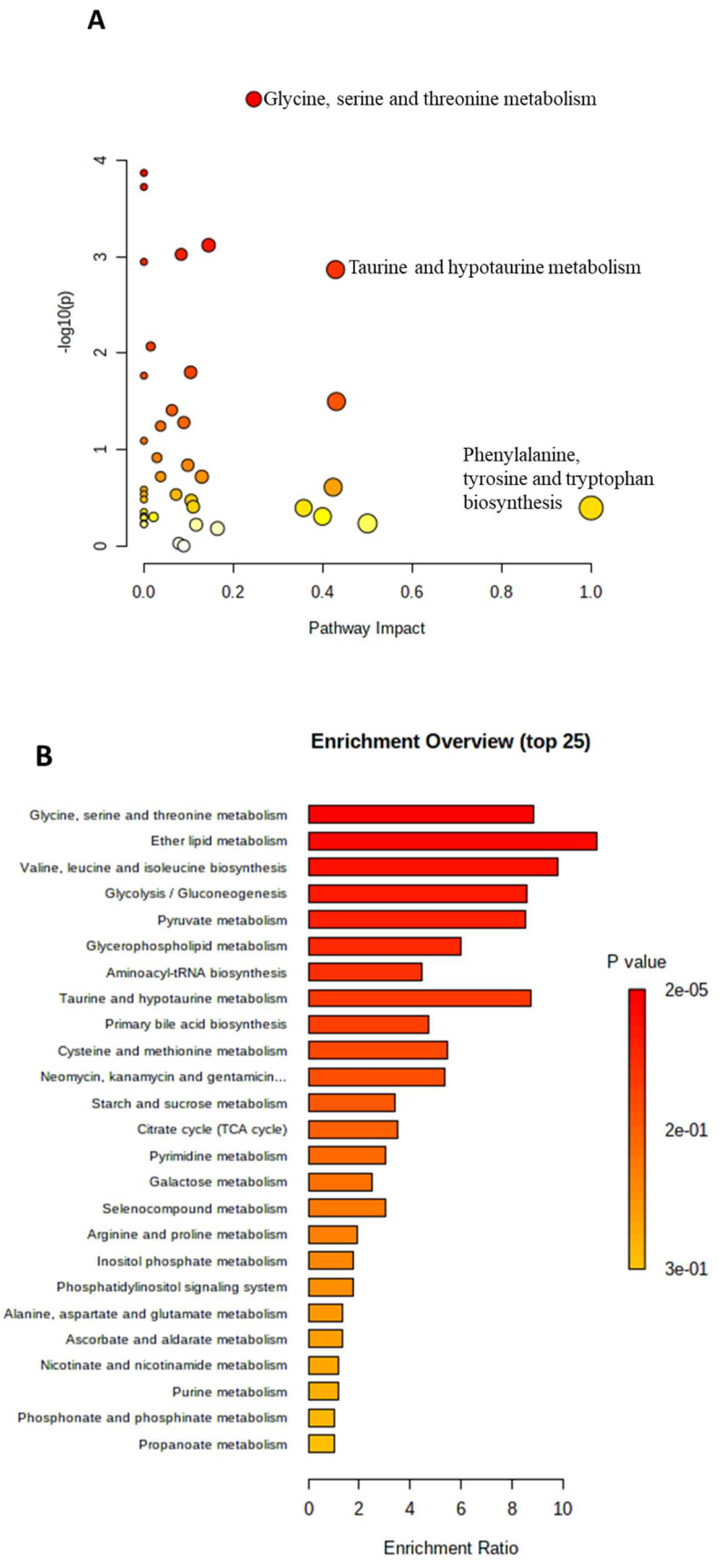

Figure S 53 (A) The metabolome view map and (B) enrichment overview of CACO-2 endometabolites after treatment with IC_{50} of PAMAM G4NH$_2$ using KEGG library.

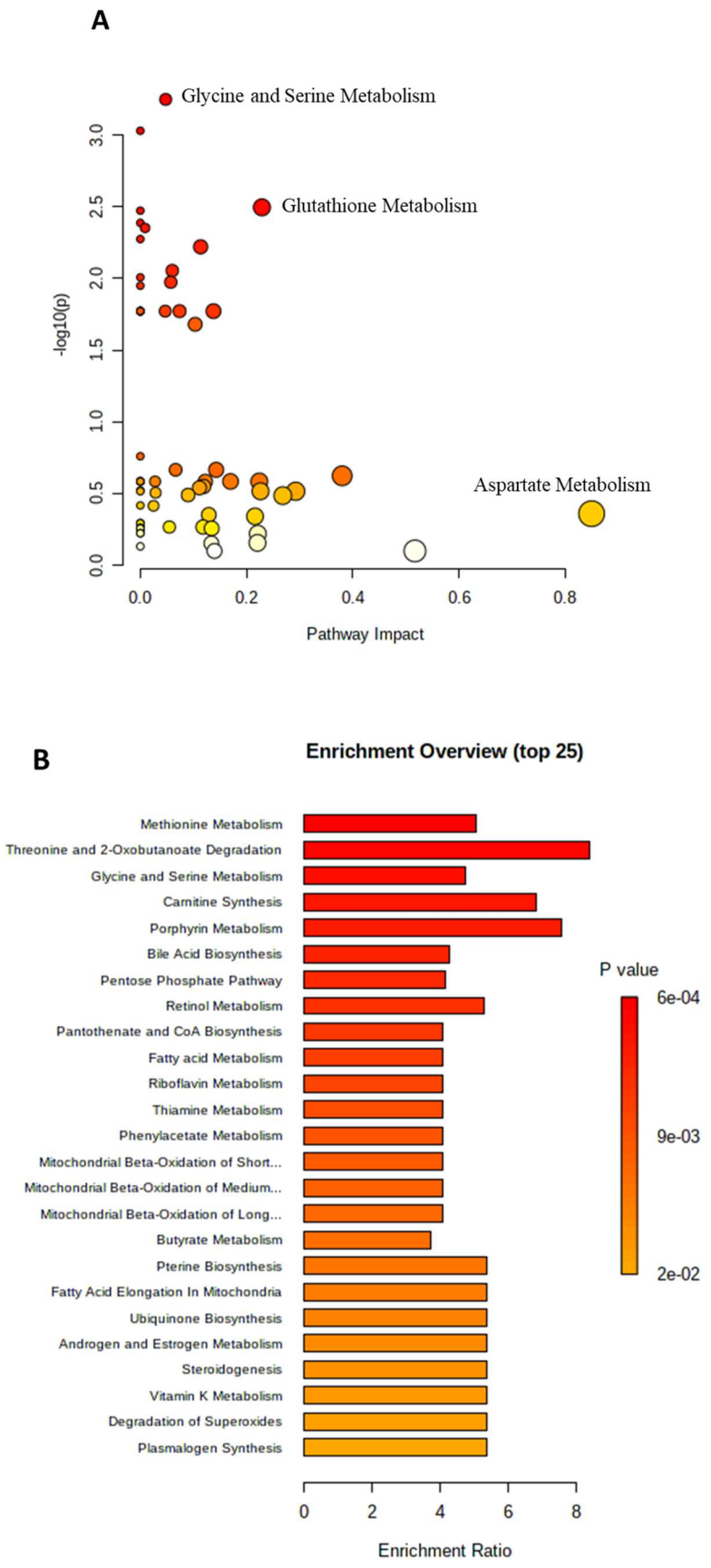

Figure S 54 (A) The metabolome view map and (B) enrichment overview of CACO-2 endometabolites after treatment with IC_{50} of PAMAM G4NH$_2$ using SMPDB library.

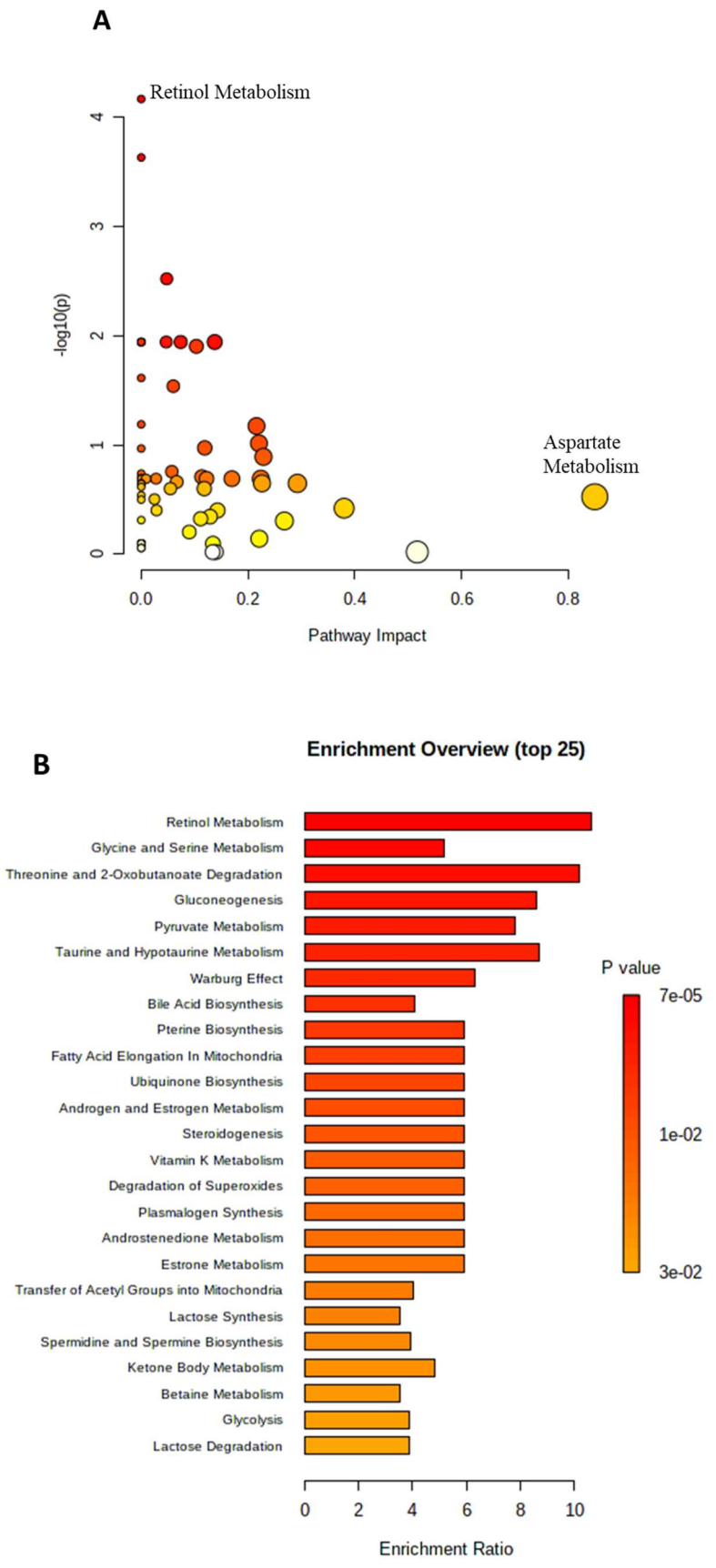

Figure S 55 (A) The metabolome view map and (B) enrichment overview of CACO-2 endometabolites after treatment with IC_{50} of PAMAM G4NH$_2$ using SMPDB library.

8. Exometabolome CACO-2 after treatment with PAMAM G4NH2

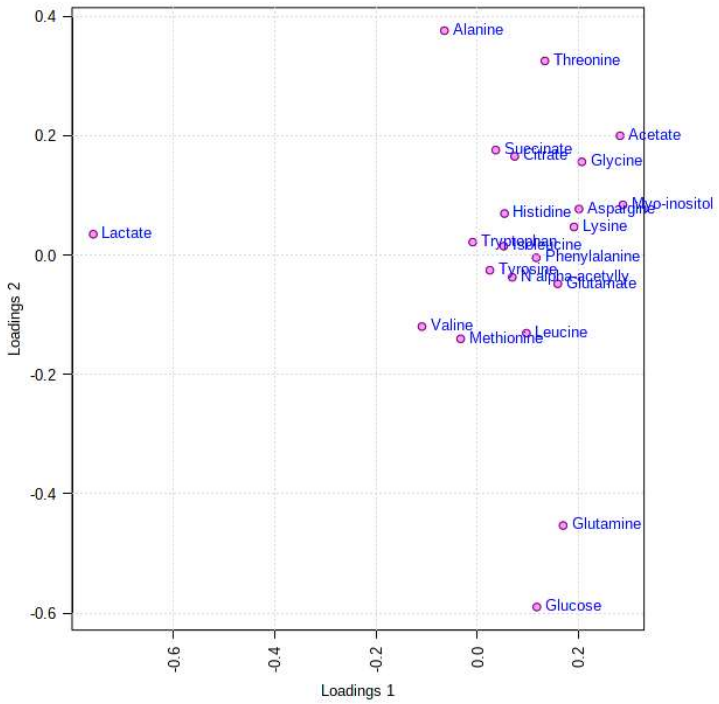

Figure S 56 PCA loading of CACO-2 exometabolites.

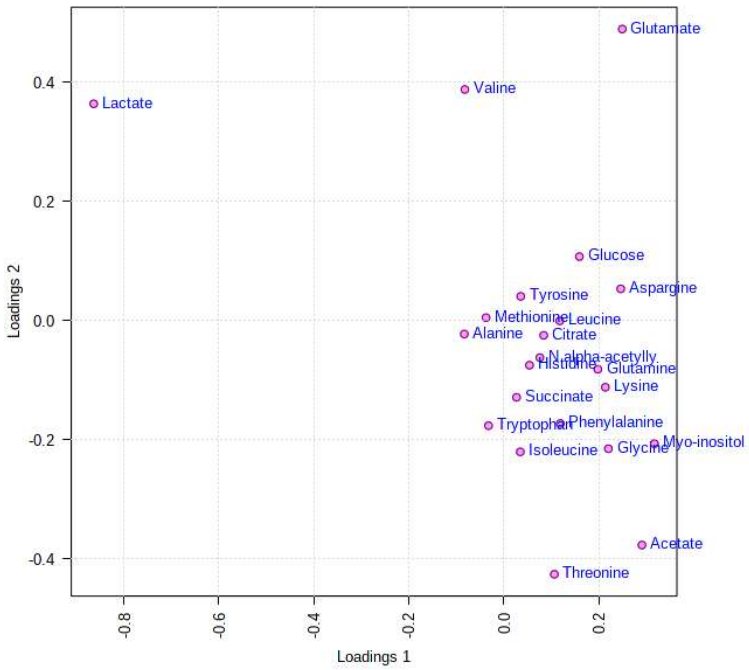

Figure S 57 PLS-DA loading of CACO-2 exometabolites.

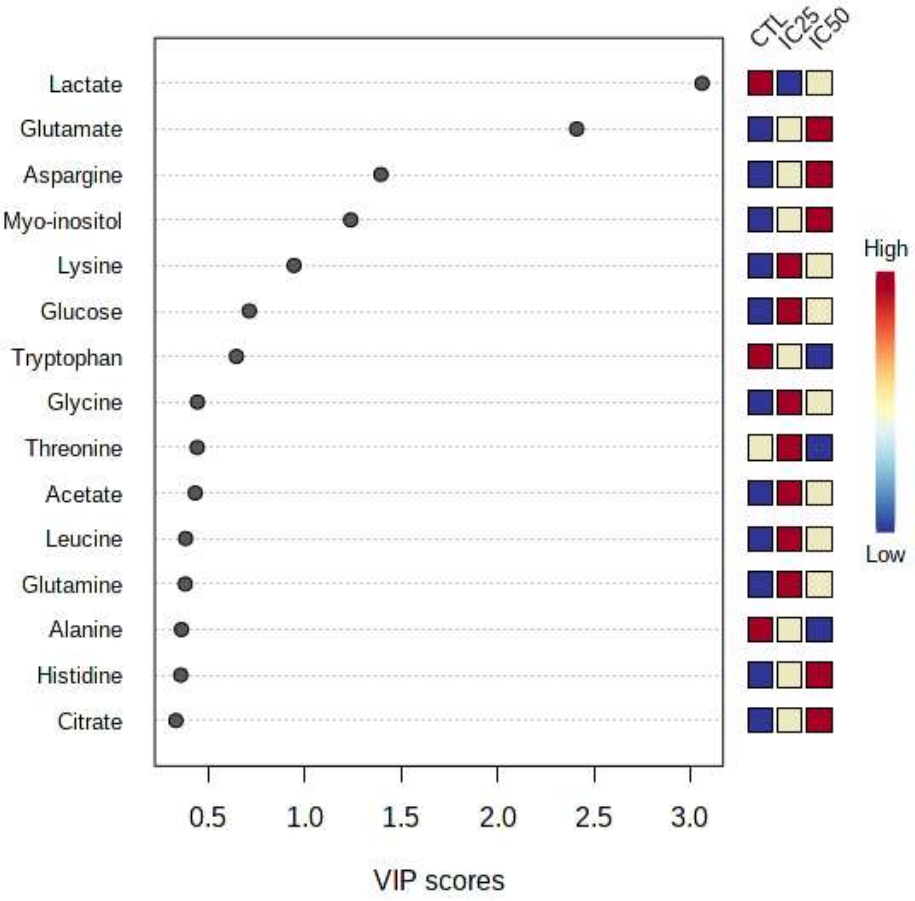

Figure S 58 VIP scores of CACO-2 exometabolites.

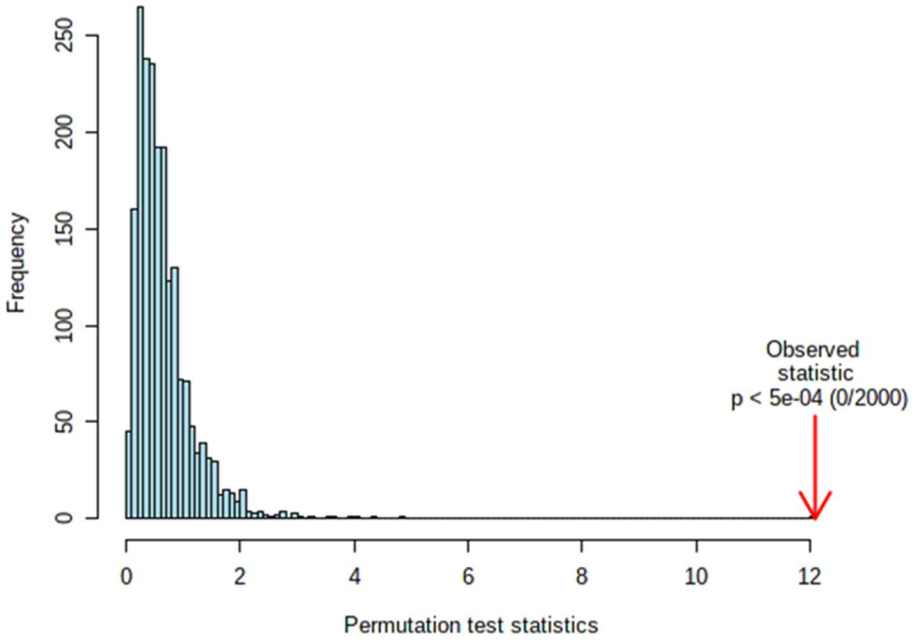

Figure S 59 Model validation by the permutation of CACO-2 exometabolites.

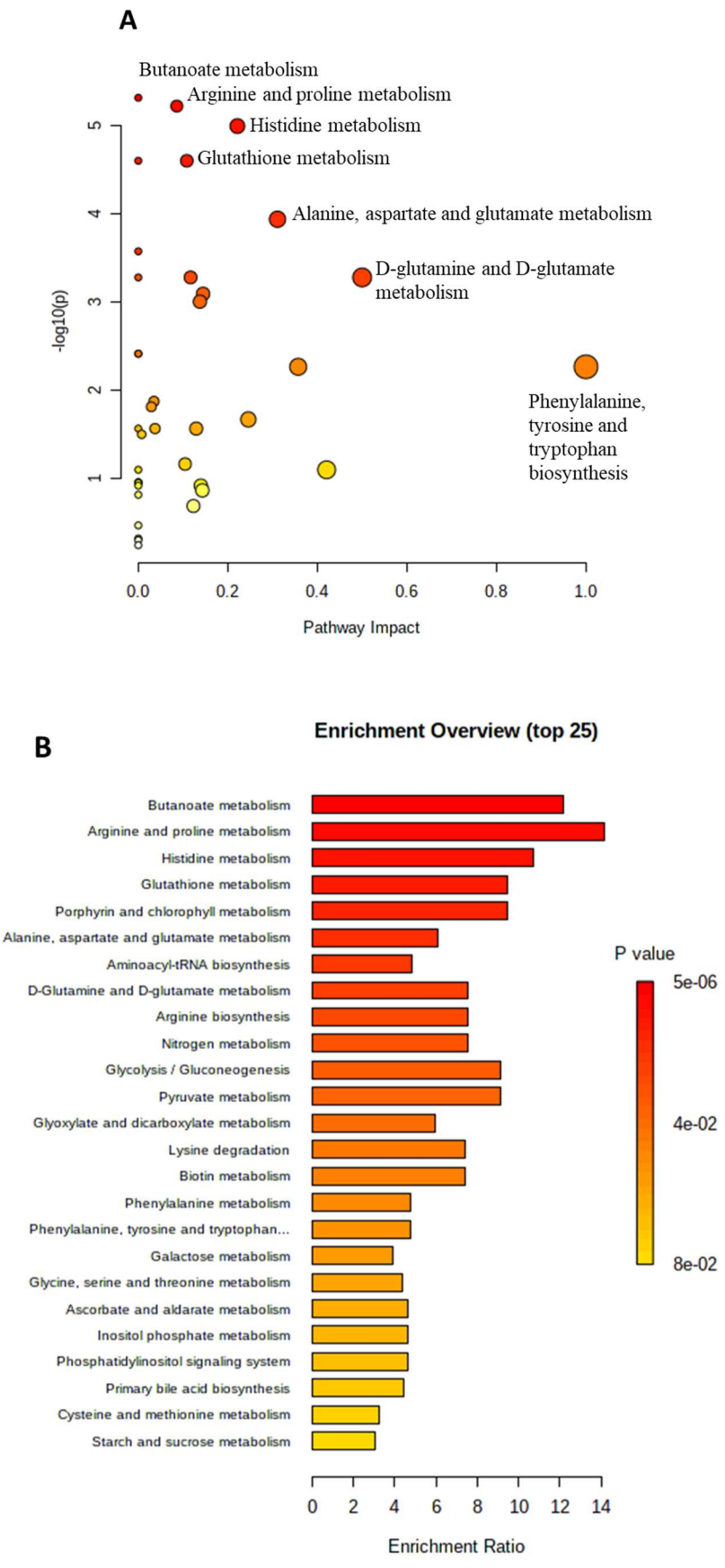

Figure S 60 (A) The metabolome view map and (B) enrichment overview of CACO-2 exometabolites after treatment with IC_{25} of PAMAM G4NH$_2$ using KEGG library.

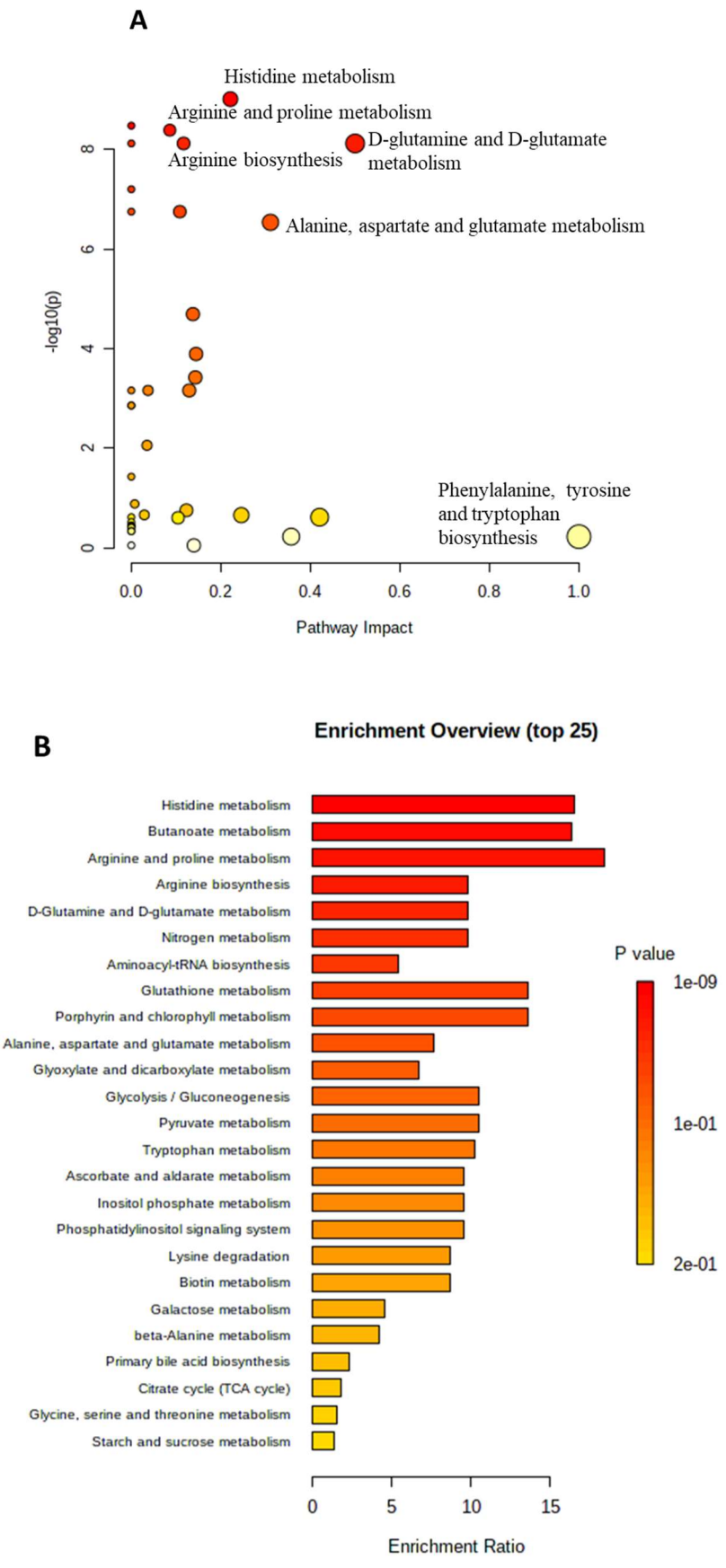

Figure S 61 (A) The metabolome view map and (B) enrichment overview of CACO-2 exometabolites after treatment with IC_{50} of PAMAM G4NH$_2$ using KEGG library.

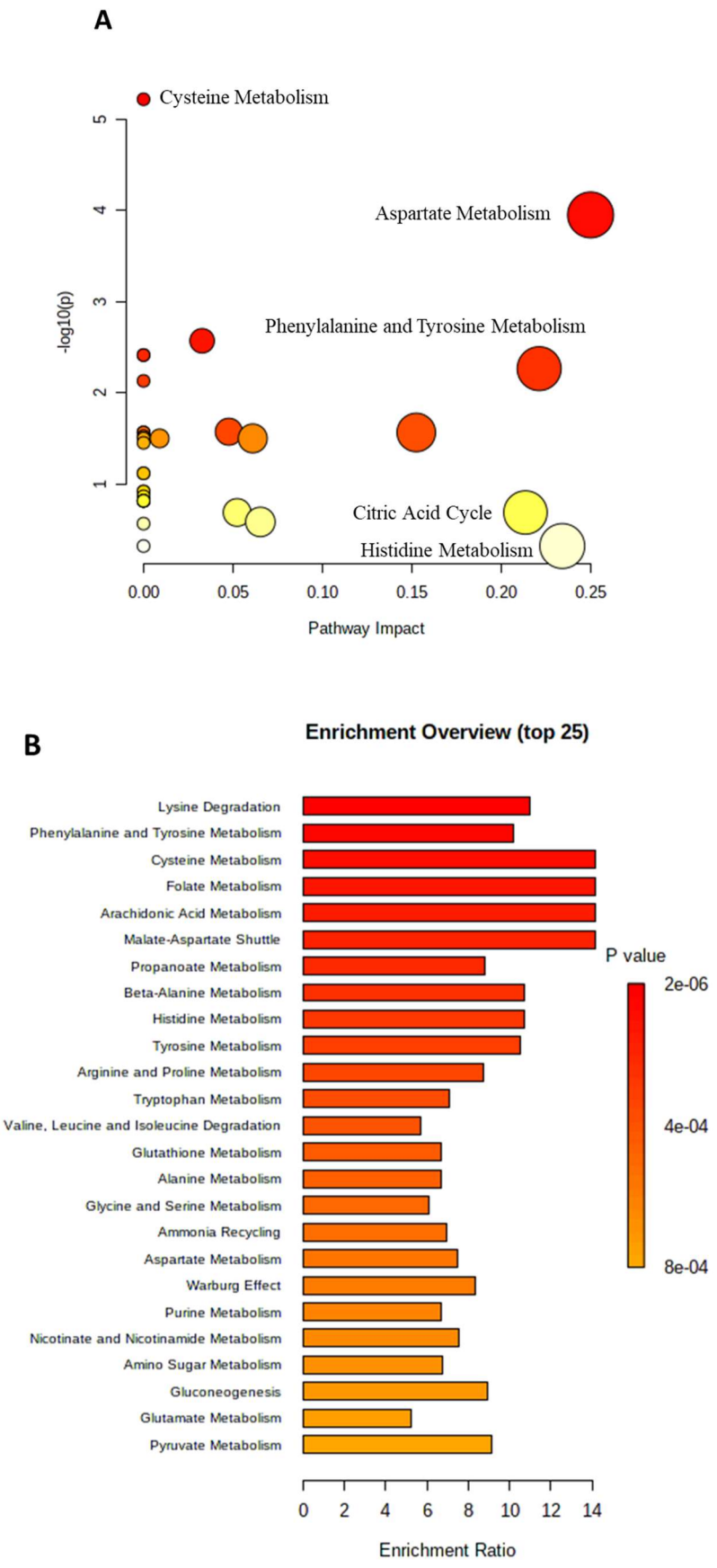

Figure S 62 (A) The metabolome view map and (B) enrichment overview of CACO-2 exometabolites after treatment with IC_{25} of PAMAM G4NH$_2$ using SMPDB library.

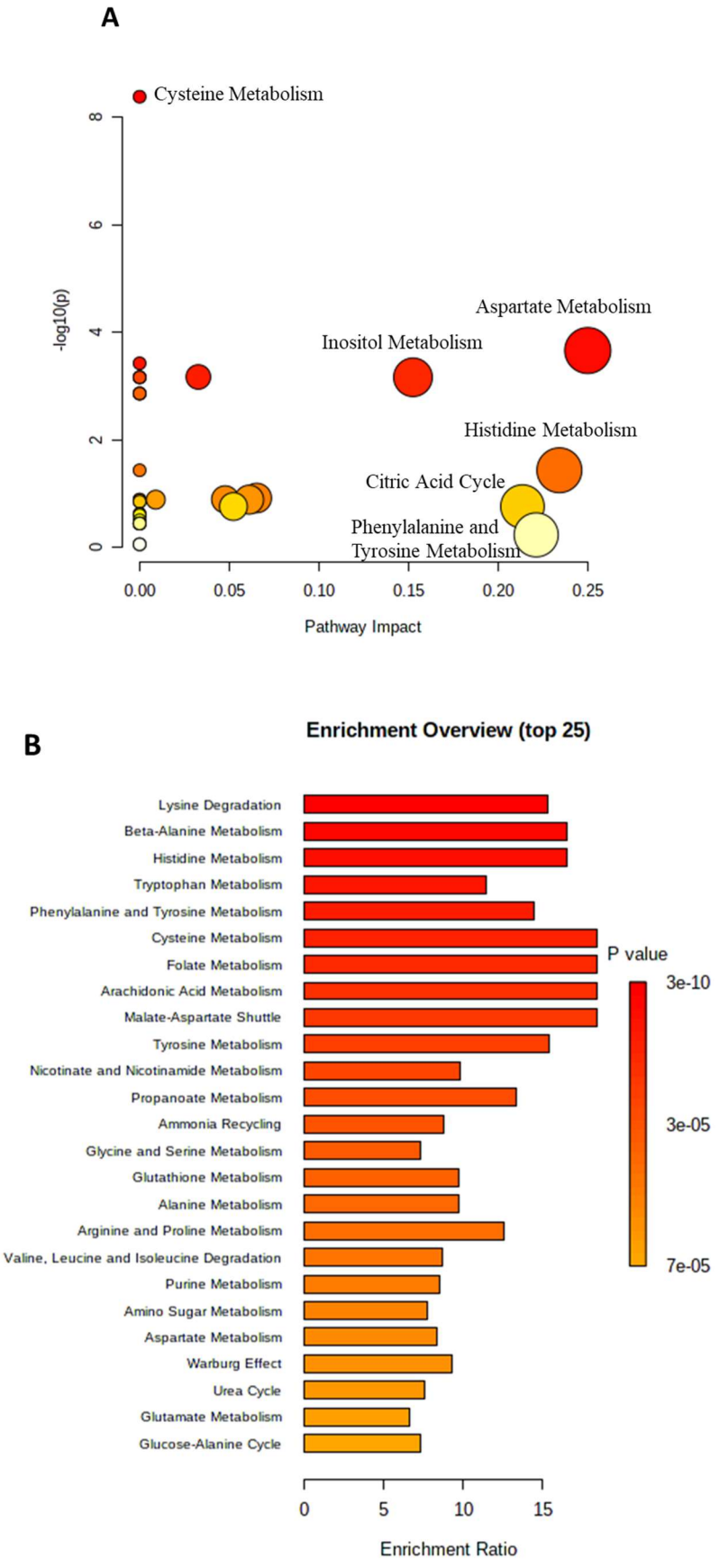

Figure S 63 (A) The metabolome view map and (B) enrichment overview of CACO-2 exometabolites after treatment with IC_{50} of PAMAM G4NH$_2$ using SMPDB library

9. Pathway analysis

Table S 7. Pathway analysis using KEGG library.

		IC_{25}		IC_{50}	
		Pathway	Enrichment	Pathway	Enrichment
CAL-72	Endometabolome	Ubiquinone and other terpenoid-quinone biosynthesis Tyrosine metabolism Starch and sucrose metabolism Phenylalanine metabolism Phenylalanine, tyrosine, and tryptophan biosynthesis	Ubiquinone and other terpenoid-quinone biosynthesis Tyrosine metabolism Galactose metabolism Starch and sucrose metabolism Phenylalanine metabolism	Valine, leucine and isoleucine degradation Starch and sucrose metabolism Phenylalanine metabolism Phenylalanine, tyrosine, and tryptophan biosynthesis	Valine, leucine and isoleucine degradation Neomicyn, kanamycin and gentamicin biosynthesis Galactose metabolism Starch and sucrose metabolism Phenylalanine metabolism
	Exometabolome	Aminoacyl-tRNA biosynthesis Pyruvate metabolism Starch and sucrose metabolism Phenylalanine metabolism Phenylalanine, tyrosine and tryptophan biosynthesis	Aminoacyl-tRNA biosynthesis Glycolysis/Gluconeogenesis Pyruvate metabolism Valine, leucine and isoleucine biosynthesis Galactose metabolism	Aminoacyl-tRNA biosynthesis Pyruvate metabolism Starch and sucrose metabolism Phenylalanine metabolism Phenylalanine, tyrosine and tryptophan biosynthesis	Aminoacyl-tRNA biosynthesis Glycolysis/Gluconeogenesis Pyruvate metabolism Valine, leucine and isoleucine degradation Valine, leucine and isoleucine biosynthesis
A2780	Endometabolome	Propanoate metabolism Glutathione metabolism Inositol phosphate metabolism Alanine, aspartate and glutamate metabolism D-glutamine and D-glutamate metabolism Phenylalanine, tyrosine and tryptophan biosynthesis	Propanoate metabolism Glutathione metabolism Porphyrin and chlorophyll metabolism Aminoacyl-tRNA biosynthesis Selenocompound metabolism	Selenocompound metabolism Arginine and proline metabolism Inositol phosphate metabolism Alanine, aspartate and glutamate metabolism Arginine biosynthesis D-glutamine and D-glutamate metabolism Phenylalanine metabolism Phenylalanine, tyrosine and tryptophan biosynthesis	Selenocompound metabolism Arginine and proline metabolism Galactose metabolism Butanoate metabolism Histidine metabolism
	Exometabolome	Glyoxylate and dicarboxylate metabolism Pyruvate metabolism D-glutamine and D-glutamate metabolism Alanine, aspartate and glutamate metabolism Starch and sucrose metabolism Phenylalanine, tyrosine and	Glyoxylate and dicarboxylate metabolism Glycolysis/gluconeogenesis Pyruvate metabolism D-glutamine and D-glutamate metabolism Nitrogen metabolism	Neomycin, kanamycin and gentamicin biosynthesis Galactose metabolism Starch and sucrose metabolism Glyoxylate and dicarboxylate metabolism D-glutamine and D-glutamate metabolism	Galactose metabolism Starch and sucrose metabolism Neomycin, kanamycin and gentamicin biosynthesis Glyoxylate and dicarboxylate metabolism D-glutamine and D-glutamate metabolism

		IC_{25}		IC_{50}	
		Pathway	Enrichment	Pathway	Enrichment
		tryptophan biosynthesis		Alanine, aspartate and glutamate metabolism Phenylalanine, tyrosine and tryptophan biosynthesis	
NIH 3T3	Endometabolome	Alanine, aspartate and glutamate metabolism Taurine and hypotaurine metabolism Selenocompound metabolism D-glutamine and D-glutamate metabolism Phenylalanine, tyrosine and tryptophan biosynthesis	Alanine, aspartate and glutamate metabolism Taurine and hypotaurine metabolism Selenocompound metabolism Aminoacyl-tRNA biosynthesis Valine, leucine and isoleucine biosynthesis	Selenocompound metabolism Alanine, aspartate and glutamate metabolism Phenylalanine, tyrosine and tryptophan biosynthesis	Selenocompound metabolism Alanine, aspartate and glutamate metabolism Aminoacyl-tRNA biosynthesis Pyruvate metabolism Glycolysis/gluconeogenesis
	Exometabolome	Biotin metabolism Lysine degradation Phenylalanine, tyrosine and tryptophan biosynthesis	Biotin metabolism Lysine degradation Aminoacyl-tRNA biosynthesis Propanoate metabolism Butanoate metabolism	Biotin metabolism Lysine degradation Phenylalanine, tyrosine and tryptophan biosynthesis	Biotin metabolism Lysine degradation Aminoacyl-tRNA biosynthesis Citrate cycle (TCA cycle) Cysteine and methionine metabolism
CACO-2	Endometabolome	Glycine, serine and threonine metabolism Phenylalanine, tyrosine and tryptophan biosynthesis	Glycine, serine and threonine metabolism Valine, leucine and isoleucine biosynthesis Aminoacyl-tRNA biosynthesis Primary bile acid biosynthesis Purine metabolism	Glycine, serine and threonine metabolism Taurine and hypotaurine metabolism Phenylalanine, tyrosine and tryptophan biosynthesis	Glycine, serine and threonine metabolism Ether lipid metabolism Valine, leucine and isoleucine biosynthesis Glycolysis/gluconeogenesis Pyruvate metabolism
	Exometabolome	Butanoate metabolism Arginine and proline metabolism Histidine metabolism Glutathione metabolism Alanine, aspartate and glutamate metabolism D-glutamine and D-glutamate metabolism Phenylalanine, tyrosine and tryptophan biosynthesis	Butanoate metabolism Arginine and proline metabolism Histidine metabolism Glutathione metabolism Porphyrin and chlorophyll metabolism	Histidine metabolism Arginine and proline metabolism D-glutamine and D-glutamate metabolism Arginine biosynthesis Alanine, aspartate and glutamate metabolism Phenylalanine, tyrosine and tryptophan biosynthesis	Histidine metabolism Butanoate metabolism Arginine and proline metabolism Arginine biosynthesis D-glutamine and D-glutamate metabolism

Table S 8. Pathway analysis using SMPDB library.

		IC_{25}		IC_{50}	
		Pathway	Enrichment	Pathway	Enrichment
CAL-72	Endometabolome	Catecholamine Biosynthesis Phenylalanine and Tyrosine Metabolism Nucleotide Sugars Metabolism Beta-Alanine Metabolism Aspartate Metabolism	Catecholamine Biosynthesis Thyroid hormone synthesis Transfer of acetyl groups into mitochondria Glycolysis Lactose degradation	Valine, Leucine, and Isoleucine Degradation Phenylalanine and Tyrosine Metabolism Beta-Alanine Metabolism Aspartate Metabolism Nucleotide Sugars Metabolism	Transfer of acetyl groups into mitochondria Sphingolipid metabolism Glycolysis Lactose degradation Galactose degradation
	Exometabolome	Threonine and 2-Oxobutanoate Degradation Phenylalanine and Tyrosine Metabolism Histidine Metabolism	Threonine and 2-Oxobutanoate Degradation Pyruvate Metabolism Gluconeogenesis Warburg Effect Glucose-alanine cycle	Valine, Leucine and Isoleucine Degradation Phenylalanine and Tyrosine Metabolism Histidine Metabolism	Pyruvate Metabolism Warburg Effect Valine, Leucine and Isoleucine Degradation Gluconeogenesis Etanhol degradation
A2780	Endometabolome	Porphyrin Metabolism Bile Acid Biosynthesis Inositol Metabolism Beta-Alanine Metabolism Aspartate Metabolism	Methionine Metabolism Threonine and 2-Oxobutanoate Degradation Glycine and Serine metabolism Carnitine Synthesis Porphyrin Metabolism	Cysteine Metabolism inositol Phosphate Metabolism Inositol Metabolism Aspartate Metabolism	Retinol Metabolism Glycine and Serine metabolism Threonine and 2-Oxobutanoate Degradation Gluconeogenesis Pyruvate Metabolism
	Exometabolome	Cysteine Metabolism Aspartate Metabolism Phenylalanine and Tyrosine Metabolism	Ammonia Recycling Purine Metabolism Aspartate Metabolism Pyruvate Metabolism Warburg effect	Cysteine Metabolism Aspartate Metabolism	Glucose-Alanine Cycle Sphingolipid Metabolism Glycolysis Galactose Metabolism Lactose Synthesis
NIH 3T3	Endometabolome	Bile Acid Biosynthesis Nucleotide Sugars Metabolism Aspartate Metabolism	Glucose-alanine cycle Taurine and Hypotaurine metabolism Tryptophan metabolism Urea Cycle Selenoamino Acid Metabolism	Porphyrin Metabolism Bile Acid Biosynthesis Glutathione Metabolism Nucleotide Sugars Metabolism Aspartate Metabolism	Selenoamino Acid Metabolism Glucose-alanine cycle Urea Cycle Tryptophan metabolism Alanine Metabolism

		IC_{25}		IC_{50}	
		Pathway	Enrichment	Pathway	Enrichment
CACO-2	Exometabolome	Biotin Metabolism Lysine degradation Citric Acid Cycle Phenylalanine and Tyrosine Metabolism Histidine Metabolism	Lysine degradation Biotin Metabolism Carnitine Synthesis Oxidation of branched chain fatty acids Ketone body metabolism	Biotin Metabolism Lysine degradation Citric Acid Cycle Phenylalanine and Tyrosine Metabolism Histidine Metabolism	Lysine degradation Biotin Metabolism Carnitine Synthesis Citric Acid Cycle Betaine metabolism
	Endometabolome	Glycine and Serine Metabolism Glutathione Metabolism Aspartate Metabolism	Methionine Metabolism Threonine and 2-Oxobutanoate Degradation Glycine and Serine metabolism Carnitine Synthesis Porphyrin Metabolism	Retinol Metabolism Aspartate Metabolism	Retinol Metabolism Glycine and Serine metabolism Threonine and 2-Oxobutanoate Degradation Gluconeogenesis Pyruvate Metabolism
	Exometabolome	Cysteine Metabolism Aspartate Metabolism Phenylalanine and Tyrosine Metabolism Citric Acid Cycle Histidine Metabolism	Lysine degradation Phenylalanine and Tyrosine Metabolism Cysteine Metabolism Folate Metabolism Arachidonic acid Metabolism	Cysteine Metabolism Aspartate Metabolism Inositol Metabolism Histidine Metabolism Citric Acid Cycle Phenylalanine and Tyrosine Metabolism	Lysine degradation Beta-Alanine Metabolism Histidine Metabolism Tryptophan metabolism Phenylalanine and Tyrosine Metabolism

Chapter 4. CATDEN cinnamic acid terminated dendrimers

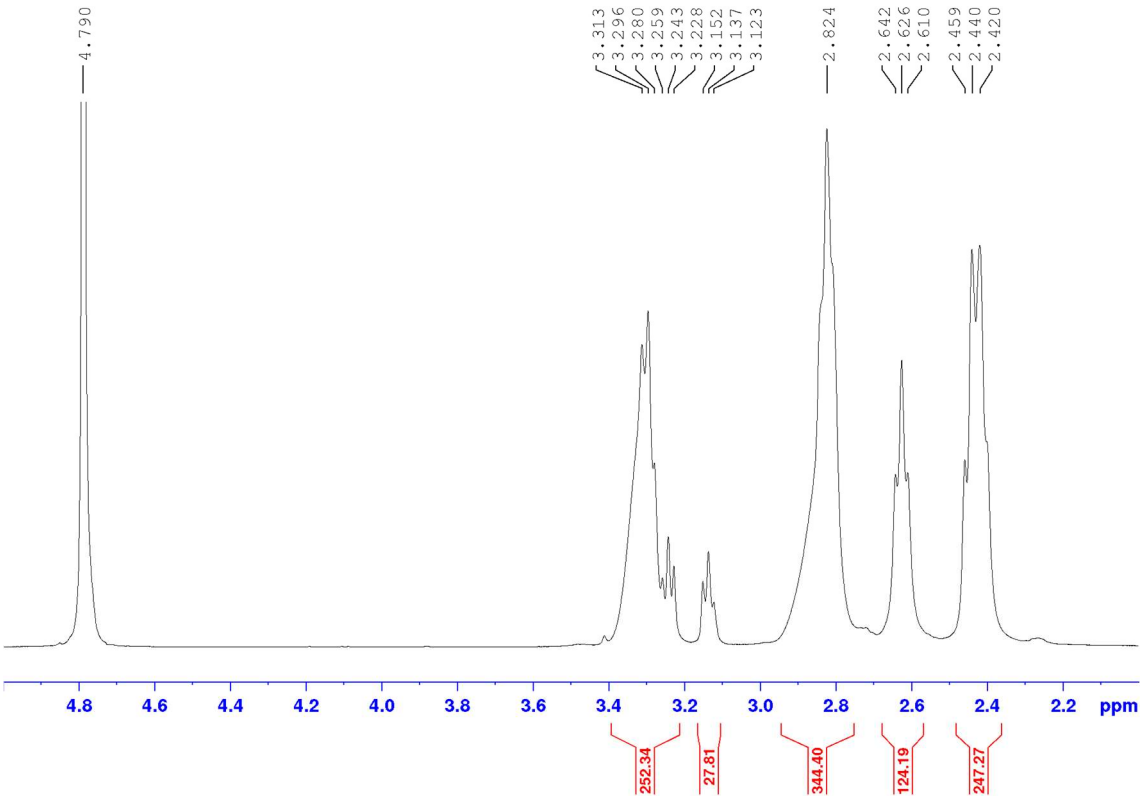

Figure S 64 ^{1}H NMR of PAMAM G4NH$_2$ in D$_2$O.

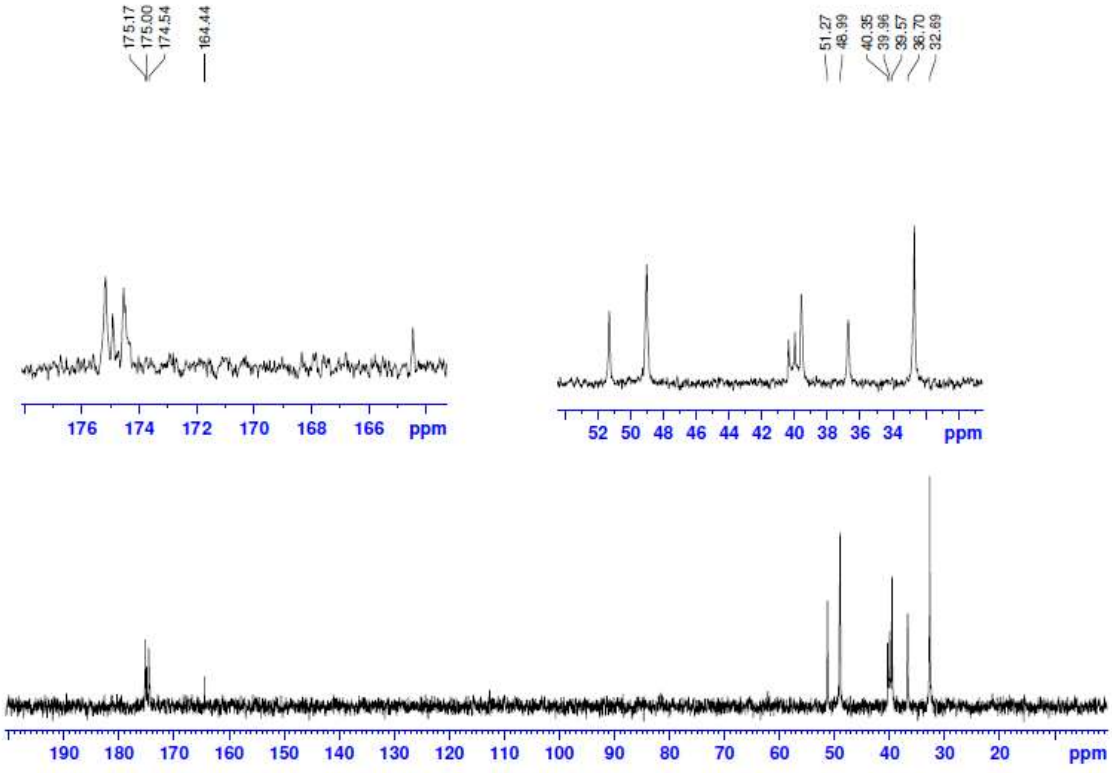

Figure S 65 ^{13}C NMR of G4NH2 in D$_2$O.

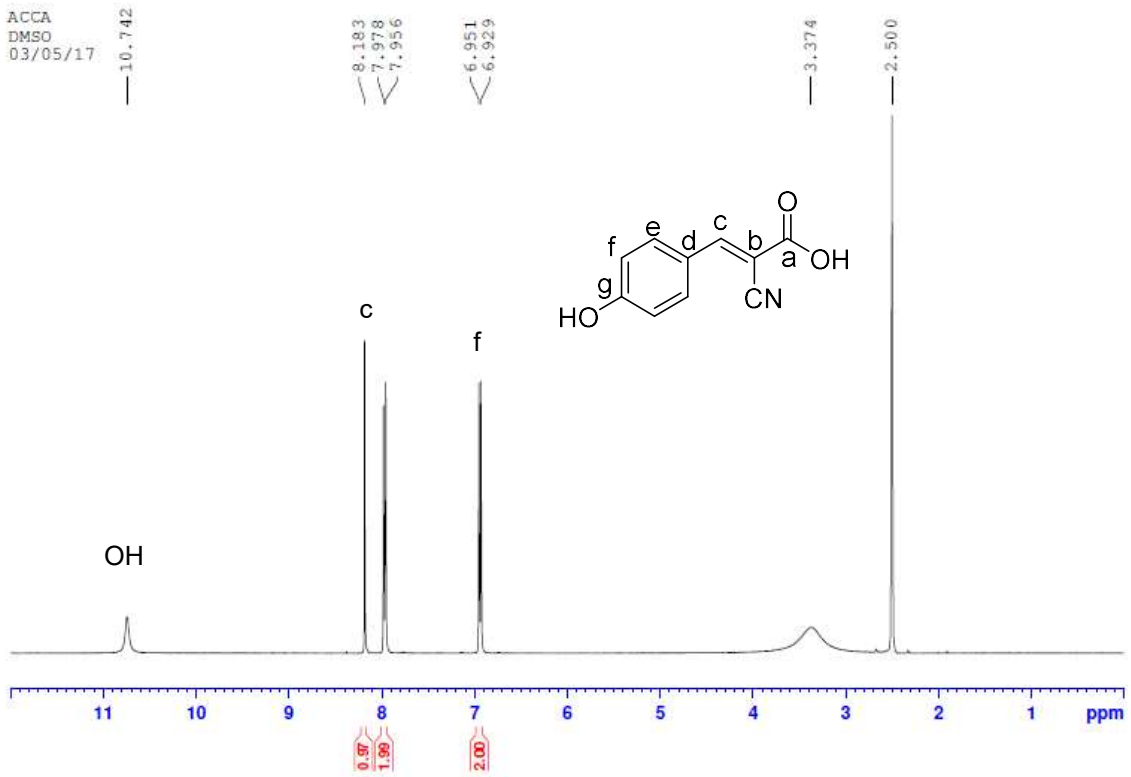

Figure S 66 [1]H NMR of ACCA in DMSO.

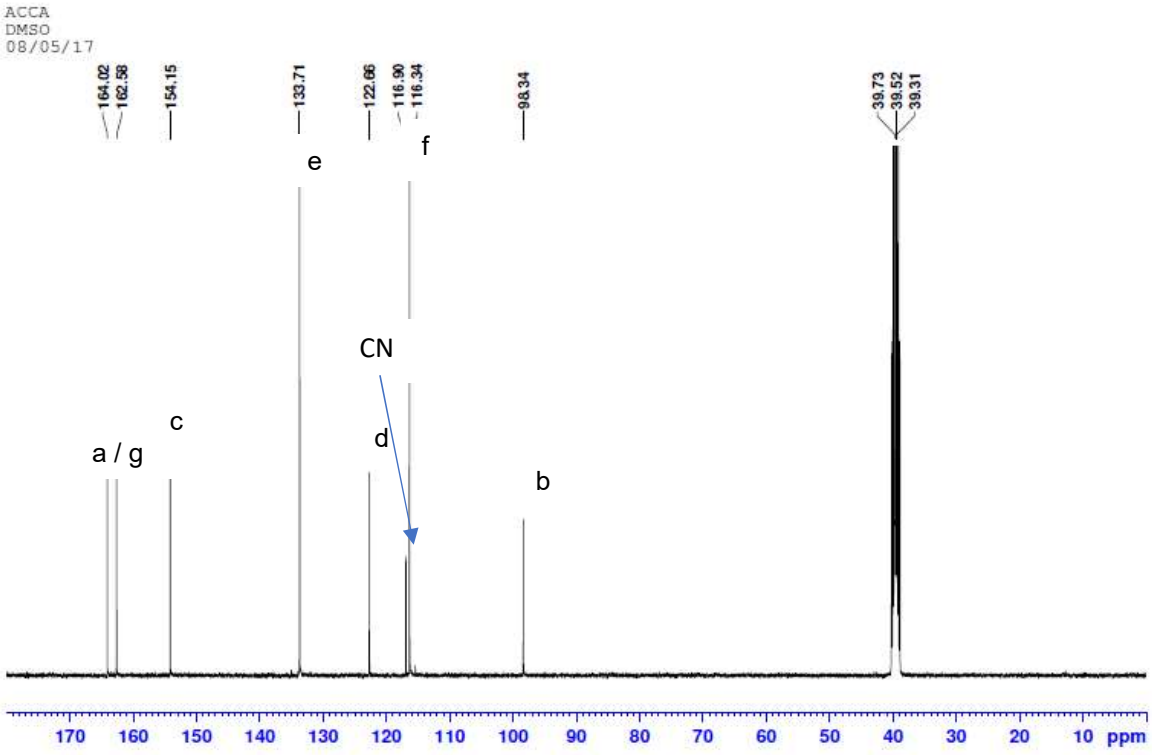

Figure S 67 [13]C NMR of ACCA in DMSO.

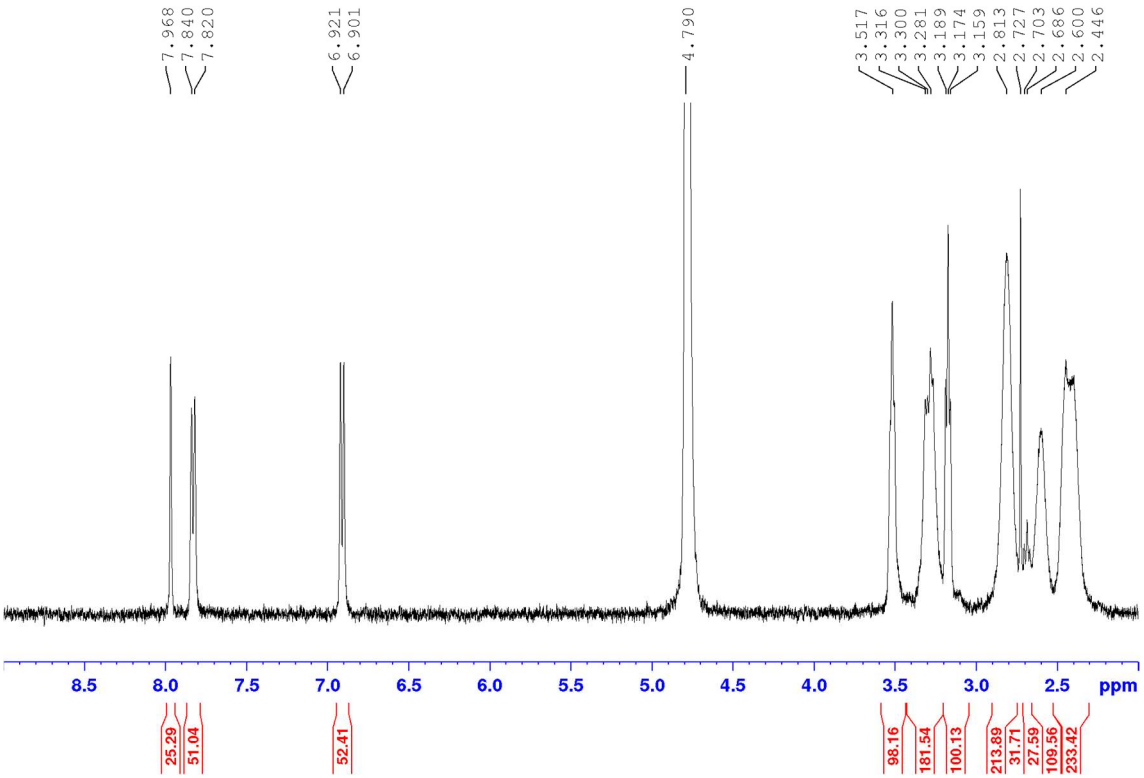

Figure S 68 ^{1}H NMR of PAMAM G4NH$_2$-25ACCA in D$_2$O.

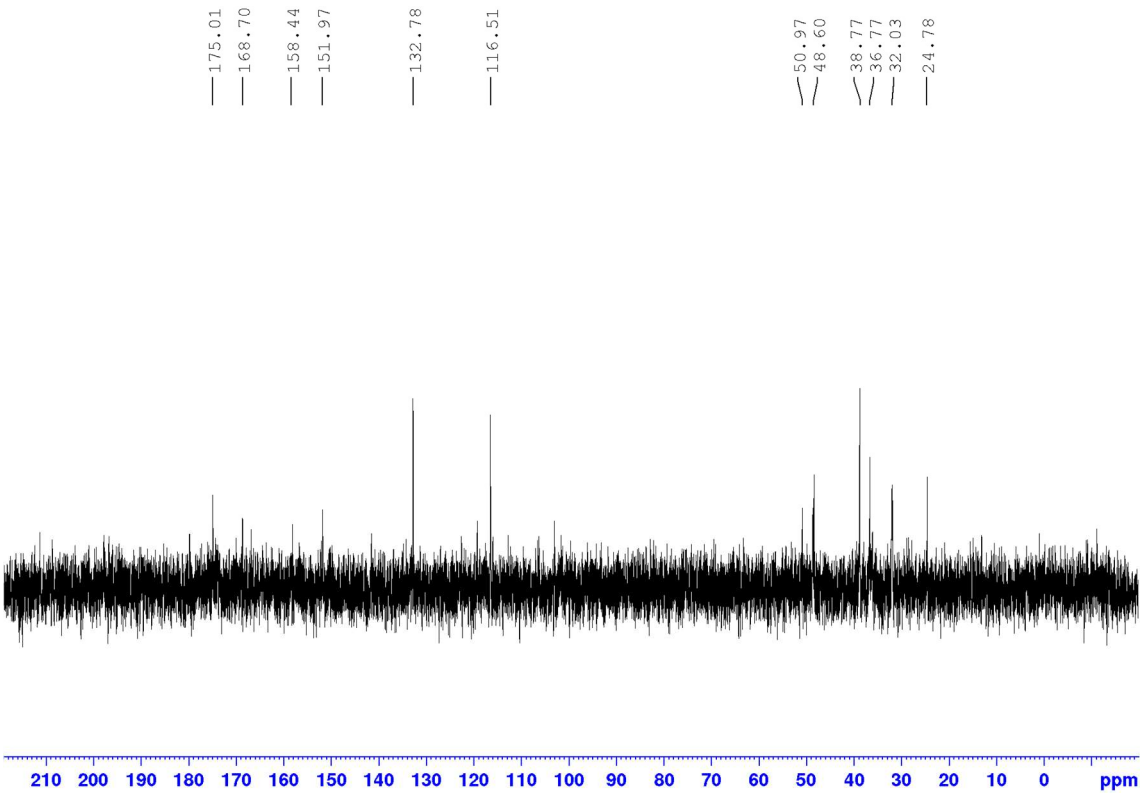

Figure S 69 ^{13}C NMR of PAMAM G4NH$_2$-25ACCA in D$_2$O.

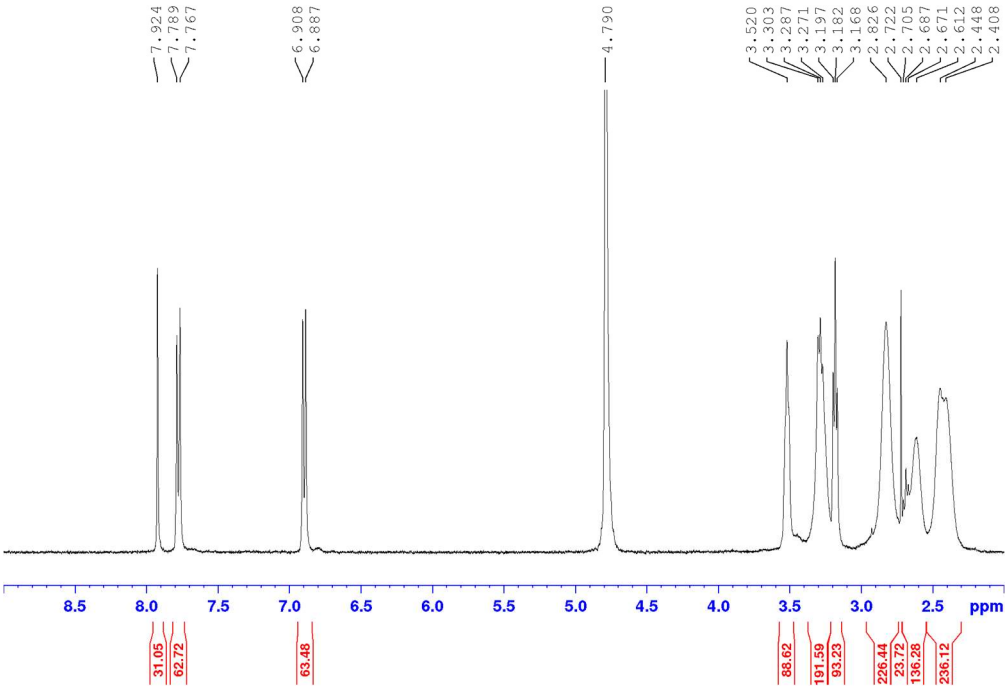

Figure S 70 ^{1}H NMR of G4NH₂-32ACCA in D_2O.

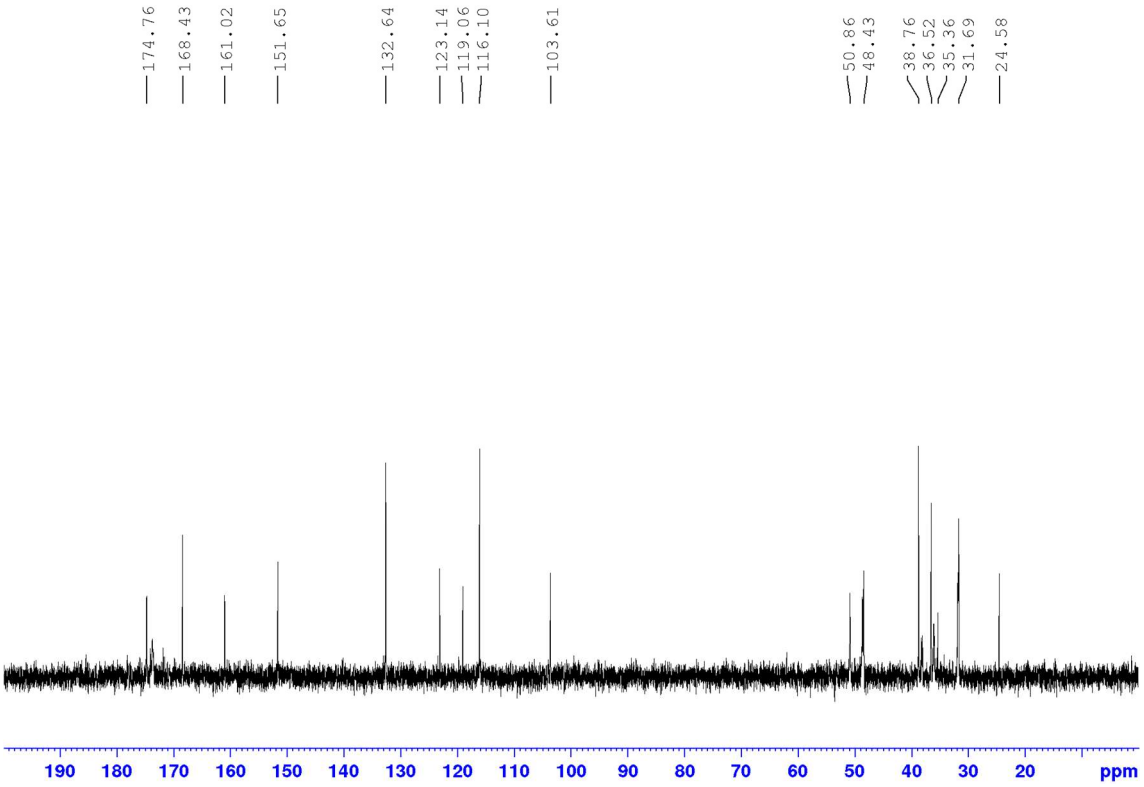

Figure S 71 ^{13}C NMR of PAMAM G4NH₂-32ACCA in D_2O.

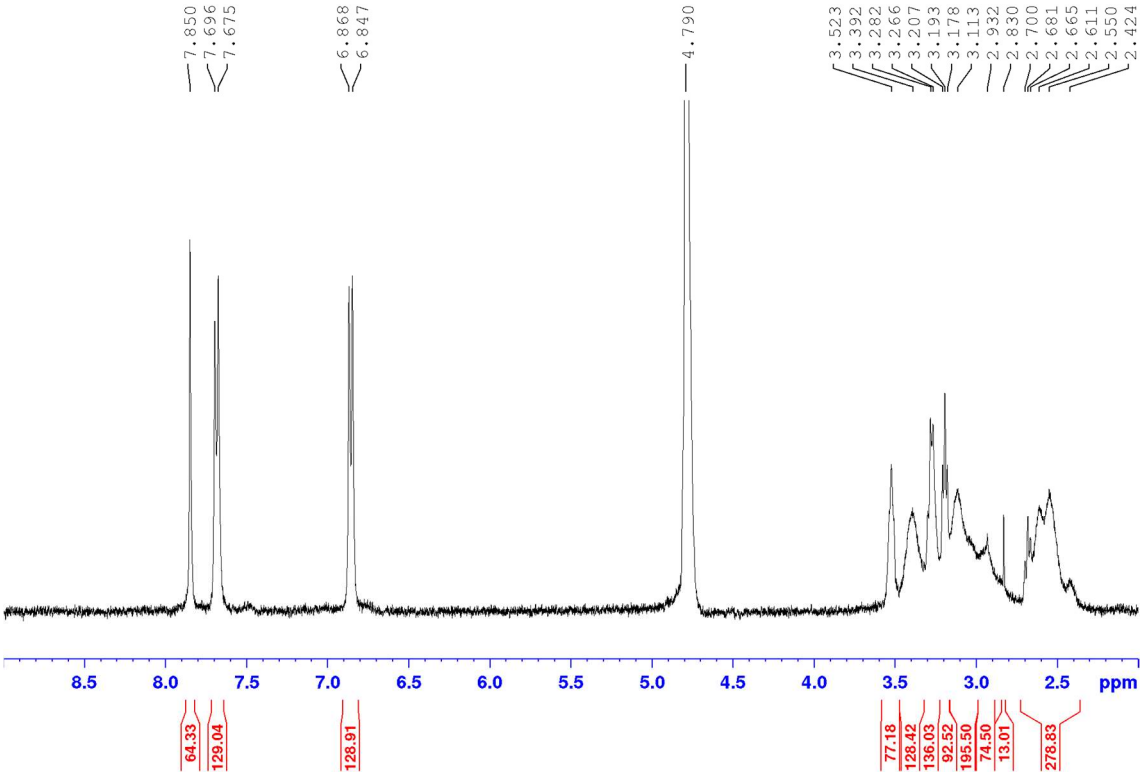

Figure S 72 ^{1}H NMR of G4NH$_2$-64ACCA in D$_2$O.

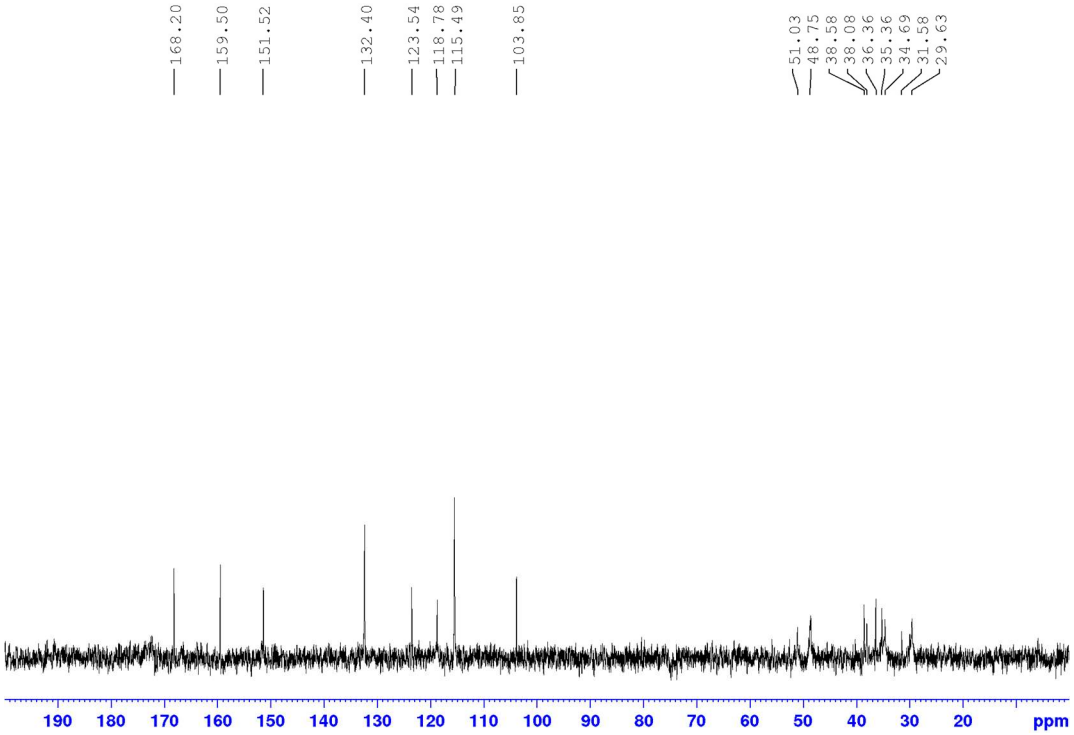

Figure S 73 ^{13}C NMR of PAMAM G4NH$_2$-64ACCA in D$_2$O.

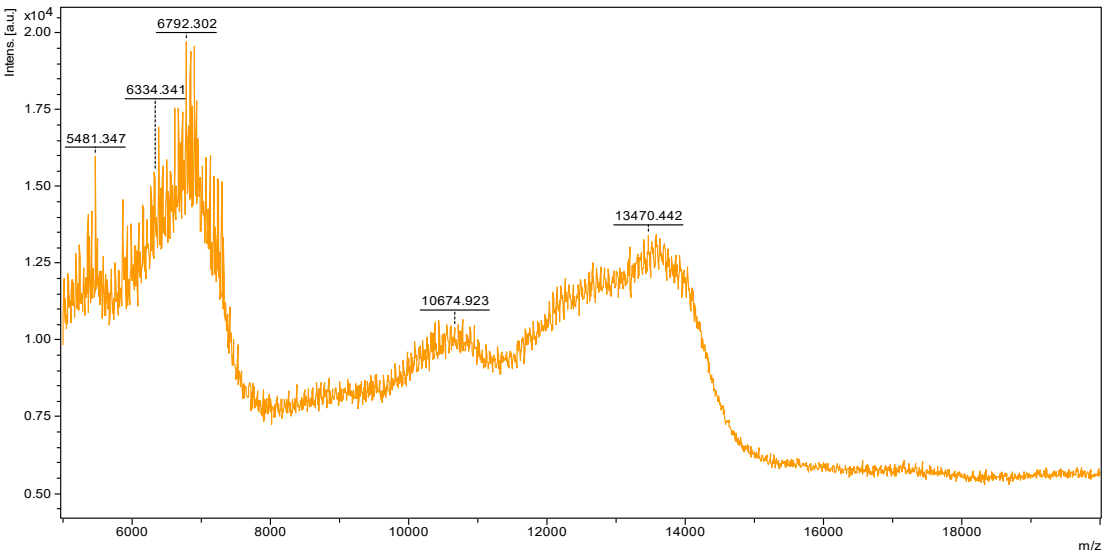

Figure S 74 MALDI-TOF of PAMAM G4NH2.

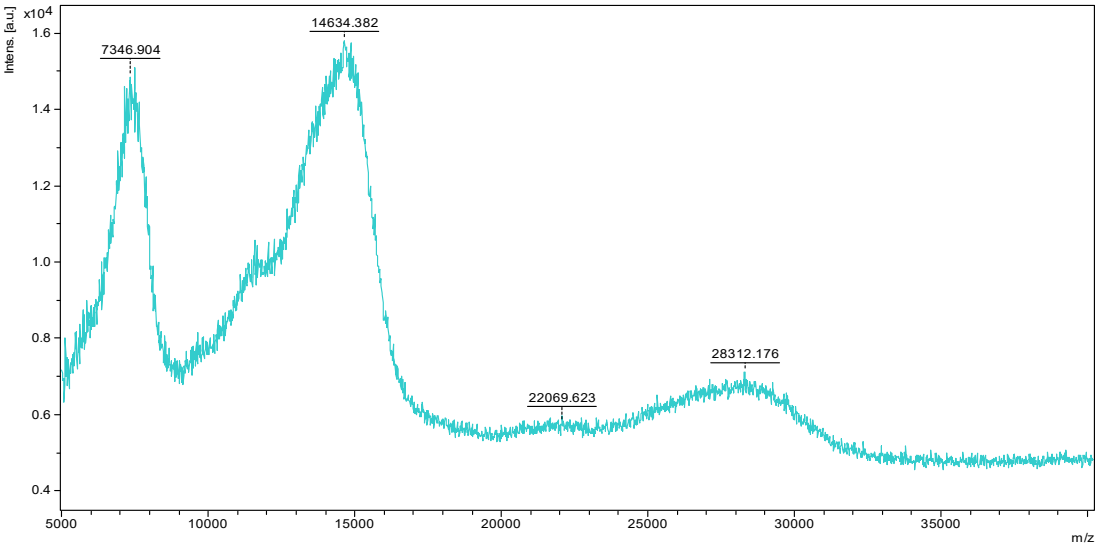

Figure S 75 MALDI-TOF of PAMAM G4NH$_2$-25ACCA.

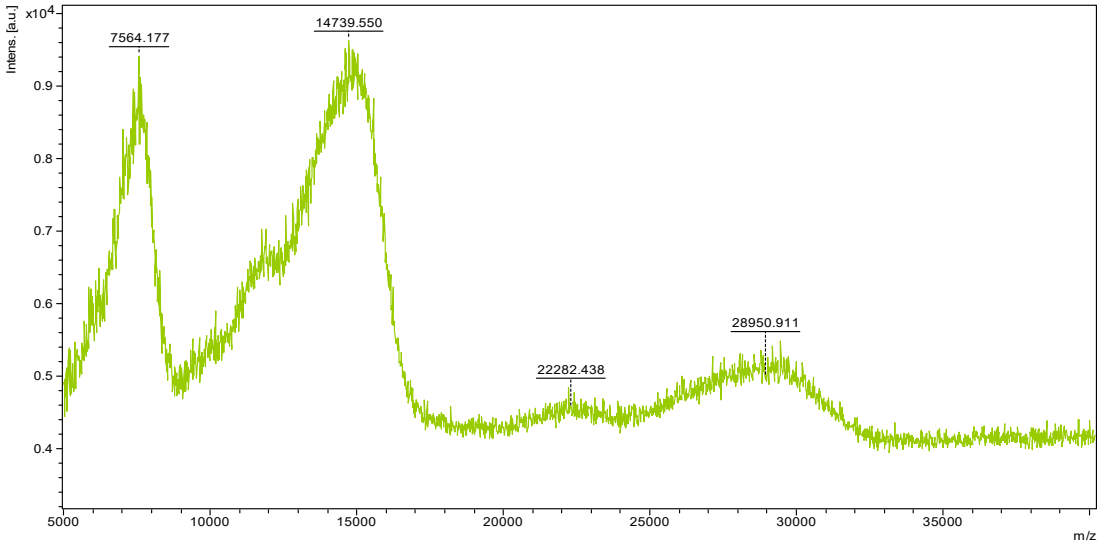

Figure S 76 MALDI-TOF of PAMAM G4NH$_2$-32ACCA.

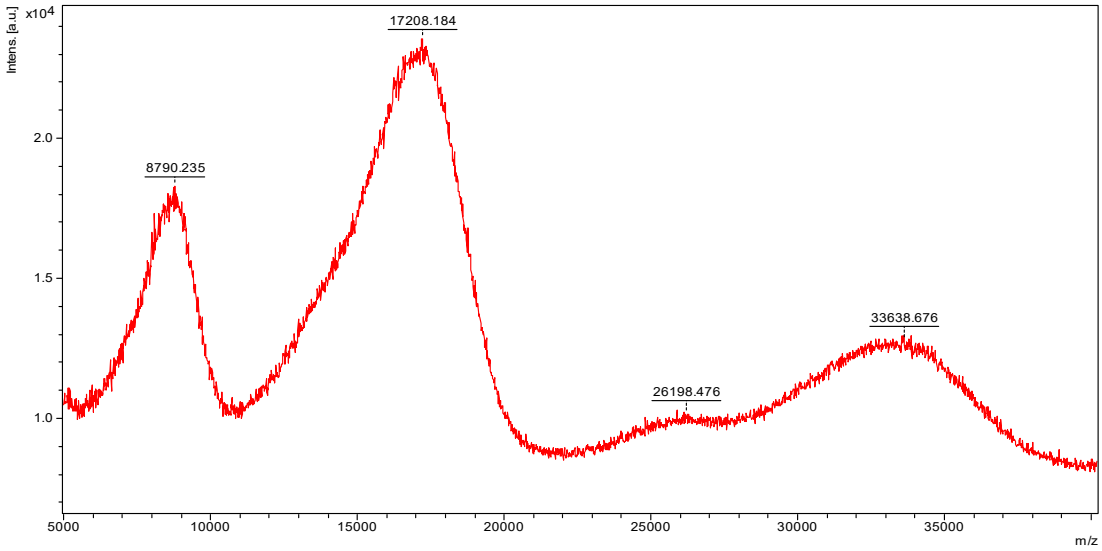

Figure S 77 MALDI-TOF of PAMAM G4NH$_2$-48ACCA.

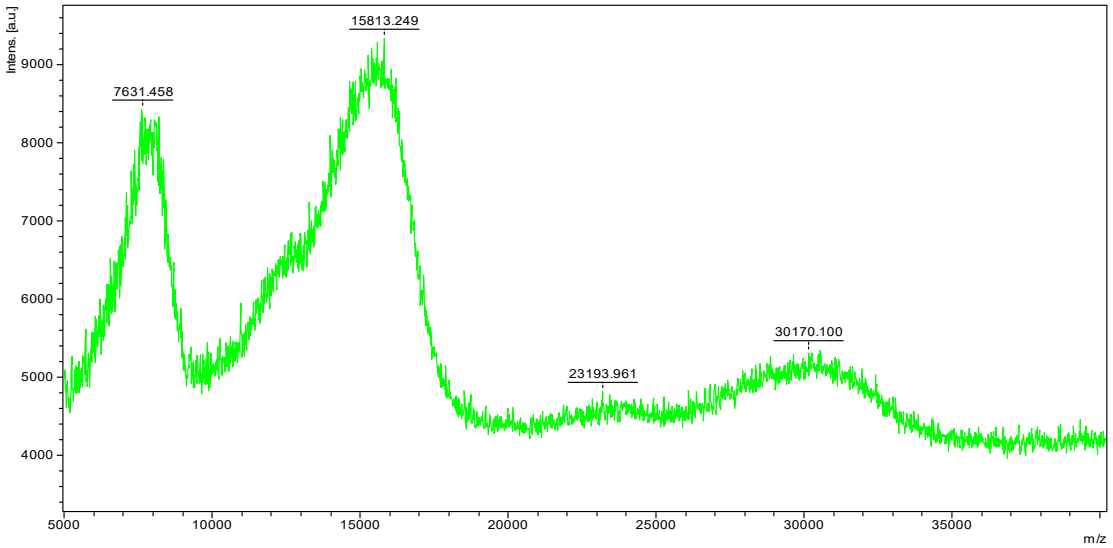

Figure S 78 MALDI-TOF of PAMAM G4NH$_2$-64ACCA.

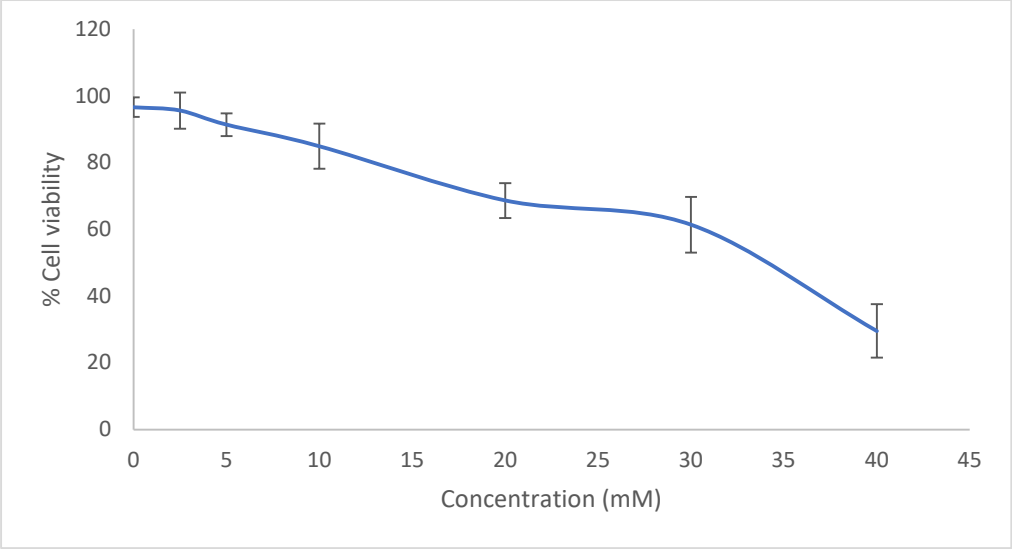

Figure S 79 Cell viability of commercial ACCA in CA-72 cell line.

Chapter 5. ^{1}H NMR metabolomics of CATDEN

Table S 9. Main endometabolite variations in cell culture media of CAL-72, exposed to IC_{25} and IC_{50} of PAMAM G4NH2-48ACCA in relation to the control cells medium, expressed as percentage of of variation.

		IC_{25}	IC_{50}
Leucine	%Var	8.37	17.53
	±	12.98	11.45
Valine	%Var	5.68	9.91
	±	10.1	18.32
Isoleucine	%Var	4.48	3.36
	±	16.06	19.46
Lactate	%Var	4.34	8.25
	±	10.03	17.10
Acetoin	%Var	71.42	85.79
	±	164.05	163.35
Alanine	%Var	23.40	17.25
	±	130.09	83.06
Nα-acetyllysine	%Var	21.42	64.32
	±	52.60	60.93
Acetate	%Var	3.71	1.25
	±	22.54	23.58
Glutamate	%Var	0.19	5.88
	±	46.10	43.20
Succinate	%Var	-11.54	-8.34
	±	30.7	23.97
β-Alanine	%Var	83.26	88.55
	±	166.87	137.75
Methionine	%Var	14.95	79.57
	±	31.00	70.39
Dimethylamine	%Var	55.34	69.11
	±	105.78	52.40
Aspartate	%Var	26.24	33.84
	±	20.16	59.00
Creatine	%Var	117.72	155.00
	±	236.56	233.51
Creatine Phosphate	%Var	29.63	3.72
	±	122.24	65.53
1,3- Diaminopropane	%Var	58.10	82.36
	±	80.13	68.82
Choline	%Var	40.07	41.45
	±	109.83	50.18
Acetylcholine	%Var	22.73	20.68
	±	52.67	37.23
Phosphoscholine	%Var	64.82	48.60
	±	126.74	82.22
Glycero phosphocholine	%Var	-38.87	-46.16
	±	24.86	32.45
Taurine	%Var	-12.32	-26.73
	±	37.48	22.61

		IC_{25}	IC_{50}
Glycine	%Var	-9.33	7.88
	±	21.36	26.14
Threonine	%Var	10.93	18.38
	±	77.54	71.15
Glucose	%Var	10.30	-45.86
	±	121.77	45.71
UDP-N-Acetylglucosamine	%Var	40.50	22.43
	±	73.92	55.65
UDP-Glucose	%Var	55.97	28.87
	±	82.17	78.74
UMP	%Var	7.05	-14.79
	±	49.34	17.91
ATP	%Var	38.10	57.12
	±	58.45	105.57
AMP	%Var	9.54	26.91
	±	49.21	91.01
Fumarate	%Var	100.89	31.39
	±	190.77	113.71
Tyrosine	%Var	8.34	18.08
	±	5.23	13.03
Phenylalanine	%Var	11.50	16.30
	±	5.83	21.87
NADP+	%Var	86.00	66.60
	±	133.24	90.96

Table S 10. Main exometabolite variations in cell culture media of CAL-72, exposed to IC_{25} and IC_{50} of PAMAM G4NH2-48ACCA in relation to the control cells medium, expressed as percentage of variation.

		IC_{25}	IC_{50}
Leucine	%Var	-6.36	-19.38
	±	24.06	20.40
Valine	%Var	-2.80	-8.60
	±	18.72	13.47
Isoleucine	%Var	-5.06	-9.31
	±	18.85	20.89
Lactate	%Var	15.47	27.90
	±	29.73	23.67
Alanine	%Var	-17.18	-19.07
	±	27.13	24.83
N alpha-acetyllysine	%Var	-1.08	-13.34
	±	38.61	30.31
Acetate	%Var	-10.71	-29.53
	±	22.11	12.14
Lysine	%Var	-9.52	-12.49
	±	20.31	15.71
Glutamine	%Var	-12.83	-16.55
	±	17.14	17.37
Succinate	%Var	-9.95	-19.09
	±	16.29	5.85
Methionine	%Var	-1.40	-27.74
	±	41.42	21.17
Glucose	%Var	-15.46	-30.16
	±	25.61	25.45
Glycine	%Var	3.02	-12.24
	±	60.85	32.27
Threonine	%Var	-1.81	-15.25
	±	26.79	14.00
Tyrosine	%Var	-6.52	-13.90
	±	18.61	18.35
Histidine	%Var	-5.39	-6.78
	±	23.30	22.22
Phenylalanine	%Var	-7.07	-19.47
	±	24.16	11.72
Tryptophan	%Var	13.90	-6.58
	±	37.28	38.17

1. Endometabolome of CAL-72 treated with G4NH$_2$-48ACCA

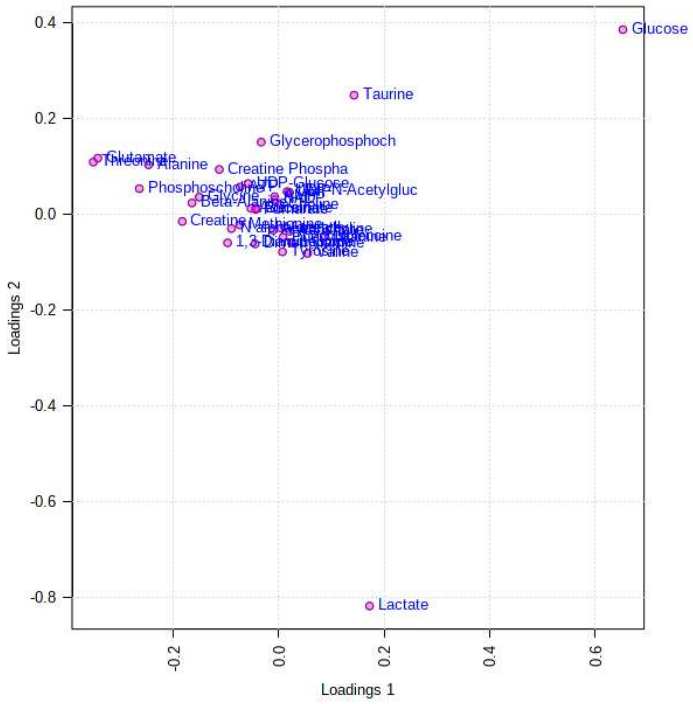

Figure S 80 PCA loading of endometabolome of CAL-72.

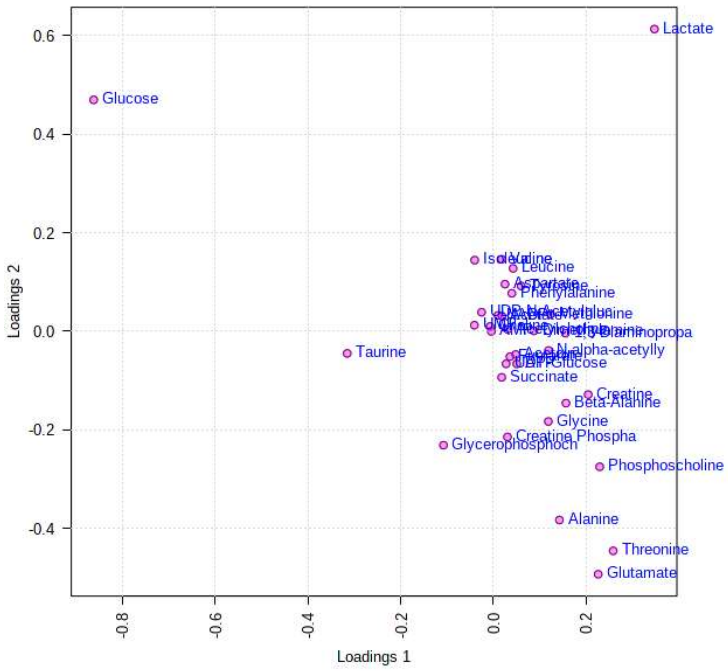

Figure S 81 PLS-DA loading of endometabolome of CAL-72.

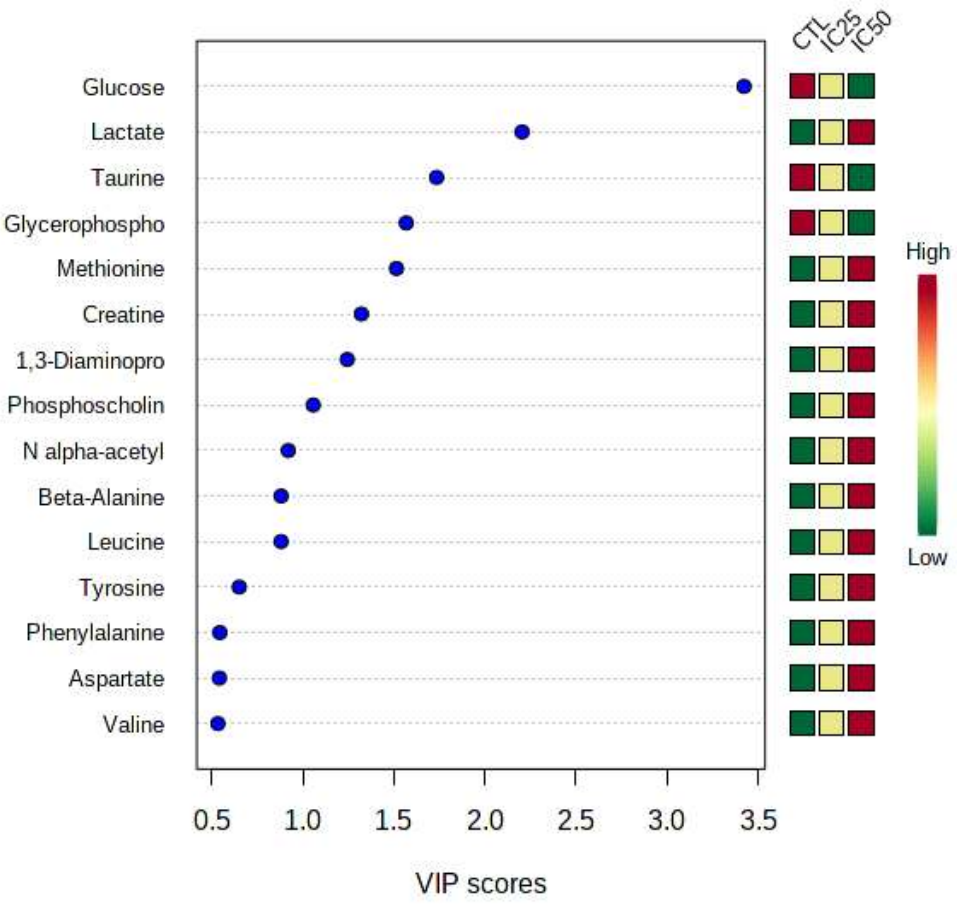

Figure S 82 VIP scores of endometabolome of CAL-72.

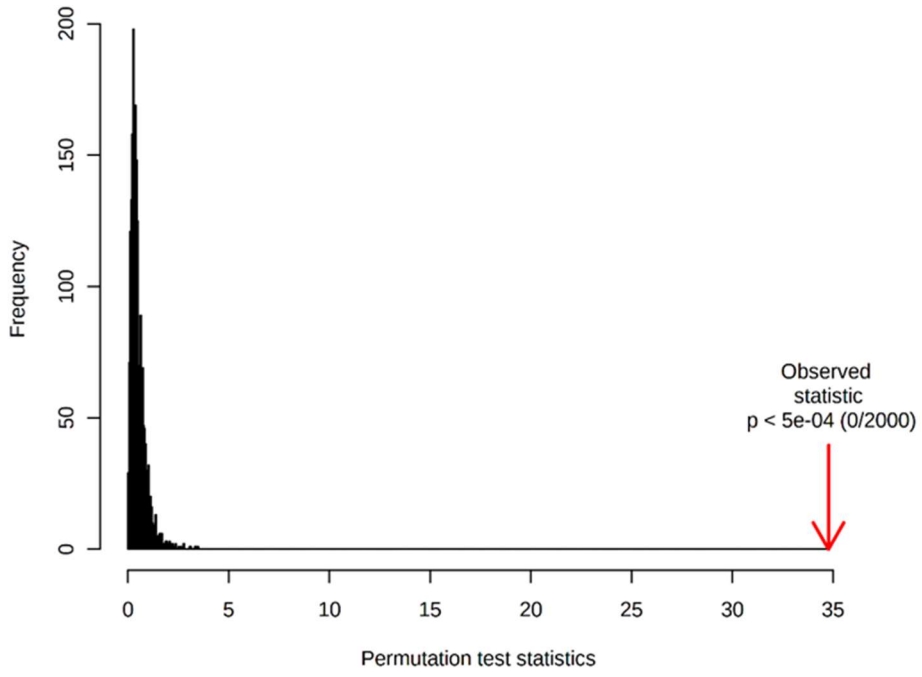

Figure S 83 Model validation by the permutation of endometabolome of CAL-72.

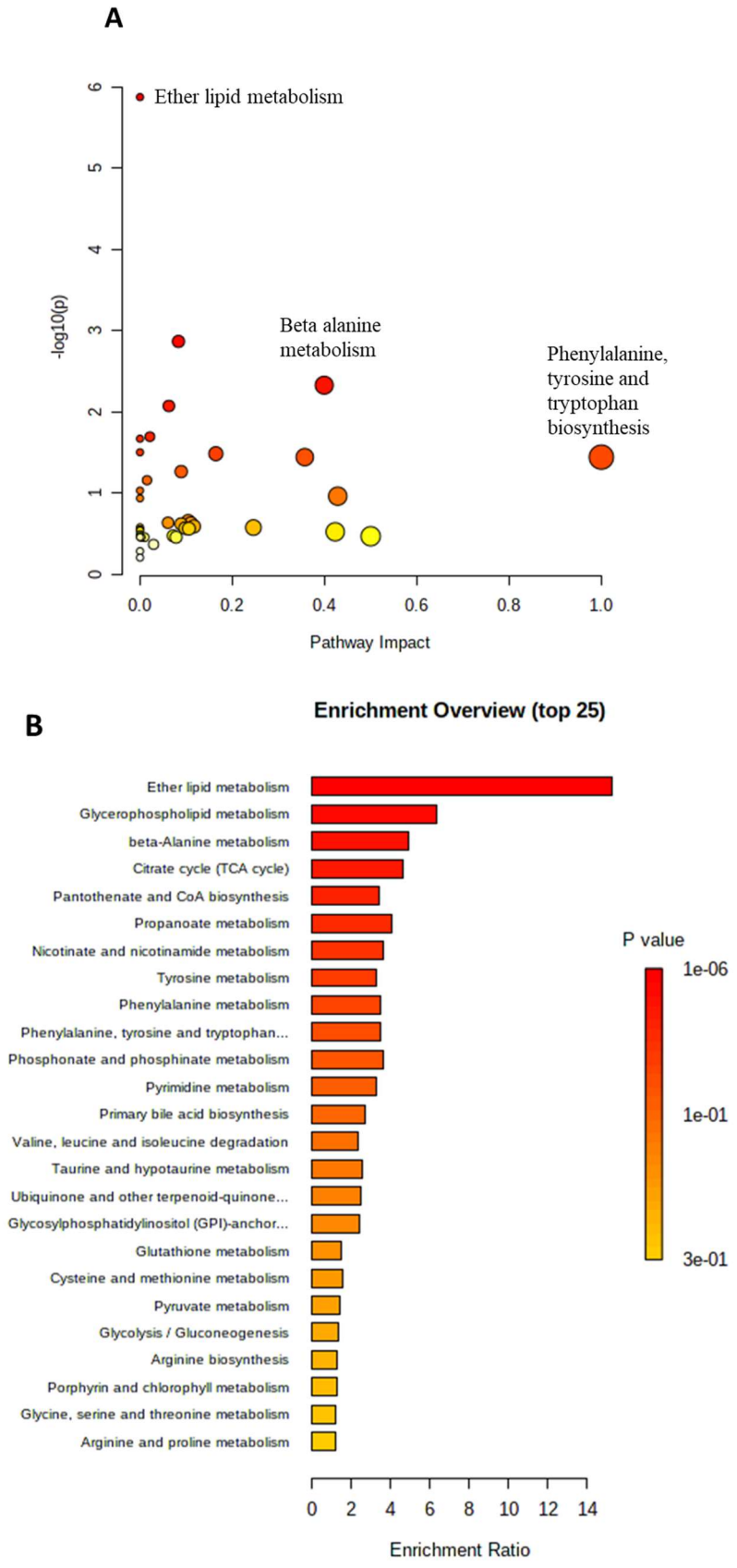

Figure S 84 (A) The metabolome view map and (B) enrichment overview of CAL-72 endometabolites after treatment with IC_{25} of PAMAM G4NH$_2$-48ACCA using KEGG library.

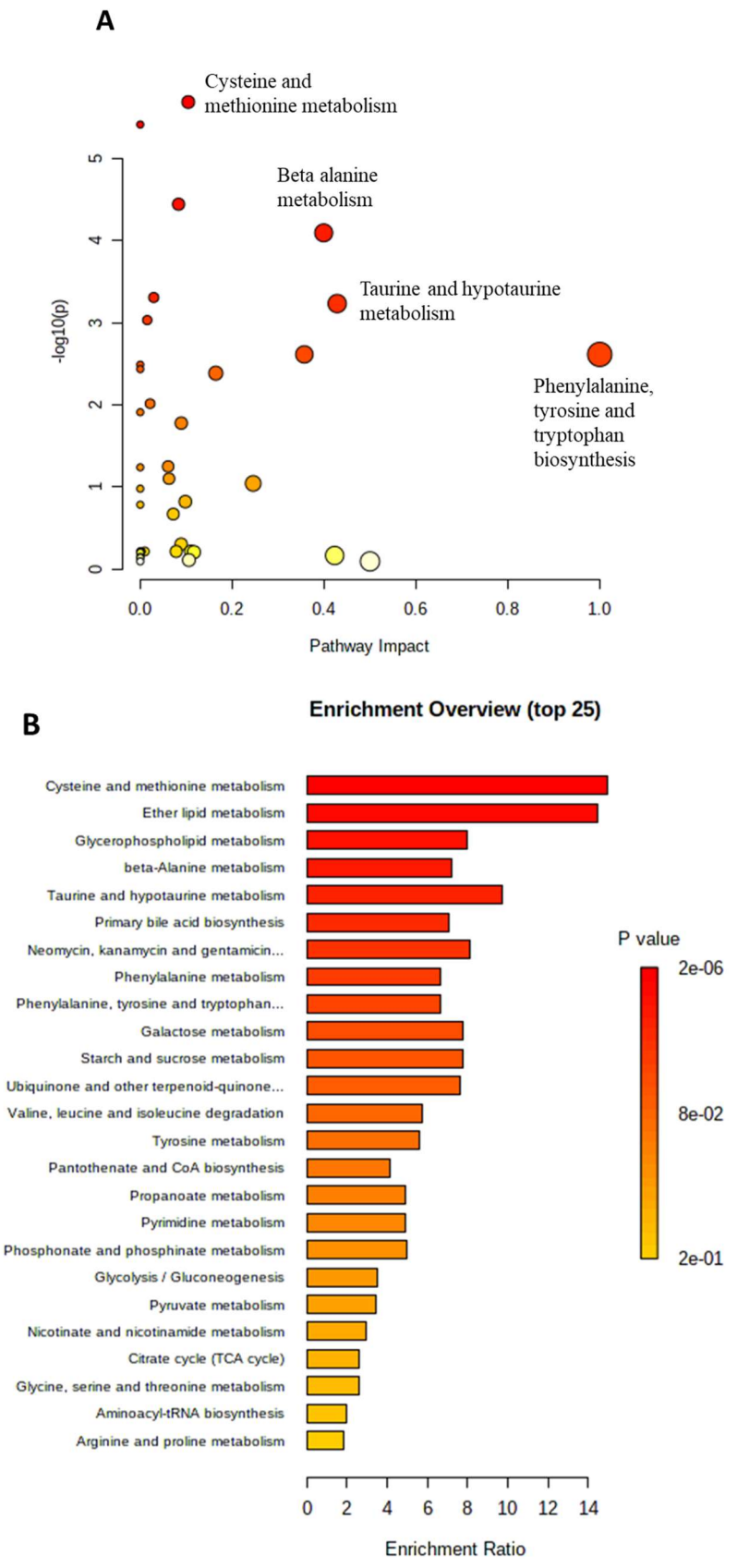

Figure S 85 (A) The metabolome view map and (B) enrichment overview of CAL-72 endometabolites after treatment with IC_{50} of PAMAM G4NH$_2$-48ACCA using KEGG library.

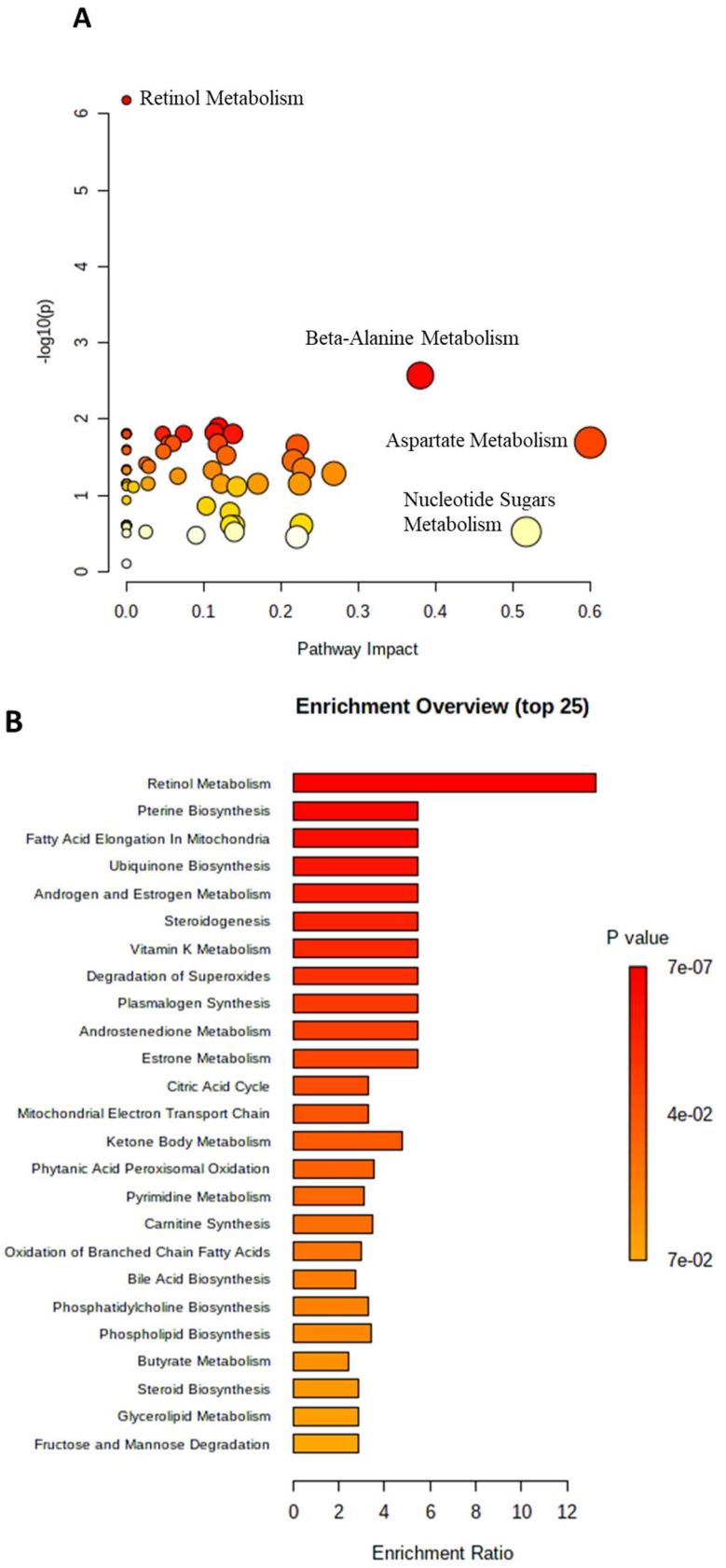

Figure S 86 (A) The metabolome view map and (B) enrichment overview of CAL-72 endometabolites after treatment with IC_{25} of PAMAM G4NH$_2$-48ACCA using SMPDB library.

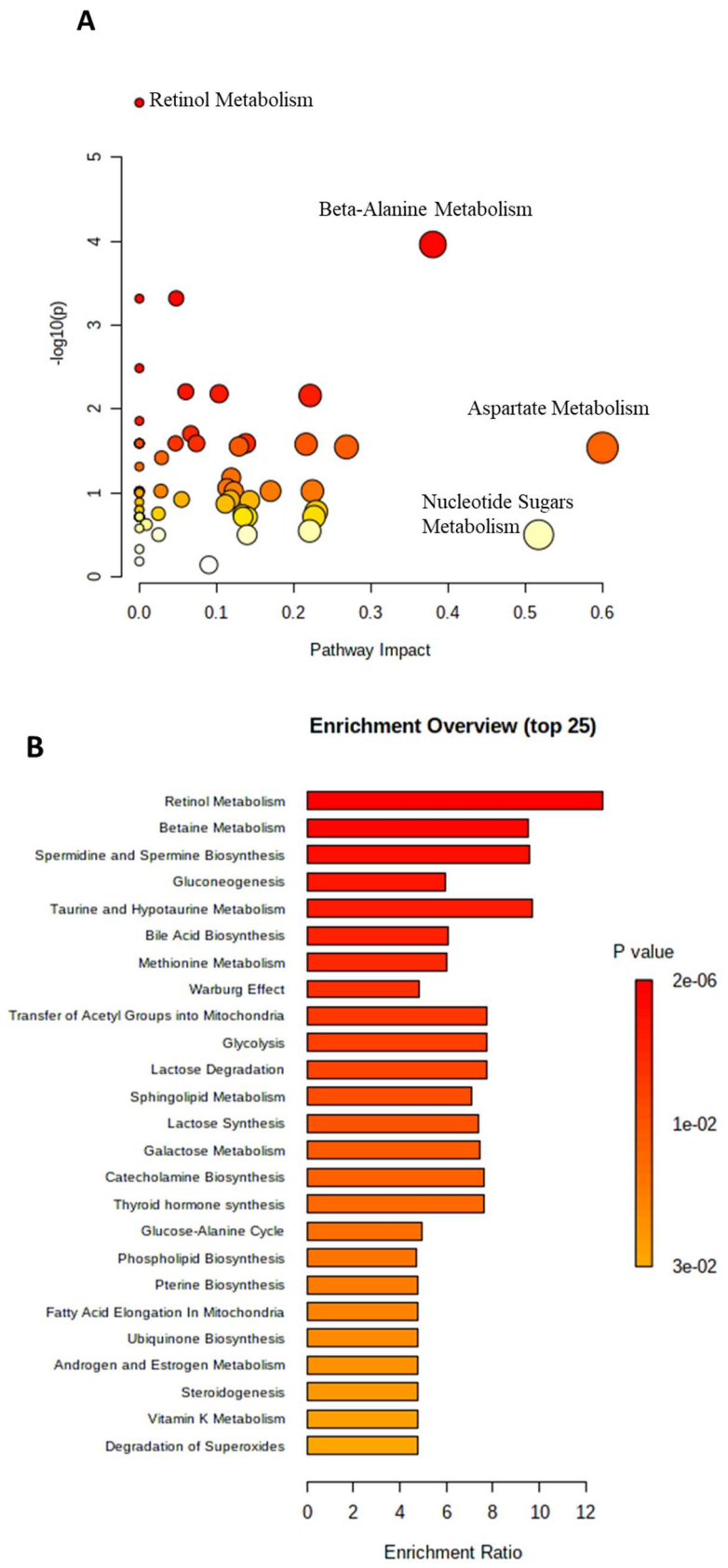

Figure S 87 (A) The metabolome view map and (B) enrichment overview of CAL-72 endometabolites after treatment with IC_{50} of PAMAM G4NH$_2$-48ACCA using SMPDB library.

2. Exometabolome of CAL-72 treated with G4NH$_2$-48ACCA

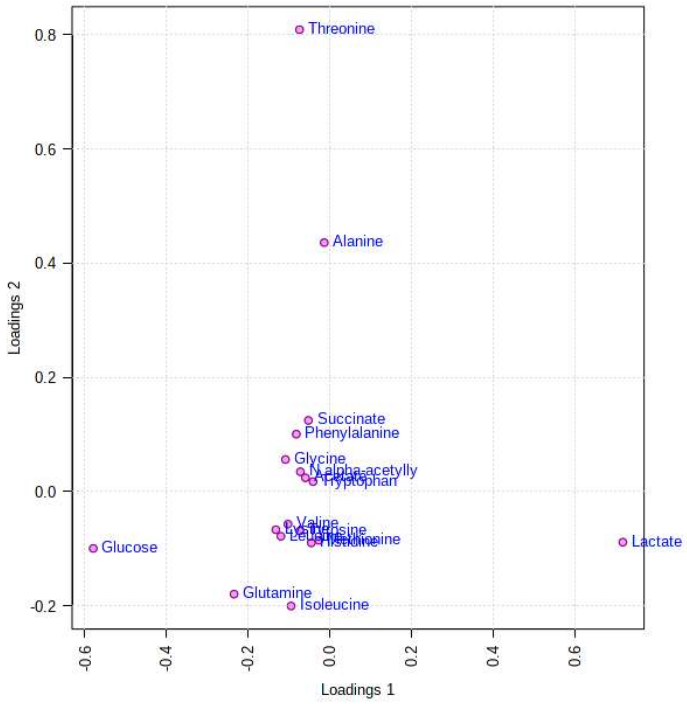

Figure S 88 PCA loading of exometabolome of CAL-72.

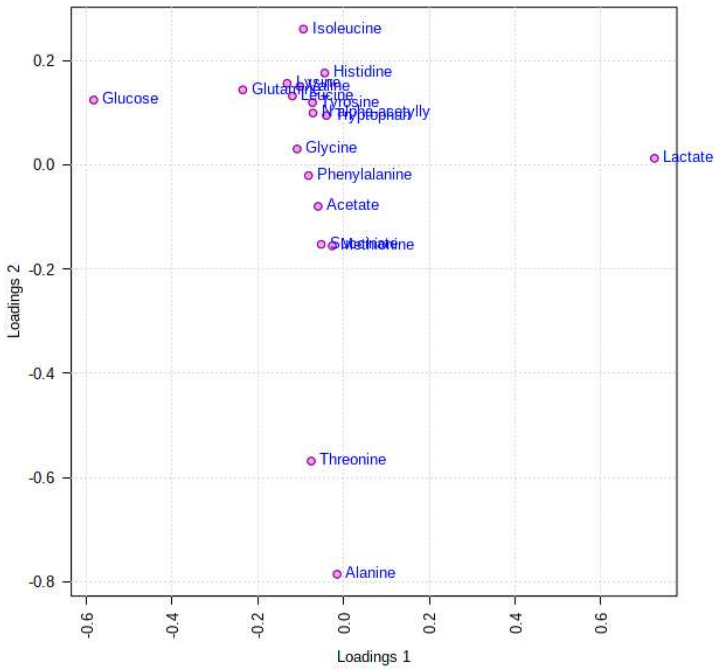

Figure S 89 PLS-DA loading of exometabolome of CAL-72.

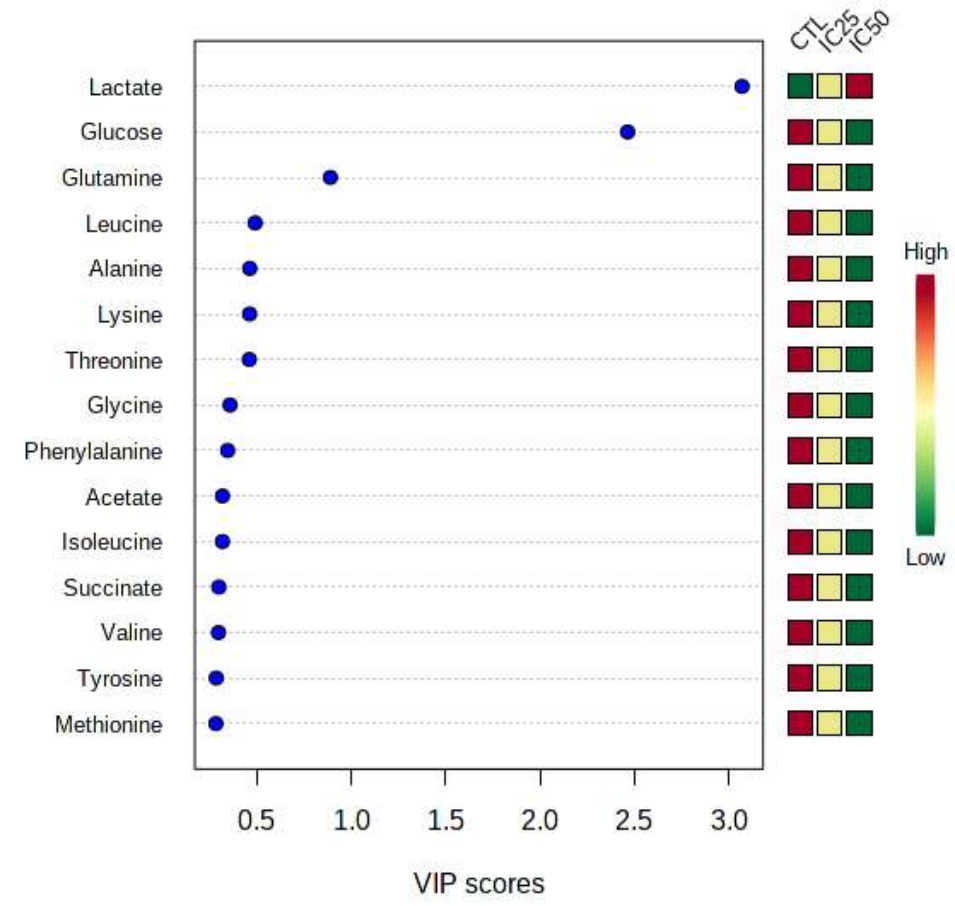

Figure S 90 VIP score of exometabolome of CAL-72.

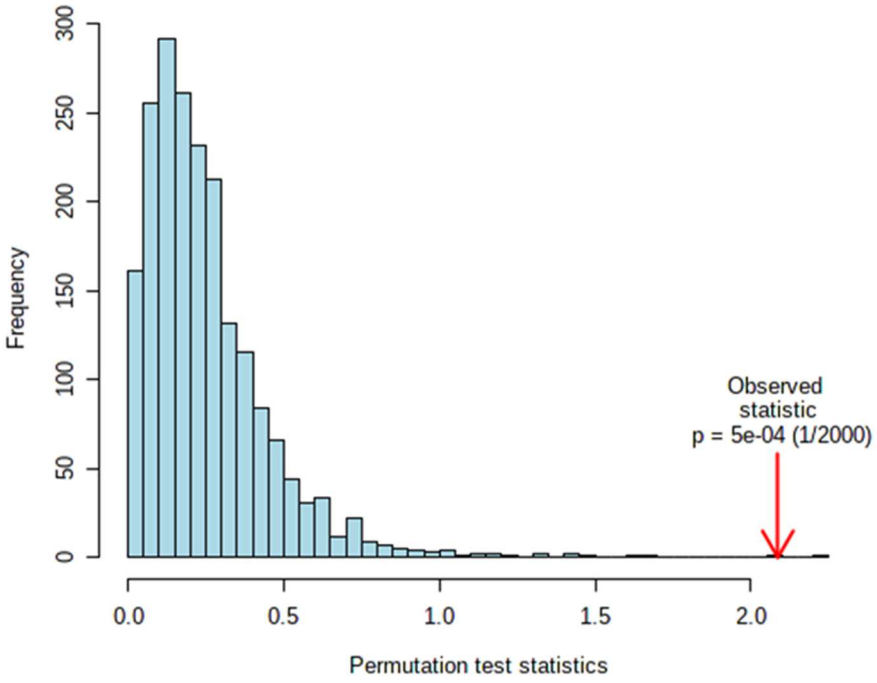

Figure S 91 Model validation by the permutation of exometabolome of CAL-72.

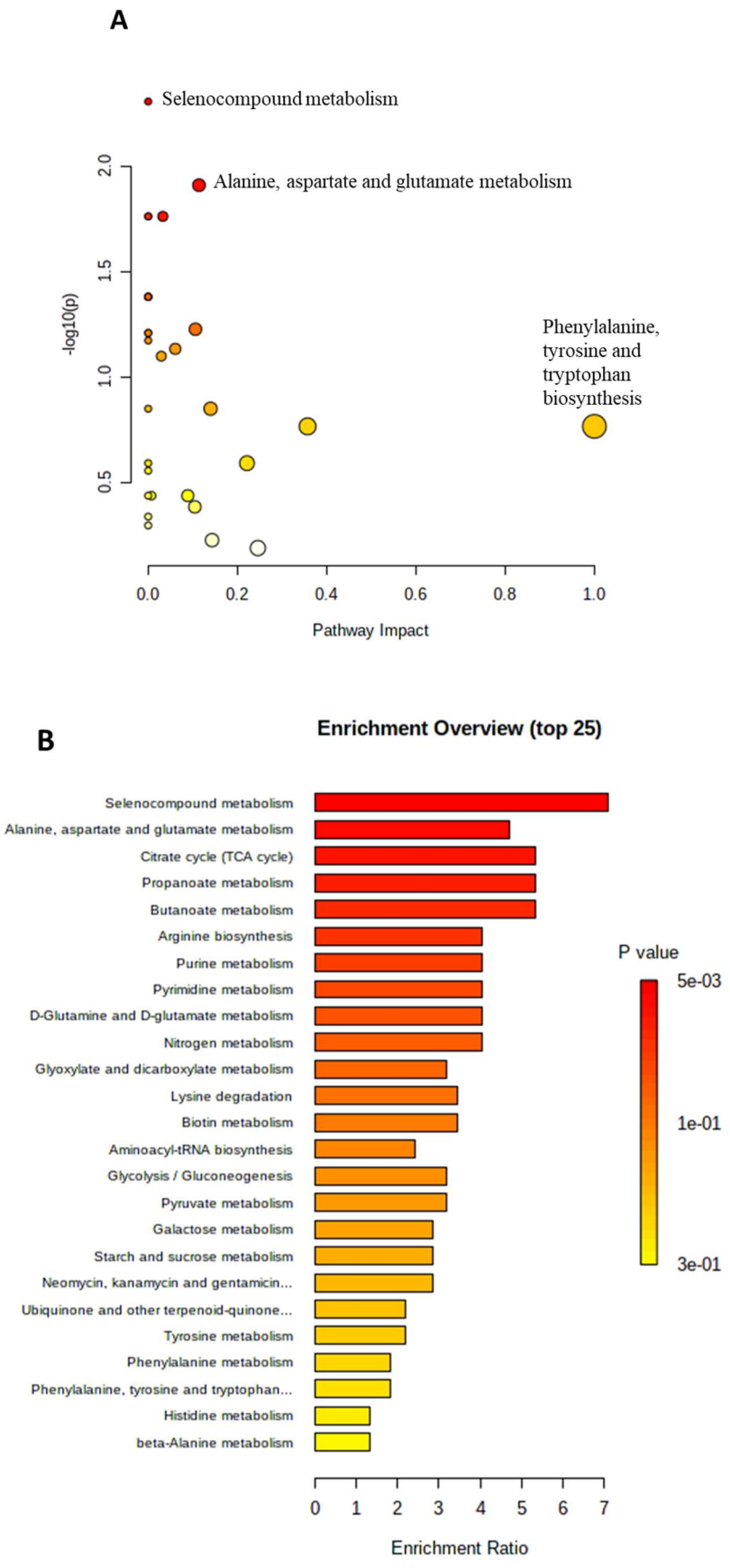

Figure S 92 (A) The metabolome view map and (B) enrichment overview of CAL-72 exometabolites after treatment with IC_{25} of G4NH$_2$-48ACCA using KEGG library.

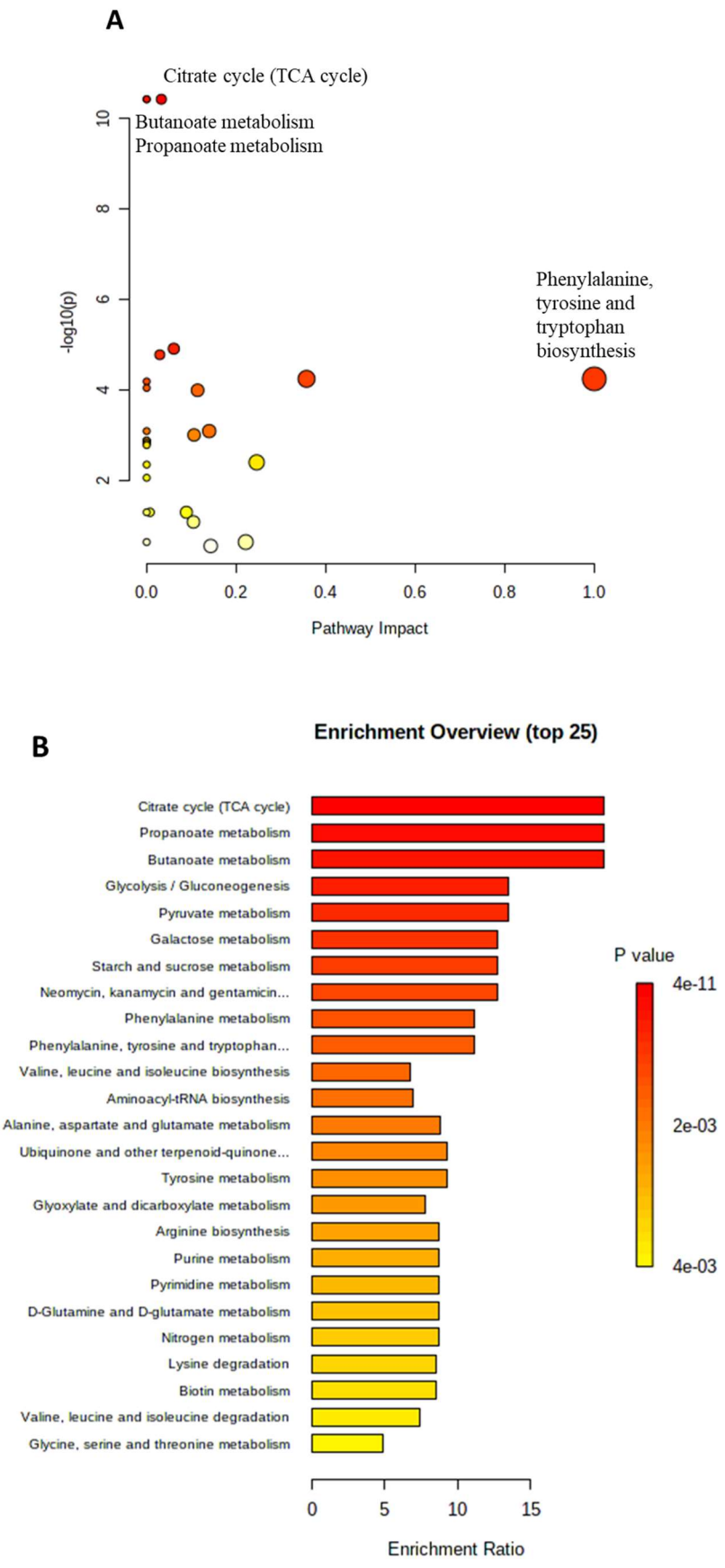

Figure S 93 (A) The metabolome view map and (B) enrichment overview of CAL-72 exometabolites after treatment with IC_{50} of G4NH$_2$-48ACCA using KEGG library.

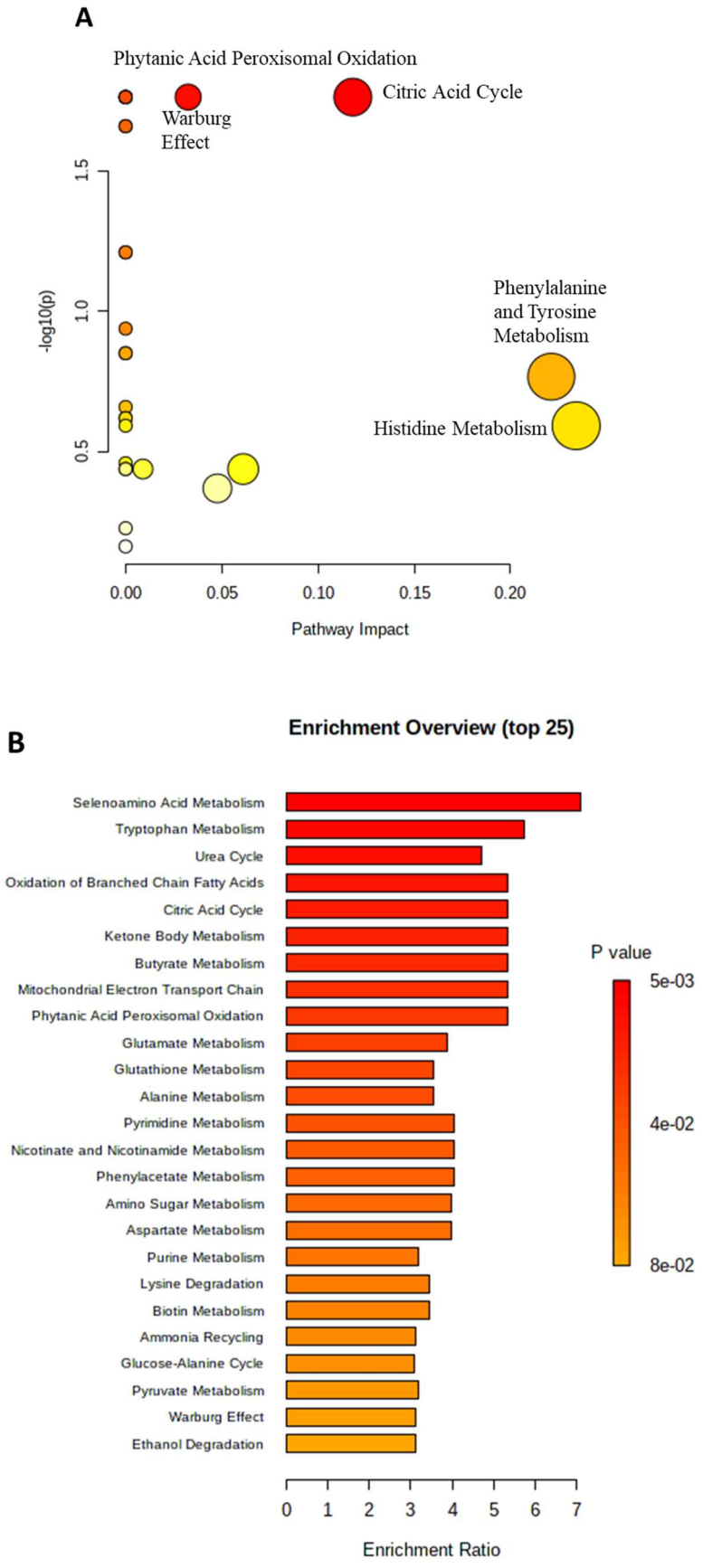

Figure S 94 (A) The metabolome view map and (B) enrichment overview of CAL-72 exometabolites after treatment with IC_{25} of $G4NH_2$-48ACCA using SMPDB library.

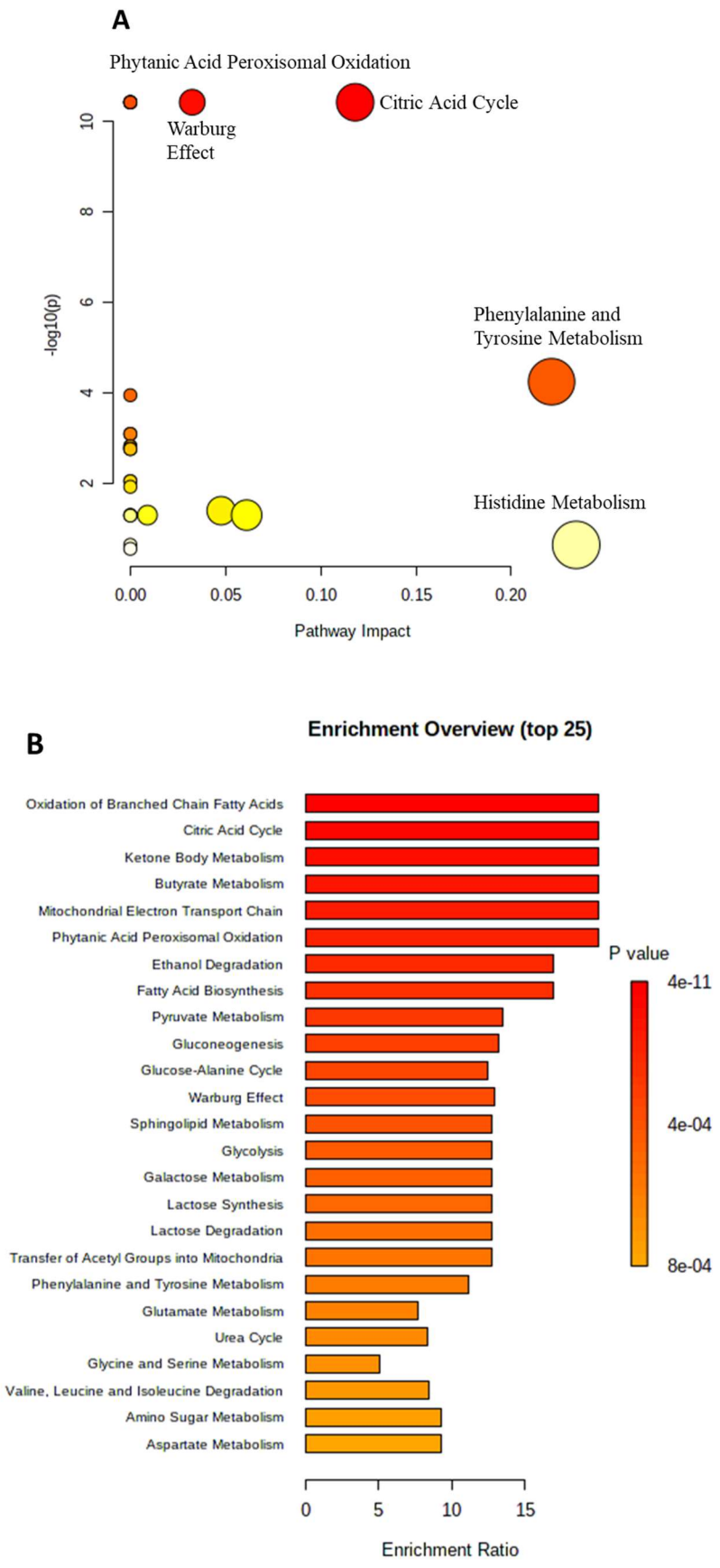

Figure S 95 (A) The metabolome view map and (B) enrichment overview of CAL-72 exometabolites after treatment with IC_{50} of G4NH$_2$-48ACCA using SMPDB library.

FCT Fundação para a Ciência e a Tecnologia
MINISTÉRIO DA CIÊNCIA, TECNOLOGIA E ENSINO SUPERIOR

Base Fund UIDB/00674/2020
Programmatic Fund UIDP/00674/2020

M1420-01-0145-FEDER-000005 - CQM+
(Madeira 14-20 Program)

Projet M1420 - 09-5369-FSE-000001- Ph.D Grant

Doctoral Program in Nuclear Magnetic Resonance Applied to Chemistry, Materials and Biosciences (PTNMR Ph.D)

Cofinanciado por: